



**NTNU – Trondheim**  
Norwegian University of  
Science and Technology

# Energy-economic optimization of heating system with solar collectors

**Live Holmedal Qvistgaard**

Master of Energy and Environmental Engineering

Submission date: June 2014

Supervisor: Natasa Nord, EPT

Norwegian University of Science and Technology  
Department of Energy and Process Engineering



EPT-M-2014-91

**MASTER THESIS**

for

Student Live Holmedal Qvistgaard

Spring 2014

Energy-economic optimization of heating system with solar collectors

*Energiøkonomisk optimalisering av varmesystem med solfangere***Background and objective**

Solar collectors for residential houses are usually sized to cover the hot water needs for the day with the highest insolation per year. However, the marginal cost of expanding the solar collector area is relatively small compared to the system cost, the problem is when the excess heat occurs. Therefore, this project will look at the different storage options relevant to establish interface between the solar collector and heat pump. Dahl Brothers will build a detached demo house in Larvik area with an integrated energy supply solution, including solar collector, ground source heat pump and a combination unit with ventilation and hot tap water systems. Within this project the student will analyze and simulate the energy solutions by using the simulation program IDA-ICE. During the project assignment the student developed a simulation model in IDA-ICE. This model might be further use and developed. The demo detached house project at Dahl Brothers is demo project within the Zero Emission Buildings - ZEB project.

The aim of this project is to analyze the energy supply solutions for the detached house with extended solar collectors and the heat pump combination unit. Design optimization and parameters analysis should be performed for the suggested energy supply solution.

This project work is closely related to The Research Centre on Zero Emission Building at NTNU and SINTEF (FME ZEB) that has the vision to eliminate the greenhouse gas emissions caused by buildings. This national research center will place Norway in the forefront with respect to research, innovation and implementation within the field of energy efficient zero-emission buildings. The main objective of FME ZEB is to develop competitive products and solutions for existing and new buildings that will lead to market penetration of buildings that have zero emissions of greenhouse gases related to their production, operation and demolition. The Centre encompasses both residential and commercial buildings, as well as public buildings.

**The following tasks are to be considered:**

1. Literature study on the heat pump systems integrated with solar collector. Literature study should include an overview of the technical, practical and financial assumptions.
2. Implement the collected data about the demo house in the simulation model. If necessary develop and improve the developed model in IDA-ICE.

3. Start with a parametric study of the most important design parameters. Perform optimization of the design and operation parameters with the aim to achieve the lowest total energy use.
4. Present and discuss the results. Specifically present parametric study and optimization results. Suggest ideas for the future work.

-- " --

Within 14 days of receiving the written text on the master thesis, the candidate shall submit a research plan for his project to the department.

When the thesis is evaluated, emphasis is put on processing of the results, and that they are presented in tabular and/or graphic form in a clear manner, and that they are analyzed carefully.

The thesis should be formulated as a research report with summary both in English and Norwegian, conclusion, literature references, table of contents etc. During the preparation of the text, the candidate should make an effort to produce a well-structured and easily readable report. In order to ease the evaluation of the thesis, it is important that the cross-references are correct. In the making of the report, strong emphasis should be placed on both a thorough discussion of the results and an orderly presentation.

The candidate is requested to initiate and keep close contact with his/her academic supervisor(s) throughout the working period. The candidate must follow the rules and regulations of NTNU as well as passive directions given by the Department of Energy and Process Engineering.


Risk assessment of the candidate's work shall be carried out according to the department's procedures. The risk assessment must be documented and included as part of the final report. Events related to the candidate's work adversely affecting the health, safety or security, must be documented and included as part of the final report. If the documentation on risk assessment represents a large number of pages, the full version is to be submitted electronically to the supervisor and an excerpt is included in the report.

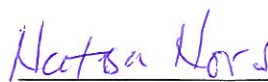
Pursuant to "Regulations concerning the supplementary provisions to the technology study program/Master of Science" at NTNU §20, the Department reserves the permission to utilize all the results and data for teaching and research purposes as well as in future publications.

The final report is to be submitted digitally in DAIM. An executive summary of the thesis including title, student's name, supervisor's name, year, department name, and NTNU's logo and name, shall be submitted to the department as a separate pdf file. Based on an agreement with the supervisor, the final report and other material and documents may be given to the supervisor in digital format.

- Work to be done in lab (Water power lab, Fluids engineering lab, Thermal engineering lab)  
 Field work

Department of Energy and Process Engineering, 16. January 2014

  
\_\_\_\_\_  
Olav Bolland  
Department Head

  
\_\_\_\_\_  
Natasa Nord  
Academic Supervisor

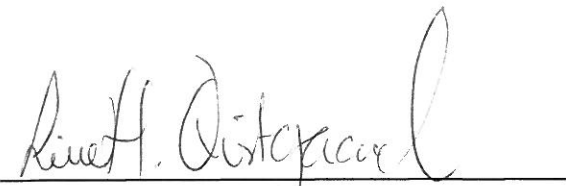
Research Advisor:  
Harald Amundsen, Brødrene Dahl, Harald.Amundsen@dahl.no

## PREFACE

This master thesis was completed in the spring of 2014 at the Norwegian University of Science and Technology in Trondheim. The thesis is written at the Department of Energy and Process Engineering as the final part of the study program Energy and Environmental Engineering. The master thesis is a continuation of the specialization project written during the autumn in 2013, where the foundation of this report was created.

I would especially like to thank my supervisor Natasa Nord for good guidance and advice during this work. Thanks to Harald Amundsen from Brødrene Dahl for being available for advice and information regarding the ZEB demo house and the system design. I would also like to send my gratitude to Jörgen Eriksson from Equa Solutions AB for answering the many questions I had regarding IDA ICE, and for helping me design the rather complicated exhaust air heat pump☺.

A special thanks to Maren Eline Ingebretsen who has always been available for advice, despite working with her own master thesis☺. Thanks to my friends and family for support.



---

Live Holmedal Qvistgaard  
Trondheim, June 2, 2014



## ABSTRACT

This study examines a suggested system solution consisting of flat plate solar thermal collectors in combination with a ground-source heat pump for building heating and cooling, and production of domestic hot water. The solar collectors are intended to constitute a part of the roof construction. The system design is suggested as an energy solution for a 202 m<sup>2</sup> single-family demo dwelling of Zero Emission Building standard. The demo project is a collaboration between Brødrene Dahl and the Research Centre on Zero Emission Buildings. The dwelling will be constructed in Larvik in South Norway.

A parametric study of the main design and operation parameters were conducted in order to find the optimum values which would result in the lowest total electricity use in the system. The design and operating parameters which were optimized included collector area, orientation and tilt angle, fluid type for both collectors and ground-source heat exchanger, collector mass flow rate, storage tank design, heat exchanger effectiveness, collector heat loss, design of ground-source heat exchanger, control settings, supply air and zone set point temperature, supply air volume flow rate, night setback control and heat distribution temperature. The optimum values were determined by using the dynamic simulation software tool IDA Indoor Climate and Energy 4.6. Scenarios with different configurations of optimized design and/or operating parameters were developed in order to investigate the effect of optimizing few, several or all of the components in the system, thus finding the composition which resulted in the lowest electricity use. As the marginal cost of expanding the solar collector area is relatively small compared to the system cost, the share of utilized renewable energy for space heating and domestic hot water was investigated for the optimized scenario with both 8 m<sup>2</sup> and 16 m<sup>2</sup> of installed solar collector area.

The results showed that by optimizing the design of the storage tanks, a 5 % reduction in electricity use was achieved. Optimizing the tilt angle, orientation and heat loss coefficients of the solar collectors resulted in a 4 % reduction in electricity use. The results revealed that changing the operating parameters had the greatest effect on the electricity use relative to parameter changes. A total reduction of 7 % was obtained by optimizing the main system operating parameters. With all main design and operating parameters optimized, a total reduction of 18 % in electricity use was obtained with 16 m<sup>2</sup> of solar collector area installed. A total reduction of 14 % in electricity use was obtained with 8 m<sup>2</sup> of solar collectors installed. Without optimizing the solar collectors, a total reduction of 14 % was obtained with a collector area of 16 m<sup>2</sup>. The highest amount of renewable energy covering the total heating load was obtained with 16 m<sup>2</sup> of solar collector area installed and all main design and operating parameters optimized. It was found that 85 % of the total heating demand was covered by renewable energy. The results showed that by utilizing solar energy the optimized system could provide 85-92 % and 12-70 % of the domestic hot water demand in summer and winter respectively, and 2.5-100 % of the space heating demand.

It can be concluded that by installing a larger solar collector area in combination with a ground-source heat pump, a higher share of utilized renewable energy as well as a higher reduction in delivered energy is obtained. By tilting and orientating the solar collectors towards optimum directions, half the solar collector area is needed in order to obtain the same result as if the solar collector tilt angle and orientation are not optimized.





## SAMMENDRAG

I denne rapporten skal en systemløsning hvor flate termiske solfangere kombineres med en grunnvarmepumpe undersøkes. Varmesystemet som er foreslått skal forsyne en demo-enebolig med energi til oppvarming, kjøling og produksjon av varmt forbruksvann. Det er tenkt at solfangerne skal utgjøre en del av takkonstruksjonen i bygningen. Eneboligen som skal være av null-energi standard og ha et gulvareal på 202 m<sup>2</sup> skal bygges i Larvik i Sør-Norge. Demoprojektet er et samarbeid mellom Brødrene Dahl og Forskningscenteret for Zero Emission Buildings.

For å oppnå et system som bruker minst mulig tilført elektrisitet må systemets hoved design- og driftsparametere optimaliseres. Det ble utført en parametrisk analyse av de design- og driftsparametere som ble ansett for å være systemets viktigste. Hovedfokuset ble lagt på parametere som solfangerareal, solfangerens orientering, helningsvinkel, varmeoverføringsmediet i både solfangere og grunnvarmeveksler, massestrøm i solfangerne, design av lagringstank, varmevekslernes effektivitet, solfangernes varmetap, design av grunnvarmeveksler, kontroll, temperatur på tilluft og settpunktstemperatur i boligen, volumstrøm i ventilasjonsaggregatet, nattsinking og turtemperatur til varmfordelingssystemet. For å finne optimale verdier ble det dynamiske simuleringsverktøyet IDA Indoor Climate and Energy 4.6 benyttet. De optimerte parametere ble deretter satt sammen i ulike scenarier for å kartlegge oppnådd reduksjon i elektrisitetsforbruk ved å optimere både ulike deler av systemet og hele systemet. Siden marginalkostnaden for å utvide solfangerarealet er relativt liten i forhold til systemkostnaden, ble det systemet som viste seg å være optimalt evaluert og analysert med både 8 m<sup>2</sup> og 16 m<sup>2</sup> installert solfangerareal

Resultatene viste at ved å optimere designet av lagringstankene ble det totale elektrisitetsforbruket redusert med 5 %. Ved å optimere solfangernes helningsvinkel, orientering og varmetapstall ble elektrisitetsforbruket redusert med 4 %. Resultatene viste også at driftsparametere hadde størst innvirkning på endringen i elektrisitetsforbruket når den relative differansen ble tatt i betraktning. Ved å optimere systemets driftsparametere ble en reduksjon på 7 % oppnådd. Med alle hoved design- og driftsparametere optimert ble det oppnådd en total reduksjon på 18 % med 16 m<sup>2</sup> solfangerareal installert. En total reduksjon på 14 % ble oppnådd med 8 m<sup>2</sup> solfangerareal. Ved å ikke optimere solfangerne ble en total reduksjon på 14 % oppnådd med 16 m<sup>2</sup> installert solfangerareal. Den høyeste andel av det totale varmebehovet dekket av fornybar energi ble oppnådd med 16 m<sup>2</sup> solfangerareal og alle hoved design- og driftsparametere optimert. Hele 85 % av eneboligens totale varmebehov ble dekket av fornybar energi. Resultatene viste at ved å utnytte solenergi så kunne det optimerte systemet dekke 85-92 % og 12-70 % av varmtvannsbehovet i løpet av henholdsvis sommermånedene og vintermånedene, og 2.5-100 % av romoppvarmingsbehovet.

Det kan konkluderes med at man ved å installere et større solfangerareal i kombinasjon med en grunnvarmepumpe vil dekke en større andel av varmebehovet med fornybar energi, og vil oppnå en høyere reduksjon i levert elektrisk energi. Ved å installere solfangerne med optimert helningsvinkel og orientering, er det kun nødvendig å installere halve solfangerarealet for å oppnå samme resultat som hvis solfangerne ikke var optimert.



## LIST OF FIGURES

Figure 1 - Net ZEB balance (Alonso & Stene, 2013).....	23
Figure 2 - ZEB ambition level (Dokka, et al., 2013) .....	24
Figure 3 - Solar irradiation in Norway for January and June respectively (Fornbybar, 2007).....	26
Figure 4 - Monthly solar irradiation in Larvik. Simulated towards south with optimized tilt angle (European Commission, 2013).....	26
Figure 5 - Monthly energy demand for dwellings of different energy requirements (Dokka & Hermstad, 2005). .....	27
Figure 6 - Energy demand for space heating for passive house standard in Larvik (Stene, 2013). .....	28
Figure 7 - Underground TES technologies (Olesen & Pavlov, 2012).....	29
Figure 8 - Ground-source vertical borehole with u-pipe.....	30
Figure 9 - Single-family dwelling with solar thermal collectors and ground-source heat pump (Kjellsson, 2009). .....	33
Figure 10 - Annual installed capacity of solar collectors in Europe 2000-2011 [MWth/a].....	34
Figure 11 - Number of sold brine/water heat pumps in Norway from 1992-2006 (Midttømme, et al., 2008). .....	34
Figure 12 - Flat plate solar collector (Southface, 2013).....	38
Figure 13 - Evacuated tube solar collector (NorthernLights, u.d.).....	38
Figure 14 - Ground temperature in August, November, February and May .....	40
Figure 15 - Working principle of the exhaust air heat pump (Stene, 2008).....	42
Figure 16 - Compact Ventilation and Heating Device for Passive House dwelling (Stene, 2013). 43	
Figure 17 - Compact P by NILAN (NILAN, u.d.) .....	44
Figure 18 - Solar irradiation for Larvik through the year, south orientation (EC-JRC, 2014).....	46
Figure 19 - Mantle and spiral tank (Furbo, 2004).....	48
Figure 20 - Design of storage tank for a Solar Combi-system (Weiss, 2003).....	50
Figure 21 - Horizontal and vertical ground heat exchangers (Sintef, 2011).....	53
Figure 22 - Polysun Simulation Software.....	57
Figure 23 - "Multikomfort Hus" single-family dwelling.....	61
Figure 24 - North-east cross section of the "Multikomfort" dwelling.....	62
Figure 25 - Ground floor in the "Multikomfort" dwelling .....	62
Figure 26 - First floor in the "Multikomfort" dwelling .....	63
Figure 27 - System design, including solar thermal system and ground-source heat pump. ....	64
Figure 28 - Illustration of the exhaust air heat pump unit in combination with the counter flow heat exchanger and the DHW storage tank (NILAN, u.d.).....	65
Figure 29 - Storage tank for space heating. Applicable for both low and high temperature energy source (OSOHOTwater, 2014).....	66
Figure 30 - Hewalex KS2000SLP .....	68
Figure 31 - Illustration of temperatures in the solar collector heating system .....	72
Figure 32 - Temperature in storage tank.....	72
Figure 33 - Illustration of the ground-source heat pump system.....	73
Figure 34 - Illustration of the exhaust air heat pump.....	75
Figure 35 - COP air/water (NILAN, u.d.) .....	75
Figure 36 - Exhaust air heat pump with outlet exhaust air temperature and outlet hot water temperature .....	76
Figure 37 - Building design in IDA ICE 4.6.....	78

Figure 38 - Direct and diffuse solar radiation Oslo/Fornebu .....	78
Figure 39 - Dry-bulb temperature Oslo/Fornebu .....	79
Figure 40 - Ground and first floor in "Multikomfort" building model designed in IDA ICE.....	79
Figure 41 - Distribution of hot water usage.....	81
Figure 42 - Maximum heat supplied to the dwelling [W/m <sup>2</sup> ].....	83
Figure 43 - Floor heating system in the "Multikomfort" dwelling.....	84
Figure 44 - The Air handling unit (AHU) for the building model in IDA ICE .....	85
Figure 45 - System solution designed in IDA ICE.....	87
Figure 46 - Control of circulation pump P1, DHW preparation .....	89
Figure 47 - Control of circulation pump P2, space heating preparation.....	89
Figure 48 - Control of circulation pump P3, recharging the borehole .....	90
Figure 49 - DHW Tank.....	91
Figure 50 - Space heating Tank.....	93
Figure 51 - Annual incoming solar radiation per solar collector area .....	95
Figure 52 - Annual collected heat.....	96
Figure 53 - Outlet temperature solar collector.....	97
Figure 54 - Temperature difference, outlet and inlet solar collector temperature .....	97
Figure 55 - Mass flow rate through the solar collectors .....	98
Figure 56 - Mass flow rate, circulation pump P1, DHW circuit.....	99
Figure 57 - Mass flow rate, circulation pump P2, space heating circuit.....	99
Figure 58 - Mass flow rate, circulation pump P3, recharging the borehole.....	99
Figure 59 - Operation of circulation pump P1 2013-06-01 .....	100
Figure 60 - Operation of circulation pump P2 2013-04-18.....	101
Figure 61 - Operation of circulation pump P2 2013-07-06.....	101
Figure 62 - Operation of circulation pump P3 2013-06-20.....	102
Figure 63 - Heat flow from solar circuit to DHW tank, SH Tank and to ground.....	103
Figure 64 - Entering brine and leaving water temperature GSHP.....	104
Figure 65 - Temperature Layer 7 SH tank .....	104
Figure 66 - Ground-source heat pump compressor power .....	105
Figure 67 - Annual performance ground-source heat pump .....	105
Figure 68 - Ground-source heat pump COP .....	106
Figure 69 - Annual performance exhaust air heat pump.....	106
Figure 70 - Evaporator inlet temperature and condenser outlet temperature .....	107
Figure 71 - Compressor power exhaust air heat pump.....	108
Figure 72 - Correlation between compressor power and inlet temperature to EAHP condenser 2013-01-04.....	108
Figure 73 - DHW draw-off pattern a regular day.....	109
Figure 74 - Tank temperature layers, DHW tank.....	109
Figure 75 - Domestic hot water draw-off temperature.....	110
Figure 76 - Inlet temperatures to tank from exhaust air HP.....	110
Figure 77 - Inlet temperature to tank from EAHE, 2013-01-06 .....	111
Figure 78 - Electrical boiler heating effect, 2013-01-06.....	111
Figure 79 - Temperature Layer 9 DHW tank, 2013-01-06 .....	112
Figure 80 - Heat input from exhaust air heat pump to DHW tank.....	112
Figure 81 - Heat input form electric boiler to DHW tank.....	112
Figure 82 - Heat input from solar circuit to DHW tank.....	113
Figure 83 - Inlet temperature to tank from solar circuit.....	113

Figure 84 - Layer temperatures in space heating tank.....	114
Figure 85 - Outlet temperature to zone heating and AHU heating.....	115
Figure 86 - Heat input to space heating tank from solar heat exchanger.....	116
Figure 87 - Heating power from electrical boiler to space heating tank.....	116
Figure 88 - Delivered energy.....	117
Figure 89 - Energy demand, utilized free energy and solar fraction.....	118
Figure 90 - Monthly solar fractions for different solar collector areas.....	120
Figure 91 - Tilt angles 19°, 40°, 55° and 60° towards the south-east.....	121
Figure 92 - Tilt angles 19°, 40°, 55° and 60° towards the south.....	122
Figure 93 - Tilt angles of 19°, 40°, 55° and 60° towards the south-east.....	122
Figure 94 - Annual solar fraction and annual specific delivered energy - south orientation.....	123
Figure 95 - Monthly solar fractions for each solar collector type.....	124
Figure 96 - Annual solar fraction as a function of the volume of the DHW tank.....	126
Figure 97 - Annual solar fraction and specific delivered energy as a function of SH tank volume .....	127
Figure 98 - Annual solar fraction and delivered energy as a function of h/d ratio, DHW Tank..	128
Figure 99 - Annual solar fraction and specific delivered energy as a function of h/d-ratio, SH tank .....	128
Figure 100 - Net utilized solar energy and specific delivered energy as a function of auxiliary electric volume in DHW tank.....	129
Figure 101 - Annual solar fraction and specific delivered energy as a function of heat exchange capacity rate.....	130
Figure 102 - Different pipe inlet and outlet locations, DHW Tank.....	132
Figure 103 - Annual solar fraction and specific delivered energy for different pipe inlet and outlet locations, DHW Tank.....	133
Figure 104 - Inlet and outlet locations, SH tank.....	134
Figure 105 - Annual solar fraction and specific delivered energy for different pipe inlet and outlet locations, SH tank.....	135
Figure 106 - Annual solar fraction and specific delivered energy as a function of the borehole depth.....	136
Figure 107 - Annual solar fraction and annual specific delivered energy as a function of the collector mass flow rate.....	139
Figure 108 - Set point temperature DHW tank.....	141
Figure 109 - DHW demand covered by solar energy during the summer months.....	141
Figure 110 - Temperature sensor location in DHW store, annual specific delivered energy.....	143
Figure 111 - Annual specific delivered energy, zone set point temperature of 21°C and varying supply air temperature.....	144
Figure 112 - Annual specific delivered energy, zone set point temperature of 20°C and varying supply air temperature.....	144
Figure 113 - Annual specific delivered energy, zone set point temperature of 19°C and varying supply air temperature.....	144
Figure 114 - Annual specific delivered energy as a function of air volume flow rate.....	146
Figure 115 - Design and operation parameters which gave the greatest reduction in electric energy use.....	148
Figure 116 - Optimized Scenarios, specific delivered energy.....	151
Figure 117 - Sensitivity analysis, Scenario 15.....	152

Figure 118 - Total heating demand, AHU heat recovery, utilized free energy and electrical heating for Scenario 17, 16 and 8 m <sup>2</sup> collector area.....	154
Figure 119 - Amount of utilized free energy in DHW Tank, Scenario 17.....	155
Figure 120 - Fraction of monthly DHW demand covered by solar heat, Scenario 17 .....	156
Figure 121 - Amount of utilized free energy for space heating, Scenario 17 .....	157
Figure 122 - Amount of utilized solar energy for recharging of borehole, Scenario 17 .....	158
Figure 123 - Total heating demand, AHU heat recovery, utilized free energy and electrical heating for Scenario 15, 16 and 8 m <sup>2</sup> collector area.....	159
Figure 124 - Amount of utilized free energy in DHW Tank, Scenario 15.....	160
Figure 125 - Fraction of monthly DHW demand covered by solar heat, Scenario 15 .....	161
Figure 126 - Amount of utilized free energy for space heating, Scenario 15 .....	162
Figure 127 - Amount of utilized solar energy for recharging of borehole, Scenario 15 .....	163

## LIST OF TABLES

Table 1 - Required solar collector area for single-family dwellings (Zijdemans, 2012).	46
Table 2 - Concentration and freezing point of propylene glycol	47
Table 3 - Estimation of ground heat exchanger lengths	53
Table 4 - Thermodynamic data for different ground-source heat exchanger brines (Kjellsson, 2009).	54
Table 5 - Basic system design parameters.	66
Table 6 - Solar collector parameters	68
Table 7 - Specific heat capacity and density of 33 % glycol/water mixture.	69
Table 8 - Solar collector efficiency	69
Table 9 - Produced useful power according to aperture area	70
Table 10 - Solar collector outlet and inlet temperature.	70
Table 11 - DHW tank temperature	72
Table 12 - Changing parameters for solar heating system	73
Table 13 - Coefficient of performance exhaust air heat pump	74
Table 14 - Changing Carnot efficiency	77
Table 15 - U-values and normalized thermal bridge value according to NS 3700:2013.	80
Table 16 - SFP-factor, infiltration and domestic hot water settings in IDA ICE 4.6.	81
Table 17 - Control Setpoints for the simulation model	81
Table 18 - Internal loads, equipment and lighting	82
Table 19 - Distribution system losses	82
Table 20 - Heating effect and specific heating effect	83
Table 21 - Supply and exhaust air flow rates	85
Table 22 - Borehole properties	87
Table 23 - Main characteristics of DHW Tank	92
Table 24 - Main characteristics of SH Tank	94
Table 25 - Specific delivered energy, specific heating demand and annual solar fraction	118
Table 26 - Annual solar fraction and specific delivered energy for different solar collector areas	120
Table 27 - Characteristics of different solar collectors from Hewalex	124
Table 28 - Total annual solar fraction and specific delivered energy for different solar collector types	125
Table 29 - Annual solar fraction and specific delivered energy for each borehole diameter	136
Table 30 - Brine liquid in ground-source heat exchanger	140
Table 31 - Specific delivered energy with night setback control	145
Table 32 - Specific delivered energy with different heating system supply temperatures	147
Table 33 - Relative change in parameter	149
Table 34 - Optimized scenarios	150
Table 35 - Specific delivered energy, specific heat demand and total heat demand for Scenario 15 and 17	153
Table 36 - Amount of utilized free energy, Scenario 17	155
Table 37 - Space heating demand covered by solar energy, Scenario 17	157
Table 38 - Annual solar fraction, Scenario 17	158
Table 39 - Amount of utilized free energy, Scenario 15	160
Table 40 - Space heating demand covered by solar energy, Scenario 15	162
Table 41 - Annual solar fractions for 16 and 8 m <sup>2</sup> collector area, Scenario 15	163

# APPENDIX

<b>A. 1 VEKSLER</b> .....	175
Figure B. 1 - External blinds schedule north-east.....	177
Figure B. 2 - External blinds schedule north-west.....	177
Figure B. 3 - External blinds schedule south-east.....	178
Figure B. 4 - External blinds schedule south-west.....	178
Figure C. 1 - Schedule for equipment and lighting.....	179
Figure C. 2 - Presence occupants kitchen and living room (Number of occupants = 4).....	179
Figure C. 3 - Presence occupants bedroom (Number of occupants = 4).....	179
Figure D. 1 - System design in IDA ICE 4.6.....	180
Figure E. 1 - Operation of circulation pump P10 and P11.....	181
Table F. 1 - Effect of solar HE volume.....	182
Figure F. 1 - Temperatures for zone and AHU heating - optimized inlet and outlet locations ....	182
Figure F. 2 - Effect of GHE diameter and thickness - Vertical loop.....	182
Figure G. 1 - Effect of glycol percentage in collector fluid – Monthly solar fraction.....	183
Figure G. 2 - Effect of glycol percentage in collector fluid - Net utilized solar energy and delivered energy .....	183
Figure G. 3 - Effect of ground-source heat exchanger brine - Delivered energy.....	184
Figure G. 4 - Effect of GSHE mass flow rate - Delivered energy .....	184
Figure G. 5 - Operation of EAHP with new temperature sensor location 2013-01-04 .....	185
Figure H. 1 - Indoor air temperature - Optimized scenario.....	186



# TABLE OF CONTENTS

Abstract.....	V
Sammendrag .....	VII
List of Figures .....	IX
List of Tables .....	XIII
Appendix.....	XIV
Terms and Definitions.....	XIX
1 Introduction.....	21
1.1 Background and Objective .....	21
1.2 Structure of the Report and Limitations .....	22
2 Zero Emission Building.....	23
3 Solar Irradiation and Energy Demand.....	25
3.1 Solar Irradiation .....	25
3.2 Space Energy Demand .....	27
4 Thermal Energy Storage.....	29
4.1 Borehole Thermal Energy Storage .....	30
4.1.1 Seasonal Storage of Solar Energy .....	31
5 Possibilities with Solar Collectors in Combination with Ground-Source Heat Pump.....	34
5.1 Technical Advantages .....	35
5.2 Environmental Advantages .....	36
5.3 Challenges.....	36
6 Components.....	37
6.1 Solar Heating System .....	37
6.1.1 Flat Plate Solar Collector and Evacuated Tube .....	37
6.1.2 Economy and Lifetime .....	39
6.2 Circulation Pump .....	39
6.3 Ground-Source Heat Pump.....	39
6.3.1 Borehole and Ground Heat Exchanger .....	41
6.3.2 Economy and lifetime.....	41
6.4 Exhaust Air Heat Pump .....	42
6.4.1 Economy and Lifetime .....	42
6.5 Compact Ventilation and Heating Device .....	43
7 Recommended Design and Operation of Solar Heating System and Ground-Source Heat Pump.....	45
7.1 Solar Thermal Collectors .....	45

7.1.1	Optimum Solar Collector Tilt Angle and Orientation .....	45
7.1.2	Required Solar Collector Area .....	46
7.1.3	Solar Heat Transfer Fluid.....	47
7.1.4	Solar Collector Mass Flow Rate .....	48
7.1.5	Solar Collector Heat Loss and Absorber Plate.....	48
7.1.6	Control.....	49
7.2	Design of the Storage Tank.....	50
7.2.1	Storage Tank Heat Loss .....	51
7.2.2	Storage Tank Volume and Height/Diameter Ratio .....	52
7.3	Ground-Source Heat Pump System .....	53
7.3.1	Ground Heat Exchanger Length and Diameter .....	53
7.3.2	Ground Heat Exchanger Fluid.....	54
7.3.3	Control of Ground-Source Heat Pump.....	55
8	Relevant Simulation Tools.....	56
8.1	IDA Indoor Climate and Energy .....	56
8.2	TRNSYS .....	56
8.3	Polysun.....	57
8.4	EnergyPlus.....	58
9	Method.....	60
10	Description of the “Multikomfort Hus” .....	61
10.1	Building Model.....	61
10.2	Suggested “Multikomfort” System Design.....	64
10.2.1	System Description.....	64
10.2.2	Operation Modes.....	67
10.2.3	Steady State Calculations .....	68
11	IDA ICE 4.6.....	78
11.1	Location and Climate Settings .....	78
11.2	Building Envelope and Energy use .....	79
11.3	Internal Loads and Heat Loss .....	82
11.4	Heat Distribution System .....	83
11.5	Ventilation System .....	84
11.6	Plant .....	86
11.6.1	The Solar Circuit .....	88
11.6.2	The Ground-Source Heat Pump Circuit.....	90
11.6.3	The Exhaust Air Heat Pump Circuit.....	91

11.6.4	The Domestic Hot Water Tank .....	91
11.6.5	The Space Heating Storage Tank .....	93
12	System Performance .....	95
12.1	The Solar Circuit.....	95
12.1.1	Incoming Radiation per Solar Collector Area and Collected Heat .....	95
12.1.2	Temperature Difference.....	96
12.1.3	Mass Flow Rate .....	98
12.1.4	Control of the Circulation Pumps .....	100
12.1.5	Solar Energy in the Solar Circuit.....	103
12.2	The Ground-Source Heat Pump .....	104
12.3	The Exhaust Air Heat Pump .....	106
12.4	The DHW Tank.....	109
12.5	The Space Heating Tank.....	114
12.6	Energy Demand, Utilized Free Energy and Solar Fraction .....	117
13	Optimal System Design and Operation.....	119
13.1	Study of Optimal Design Parameters.....	119
13.1.1	Effect of Solar Collector Area.....	119
13.1.2	Effect of Solar Collector Orientation and Tilt Angle.....	121
13.1.3	Effect of Solar Collector Heat Loss .....	124
13.1.4	Effect of the Tank Volume.....	125
13.1.5	Effect of the Height/Diameter Ratio.....	127
13.1.6	Effect of Auxiliary Electrical Volume.....	129
13.1.7	Effect of Spiral Heat Exchanger Capacity Rate and Spiral Length.....	130
13.1.8	Effect of Tank Pipe Inlet and Outlet Locations.....	132
13.1.9	Effect of Vertical Borehole Depth .....	135
13.1.10	Effect of Vertical Borehole Diameter .....	136
13.1.11	Effect of Horizontal Heat Exchanger Length.....	137
13.1.12	Effect of Ground-Source Heat Exchanger Diameter and Thickness .....	137
13.2	Study of Optimal Operation Parameters.....	138
13.2.1	Effect of Heat Transfer Fluid in Solar Circuit.....	138
13.2.2	Effect of the Collector Mass Flow Rate .....	138
13.2.3	Effect of Brine Liquid in the Ground-Source Heat Exchanger .....	140
13.2.4	Effect of the Ground-Source Heat Exchanger Mass Flow Rate .....	140
13.2.5	Effect of Control Settings.....	140
13.2.6	Effect of Supply Air and Zone Set Point Temperature .....	143

13.2.7	Effect of Night Setback Control.....	145
13.2.8	Effect of Air Volume Flow Rate.....	146
13.2.9	Effect of Heating System Supply Temperature.....	147
13.3	Summary of the Design and Operation Parameter Optimization.....	148
13.4	Optimized Scenarios.....	150
13.5	Sensitivity Analysis.....	152
13.6	System with Optimized Design and Operation Parameters.....	153
13.6.1	Electricity Use and Energy Demand.....	153
13.6.2	Utilized Free Energy – Scenario 17.....	154
13.6.3	DHW Demand.....	155
13.6.4	Space Heating Demand.....	157
13.6.5	Solar Energy Transferred to the Ground.....	158
13.7	Utilized Free Energy – Scenario 15.....	159
13.7.1	DHW Demand.....	160
13.7.2	Space Heating Demand.....	162
13.7.3	Solar Energy Transferred to the Ground.....	163
14	Discussion.....	164
15	Conclusion.....	166
16	Future Work.....	168
17	Bibliography.....	169
	Appendix A - VEKSLER.....	175
	Appendix B – Schedules for External Blinds.....	177
	Appendix C – Occupant and Equipment/lighting Schedules.....	179
	Appendix D – System Design in IDA ICE 4.6.....	180
	Appendix E – Operation of P10 and P11.....	181
	Appendix F – Design Parameter Study.....	182
	Appendix G – Operation Parameter Study.....	183
	Appendix H – Indoor Air Temperatures.....	186

## TERMS AND DEFINITIONS

The terms and definitions presented are quoted from EN ISO 9488 – *Solar energy Vocabulary* (EN9488, 1999).

<b>Aperture area</b>	Maximum projected area through which unconcentrated solar radiation enters the collector.
<b>Gross collector area</b>	Maximum projected area of the complete collector, excluding any integral means of mounting and connecting fluid pipework.
<b>Irradiance</b>	Power density of radiation incident on a surface.
<b>Optical efficiency</b>	Represents the heat gain when the heat losses are zero.
<b>Selective surface</b>	Surface whose optical properties of reflectance, absorptance, transmittance and emittance are wave-length-dependent.
<b>Solar fraction</b>	Energy supplied by the solar part of a system divided by the total system load.
<b>Stagnation</b>	Status of a collector or system when no heat is being removed by a heat transfer fluid.
<b>Thermal stratification</b>	Horizontal layers of differing densities produced in a storage tank by temperature changes at different depths.
<b>Tilt angle</b>	Angle between the horizontal plane and the plane of the specified surface.



# 1 INTRODUCTION

## 1.1 BACKGROUND AND OBJECTIVE

The annual energy demand in the building sector in Norway represents about 40 % of the total national energy use. In residential buildings, space heating and domestic hot water production represent approximately 70 % of the total energy consumption (NVE, 2011). The building sector can therefore be seen as the key to obtain higher energy savings nationwide, and predictions indicate that the Norwegian energy consumption for residential purposes will be reduced by 75 % in 40 years from now. In order to realize this, the Climate Agreement of March 2012 and the building policy conducted by the Norwegian Government indicates that a passive house standard must be a regulatory requirement by 2015 and nearly zero energy level by 2020. Simultaneously there is a desire to reduce the greenhouse emissions as much as possible in order to assure an effective protection of the climate for future generations. A reduction of CO<sub>2</sub> emissions will demand conversion to a sustainable supply of renewable energy.

Construction of new residential buildings represents an opportunity to limit the energy use due to new energy efficient architectural design and implementation of new technologies. The development of optimal systems that improve the energy integration between renewable energy sources and thermal requirements, while guaranteeing a comfortable indoor climate is crucial.

In this report an example of the new generation of single-family dwellings will be investigated. The majority of the energy demand will be covered by renewable energy sources available on site. The residential building is called the “Multikomfort” dwelling and is a demo project conducted by Brødrene Dahl and the Research Centre on Zero Emission Buildings (ZEB). The “Multikomfort” dwelling will be located in Larvik and is a ZEB detached home with ambition level of ZEB-O&M. The heating system in the dwelling is an integration of thermal solar collectors, ground-source heat pump (GSHP) and a combination unit for ventilation and domestic hot water where an exhaust air heat pump (EAHP) is utilized for domestic hot water production. The design of the heating system is only a suggestion and further optimization and improvements may be done before the system design is chosen as the final energy solution for the demo detached house.

The marginal cost of expanding the solar collector area is small compared to the system cost, and a larger solar collector system is under consideration. Extending the collector area allows for the ability to utilize more solar heat during spring and autumn, but during summer the demand is less than the potential output, which results in overproduction of solar heat. It is therefore interesting to investigate different possibilities of utilizing the excess solar heat, and thermal energy storage is an option with potential.

The aim of this report is to investigate and analyze the possibilities by combining solar thermal collectors with ground-source heat pump for a single-family dwelling, and how this combination may result in better performance and higher energy efficiency of the system. The system designed for the “Multikomfort” dwelling includes additional renewable energy sources, but the focus will be on the collaboration between the solar collectors, the exhaust air heat pump and the vertical ground-source heat pump. The aim is to optimize the system’s main design and operation parameters, thus achieving a system solution with the lowest total electricity use. How changing the installed solar collector area from 8 m<sup>2</sup> to 16 m<sup>2</sup> will affect the system performance,

and how the share of utilized free energy for space heating and domestic hot water differs from one scenario to the other will be studied for the optimal system design.

## 1.2 STRUCTURE OF THE REPORT AND LIMITATIONS

The report will be divided into two main parts, a literature study and a case study. In the literature study, the possibilities of implementing thermal energy storage will be analyzed as well as the possibilities of combining solar and ground-source energy in a system solution. Advantages and challenges of the solution will be emphasized, and the different components which constitute the system will be reviewed from both a technical and a financial perspective. Recommended design and operating parameters for the heating system consisting of solar thermal collectors and ground-source heat pump will be investigated as well. A short literature study on relevant simulation tools will be performed. In the second part, the “Multikomfort” dwelling will be presented and the system design will be analyzed with possible operation modes and with subsequent steady state calculations. A model of the “Multikomfort” system design is created in the dynamic simulation program IDA Indoor Climate and Energy (ICE) and chapter *12 System Performance* is included in order to verify that the heating system works as desired. Further examination and optimization of the main design and operation parameters will be performed by using IDA ICE. A parametric analysis as well as a sensitivity analysis of the optimum system design will be presented. The optimization results will be presented and discussed along with the effect of changing the installed solar collector area.

The customized “Multikomfort” system was designed in the IDA ICE plant model, but due to limitations in IDA ICE it was not possible to include grey water as an energy source, an outdoor swimming pool or the horizontal ground heat exchanger. The program did not work properly when a horizontal ground heat exchanger was used. A more detailed explanation of this can be found in *13.1.11 Effect of Horizontal Heat Exchanger Length*.



## 2 ZERO EMISSION BUILDING

The Norwegian Research Centre on Zero Emission Buildings was established in 2009, and has the following main objective:

*“.. to develop competitive products and solutions for existing and new buildings that will lead to market penetration of buildings that have zero emissions of greenhouse gases related to their production, operation and demolition. The Centre encompasses both residential and commercial buildings, as well as public buildings.” (ZEB, 2013).*

In order to fulfill the objective, work is concentrated into five focus areas:

- Material technology
- Low-energy envelope technologies
- Energy supply system and services
- Energy efficient use and operation
- Concepts and strategies for ZEBs

The Norwegian definition is, for the time being, based on nine criteria (Alonso & Stene, 2013):

- Ambition level
- Basis for calculation
- System boundaries
- CO<sub>2</sub> – factors
- Energy quality
- Mismatch production and demand
- Minimum requirements for energy efficiency
- Requirements for indoor climate
- Verification in use

With a Zero Emission Building it is understood that the energy demand is greatly reduced, and that the building is able to generate electricity with renewable energy sources. A building can be characterized as a ZEB when it is able to export excess energy, generated by photovoltaic (PV) modules for instance, to the grid and achieve an annual net balance between demand and supply. The ZEB balance is illustrated in Figure 1, where the net zero balance line represents the relation between the weighted supply and the weighted demand.

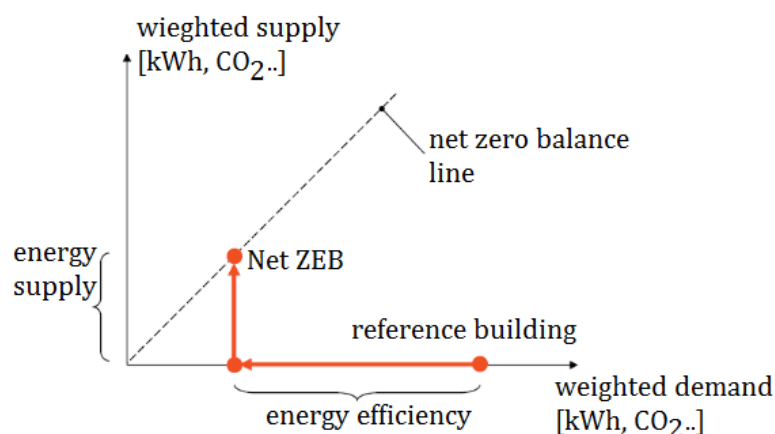


Figure 1 - Net ZEB balance (Alonso & Stene, 2013)

Within the Zero Emission Building definition different ambition levels are defined. The different levels take into account different emission items, and are visualized in Figure 2.

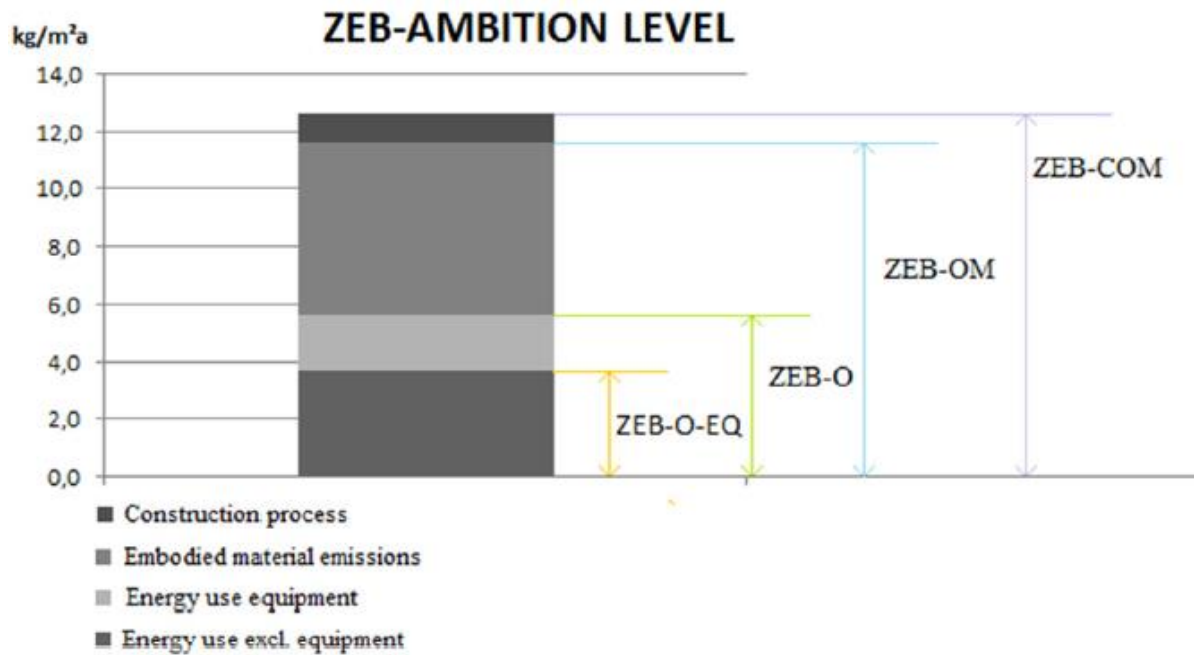


Figure 2 - ZEB ambition level (Dokka, et al., 2013)

For buildings with the most ambitious level, ZEB-COM, emissions related to all operational energy use plus emissions from materials and emissions during the construction phase of the building must be zero.

The minimum requirements of energy efficiency for a ZEB single-family dwelling are stated in the standard describing the requirements for passive houses and low energy buildings, NS 3700:2013 – *Criteria for passive houses and low energy buildings – Residential buildings* (NS3700, 2013).

### 3 SOLAR IRRADIATION AND ENERGY DEMAND

In order to save energy in the building sector in Norway, the Norwegian government's goal is to introduce passive houses by 2015 and zero emission buildings by 2020. With passive residential buildings the objective is to minimize the use of electricity. To achieve this goal, internal loads should be reduced by introducing energy effective equipment, and the building heating system should be based on renewable energy.

Passive residential buildings are characterized by an enhanced building envelope, where the consequence is reduced specific design power demand ( $\text{W}/\text{m}^2$ ), reduced annual specific energy demand ( $\text{kWh}/\text{m}^2\cdot\text{year}$ ) and an increased share of annual heat demand for domestic hot water (DHW). As the building envelope becomes tighter, the development of domestic hot water systems becomes of equal or greater importance than space heating (SH) systems. In passive residential buildings for instance, the hot water demand represents 40 – 85 % of total annual heating demand (Stene, 2008). Developing sustainable solutions for domestic hot water systems based on solar energy is therefore highly relevant.

Even though solar thermal energy is a relatively underexploited resource in Norway, the potential for utilizing solar energy is present. As the focus on energy effective and environmental friendly solutions increases, the market for solar heating systems becomes of great importance. With the increased development of highly energy efficient buildings it is possible to design a heating system where solar heat is utilized to cover a large part of the heating demand.

In 2011 KanEnergi and SINTEF Byggforsk performed a research where the objective was to identify the potential for solar energy in Norway by 2020. The survey was based on calculations which showed that building integrated solutions will be the most competitive in the market. They also concluded that solar heating systems will be able to cover 60 % of the domestic hot water demand and 30 % of the space heating demand in all new residential buildings for a year. The theoretical potential for solar heating by 2020 was calculated to be 65 GWh/year for space heating and 131 GWh/year for domestic hot water for new residential buildings of passive house standard. Assuming that a solar collector can deliver  $300 \text{ kWh}/\text{m}^2$  on a yearly basis, 0.65 million  $\text{m}^2$  of solar collectors are needed to cover 196 GWh/year (Halvorsen, et al., 2011).

#### 3.1 SOLAR IRRADIATION

Approximately  $1.5 \cdot 10^{18}$  kWh of solar radiation hits the earth every year. This constitutes about 15 000 times the annual energy need of the entire world. Even in Norway, the sun provides 1 500 times more energy than what is used (Andresen, 2008). The annual global solar irradiation depends on latitude and with increasing latitudes the solar irradiation decreases. One of the reasons for this is due to the distance which the solar radiation has to travel in the atmosphere. At higher latitudes the distance is longer and larger parts of the solar radiation is absorbed and reflected before it reaches the earth. High latitudes result in high incidence angles of solar irradiance, and lower radiance hits the horizontal ground. By tilting the solar collectors a larger share of the solar irradiation can be collected (Kjellsson, 2009).

The annual solar irradiation in Norway varies from  $700 \text{ kWh}/\text{m}^2$  in the north to  $1100 \text{ kWh}/\text{m}^2$  in the south due to different latitudes. During summer higher solar irradiation is available compared to winter as seen in Figure 3, where the horizontal solar irradiation for January and June is illustrated. Due to this variation it is not possible to rely 100 % on solar heat unless the possibility for storing the solar energy from summer to winter is available.



Figure 3 - Solar irradiation in Norway for January and June respectively (Fornbybar, 2007).

Larvik is one of the more favorable locations in Norway for utilization of solar energy. The annual solar irradiation is approximately 1100 kWh/m<sup>2</sup> (Fonkalsrud, et al., 2003). Figure 4 illustrates the solar irradiation through the year in Larvik.

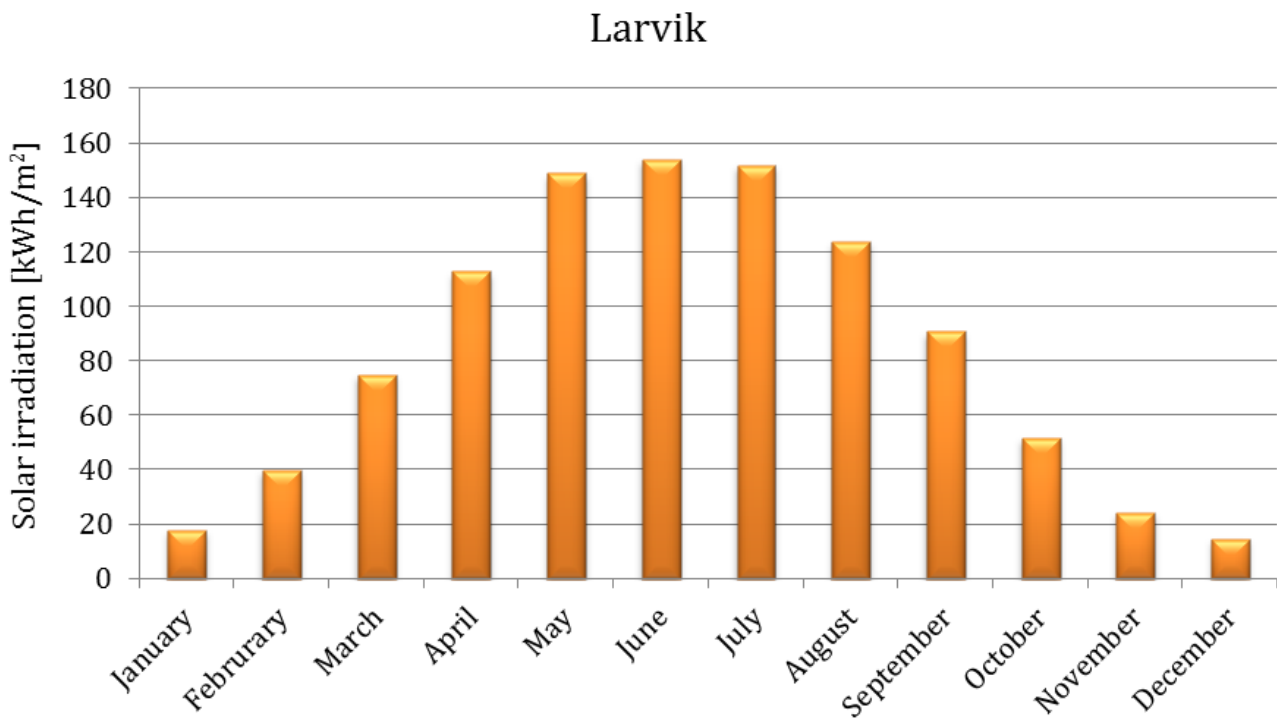


Figure 4 - Monthly solar irradiation in Larvik. Simulated towards south with optimized tilt angle (European Commission, 2013).

### 3.2 SPACE ENERGY DEMAND

In order to reach the passive house standard, installation of highly energy effective equipment, heat recovery units with high efficiency and construction of extremely airtight building envelopes are needed. Figure 5 shows a comparison of energy demand between dwellings built according to the building code of 97, Low energy building, and Passive houses. For the A+ Passive house concept the heat loss is reduced to 1/3 of the heat loss found in buildings built in accordance with the 97 building code (Dokka & Hermstad, 2005).

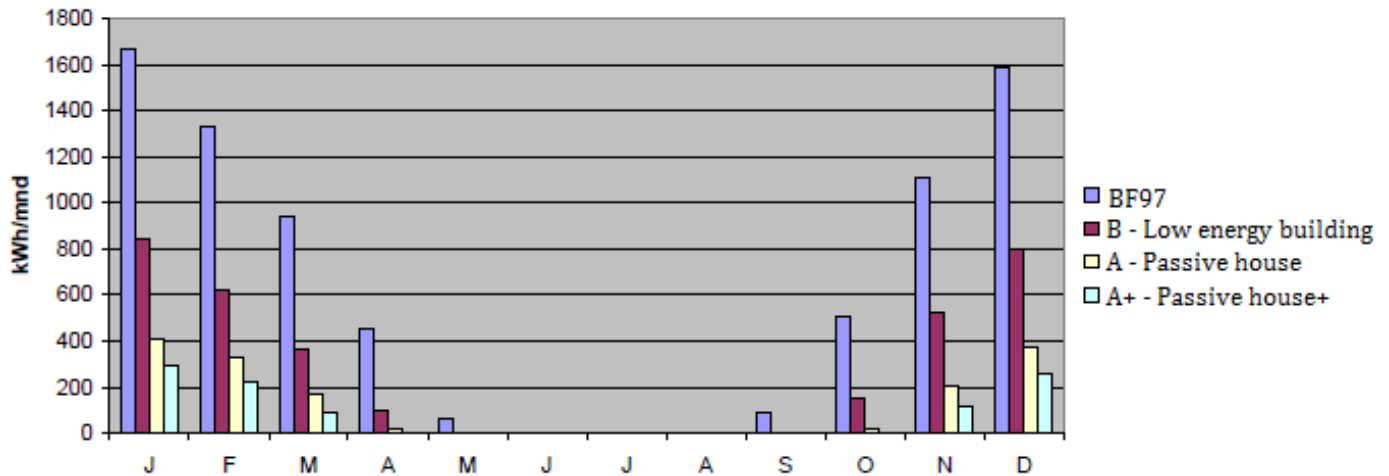


Figure 5 - Monthly energy demand for dwellings of different energy requirements (Dokka & Hermstad, 2005).

As illustrated, the energy demand has been reduced significantly, and for a dwelling with A+ Passive House+ standard, the maximum energy demand is found in the two coldest winter months, January and December.

The required specific heating demand for dwellings of Passive house standard is 15 kWh/m<sup>2</sup>, while the specific heating effect is 10 W/m<sup>2</sup> (Stene, 2008). Achieving these requirements are however difficult in Norway due to a colder climate compared to Germany, where the requirements were first introduced. The Norwegian standard, NS 3700:2013, operates with a maximum specific heating demand adjusted according to climate and thereby the annual average temperature on the specific location.

In addition to the annual average temperature, the specific heating demand is adjusted according to heated dwelling floor area, where the distinction lies between dwellings with a heated floor area above or below 250 m<sup>2</sup>.

According to NS 3700:2013, the specific heat demand for a dwelling with an annual average temperature equal to or above 6.3°C and a floor area below 250m<sup>2</sup> is calculated according to Equation 1.

$$\text{Specific heat demand} = 15 + 5.4 \cdot \frac{(250 - A_{fl})}{100} \left[ \frac{\text{kWh}}{\text{m}^2} \right] \quad (1)$$

where,

$A_{fl}$  is the heated floor area [m<sup>2</sup>]

The specific heating demand for a dwelling with a floor area above 250 m<sup>2</sup> is 15 kWh/m<sup>2</sup>, but if the annual average outdoor temperature is less than 6.3°C the specific heating demand for a dwelling with floor area below and above is calculated according to Equation 2 and Equation 3 respectively.

$$\text{Specific heating demand} = 15 + 5.4 \cdot \frac{(250 - A_{fl})}{100} + \left( 2.1 + 0.59 \cdot \frac{(250 - A_{fl})}{100} \right) \cdot (6.3 - \theta_{ym}) \left[ \frac{kWh}{m^2} \right] \quad (2)$$

$$\text{Specific heating demand} = 15 + 2.1 \cdot (6.3 - \theta_{ym}) \left[ \frac{kWh}{m^2} \right] \quad (3)$$

where,

$\theta_{ym}$  is the annual average temperature

Figure 6 illustrates the required heat demand in Larvik for passive houses with floor areas ranging from 100 m<sup>2</sup> to 250 m<sup>2</sup>. The annual average temperature in Larvik is 6.3°C and as seen in Figure 6, the specific heating demand for passive houses with a floor area of 250 m<sup>2</sup> is 15 kWh/m<sup>2</sup>. With a floor area of 100 m<sup>2</sup> the specific heating demand is approximately 22 kWh/m<sup>2</sup>. The net energy demands for space heating illustrated in Figure 6 are calculated according to Equation 1, 2 and 3.

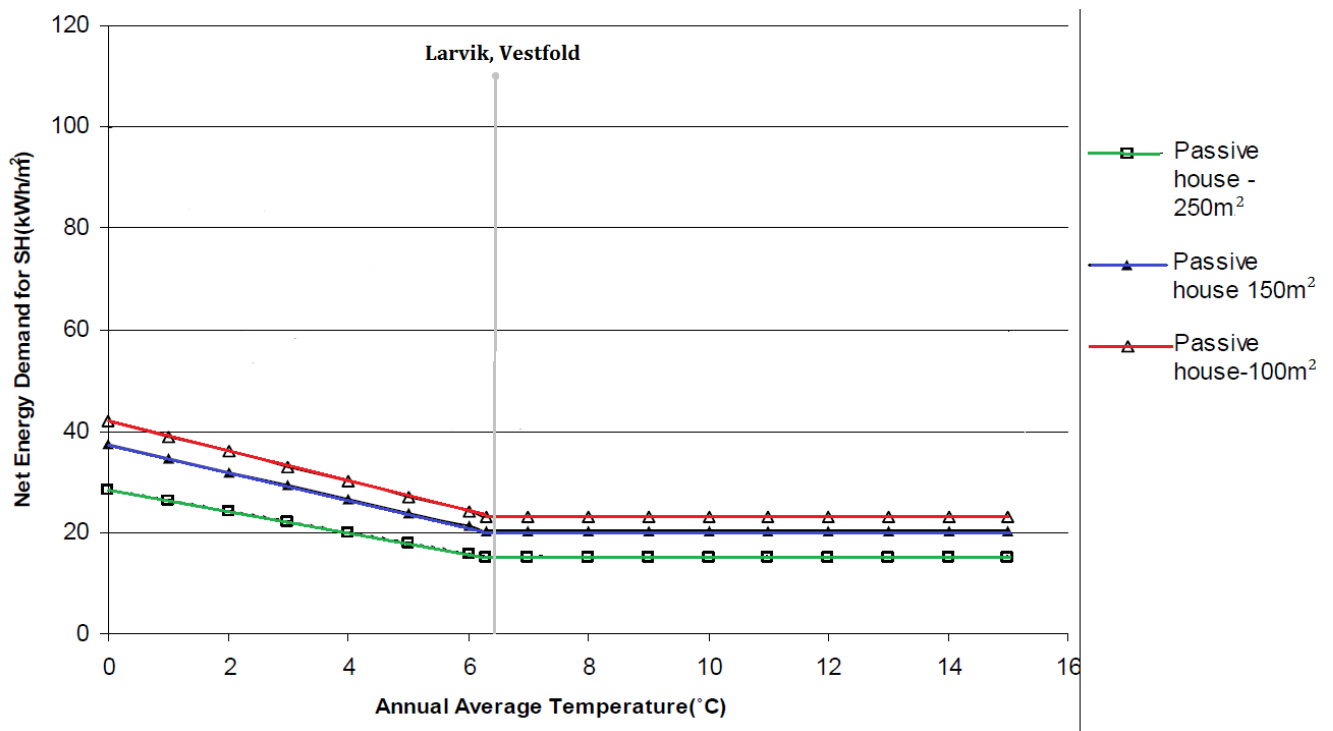


Figure 6 - Energy demand for space heating for passive house standard in Larvik (Stene, 2013).

## 4 THERMAL ENERGY STORAGE

The marginal cost of expanding a solar collector area is relatively small compared to the system cost, the problem arises when excess solar heat is produced. Developing a solution which makes it possible to use the excess heat and thereby utilize the full potential of the solar thermal technology is therefore crucial. Efficient energy storages may represent such a solution. Being able to store the excess heat is particularly important for cold climate countries with a high latitude location due to the imbalance between available solar energy and the space heating demand. In Norway, for instance, there is a significant seasonal dependent variation in solar irradiation, and the residential energy consumption is dominated by varying heating loads throughout the year. Having the possibility to store excess solar heat collected during transition and summer time, is therefore an important aspect when the share of renewable energy must increase.

Thermal energy storages (TES) must be carefully matched to each specific application, and the selection of a TES system is highly dependent on storage period required, economic viability and operating conditions. It is stated that one of the main issues impeding the utilization of natural energy sources for space heating and heating of domestic hot water is the development of economically competitive and reliable means for seasonal storage of thermal energy (Olesen & Pavlov, 2012). However, storage of thermal energy has the potential of making the use of HVAC systems more effective and, if well designed, the system can reduce initial and maintenance costs and improve energy efficiency (Olesen & Pavlov, 2012).

Different TES-technologies for heating and cooling purposes have been investigated and analyzed during the past decades. As TES-systems require large volumes, preferably inexpensive, the most promising technology is found using the ground as storage. The ground has the advantage of having relatively stable temperatures compared to storages above ground, where the ambient temperature varies throughout the year causing higher thermal losses to the surroundings. There are mainly four types of underground thermal energy storages (UTES), see Figure 7.

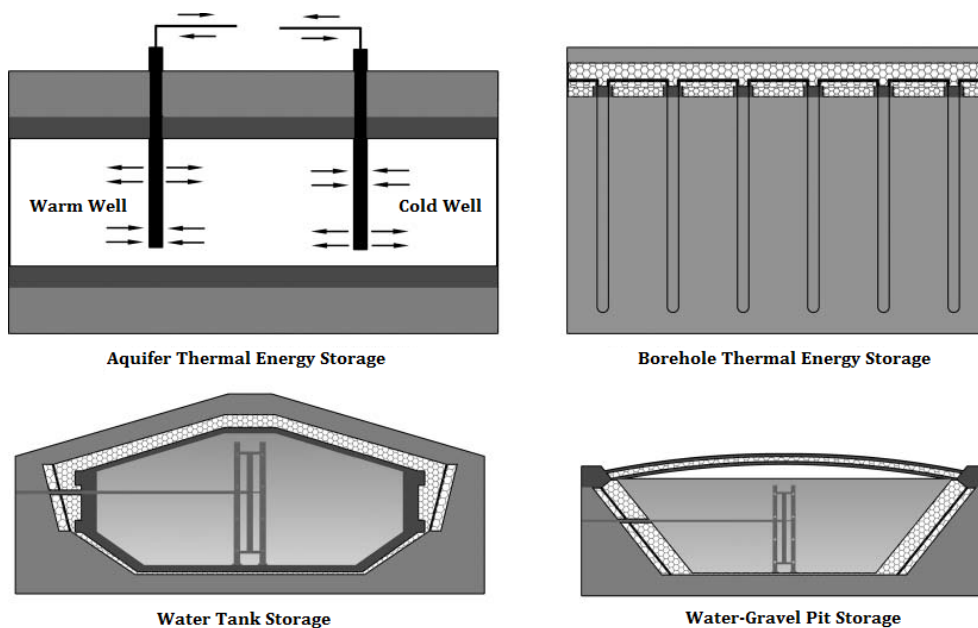


Figure 7 - Underground TES technologies (Olesen & Pavlov, 2012).

## 4.1 BOREHOLE THERMAL ENERGY STORAGE

For a heating system with a combination of solar collectors and a ground-source heat pump it is relevant to look into the borehole TES technology for storing. In borehole TES, heat is stored directly in the ground and the geological formation of the ground is therefore of great importance to the system's efficiency.

The heat transfer between the heat carrier fluid and the surrounding ground is determined by the arrangement of flow channels in the boreholes, the convective heat transfer in the ducts and the thermal properties of the materials involved in the thermal process. Obtaining good thermal contact between the heat exchanger and the borehole wall is important in order to allow a good heat transfer rate per unit area of the heat exchanger tube (Olesen & Pavlov, u.d.). The flow between the two surfaces is determined by the temperature difference and the thermal resistance between the heat carrier fluid and the borehole wall. This resistance,  $R_b$ , is defined by Equation 4.

$$T_f - T_b = q \cdot R_b \text{ [K]} \quad (4)$$

where,

$T_f$  is the temperature of the fluid [K]

$T_b$  is the temperature of the borehole wall [K]

$q$  is the heat injection/extraction rate [W/m]

The thermal resistance between the heat exchanger and the borehole wall depends on the convective heat transfer between the fluid in the pipes and the pipe walls, the thermal resistance over the pipe walls, the convective heat flow outside the pipes in the water or refill and the conductive heat flow in the ground outside the borehole. In order to extract as much energy as possible it is important to reduce the thermal resistance to a minimum. The overall thermal resistance is important to calculate in order to size the borehole depth correctly. Figure 8 shows an example of a ground source heat exchanger with U-pipe.

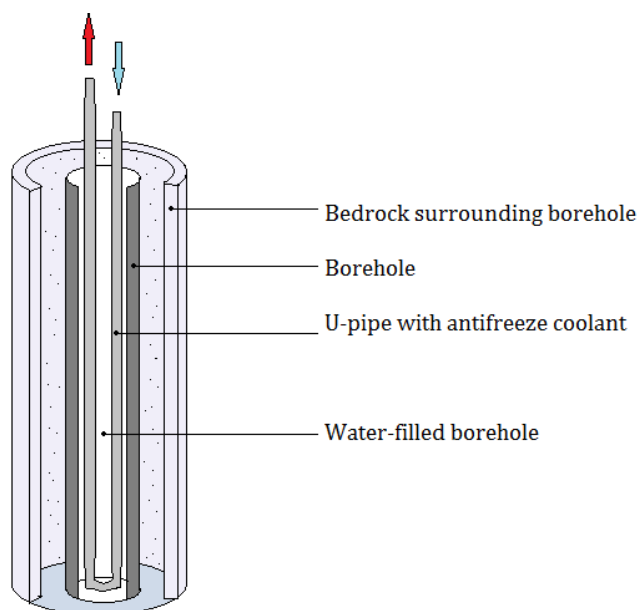


Figure 8 - Ground-source vertical borehole with u-pipe



To increase the thermal contact between the heat carrier pipes and the borehole wall, the borehole is filled with a highly conductive material, often groundwater. The local heat transfer in and near the borehole is very important for the heat transfer capacity of the ground heat exchanger. When the borehole is filled with groundwater, the heat transfer will induce free convection. A laboratory experiment performed by Kjellson and Hellström (Kjellsson, 2009), where different pipe materials and pipe geometries were studied for different fluid temperature levels and specific heat transfer rates, showed a substantial reduction of borehole thermal resistance due to natural convection. They confirmed that free convection in the groundwater in the borehole influences the borehole thermal resistance, and the higher the heat transfer is, the more reduction in borehole thermal resistance is achieved. It was found that boreholes filled with groundwater got improved thermal properties compared to boreholes with fixed filling.

As mentioned earlier, the thermal characteristics of the ground must be identified in order to calculate the required quantity and length of the boreholes. Geological characteristics are usually created based on geological research performed by national institutions for geological knowledge. In Norway they are performed by NGU. The geological characteristics of the thermal properties in the ground may change over time due to natural seasonal change of temperature or underground water flow, but also due to thermal exploitation of the boreholes (Danielewicz, et al., 2013). In order to achieve good operational conditions for the borehole and the accompanying heat pump, the ground loads must be balanced. In case of heating dominated buildings, a thermal heat depletion of the soil may occur and the temperature in the soil will descend year after year. As a result, the heat pump's COP will decline gradually and the installation will become less efficient (Trillat-Berdal, et al., 2006).

Maintaining an energy balance will keep the average ground temperature relatively constant, and avoid operational problems for the heat pump provoked by overheating or overcooling of the ground.

#### *4.1.1 SEASONAL STORAGE OF SOLAR ENERGY*

Combining solar collectors with a ground-source heat pump has been increasingly recognized in Europe since the oil crises in the 1970s, but the technology has not been widely adopted (Trillat-Berdal, et al., 2006). Experiments and studies on this kind of heating system used in single-family dwellings are relatively scarce, especially in Norway. Even though seasonal storage of solar heat in boreholes for detached houses is not widely examined, theoretical calculations show that charging the borehole with solar heat is beneficial (Ramstad, 2013). The question is whether the benefit outweighs the cost. An illustration of a single-family dwelling with solar thermal collectors and ground-source heat pump can be seen in Figure 9.

Incorporating the ground-source heating system with supplementary components, such as thermal solar collectors, can remedy for the imbalance which occurs in the soil due to thermal heat depletion. Solar seasonal thermal storage is defined as the collection of solar energy from spring to autumn, where the excess solar heat produced on days with high solar irradiation is injected into the borehole through ground heat exchangers and stored until heating season. The advantage of combining thermal solar collectors with a ground-source heat pump is not only that the imbalance in the soil is reduced, but it also prevents overheating problems in the solar collector. Recharging is also an alternative when the outlet temperature of the solar collector is too low and insufficient for domestic hot water production.

An experimental study of a heating system which combined ground source heat pumps and thermal solar collectors, performed by Trillat-Berdal et al. (2006), showed that the COP of the heat pump gradually decreased as the heating season advanced. A reduction of 14 % of the heat pump COP was the result due to heat depletion of the ground. Injecting excess solar heat into the boreholes consequently increased the heat pump COP, and improved the operational conditions of the system (Trillat-Berdal, et al., 2006). Xi et al. (2011) also presented an experimental study on a combined ground-source heat pump and solar thermal collectors. He compared a system where a continuous space heating demand was provided with the soil as the only heat source with a system where both the soil and solar energy were the heat sources. In the latter system, the solar collectors were installed in series with the ground heat exchanger. The study showed that with both soil and solar energy as heat sources the average evaporator inlet temperature improved by 35 %. He concluded that a solar-assisted heating process has a significant effect on the improvement of the borehole temperature and energy efficiency (Xi, et al., 2011).

When recharging the borehole the fluid temperature in the U-pipe will increase. This enables the possibility of using shorter boreholes and thereby decrease the borehole investment cost. The possibility of a higher heat extraction rate from the borehole is also present when recharging the borehole. Chiasson (2003) performed an assessment of the viability of a ground heat pump coupled with solar thermal collectors in heating dominated buildings. He based the analysis on an example building with six different climates from six different U.S. cities. The study showed that combining solar collectors with a GSHP reduced the borehole length at the design step with a reduction per solar collector area ranging from 4.5 (Omaha and Nebraska) to 7.7 m/m<sup>2</sup> solar collector area (Cheyenne and Wyoming) (Chiasson & Yavuzturk, 2003).

Having the possibility of recharging the borehole is an advantage if the borehole turns out to be undersized due to a higher heating demand than expected, or if the ground thermal conductivity or level of ground water is lower than predicted. The recharging process will increase the temperature to the evaporator and compensate for the problems caused by an undersized borehole. In densely populated areas, the boreholes may be drilled too close to each other and thereby influencing each other negatively. Being able to charge the boreholes with excess solar heat is therefore beneficial (Kjellsson, 2009).

An experimental study of a solar-assisted ground-source heat pump system with solar seasonal thermal storage was performed by Xiao Wang et al. (2010) in Harbin, China. Harbin is a location with a severely cold climate. During the measuring period, the average outdoor temperature was -7.6°C. The system was conducted for a detached house with 500 m<sup>2</sup> floor area, 50 m<sup>2</sup> of high efficient flat plate solar collectors and 12 ground heat exchangers with depths of 50 m. The survey showed that after a year of operation, the heat injected to the soil was higher than the heat extracted during heating season, which implied that the heat extracted by the heat pump completely came from the solar energy. The heat pump's COP increased in line with the increasing soil temperature, which may seem favorable. However, at some point, the soil temperature can reach too high levels and counteract the possibility of free space cooling from the soil. The analysis promoted the importance of an efficient control system to reduce the operating time of solar collectors in order to reach a balanced ground load (Xiao Wang, 2010). Even though the solar insolation is considerably higher and enables a longer period of heat injection to the soil in Harbin, China than in Larvik, Norway, the heat demand in a ZEB detached house is lower and less heat needs to be extracted from the soil. The possibility of overheating

the soil is present and should be avoided in order to meet the high cooling demand that can occur in a Zero Energy Building. It should also be stated that a heating system for a single-family dwelling of ZEB standard only needs a limited number of boreholes to cover the heat demand, normally only one borehole is needed. The possibility of neighboring boreholes influencing each other and causing a rapid temperature decrease in the soil is therefore limited. With only one borehole, the soil has a faster natural heat recovery and the possibility of overheating the soil when solar energy is injected is therefore present. The solution may therefore seem to be worthless. However, if adjacent boreholes will be drilled at a later stage, the possibility of recharging is convenient.

An important aspect when considering the durability and reliability of a solar heating system is the undesired situation when too high temperatures are reached in the solar collector. High temperatures occur if the heat transfer media is not able to emit enough heat to the water in the storage tank, and as a result of too high temperatures high pressure, material degradation and thermal shock may occur. Having the opportunity to emit power by charging a borehole may therefore be a solution to the problem. Even though it may not be meaningful to inject solar heat into the ground with only on borehole in the system, it may be beneficial in order to prevent problems with solar collectors overheating.

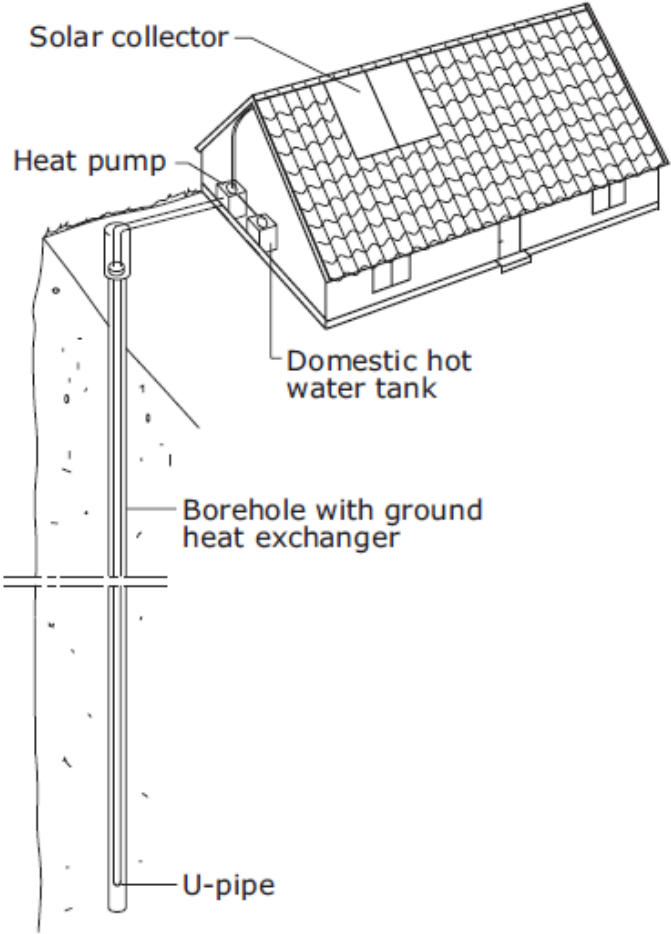


Figure 9 - Single-family dwelling with solar thermal collectors and ground-source heat pump (Kjellsson, 2009).

## 5 POSSIBILITIES WITH SOLAR COLLECTORS IN COMBINATION WITH GROUND-SOURCE HEAT PUMP

The demand for solar heating systems which combine domestic hot water production and space heating is rapidly growing in several countries in Europe. This kind of system is referred to as a combi-system, and the energy sources are solar energy combined with auxiliary energy sources such as biomass, electricity, oil, gas or heat pumps. In 2001 the share of solar combi-systems in Sweden was significantly larger than the share of solar heating systems installed for only DHW production. In Norway and Denmark, the share of solar combi-systems and the share of solar domestic hot water systems were almost the same (Weiss, 2003). Figure 10 shows the annual installed capacity of flat plate and evacuated tube collectors in Europe from 2000 to 2011.

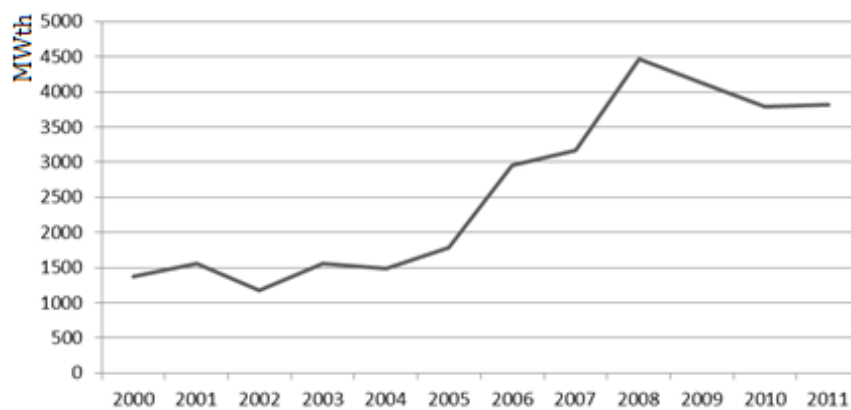


Figure 10 - Annual installed capacity of solar collectors in Europe 2000-2011 [MWth/a]

At the end of 2011 a total solar collector area (both flat plate and evacuated tube collectors) of 18 840 m<sup>2</sup> with a total capacity of 10.8 MWth was installed in Norway (Mauthner & Weiss, 2013).

Ground-source heat pumps are one of the fastest growing installations of renewable energy in the world. An annual increase of 10 % in about 30 countries was recorded from 1995 to 2005 (Curtis, et al., 2005). In Norway there exists approximately 15 000 GSHP systems which extracts 1.5 TWh from the ground. Compared to Sweden, which is a leading country using GSHP and has approximately 200 000 GSHP systems installed, this is a relatively small number. However, Norway is up and coming, which is illustrated in Figure 11.

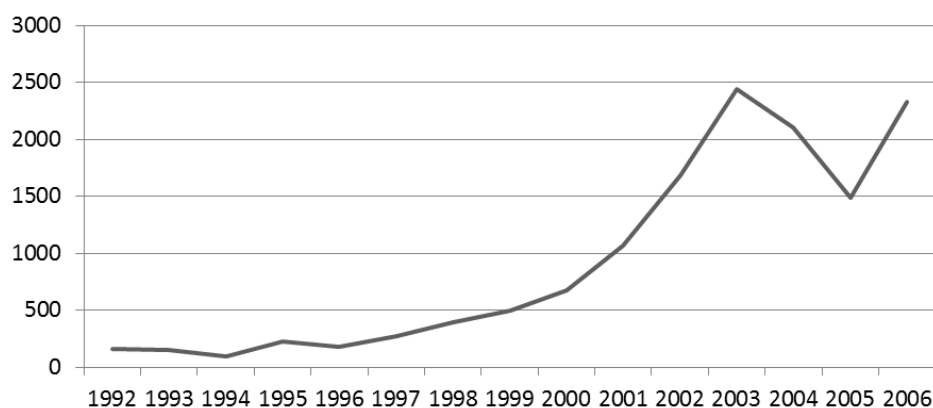


Figure 11 - Number of sold brine/water heat pumps in Norway from 1992-2006 (Midttømme, et al., 2008).

Figure 10 and Figure 11 show that there is an increase in installation of solar collectors and ground-source heat pumps in Norway.

## 5.1 TECHNICAL ADVANTAGES

As the share of residential buildings with high insulation level increases, the thermal quality of the building envelope increases. With a high thermal quality of the building, the heat distribution system can be operated with lower temperatures. This allows for the integration of highly efficient heating devices operating at low temperatures such as heat pumps and solar combi-systems. The potential for utilizing solar thermal energy for space heating as well as domestic hot water preparation is highly relevant with the increasing installation of low temperature heat distribution systems, such as simple radiator and floor heating systems.

By combining heat pump and solar energy systems it is possible to alleviate many of the disadvantages which occur if the systems operate separately. If optimal design and control of the system is achieved, combining solar collectors with ground-source heat pumps can result in new operational conditions which provide better efficiency, better use of renewable energy and minimize the energy costs. Combined with GSHP, solar collectors can produce useful energy at lower temperatures, which increases the solar system's efficiency due to decreased thermal losses and extended operational time as the lower levels of irradiation may be utilized (Kjellsson, 2009).

As seen in Figure 4, useful solar irradiation is present in Larvik during spring and autumn as well as summer. Even though the outlet temperature from the solar collectors is not as high as during the summer months, useful energy can be produced and used for space heating, especially when the dwelling is integrated with a low temperature heat distribution system. The solar energy system may be designed to deliver energy to a storage tank for space heating if the set point temperature for domestic hot water is reached. By contributing to a temperature rise in the water stored for space heating, a decrease in operation time for the heat pump may be achieved. During the day when the solar irradiation is intense, solar energy can be stored in the tank, and be utilized at the evening when the heating demand appears. If the solar collectors are capable of delivering enough energy to the space heating storage tank, the heat pump can be completely turned off. This gives the borehole a natural recovery and may give the heat pump a longer lifetime, as the number of starts and stops is reduced (Kjellsson, et al., 2009).

Compared to conventional solar heating systems where the solar energy is only utilized to produce domestic hot water and the collectors are turned off when the desired temperature in the storage tank is reached, this system solution promotes a longer operational time for the solar collectors when the excess heat can be used to recharge the boreholes or a swimming pool. As a result, the solar collectors achieve a better efficiency which has an economical benefit. In addition, during wintertime the solar radiation is limited and only low temperatures can be reached in the solar collectors. Even though these temperatures are useless for domestic hot water or space heating, the produced solar heat can be used to recharge the borehole. This may increase the borehole temperature and may provide the heat pump with better operational conditions, as earlier described (Kjellsson, et al., 2009).

## 5.2 ENVIRONMENTAL ADVANTAGES

The ground-source heat pump is not only recognized as a highly efficient component for delivery of renewable energy, but it also contributes to a reduction of CO<sub>2</sub> emission in association with heating and cooling of buildings. According to IEA Heat Pump Centre, approximately 6 % of the global CO<sub>2</sub> emissions are cut due to installation of the heat pump, which is one of the largest reductions a single technology can offer (Curtis, et al., 2005). Utilizing heat pumps with high COP value means that energy efficient systems provide a significant reduction in level of CO<sub>2</sub>, NO<sub>x</sub> and SO<sub>2</sub> emissions (Omer, 2006).

## 5.3 CHALLENGES

One of the main drawbacks with the combination of solar collectors and ground-source heat pump is that the solution represents a rather complex system, which results in difficulties of realizing optimal system design and operational control. With the increasing degree of complexity, the possibility of operational problems and failures in the system increases. In order for the system to work profitably the energy sources must complement each other, which requires a well-planned and well-designed control strategy.

Another aspect is the investment cost, which increases in line with the degree of complexity of the system. With a system like this, the investment costs are high, and the question is whether or not it would be beneficial for a single-family dwelling. The experience with a solar heating system combined with ground-source heat pumps for single-family dwellings is limited in Norway, and there is little to no information about whether a solution like this would be profitable or not. Designing a system similar to this, which provides several single-family dwellings, apartment buildings or non-residential buildings with energy, is more likely to be beneficial due to the enlarged energy demand. The investment costs might not be as high compared to the cost of the saved energy.

Another drawback is the operational cost of the circulation pumps. Circulation pumps are needed in the solar collector subsystem, the ground-source heat pump subsystem and in the space heating system. Due to longer operational time for the solar collectors, the operational time for the circulation pumps is extended as well, causing an increase in cost. Conventional circulation pumps used in the solar collector circuit and in the ground-source circuit are relatively cheap and have low efficiency, which indicates that the control of the pumps must be optimized. However, if new, highly efficient circulation pumps are used longer operational times can be accepted.

It should also be stated that if the borehole reaches too high temperatures, due to charging with excess solar heat, it will not fully function as a free cooling mechanism during the summer months. The heat pump must be used as a cooling machine instead, which will result in higher power consumption. Recharging of the borehole must always be evaluated based on the heating and cooling demand of the building.

## 6 COMPONENTS

A description of the different components in a combined ground-source heat pump and solar collector solution is given in this chapter. An exhaust air heat pump will also be discussed since it may be utilized as an auxiliary energy source for domestic hot water production, and heating of the supply air in the ventilation aggregate. A suggestion for how a system may be designed when combining solar thermal collectors with a ground-source heat pump can be seen in chapter 10.2 *Suggested "Multikomfort" System Design*.

### 6.1 SOLAR HEATING SYSTEM

For Nordic climates the solar thermal system is usually designed as an active closed loop system which includes solar collectors, circulation pump, heat exchangers and a storage tank. Due to the good freeze protection provided by a closed loop system, these systems are especially popular in areas subject to cold climates. Glycol-water mixtures are often used as solar collector fluid in order to protect the solar collector loop and the collector from freezing (Morrison, u.d.). The heat transfer fluid is pumped through the solar collectors and the heat exchange spiral and transfers thermal energy, which is absorbed in the collector, to the water in the storage tank.

#### 6.1.1 FLAT PLATE SOLAR COLLECTOR AND EVACUATED TUBE

For domestic hot water production or space heating, flat plate glazed solar collectors may be utilized. Glazed solar collectors are needed when high temperatures in the system are desired. Unglazed flat plate solar collectors are used when low-temperatures are required, e.g. for swimming pool heating.

In order to evaluate the collector performance, the collector efficiency, which refers to the ability of the collector to convert solar radiation to useful heat, can be calculated by using Equation 10 found in 10.2.3.1 *Solar Collectors*. The collector efficiency is expressed as the ratio between the useful output (solar-heated water) and the input (incident solar energy), and is expressed as a percentage between 0 and 100. Typical maximum values for factory-made collectors range from 50 to 90 %. Even though the collector is an important component, the overall performance of the system depends on the quality of all the components in the system (Laughton, 2010).

A conventional flat plate solar collector is constructed using an absorber containing pipes or passageways and a flat glazing. In the absorber, which is made of metal with high absorbance and low emittance, the solar energy is transferred to the solar collector fluid. The absorber is enclosed by a box covered with glass or plastic. To reduce thermal losses from the box, an insulation layer is inserted below the absorber and at the sides of the box. The lower the absorber temperature is, the lower the heat losses are and a more efficient operation of the collector is achieved. Illustrations of a flat plate solar collector with the main components can be seen in Figure 12.

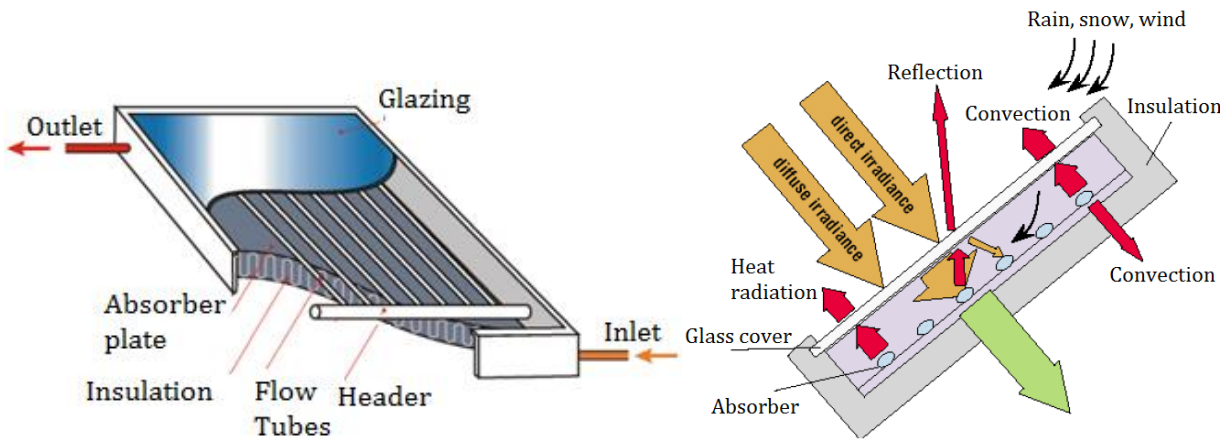


Figure 12 - Flat plate solar collector (Southface, 2013).

The flat plate solar collector is characterized by a high transmission cover, good contact between the heat removal fluid passageways and the absorber plate, and a weather-proof glazed cover. Compared to other solar collectors, the flat plate solar collector has the largest heat absorbing area, but it also has the highest heat loss. Due to the high heat losses the operating temperature is usually 80°C (Morrison, u.d.). The primary advantage of the flat plate solar collector is that it is able to collect both direct and diffuse solar irradiation, it is inexpensive to manufacture and can be integrated as a part of the roof construction, which makes it even more economically feasible.

In Norway, evacuated solar collectors are an alternative to flat plate solar collectors. Due to the vacuum enclosing the absorbing surface, convective heat loss is eliminated and the performance of the solar collector is higher than for flat plate solar collectors. The main disadvantage with the evacuated solar collector is the increased investment cost (Dokka, et al., 2009). In addition, the evacuated solar collectors cannot be mounted as an integrated part of the roof and is not as weather-proof as the flat plate collector. An illustration of the evacuated tube solar collector can be seen in Figure 13.

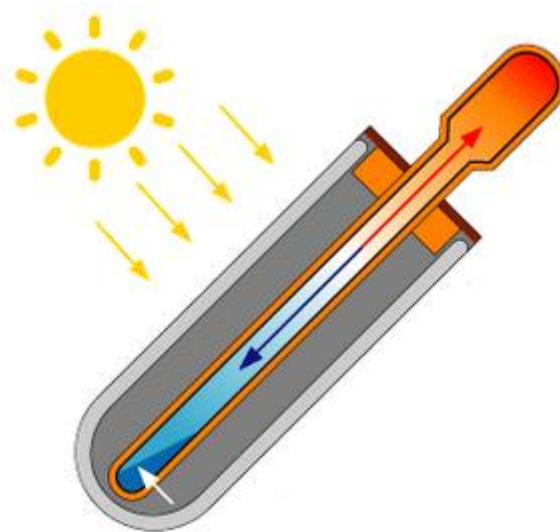


Figure 13 - Evacuated tube solar collector (NorthernLights, u.d.)



### 6.1.2 ECONOMY AND LIFETIME

A solar heating system is characterized by high investment costs, but low operational costs. By installing a solar heating system the energy which the solar heating system will produce through its lifetime is prepaid. The investment is economically beneficial if the cost of conventional energy, such as oil, electricity and gas, increases. Even though the price for electricity in Norway is low compared to the rest of Europe, predictions indicate that the prices will increase, making the solar heating system competitive compared to electricity. Due to the scarce experience with solar heating systems in Norway, presenting representative cost figures on such systems are difficult. Calculations performed by Enova show that the minimum price for a complete solar combi-system is approximately 100 000 NOK. The savings achieved by installing such a system may vary, but according to Enova the savings of a combi-system with 25 m<sup>2</sup> solar collectors located in Oslo would be 7 800 NOK/year. The calculation is based on an alternative energy price of 1 NOK/kWh (ENOVA, 2012). The economic lifetime for a solar heating system is estimated to 20 years (Rindal & Salvesen, 2008).

### 6.2 CIRCULATION PUMP

The circulation pump is the most vital component in the system. It is used to transfer the heat stored in the solar collector fluid to the heat storage, and is controlled by a regulator which starts the pump when the temperature in the solar collector reaches desired values. One of the main quality requirements is that the pump is able to handle many dense starts and stops.

Several circulation pumps are needed when solar thermal collectors are combined with a ground-source heat pump. In a system like this, solar energy may be utilized for space heating, domestic hot water production, recharging of boreholes or heating of a swimming pool. This means that the circulation pumps will have longer operating times compared to a system where the solar energy is only utilized to heat domestic hot water. Increased operating time of the circulation pumps results in increased electricity consumption. For new, highly efficient circulation pumps this disadvantage decreases and longer operating times for recharging can be accepted.

In order to reduce the energy consumption, the circulation pumps should have sequential operation. A study performed by Trilliat-Berdal et al. (2006) on a ground-source heat pump combined with thermal solar collectors system, showed that the system's COP in heating mode, when the circulation pumps were working at the same time as the heat pump, was maintained at an acceptable level. But when one of the pumps was working continuously the system's COP decreased with 20 %. Even though the circulation pump power may seem low compared to the compressor power, the choice of control system is essential to optimize the system's COP (Trilliat-Berdal, et al., 2006)

### 6.3 GROUND-SOURCE HEAT PUMP

A ground-source heat circuit is an indirect system which consists of a vertical or horizontal ground heat exchanger (GHE) and a ground-source heat pump. The ground-source heat exchanger, where the antifreeze coolant circulates, is submerged into the ground where it collects low temperature thermal energy. The antifreeze coolant circulates in the collector loop and through the evaporator in the heat pump. In the heat pump's refrigeration system, the antifreeze solution is chilled to a temperature below the ground-temperature, and is therefore able to absorb heat from the surrounding ground. In the heat pump evaporator the heat is

transferred to the working fluid, which boils to a low temperature vapor. In the compressor, the pressure and the temperature of the working fluid increases and heat is transferred to the heat distribution system. Exiting the condenser, the refrigerant holds a vapor-liquid-phase with high pressure but lower temperature. Passing through the expansion valve, the pressure and temperature decreases and the vapor is again in liquid-phase.

When compared to primary energy sources, the heat pump represents a more energy efficient technology for covering heating demand at moderate temperatures. If the heat pump is driven by electricity produced from hydropower, which is the case in Norway, it is able to reduce the energy consumption by 50-80 % relative to direct heating based on oil, gas or electricity (Stene, 1997). The ground-source heat pump covers approximately 50-70 % of the maximum power load of a single family dwelling, and 85-95 % of the annual energy demand (Kjellsson, 2009).

According to Esen et al. (2009) there are three potential advantages with the GSHP compared to the conventional air source heat pump. With a GSHP, the outdoor fan is replaced with a water-antifreeze solution-circulating pump and eliminates the outdoor coil frost and the defrost losses. Secondly, the antifreeze coolant is a superior heat transfer fluid compared to air, and third, the ground temperature is closer to the desired indoor temperature than the outside air during extreme heat or cold; see Figure 14 (Esen, et al., 2009). For each kWh of heating the GSHP can provide, approximately 0.22-0.35 kWh of electricity is required. Compared to the seasonal power consumption of air-to-air heat pumps, this represents a reduction of 30-50 % (Sanner, et al., 2003).

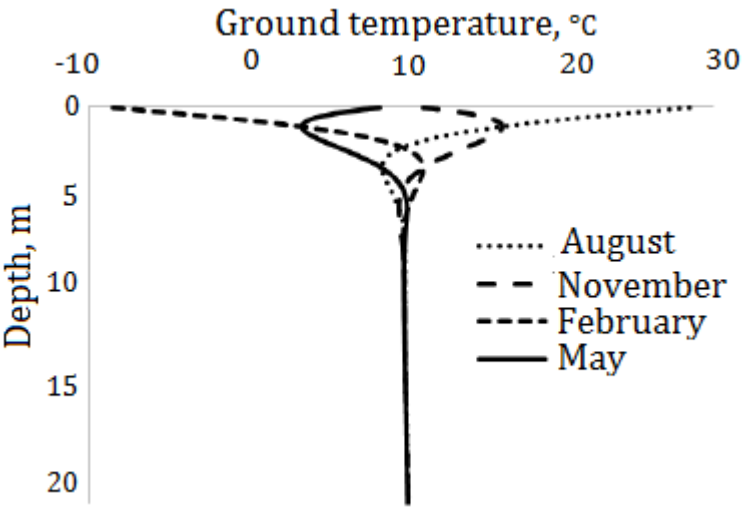


Figure 14 - Ground temperature in August, November, February and May

In order for the heat pump to work properly the heat distribution system must be sized and adjusted to the temperature level which is the basis for the design of the heat pump. A preferable solution is a floor heating system where the temperature of the circulated water does not exceed 35-40°C. A brine/water heat pump is best utilized with water temperatures up to 55°C. The higher the temperature of the supply water, the lower the COP of the heat pump (Sanner, et al., 2003).

### 6.3.1 BOREHOLE AND GROUND HEAT EXCHANGER

The conventional ground-source heat pump collects heat from boreholes, which typically range from 80-200 meters deep. For single-family dwellings one borehole is usually enough.

The heat extraction rate from vertical boreholes in Norway typically ranges from 20-60 W/m (Stene, 2004). When the depth is calculated, it is the active borehole depth that is calculated. The active borehole is characterized as the part of the borehole which is filled with material with acceptable thermal conductivity, such as water.

U-pipes, or so-called ground heat exchangers, are inserted into vertical boreholes. In Norway the ground-source system is generally designed as an indirect system where an antifreeze coolant is transported in the U-pipe and exchanges heat with the surrounding rock volume. The boreholes can either be designed with a single U-pipe or a double U-pipe. Double U-pipes are generally applied where cooling is desired. The U-pipe material should have good thermal conductivity, and the pipe should not be too thick in order to achieve acceptable heat transfer.

### 6.3.2 ECONOMY AND LIFETIME

The price is essential in the design of ground-source heat exchangers. For instance, the pipe material is often made of polyethylene (PEM), and using a single U-pipe is cheaper than a double. However, single U-pipes have the highest thermal resistance and are inoperable in deep boreholes due to the large pressure drop (Kjellsson, 2009).

There are primarily three geological aspects that influence the investment cost for the ground-source system:

- The thickness of sediment covered bedrock surface. If the share of sediments is relatively large, steel casings are needed to stabilize the ground. Inserting casings represents an uncertainty in the system cost and is up to 3-5 times more expensive than the borehole drilling (Ramstad, 2011). The sediment formation must also be taken into consideration in order to avoid operational problems due to a large portion of clay in the sediments (Prenøk, 2011).
- Temperature in the ground.
- Thermal conductivity in the ground. The thermal conductivity is related to the amount of quartz, which has a conductivity of 6 W/m·K. The thermal conductivity of the ground can vary between 2-4.5 W/m·K (NGU, 2008).

Typical costs for rigging up, drilling boreholes and installing ground heat exchangers in bedrock are approximately 150-250 NOK/m. A complete energy well with a 200 meter deep borehole costs 65 000-70 000 NOK, and with 50 meters of sediments the cost will increase with 25 000 NOK (Ramstad, 2011).

The advantages of installing ground-source heat pumps are that the boreholes can be drilled almost everywhere in Norway. They are reliable and the economic lifetime is at least 50 years for boreholes and heat exchanger. Additionally, the system provides stable temperatures through the year, which ensures power and energy savings. Minimal space is required for the system and the possibility of free cooling is present. The main disadvantage is the high investment cost.

The price of an installed ground-source heat pump for a single family dwelling varies from 100 000 NOK to 250 000 NOK, and the lifetime of the brine/water heat pump is usually 15-20 years (Oljefri.no, u.d.).

## 6.4 EXHAUST AIR HEAT PUMP

With the new building code demanding tighter building bodies, there has been a growing interest in using controlled ventilation systems with exhaust air heat pumps as heat recovery in the Nordic European countries (Sakellari & Lundqvist, 2004). The exhaust air heat pump utilizes the exhaust air in a balanced ventilation system as heat source, and is able to provide energy for domestic hot water production, supply air and space heating. The evaporator is located in the exhaust air duct and can be combined with a heat recovery unit. It is also possible to preheat the supply air with heat from vertical or horizontal GHE. By adding a supplementary heat source, such as GHE, the COP of the heat pump will increase (Stene, 2008).

In order to achieve good performance and an efficient heat pump, a factor of great importance is the availability of a cheap, dependable heat source for the evaporator. Installing a heat pump in the ventilation system, which utilizes the energy in the exhaust air to produce energy for domestic hot water production, will facilitate good working conditions. The temperature of the exhaust air is kept relatively constant through the year, which secures a dependable energy source for the evaporator. For instance, a heat pump has an easier time generating 60-70°C water if the ambient air is 24°C than if it is 1.7°C (Hepbasli & Kalinci, 2008). An illustration of the exhaust air working principle can be seen in Figure 15.

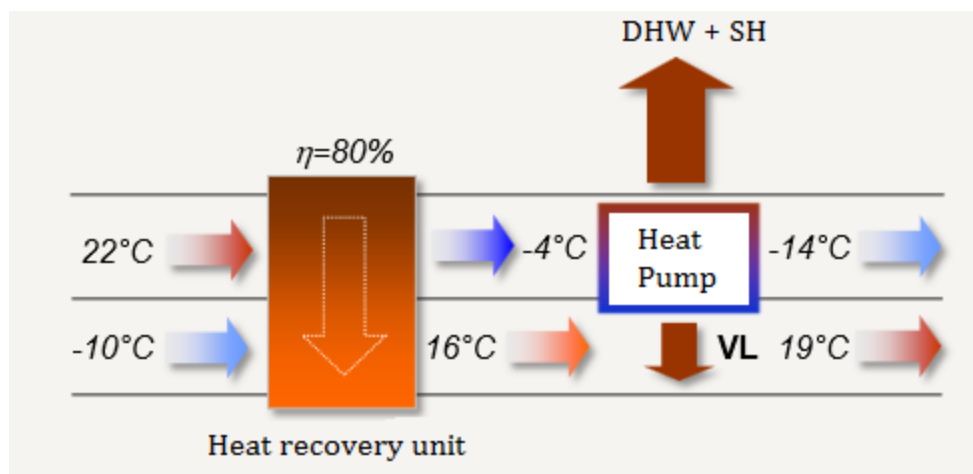


Figure 15 - Working principle of the exhaust air heat pump (Stene, 2008).

### 6.4.1 ECONOMY AND LIFETIME

An exhaust air/water heat pump has a long lifetime (15 years) due to high reliability and favorable operational conditions. The investment cost for an exhaust air/water heat pump is relative moderate and according to Enova, the cost of an efficient heat pump lies between 60 000 and 130 000 NOK (ENOVA, u.d.)

## 6.5 COMPACT VENTILATION AND HEATING DEVICE

Compact Ventilation and Heating Device (CVHD) is an aggregate well suited for application in passive house dwellings. The aggregate includes a highly effective heat recovery unit, one or two heat pump aggregates, a domestic hot water tank and electrical heating elements for peak load. It is possible to connect solar thermal collectors and vertical or horizontal ground-source heat exchangers to the CVHD. An illustration of the use of the aggregate can be seen in Figure 16.

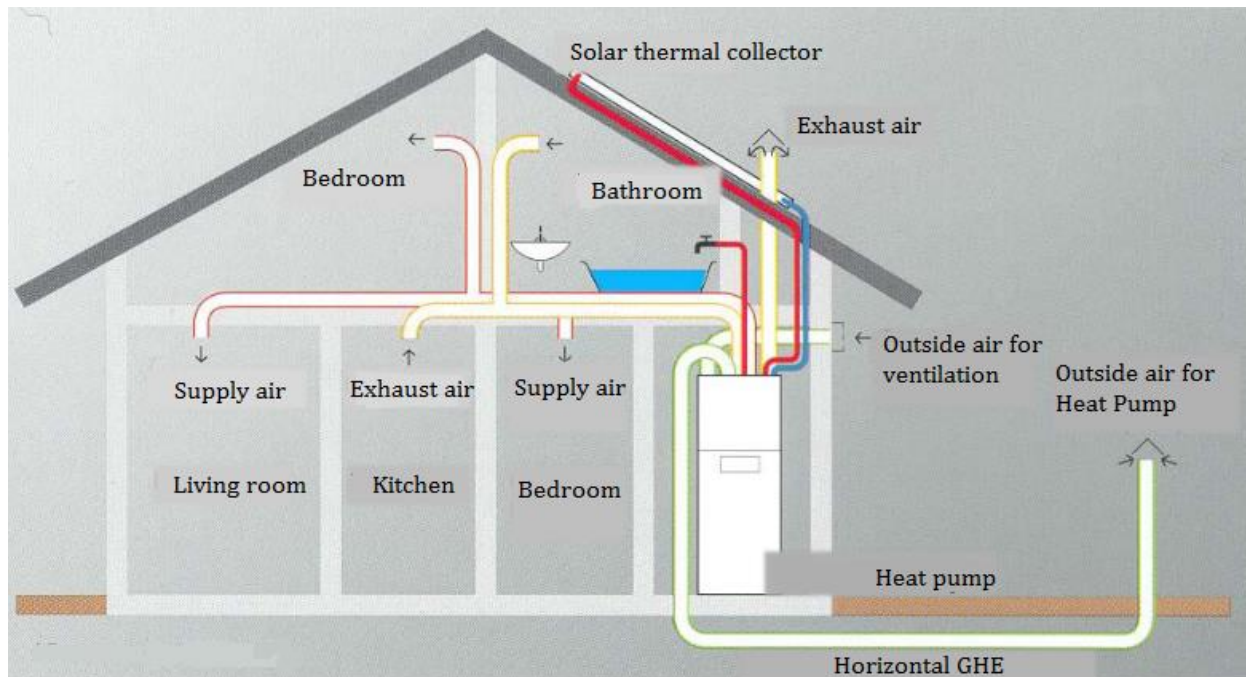


Figure 16 - Compact Ventilation and Heating Device for Passive House dwelling (Stene, 2013).

An example of a CVHD aggregate is the Compact P module produced by Nilan (NILAN, u.d.). Compact P represents a ventilation and heat pump solution developed to reach the requirements for future dwellings of low energy or passive house standard, and is certified by the Passive House Institute. Since Compact P is a modular component it provides several solutions and is able to deliver ventilation with active and passive heat recovery, comfort heat, comfort cooling, production of domestic hot water and space heating. The Compact P can be seen in Figure 17.

The heat exchange unit in the ventilation system in Compact P is a highly efficient recuperative counter-flow heat recovery unit. The high efficiency is achieved due to the close-end temperature differences, which are reached when using both high heat transfer coefficients and counter-flow arrangement. Heat is transferred from the exhaust air to the supply air by the plate exchange surfaces. Due to large surface areas, high heat transfer between the air flows is obtainable. The counter-flow heat recovery unit in Compact P is able to achieve a temperature efficiency of 85 % (NILAN, 2013). When using a counter-flow heat recovery unit in a cold climate, ice formation on the extract side can occur if the temperature on the plates is below 0°C. A defrosting procedure is therefore necessary. Problems due to condensation may also occur, and it is therefore important with a sufficient design of the unit in order to avoid extra pumps or valves. To collect the condensation, a drain should be placed at the bottom and the airflows should stream vertically. By letting the inlet air flow from the bottom to the top of the exchanger,

higher efficiency is possible (Kragh, et al., 2006). The Compact P module is equipped with a 100 % by-pass valve and a defrosting procedure to deal with these problems.

Compact P is designed to deliver a maximum airflow of 325 m<sup>3</sup>/h, and has a hot water storage tank which holds 180 liters for domestic hot water use. Solar collectors can be connected to the hot water tank through a spiral heat exchanger. For space heating, an air or ground-source heat pump can be added. A reverse heat pump is included in order to utilize the energy in the extract air.

According to Per-Erik Hansen, representative for NILAN Norway, the price for an aggregate including the ground-source heat pump would be approximately 117 000 NOK. The cost may however vary, and the cost for drilling and installation of ground-source heat exchangers and the cost for the solar thermal collectors are not included (Hansen, 2013).



Figure 17 - Compact P by NILAN (NILAN, u.d.).

## 7 RECOMMENDED DESIGN AND OPERATION OF SOLAR HEATING SYSTEM AND GROUND-SOURCE HEAT PUMP

This chapter describes recommended values for the main design and operating parameters in a solar combi-system coupled with a ground-source heat pump. The recommended values are mainly based on rules of thumb and should be regarded as general guidelines for obtaining an energy efficient system. Guidelines regarding the dimensioning of pipelines and pumps are not included.

### 7.1 SOLAR THERMAL COLLECTORS

#### 7.1.1 OPTIMUM SOLAR COLLECTOR TILT ANGLE AND ORIENTATION

The solar collector's performance is highly influenced by the solar collector tilt angle and the orientation. Both the tilt angle and the collector orientation are regarded as two of the most important parameters when planning and installing a solar heating system.

For residential buildings, solar heating systems generally consist of flat plate solar collectors which are able to collect both the direct and diffuse components of radiation. A fixed installation is the most typical installation due to its robustness, but in order to maximize the amount of collected solar heat, finding the optimum tilt angle and orientation is crucial. The flat plate collector is not able to track the sun, due to the fixed installation, and should therefore be orientated towards the equator when installed on the Nordic hemisphere. The sun has a maximum altitude at noon, and in order to absorb the largest rate of energy at this hour, the flat plate collector should be orientated towards the south or at least within 30° of south (Kalogirou, 2004). To make sure that the collector's performance is maximized, it should be facing direct sun from 9 a.m. until 3 p.m. During these hours, the solar collector receives close to 80-90 % of the total solar irradiance available through the day (Ramlow & Nusz, 2006).

In order to maximize the density of absorbed energy, the solar collector must be tilted from the horizontal. With fixed installations the collector tilt angle must be adjusted to make sure that an acceptable yearly average amount of energy is collected. For central Europe regions with latitudes of 50°N, an optimal irradiance is achieved with an orientation between south-east and south-west combined with a collector tilt angle between 30° and 60° (DGS, 2005). The common practice is to tilt the solar collector according to latitude and adjust the angle with  $\pm 10^\circ$ - $15^\circ$ . For a solar heating system located in the south of Norway, this would correspond to an orientation towards south with a tilt angle ranging from 45° to 75°.

It is common to distinguish between optimal tilt angle and recommended tilt angle. The recommended tilt angle may differ from the optimal tilt angle due to practical reasons, or simply because more useful heat is collected with this angle compared to the optimal. If the weather is mostly cloudy during the winter where the solar collectors are installed, the tilt angle should be lowered since most of the solar heat collected is during summer when the sun's position is higher (Zijdemans, 2012). When solar collectors are installed in a cold climate they may be exposed to snow during winter. In order to utilize the winter sun and for the snow to drain off, the solar collectors should have a steeper tilt angle than the optimal tilt angle. Additionally, when the solar collector area is oversized, which is common for solar combi-systems, the risk of stagnation problems is present during summer, and a larger tilt angle would limit the incoming solar radiation on the collector surface and reduce the risk. With a solar combi-system, the

collectors should have a steeper tilt angle than the optimal in order to utilize more of the solar irradiation during the year (Zijdemans, 2012).

Figure 18 shows the monthly global solar irradiation for Larvik with collectors orientated towards the south and with tilt angles ranging from 0-90°, where 40° is considered to be the optimum tilt angle.

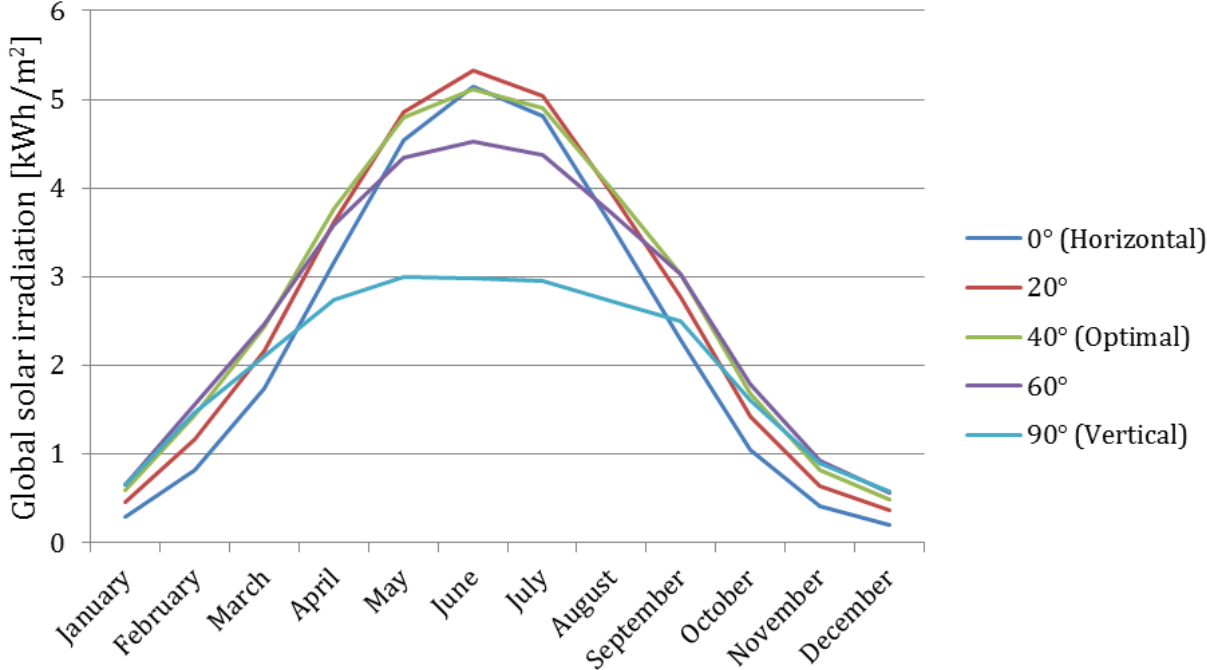


Figure 18 - Solar irradiation for Larvik through the year, south orientation (EC-JRC, 2014).

7.1.2 REQUIRED SOLAR COLLECTOR AREA

A solar heating system can be designed as a solar domestic hot water system only, or as a combi-system covering both domestic hot water and space heating demand. Designing a solar combi-system requires a larger solar collector area than a domestic hot water system. According to Zijdemans (2012), the required area can be calculated based on occupants living in the building or whether or not the building is a multi-family or single-family dwelling. Table 1 shows the required solar collector area for a single-family dwelling for both DHW preparation and combi-systems.

Table 1 - Required solar collector area for single-family dwellings (Zijdemans, 2012).

	Solar collector area	
	DHW Preparation	Combi-system
<b>Per person in a single-family dwelling</b>	1-2 m <sup>2</sup>	2-3 m <sup>2</sup>
<b>Per single-family dwelling</b>	4-6 m <sup>2</sup>	8 -12 m <sup>2</sup>

A solar collector area of 8-12 m<sup>2</sup> is recommended by Zijdemans (2012) for a single-family dwelling with a solar combi-system installed. According to Weiss (2003), on the other hand, a solar collector area ranging from 15-30 m<sup>2</sup> for a solar combi-system is recommended. This applies particularly for low solar regions where the annual horizontal irradiation is less than 950 kWh/m<sup>2</sup> and the latitude is above 50°N. Installing collector areas of this size will result in high solar fractions which are beneficial, but during the summer months when the solar



irradiation is high and the space heating demand is marginal, stagnation problems due to overheating may occur (Weiss, 2003). With too high temperatures in the solar circuit, malfunction of the system components and system leaks can occur. If an oversized solar collector area is used, it is important to make sure that adequate protection against high temperatures is available (Hausner & Fink, 2002). Allowing the solar collectors to be an integrated part of the façade is regarded as an advantageous heat protection initiative. If the solar collectors are mounted on the façade instead of on the roof with a tilt angle of 45°, the heating demand is met rather well during winter due to the low position of the sun. During the summer months the façade installation has an advantage since the irradiation is highly reduced, which results in reduced possibility for stagnation problems (Weiss, 2003).

The size of solar combi-systems may vary from one country to another, partly depending on the different conditions in the individually countries. In Sweden, Austria and Switzerland, where solar combi-systems constitutes a noteworthy share of the market, systems with solar collector areas ranging from 15-30 m<sup>2</sup> and storage tanks with 1-3 m<sup>3</sup> are installed in single-family dwellings. In countries where gas or electricity is primarily utilized as auxiliary energy, smaller systems are installed. The solar collector area may not be larger than 4-6 m<sup>2</sup> and the storage tank may hold a volume of 300 l (Weiss, 2003). Skarpnes in Arendal in southern Norway is characterized as Scandinavia's first housing estate of zero emission buildings. 17 single-family dwellings are planned, where the heating system is a combination of thermal solar collectors and ground-source heat pump. Solar heat will be utilized for both domestic hot water production and space heating. The idea is to install 9 m<sup>2</sup> of solar collectors on the façade of each dwelling. The choice of collector area corresponds with the recommendation by Zijdemans (2012), as seen in Table 1.

### 7.1.3 SOLAR HEAT TRANSFER FLUID

Due to a cold climate and the risk of frost, the solar heating systems in Norway cannot use water as heat transfer fluid, and a mixture of propylene glycol and water is commonly used today. Ethanol mixtures are not suitable for high temperature solar collectors, due to the risk of explosion (Kjellsson, 2009). Concentration and corresponding freezing point for propylene glycol-water mixture are shown in Table 2.

**Table 2 - Concentration and freezing point of propylene glycol**

<b>Propylene glycol</b>									
<b>Concentration (%)</b>	0	20	30	36	40	43	48	52	55
<b>Freezing point</b>	0	-7	-12	-18	-20	-23	-29	-34	-40

The recommended concentration of propylene glycol lies in the 40-50 % range (DGS, 2005). With a 40 % concentration the freezing point is -20°C and the boiling point is approximately 150°C or more. With a higher propylene glycol concentration in the heat transfer fluid, the specific heat capacity of the liquid decreases. It may therefore be desirable with a low concentration in order to maximize the heat transferred, as long as the freezing point is adequate according to the respective climate.

#### 7.1.4 SOLAR COLLECTOR MASS FLOW RATE

The solar collector mass flow rate depends on the installed solar collector area and the choice of storage tank. There are mainly two types of storage tanks: the low-flow mantle tank and the high-flow spiral tank, as seen in Figure 19.

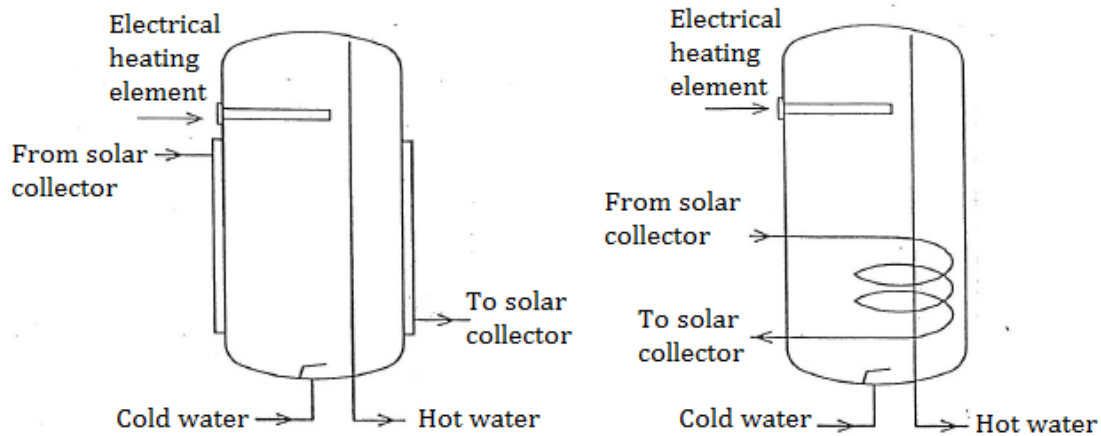


Figure 19 - Mantle and spiral tank (Furbo, 2004)

The spiral tank represents the more traditional high-flow solar heating system where a spiral heat exchanger is integrated in the storage tank. The recommended mass flow rate in a high-flow system lies between 0.013-0.019 kg/s·m<sup>2</sup> solar collector area, and the temperature rise in the collector is of the order 10-20°C. It is important that the mass flow rate circulating through the solar collectors is large enough to cool the collectors sufficiently, but if too large mass flows are utilized, adequate fluid temperatures may not be generated (DGS, 2005). With a high-flow system, it is recommended that the integrated solar heat exchanger inlet to the storage tank is located near the bottom. The store water can then be heated slowly from bottom to the top. If too low flow rates are used, the integrated solar heat exchanger may have difficulties with fully utilizing the high temperatures generated in the collectors. As a consequence, lower temperatures occur in the tank since the water in the store is mixed rapidly (Weiss, 2003).

Low mass flow rates are commonly used in the mantle storage tanks, where the solar collector fluid is slowly pumped through the mantle from top to bottom. Typical flow rates lie between 0.0016-0.0033 kg/s·m<sup>2</sup> solar collector area, and the temperature rise in the solar collector is approximately 40-50°C. Laboratory tests conducted by Furbo (2004) showed that the thermal performance of a mantle tank system with a small volume flow rate is greater than that of a spiral tank system (Furbo, 2004). The study also revealed that a system with low volume flow rate has a higher thermal performance, since thermal stratification in the storage tank is easier achieved. With a good thermal stratification, the inlet temperature to the solar collector is highly reduced, which results in better thermal performance of the solar collectors. Even after a short time of sunshine, adequate temperatures are reached at the top of the tank and the electrical heating element can be turned off.

#### 7.1.5 SOLAR COLLECTOR HEAT LOSS AND ABSORBER PLATE

The absorber plate is the most central component of any solar collector, as the thermal performance of the collector depends on the optical and thermal properties as well as the design of the absorber. The absorber receives solar irradiation and converts it into useful thermal

energy, see Figure 12. Better system performance may be achieved if a good heat transfer from the plate to the fluid is ensured. Materials with high thermal conductivity are usually chosen for the absorber plate, and steel, aluminum and copper are commonly used. A study performed by Shariah et al. (1999) was conducted in order to reveal the better absorber plate material. The study showed that by changing the absorber plate material from steel to aluminum the collector efficiency factor improved by 12-19 % and the annual solar fraction improved by 4-7 %. Replacing the aluminum with copper improved the collector efficiency by 3 % and the annual solar fraction by 1 %. It was concluded that there was no benefit from choosing copper instead of aluminum as absorber plate material (Shariah, et al., 1999).

Due to the reflection of metal surfaces, the absorber plate must be provided with a coating with high absorption and greatly reduced emittance to decrease thermal losses. To achieve optimum thermal performance, a selective coating is usually chosen. Commonly used selective coatings consist of black chrome or black nickel (DGS, 2005). The selective coating is able to separate high light radiation absorption and low heat radiation loss, and the absorption coefficient may be as high as 0.95, while the emission coefficient ranges from 0.05 to 0.2 (Furbo, 2013).

The solar collector efficiency can be improved by choosing a better absorber coating and by minimizing the heat loss from the collector. All flat plate solar collectors are provided with thermally insulated edges and backs in order to reduce heat losses to the environment. The heat loss is primarily caused by convection and radiative heat transfer through the flat plate cover, which is a function of the ambient temperature and the sky temperature. Typical values of the back and edge heat loss is 0.3-0.6 W/m<sup>2</sup> and 1.5-2.0 W/m<sup>2</sup> respectively (Morrison, u.d.). The solar collector heat loss coefficients,  $a_1$  and  $a_2$ , are given by the manufacturer of the solar collector, and common values are  $a_1 = 4.0 \pm 0.5 \text{ W/m}^2\cdot\text{K}$  and  $a_2 = 0.008 \pm 0.003 \text{ W/m}^2\cdot\text{K}^2$ .

#### 7.1.6 CONTROL

The main task of the solar heating control system is to control the circulation pumps in the solar circuit to harvest the sun's energy in the most optimum way. Two temperature sensors are needed in order to control the circulation pump: one located at the solar collector outlet, which measures the temperature at the hottest part of the circuit, and one located near the bottom of the storage tank, at height with the solar spiral heat exchanger outlet. The difference between the two measured temperatures is sent to a control unit, and the circulation pump is switched on when the switch-on temperature difference is reached. It is important that the switch-on temperature difference is high enough to overcome any heat loss in the pipes. By being aware of this, one ensures that the exchanged heat is higher than the power used by the pump (Laughton, 2010). If the pump is switched on too early, more power will be consumed than what could have been saved thermally. Standard settings for the switch-on temperature difference are 5-8 K depending on the length of the pipe from the collector to the storage tank. A longer distance requires a higher temperature difference (DGS, 2005).

Another temperature sensor can be positioned at the top of the tank, which allows for measurements of the draw-off temperature. For heat protection, an additional function to the temperature sensor located near the bottom of the tank can be established. When the maximum store temperature has been reached, the circulation pump can be turned off in order to prevent too high temperatures in the tank.

## 7.2 DESIGN OF THE STORAGE TANK

The storage tank is considered to be the most important component in a solar heating system, especially when taking the system's thermal performance and cost into account. With a well-designed storage tank the overall system performance can be increased significantly (Furbo, 2005). A good storage tank design is achieved by an optimal combination of tank operating and design parameters. Inlet fluid speed, temperature difference between inlet and outlet heat transfer fluid and climatic conditions, as well as the height/diameter ratio, wall thickness, insulation thickness and material, tank volume and pipe inlet and outlet locations are regarded as the parameters with highest influence (Dehghan & Barzegar, 2010).

Figure 20 shows the different zones of a storage tank in a solar combi-system. The necessary heat exchangers are not included in the illustration.

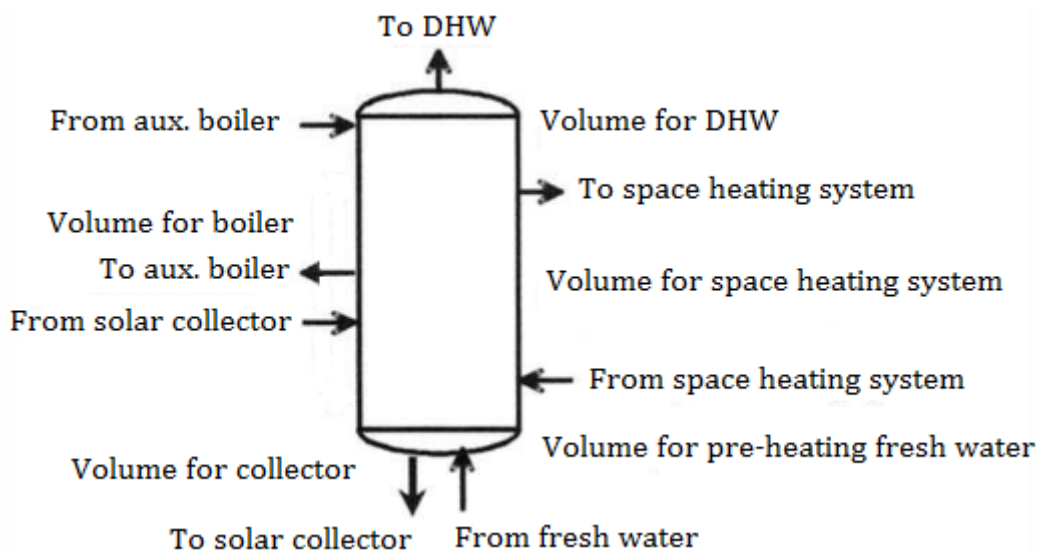


Figure 20 - Design of storage tank for a Solar Combi-system (Weiss, 2003)

When connected to a solar loop it is important that a strong thermal stratification is reached in the tank during both storage and discharge periods. Thermal stratification is a phenomenon which provides the storage tank with different temperature zones. Hot water has lower density than colder water, and due to the buoyance forces, hotter water finds it way above the layers of cold water. In this way, adequate temperatures for domestic hot water use is reached at the top of the tank, and water with lower temperatures are found at the bottom. With a strong thermal stratification, low fluid temperatures are transferred back to the solar collector and ensure high collector efficiency as more solar heat can be collected. As a result, good system performance is achieved even at periods with lower solar irradiation. According to Furbo (2004), the thermal performance of a solar heating system with a fully mixed hot water tank is close to 2-3 times lower than the performance of a solar heating system with a good thermal stratified storage tank (Furbo, 2004).

As seen in Figure 20, the solar collector spiral is integrated near the bottom of the storage tank where the water is colder. Investigations indicate that when high volume flow rates are used in the solar loop, the solar heat exchanger should not be higher than  $2/3$  of the solar tank volume, which is the total tank volume minus the auxiliary volume (Furbo, 2004). Covering 100 % of the domestic hot water demand with solar energy is not possible and an additional energy source is

needed. As illustrated in Figure 20, the auxiliary energy supply system should be located at the top of the tank to heat the top water to the desirable temperature. In this way hot water can be tapped in periods without sunshine. To ensure that adequate amounts of water can be tapped from the tank, it is important that the water volume heated by the auxiliary energy is large enough. In the Danish market an auxiliary volume of 60 l to 100 l is recommended for single-family systems (Furbo, 2005). If several heat sources are utilized in a solar storage tank, it is important to ensure that the solar volume is unaffected by the other heat sources. The solar volume should be maintained colder than the upper parts of the tank in order to ensure low inlet temperature to the solar collector (Laughton, 2010).

Degradation of the thermal stratification in the tank can be caused by several factors. The main contributors are forced convection flow through the tank, heat loss to the surroundings, thermal mixing at the inlet, natural convection flow induced by conduction within the tank walls and heat diffusion inside the tank due to vertical temperature gradient within the tank (Dehghan & Barzegar, 2010). With a good tank design the effect of these factors is reduced.

### 7.2.1 STORAGE TANK HEAT LOSS

The heat loss from the tank is caused by transmission loss from the tank to the ambient and by thermal bridges in the insulation. Location of the thermal bridges and the auxiliary equipment is of great importance to the magnitude of the heat loss from the tank. There is a considerable difference between thermal bridges located at the bottom of the tank and thermal bridges located at the top of the tank. Due to natural convection, cold water will accumulate at the bottom of the tank while hot water will rise towards the top of the tank. With a thermal bridge at the bottom of the tank, the water will be cooled relatively quickly and form an insulation layer above the thermal bridge, resulting in minimum heat loss. If the thermal bridge is located at the top of the tank, the thermal bridge will stay warm as the water cooled by the thermal bridge will be replaced by warmer water. The temperature of the thermal bridge will, as a consequence of this, stay warm and the heat loss becomes large (Furbo, 2005). Being aware of where pipe connections are made is therefore very important in order to reduce the heat loss from the tank. Pipe connections should be made at the bottom of the tank, and pipes should be carried downwards from the top. Internal circulation in the pipe, which can cause additional heat loss, is thus avoided. The domestic hot water should be drawn off through a plastic pipe which runs from the top of the tank through the bottom.

The storage tank heat loss is expressed as the product of the thermal heat loss coefficient and the temperature difference between the tank and the surroundings. The heat loss coefficient per height unit from the sides of the tank is expressed by Equation 5.

$$UA_s = \frac{\pi}{\frac{1}{2 \cdot \lambda} \ln \frac{d_i + 2e_s}{d_i} + \frac{0.13}{d_i + 2e_s}} \left[ \frac{W}{mK} \right] \quad (5)$$

where,

$\lambda$  is the thermal conductivity of the insulation material (W/m·K)

$e_s$  is the insulation thickness for the side (m)

$d_i$  is the inner diameter (m)

0.13 m<sup>2</sup>·K/W is the size of the surface resistance at the insulation surface. This is a normally used size of the surface resistance at interior surfaces in buildings (Furbo, 2005).

The heat loss coefficient from the top and the bottom of the tank are expressed by Equation 6 and Equation 7. These heat loss coefficients are difficult to calculate since the heat flow conditions in the insulation are complicated. However, Equation 6 and 7 should give adequate values.

$$UA_t = \frac{\frac{\pi}{4}(d_i + e_s)^2}{\frac{e_t}{\lambda} + 0.13} \left[ \frac{W}{K} \right] \quad (6)$$

where,

$e_t$  is the insulation thickness for the top (m)

$$UA_t = \frac{\frac{\pi}{4}(d_i + e_s)^2}{\frac{e_b}{\lambda} + 0.13} \left[ \frac{W}{K} \right] \quad (7)$$

where,

$e_b$  is the insulation thickness for the bottom (m)

The storage tank insulation is generally made of PUR foam or mineral wool with thermal conductivity of 0.037 or 0.045 W/m·K respectively (Furbo, 2005). A commonly used insulation thickness is 5 cm for top, bottom and sides. However, a thicker insulation layer at the top of the tank may be beneficial in order to reduce the tank heat loss.

### 7.2.2 STORAGE TANK VOLUME AND HEIGHT/DIAMETER RATIO

A study by Furbo (2004) was conducted in order to find the best tank design in a solar combi-system for a single-family dwelling. The study showed that the system's net utilized solar energy increased as the volume of the storage tank increased, and revealed an increase in thermal performance by 10-15 % just by increasing the tank volume from 200 l to 300 l. By reducing the tank volume from 200 l to 160 l, on the other hand, the thermal performance was decreased by 11 % (Furbo, 2004). With too small storage tanks in the system, the solar collectors will not be utilized to the fullest and the system performance deteriorates. Increasing the tank volume, on the other hand, decreases the inlet temperature to the solar collector and as a result, the collector efficiency is improved. However, an increase in tank volume increases the tank surface area and accordingly the heat loss to the surroundings. As a consequence, the storage efficiency is reduced. A storage tank volume 1-2 times the daily hot water consumption is recommended for a solar DHW system, while a volume of 400-750 l is recommended for a one store solar combi-system (Zijdemans, 2012). In a solar twin store combi-system the solar circuit charges two tanks: one storage tank for domestic hot water production and one buffer tank for space heating. The store volume for the DHW tank should be 1-2 times the daily hot water consumption, and for a family of four this gives a store volume from 100 l-300 l. The recommended volume for the buffer store for space heating is 100-200 l per kW of heat load (DGS, 2005).

A slim and tall storage tank is crucial in order to achieve good thermal stratification in the tank. The recommended height/diameter-ratio (h/d-ratio) for high-flow spiral tanks is 2:1 or higher.

For low-flow mantle tanks it is recommended that the h/d-ratio is as high as practical possible (Furbo, 2004).

### 7.3 GROUND-SOURCE HEAT PUMP SYSTEM

#### 7.3.1 GROUND HEAT EXCHANGER LENGTH AND DIAMETER

The ground heat exchangers coupled with a ground-source heat pump can either be designed as vertical loops or horizontal loops sized to meet the heating load of the respective dwelling. An illustration of the horizontal and vertical ground heat exchangers is given in Figure 21.

Horizontal ground heat exchangers are regarded as a viable option for single-family dwellings, but due to a relatively large required area, vertical boreholes are often the preferred solution (Stene, 2004). As opposed to vertical loops, horizontal loops are submerged 60-150 cm into the soil where it collects heat. The composition of the ground and its thermal conductivity determines the amount of heat which can be extracted, and thus how energy efficient the ground-source heat pump becomes. Typical ground thermal conductivity varies from 2-4 W/m·K, where 2.5-3.5 W/m·K is most common (Ramstad, 2011).

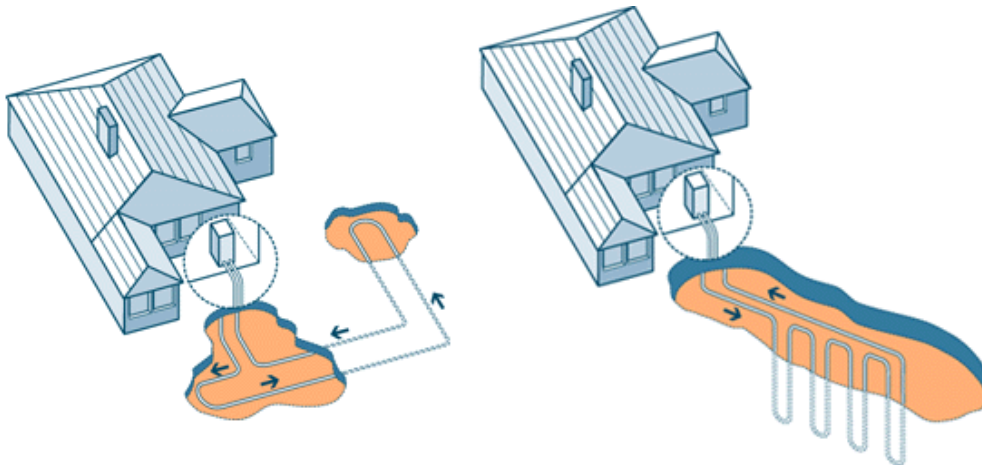


Figure 21 - Horizontal and vertical ground heat exchangers (Sintef, 2011)

Typical heat extraction rates from the ground, with either horizontal loops or vertical loops, are listed as “Rule of thumb” values in Table 3 (Sintef, 2011). Heat extraction rates of  $30 \pm 10$  W/m is normal for ground-source heating systems with vertical loops. (Ramstad, 2011).

Table 3 - Estimation of ground heat exchanger lengths

Estimation of ground heat exchanger lengths	
Horizontal loop	15-20 W/m
Vertical loop	20-60 W/m

Typical pipe diameters for horizontal and vertical loops are 32-40 mm, while the borehole diameter ranges from 130-160 mm. The ground heat exchangers are normally made of polyethylene (PEM) which has a thermal conductivity of 0.33-0.51 W/m<sup>2</sup>K, depending on whether low density or high density PEM is used. It is important that the pipe material has a good thermal conductivity and is able to provide the best heat transfer. The thickness of the tubes should be 2.0-3.7 mm (Kjellsson, 2009).

### 7.3.2 GROUND HEAT EXCHANGER FLUID

The heat transfer fluid in a closed ground-source heat exchanger loop is a mixture of an antifreeze medium and water, which tolerates temperatures down to at least  $-10^{\circ}\text{C}$ . To achieve a sufficient heat transfer from the ground, the fluid should have high specific heat capacity, high thermal conductivity, high density and low viscosity. Different ground heat exchanger fluids are listed in Table 4.

Table 4 - Thermodynamic data for different ground-source heat exchanger brines (Kjellsson, 2009).

Fluid	Freezing point ( $^{\circ}\text{C}$ )	Thermal conductivity ( $\text{W}/\text{m}\cdot\text{K}$ )	Specific heat capacity ( $\text{J}/\text{kg}\cdot\text{K}$ )	Density ( $\text{kg}/\text{m}^3$ )	Dynamic viscosity ( $\text{mPa}\cdot\text{s}$ )	Kinematic viscosity ( $\text{mm}^2/\text{s}$ )
<b>Propylene-glycol 25 % at <math>0^{\circ}\text{C}</math></b>	-10	0.450	3974	1026	5.51	5.37
<b>Propylene-glycol 25% at <math>40^{\circ}\text{C}</math></b>	-10	0.486	3991	1010	1.36	1.35
<b>Propylene-glycol 33% at <math>0^{\circ}\text{C}</math></b>	-15	0.416	3850	1035	8.17	7.90
<b>Propylene-glycol 33% at <math>40^{\circ}\text{C}</math></b>	-15	0.445	3899	1015	1.74	1.72
<b>Ethanol 24.4 % at <math>0^{\circ}\text{C}</math></b>	-15	0.426	4288	972	5.85	6.02
<b>Ethanol 30 % at <math>0^{\circ}\text{C}</math></b>	-20	0.399	4170	966	6.49	6.72
<b>VegoCool mixed at <math>0^{\circ}\text{C}</math></b>	-15	0.436	3320	1106	9.5	8.6
<b>VegoCool mixed at <math>40^{\circ}\text{C}</math></b>	-15	0.488	3510	1090	2.5	2.3

According to Kjellsson (2009), a 30 % mixture of ethanol and water is the recommended and most common brine liquid. Environmental aspects should be considered when choosing fluid for the ground-source heating system, since leakage of a toxic fluid into the ground is undesirable. VegoCool has been used as fluid for environmental reasons, but as seen in Table 4, it holds a lower specific heat capacity than the ethanol mixture (Kjellsson, 2009).

A commonly used mass flow rate in ground-source heat exchangers is  $0.5 \text{ kg/s}$  according to Wang (2007) and Eslami-nejad (2011) (Wang & Qi, 2007), (Eslami-nejad & Bernier, 2011).



### *7.3.3 CONTROL OF GROUND-SOURCE HEAT PUMP*

Due to the complex nature of solar heating systems coupled with a ground-source heat pump, controlling the system is rather difficult. The geothermal heat utilized by the ground-source heat pump is available all year, as opposed to solar energy which depends on the available solar irradiation. Using one control system for the solar collectors and one system for the ground-source heat pump may therefore be advantageous (Trillat-Berdal, et al., 2006). The ground-source heat pump may be controlled by the indoor air temperature and the outlet heat distribution system temperature, e.g. floor heating system. If the indoor air set point temperature is not met and if the heating system outlet temperature is below the set point temperature, the ground-source heat pump circuit is activated. If the measured temperatures exceed the set point temperatures, the heat pump is turned off.

## 8 RELEVANT SIMULATION TOOLS

This chapter provides a brief description of relevant simulation tools which can be utilized for detailed investigation of the performance of solar heating systems in combination with ground-source heat pumps.

### 8.1 IDA INDOOR CLIMATE AND ENERGY

IDA Indoor Climate and Energy is developed by the Swedish EQUA Simulations AB, and is defined as a transparent program where every underlying equation can be browsed and every variable can be logged (Equa, u.d.). The mathematical models are described in terms of equations in a formal language, NMF, which makes it easy to upgrade the program modules.

IDA ICE performs a whole-year detailed and dynamic multi-zone simulation, which enables analysis of the thermal indoor climate and the energy consumption of the entire building. Calculations of the full zone heat balance, which includes the impact of occupants, sun, equipment, lights, ventilation, heating and cooling devices, surface transmissions, air leakage and cold bridges, can be performed as well as wind and buoyancy driven airflows, surface heat fluxes, comfort indices, CO<sub>2</sub> levels and power levels of primary and secondary system components. In IDA ICE the building body can either be constructed or imported as a DWG-file or IFC-file. IFC-files contain information about materials and U-values, which are imported to the program. With IDA ICE, the entire building with its materials, internal loads, schedules, heat distribution systems, and energy sources as well as design of the heating system and ventilation system are constructed in one single program which enables the user to jump back and forth between tasks.

In IDA ICE a standard plant or an ESBO-plant (Early Stage Building-Optimization plant) can be chosen. The ESBO plant enables the opportunity to select between different renewable energy sources and then build the plant accordingly. The plant which then is built in ESBO is a predefined system designed by EQUA, and in order to change any of the settings good knowledge of the structure of the simulation program is needed.

### 8.2 TRNSYS

Another relevant simulation tool is TRNSYS (Transient System Simulation Tool). TRNSYS is defined as a flexible graphically based software environment used to simulate the behavior of transient systems. The development of the program started as early as in the 1970s by the Solar Energy Laboratory at the University of Wisconsin, USA, but has been developed continuously ever since. TRNSYS can be used to simulate traffic flows and biological processes, but the majority of the simulations are performed in order to assess the performance of thermal and electrical energy systems. It has a world-wide span of users, all from engineers, consultants, students to architects and is actively being used in applications such as building simulation, solar thermal processes, ground coupled heat transfer, geothermal heat pump systems, optimization, power plants and hydrogen fuel cell systems (TRNSYS, 2013). The simulation program is used by researchers to validate the performance of new energy concepts, such as solar combi-systems for instance, and for design and simulation of buildings and installations including control systems and occupant behavior.

According to Kjellsson (2009), one of the main advantages with TRNSYS is the open modular structure which provides flexible structure for different systems. Components are linked

together in order to solve a task, and are connected via inputs and outputs. For instance, a simple solar collector system consists of solar collectors, storage tank, auxiliary heat, a pump and several temperature sensors (Kjellsson, 2009).

TRNSYS consists of two parts, where the first part is an engine called the kernel. The kernel reads and processes the input files, solves the system iteratively, determines convergence and plots the system variables. Utilities that determine thermophysical properties, perform linear regression and interpolations are also found in the kernel. The other part of TRNSYS is the component library. Each component models the performance of one part of the system. TRNSYS is delivered with a standard library of 150 models ranging from pumps to cutting edge emerging technologies. It is however possible to extend and modify the existing components and create own if they are not found in the standard library. The flexibility enables the user to study the systems or the system components in detail. This requires good knowledge of both the program and the physics of the system, and may be perceived as time demanding since a large number of parameter values have to be handled with great care in order to prevent errors according to Kjellsson (2009).

As with IDA ICE, TRNSYS is capable of simulating whole year energy flows, heat losses, transmission losses, ventilation, domestic hot water demand and heating/cooling demand.

### 8.3 POLYSUN

The simulation program Polysun is developed and distributed by the company Vela Solaris, and offers support with the design, analysis and calculation of installations in the field of renewable energy, such as solar thermal, geothermal, photovoltaics or combi-systems. Polysun Simulation Software is available in two user levels: professional and designer. The professional level is very user-friendly and is intended for sales persons. The designer level on the other hand, provides flexibility for design of renewable energy systems, exact modeling of hydraulics, templates for large-scale systems, process heat and district heating. This level is more advanced and is intended for system designers, energy consultants and engineers (Solaris, 2013).

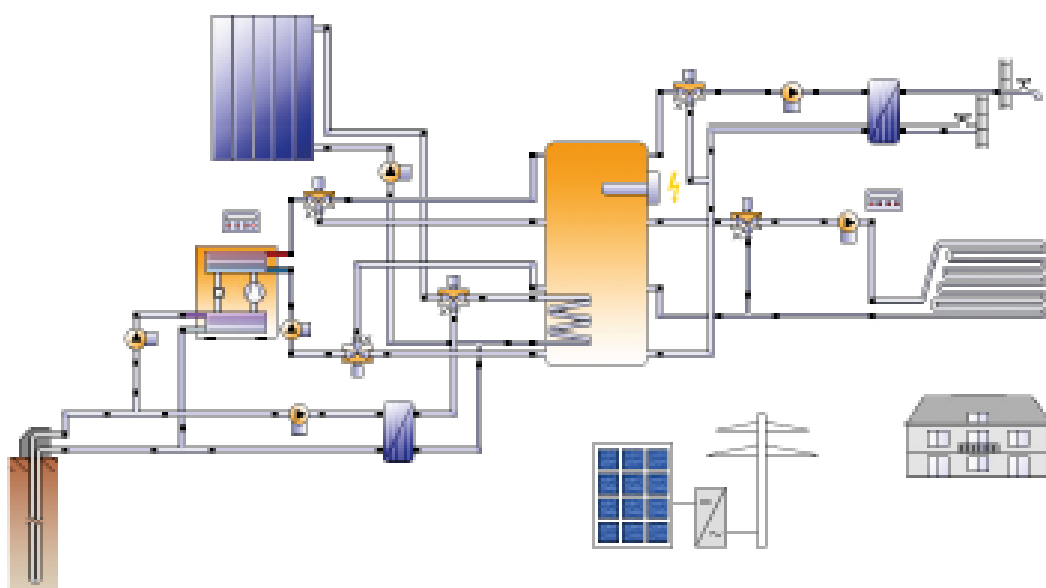


Figure 22 - Polysun Simulation Software

When a “project” is defined in Polysun the location and consumer behavior is set according to the system which will be analyzed. A “variant” defines all the components and connections in a given solar energy system. It is possible to create a new variant and simulate different variants individually and visualize and compare the results. A series of pre-defined “templates” are also available in Polysun. The templates define a solar energy system in the same way as the variants. If a template is included in the project as a variant it can be modified and simulated. The Polysun Designer enables the user to create new hydraulic schemes (Solaris, 2007). An example of a Polysun scheme is seen in Figure 22.

Unlike IDA ICE, Polysun is not able to provide detailed simulation results on indoor climate and comfort indices, but offers detailed results on the energy system performance. The simulation program also offers advanced control systems which controls temperatures, flow rates, irradiance, heating, reheating and mixing. Polysun provides results such as energy to the system or energy withdrawn from the system, energy to tank and energy withdrawn from the tank, end energy, solar energy, energy consumption and demand, auxiliary energy, energy in ventilation of building and energy transmission in building. The only modeling of the building is however definition of domestic hot water consumption and external walls based on a building catalogue.

All components available in the program, such as pumps, heat exchangers and solar collectors etc. are listed in a component library. All the available solar collectors are solar collectors which are tested by the recognized SPF Institut für Solartechnik. It is however possible to define own components and add them to the library. The program is relative easy to use, and if for instance defined set point temperatures in system are not reached, error messages occur.

#### 8.4 ENERGYPLUS

EnergyPlus is a whole building energy simulation program from 1996, which is developed by the U.S. Department of Energy. The simulation program is written in Fortran 90 and represents a flexible thermal load simulation program used by engineers, architects and researchers to model and optimize energy and water use in buildings. It is possible to model heating, cooling, lighting, ventilation, energy flows and water use with the simulation program. The building with its physical make-up and mechanical systems is designed by the user. EnergyPlus is used to calculate the necessary heating and cooling loads in order to maintain a comfortable indoor climate and the energy consumption of primary plant equipment.

EnergyPlus uses an integrated solution technique which allows the user to evaluate processes such as realistic system controls, moisture adsorption and desorption in building elements, radiant heating and cooling systems and interzone air flow. The program consists of three basic components - a simulation manager which controls the entire simulation process, a heat and mass balance simulation module, and a building systems simulation module. The building system simulation manager controls interaction and data exchange between EnergyPlus and SPARK and TRNSYS simulations (Crawley, et al., 2001).

With EnergyPlus the user is able to perform both simple and advanced simulations and analysis on individual components, single zones, thermal comfort and daylight, and is able to match the simulation with the actual system configurations. Several additional programs can be used in cooperation with EnergyPlus in order to simplify the designing process of the model. It is however possible to use an integrated text editor to design the model, but this will in some cases make the procedure disorganized. Relatively large input data are needed before a simulation can

be performed in EnergyPlus. This makes it difficult to perform a stepwise detection of potential problems along the designing phase, and the model must be relatively complete before possible problems can be solved.

## 9 METHOD

In order to gain knowledge concerning the combination of solar thermal collectors and ground-source heat pumps, relevant information regarding the system concept has been collected. Information regarding components, system advantages and possibilities, but also challenges has been gathered from relevant literature and earlier studies. In order to optimize the system, recommended values for the components main design and operating parameters has been collected and evaluated as well.

A suggestion for the system design was provided by Brødrene Dahl. In order to investigate the system's electricity use and how this can be optimized, a building simulation tool was utilized. It was predefined that the dynamic simulation tool IDA ICE would be used. As shown earlier, several dynamic simulation tools are available for solving this kind of problem, but IDA ICE is a user friendly tool which allows for detailed analysis of the indoor climate and energy demand of the entire building. With the possibility of using the ESBO-plant, which enables the opportunity to choose the relevant energy sources, IDA ICE appears to be a good choice.

The building model was created in IDA ICE 4.6 including the dwelling geometry and the combination of solar thermal collectors and ground-source heat pump. Relevant input for ventilation system, constructions, internal loads and domestic hot water demand was set in accordance with NS 3700 – *Criteria for passive houses and low energy buildings – Residential buildings*, where the criteria for passive houses were used. Simplifications were made on the interior of the dwelling and possible shadows surrounding the dwelling were not accounted for. The system design suggested by Brødrene Dahl was created in IDA ICE plant model. Due to limitations in IDA ICE, a simplified model of the system was designed. In order to optimize the system, a parametric study was performed. Both design and operating parameters were analyzed and optimized with the aim of finding the best system solution with the lowest electricity use. In the parametric study one parameter was changed at a time and a simulation was performed for each change in order to evaluate the effect on the system performance. The parameters with the greatest effect on the system's performance were combined in different scenarios, and a sensitivity analysis was performed on the best scenario in order to investigate how the result would be influenced by variations in input parameters. Two of the optimized scenarios were evaluated with two different sizes of solar collector area.

The evaluation includes analyses of the performance of the two scenarios with the specific heating demand, delivered energy and amount of utilized renewable energy.

## 10 DESCRIPTION OF THE “MULTIKOMFORT HUS”

The single-family dwelling investigated in this study is a demonstration building called “Multikomfort” dwelling designed by Snøhetta. Currently the dwelling is a preliminary project, and will be constructed in Larvik in Norway, close to Ringdalskogen. The project is a cooperation between multiple partakers, but the main contributors are Brødrene Dahl and The Research Centre on Zero Emission Buildings. The single-family dwelling is designed to accommodate a family of 4-5 members with related outdoor area, and is designed to function as a demonstration building which contradicts the prejudices towards passive houses.

A model of the building can be seen in Figure 23.

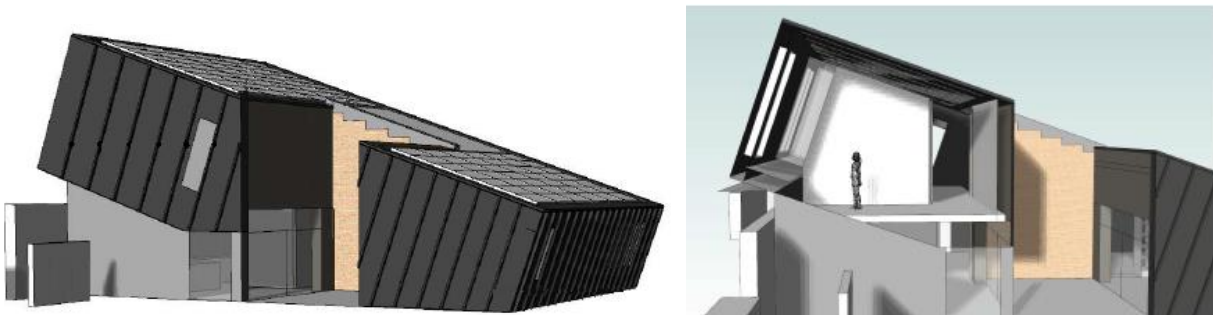


Figure 23 - "Multikomfort Hus" single-family dwelling

The objective is to create a new generation of modern and energy efficient family homes. The “Multikomfort” name is derived from its many qualifications and requirements of better energy use, tighter building envelope, comfortable indoor climate, sufficient daylight and acoustics. It is desired to design a single-family dwelling according to the Zero Emission Building definition, with the ambition level ZEB-O&M (Operation and Material), which is the second highest ambition level. The ambition level indicates that there should be zero emissions from the operation of the building and from the materials the dwelling is constructed from. In order to achieve a zero emission building, the technical solutions must be energy effective and energy saving initiatives must be implemented. The dwelling will obtain a demand and supply net balance due to the integrated PV modules installed on the roof top which will generate electricity to the grid. Achieving a plus-house that generates excess-electricity which can be used to provide an electric car with power is desirable.

The minimum requirements on energy efficiency, which will be utilized when designing the model, are stated in the standard describing the requirements for passive houses and low energy buildings, NS 3700:2013.

### 10.1 BUILDING MODEL

The concept building is a two story high family home with a floor area of 202 m<sup>2</sup>. The ground floor consists of an entrance, bathroom, media room, office, living room and kitchen. The first floor accommodates a bathroom, hall and three bedrooms. Between the kitchen and the living room is an outside atrium as seen in Figure 25. The roof has a slope of 19°, and is equipped with PV-panels and solar thermal collectors as integrated parts of the roof construction. The ventilation system is a balanced, mechanical ventilation system with constant air flows. The volume flow rate will be 240 m<sup>3</sup>/h. An outdoor swimming pool will most likely be installed.

Figure 24 to Figure 26 provide an overview of the north-east cross section and the floor plans of the building.

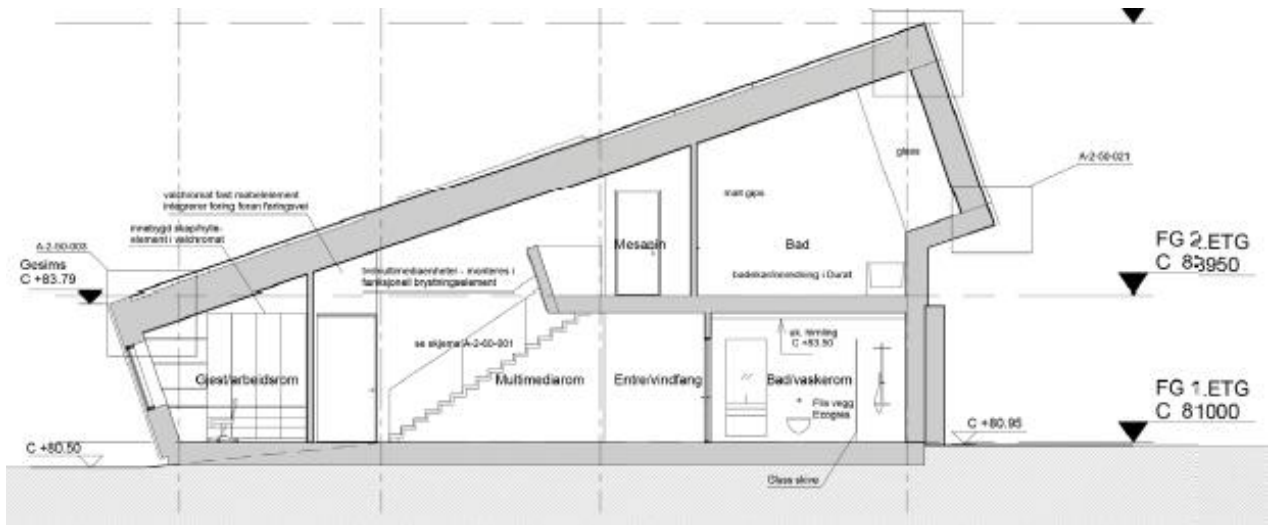


Figure 24 - North-east cross section of the "Multikomfort" dwelling

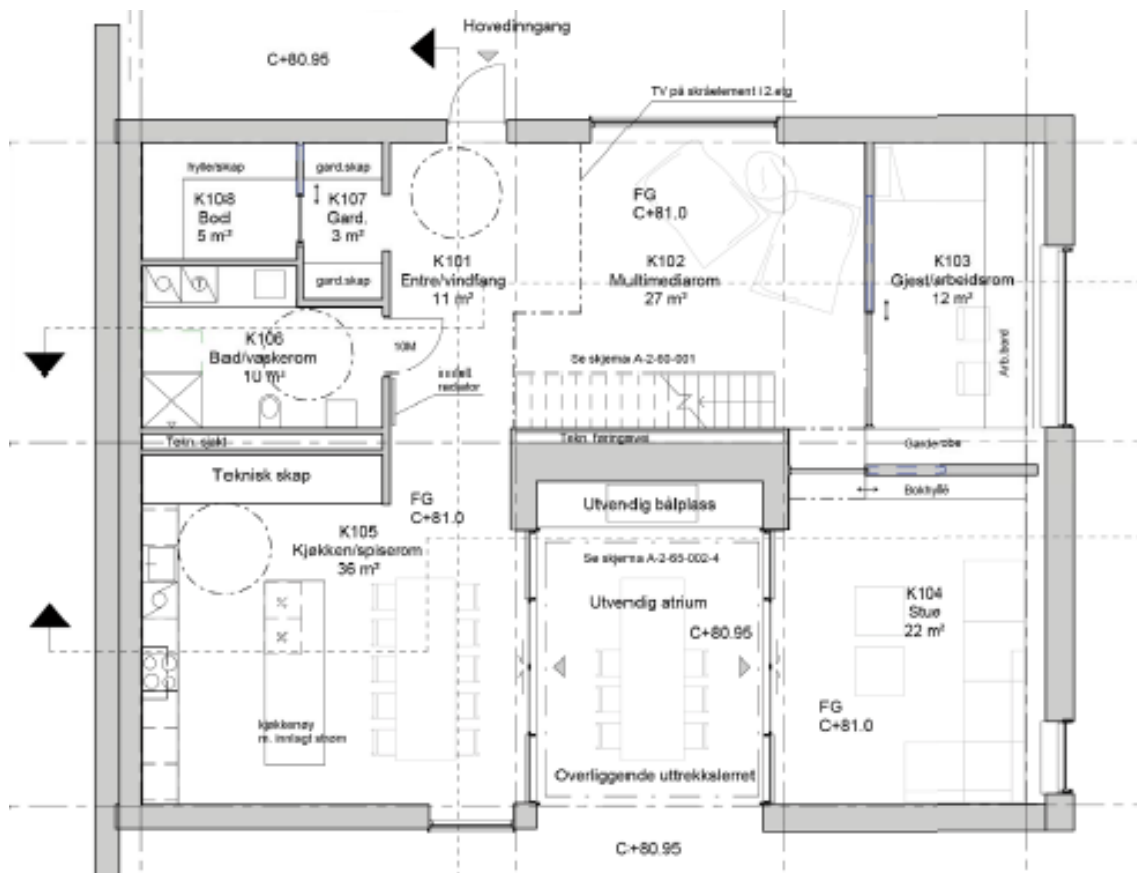
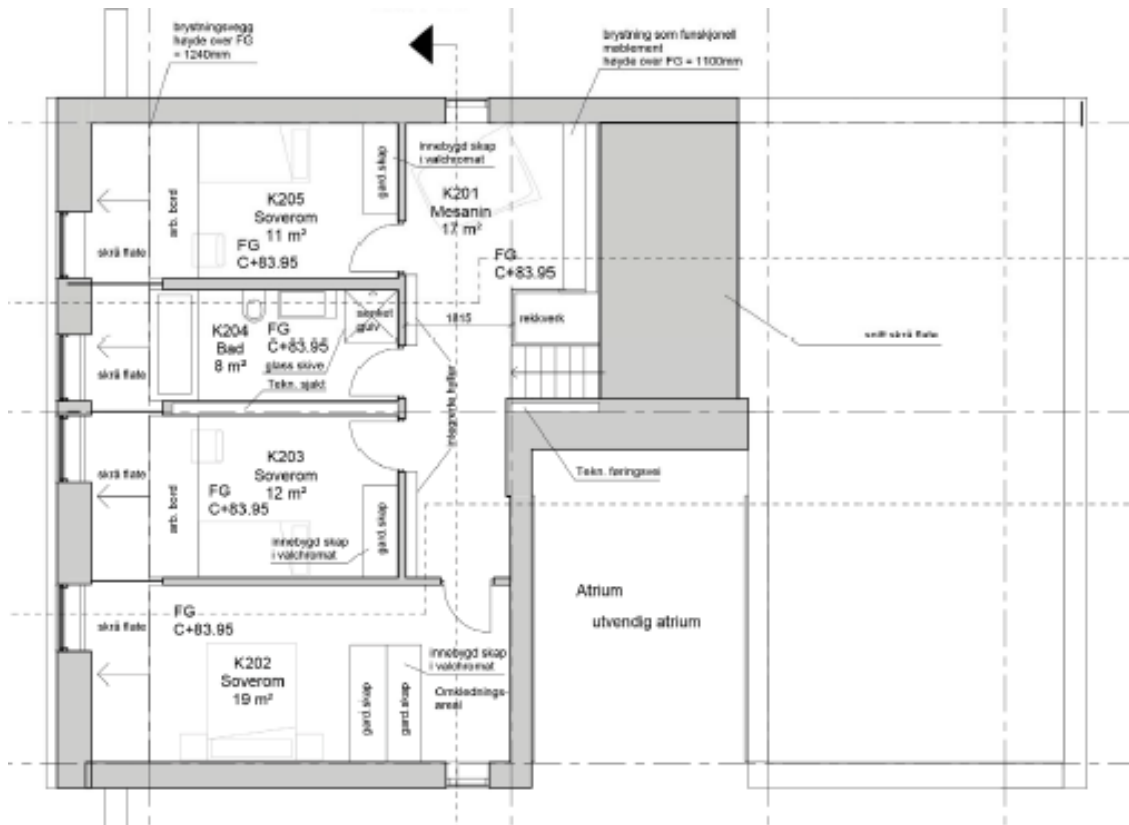


Figure 25 - Ground floor in the "Multikomfort" dwelling





**Figure 26 - First floor in the "Multikomfort" dwelling**

The annual average temperature in Larvik is 6.3°C and the "Multikomfort" floor area is 202 m<sup>2</sup>. The required specific heating demand for space heating and ventilation for the "Multikomfort" dwelling can therefore be calculated according to Equation 1 found in 3.2 *Space Energy Demand*. The specific heating demand for the demo house was calculated to be 17.6 kWh/m<sup>2</sup>, which is slightly above the German requirement of 15 kWh/m<sup>2</sup>.

## 10.2 SUGGESTED “MULTIKOMFORT” SYSTEM DESIGN

### 10.2.1 SYSTEM DESCRIPTION

The heating system for the “Multikomfort” single-family dwelling includes a ground-source heat pump, solar thermal collectors and a combination unit for ventilation and domestic hot water production. The combination unit includes an exhaust air heat pump and is called Compact P. Figure 27 shows the suggested system design for the demo detached dwelling.

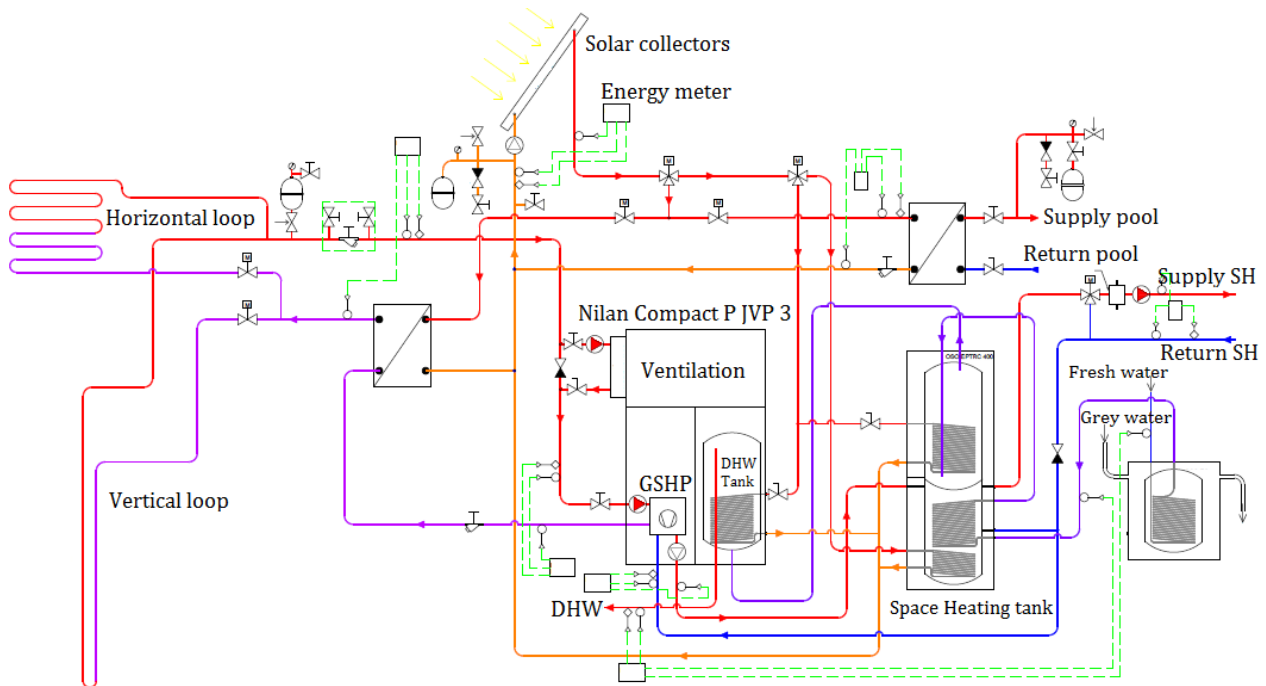
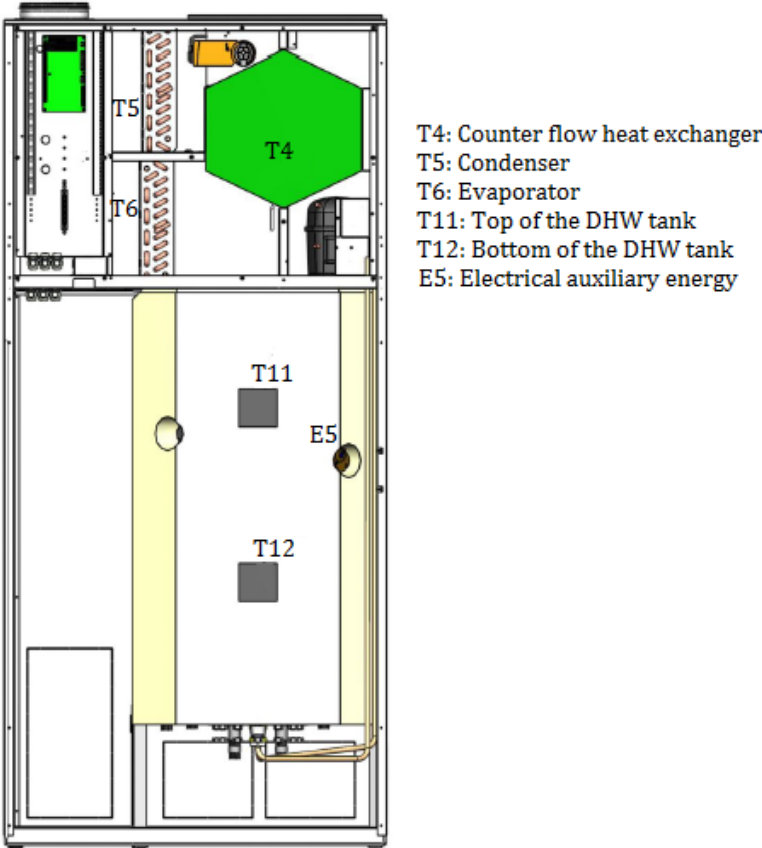


Figure 27 - System design, including solar thermal system and ground-source heat pump.

The system collects energy from five different energy sources. The main sources are solar thermal energy, ground-source energy and exhaust air from the ventilation system. The plan is to utilize the solar thermal energy for both domestic hot water production and space heating. The solar thermal energy will primarily be utilized for production of domestic hot water and secondly used to preheat water in the storage tank for space heating, as seen in Figure 27. The system presented in Figure 27 is only a suggestion and it is desired to optimize it and thus make changes if it should prove to be necessary. It is desired to optimize the system’s design and operating parameters in order to achieve a system with minimum electricity use. The heating system will be evaluated with both 8 and 16 m<sup>2</sup> of installed solar collector area. Installing 16 m<sup>2</sup> of solar collectors will probably result in overproduction of solar heat, but if possible the excess solar heat can be used to recharge the vertical borehole or a swimming pool, if the borehole temperature is too high. As seen in Figure 27, it is suggested that the ground-source heat pump extracts heat from both a vertical and a horizontal ground-source heat exchanger during heating mode.

The idea is to utilize energy from the well to preheat the supply air in the ventilation system during the winter, and similarly use it for free cooling during the summer. The preheater during heating season is a frost protection initiative for the heat recovery unit. With this initiative the supply air will be increased to -7°C, which is the frost protection temperature.

An exhaust air heat pump will be installed in the ventilation system. The heat pump will utilize energy in the exhaust air to heat the supply air before entering the occupant zone and to heat the domestic hot water. A more detailed illustration of this concept is shown in Figure 28.



**Figure 28 - Illustration of the exhaust air heat pump unit in combination with the counter flow heat exchanger and the DHW storage tank (NILAN, u.d.).**

The heating system described above will be utilized in combination with a low-temperature floor heating system. The supply and return temperature of the heat distribution system will be 35/30°C.

Both a domestic hot water tank and a storage tank for space heating are added to the system, as seen in Figure 27. The domestic hot water can be heated by the solar collectors, the exhaust air and an electrical heater. The storage tank for space heating can be preheated by grey-water and heated by the solar collectors, the GSHP and an electrical heater. The heat produced by the solar collectors will primarily be used to charge the domestic hot water tank, but if the set point temperature in the DHW tank is reached, the solar energy will secondarily be stored in the hot water tank for space heating. By utilizing short time storage, the energy can be collected during the day and used for space heating when demand arises during the evening.

A more detailed illustration of the storage tank for space heating can be seen in Figure 29.

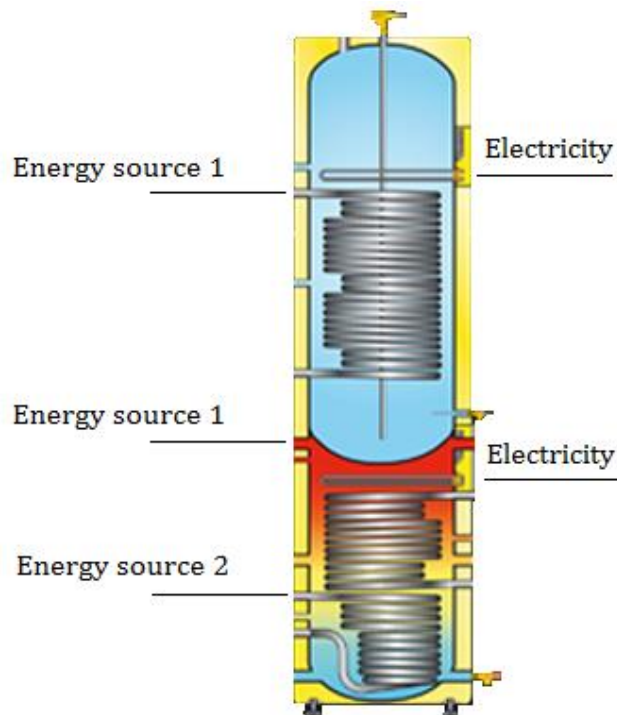


Figure 29 - Storage tank for space heating. Applicable for both low and high temperature energy source (OSOHOTwater, 2014).

The whole system can be divided into six modules, including the solar collector subsystem, the domestic hot water supply subsystem, the closed loop ground-source subsystem, the ventilation system, the ground-source heat pump subsystem and the space heating subsystem. Basic design parameters are listed in Table 5.

Table 5 - Basic system design parameters

Site location: Larvik (lat. N59°03, long.E10°02)			
Indoor/outdoor winter design temperatures		21°C/-17°C	
Borehole number		1	
Borehole depth		80 m	
Brine/water ground-source heat pump		COP	Heating capacity
		4.6	3 kW
Solar collector		Collector area	Efficiency
		8m <sup>2</sup> /16m <sup>2</sup>	60 %
Exhaust air heat pump		Air/air	Air/water
<i>COP</i>		4.6	3.9
<i>Heating capacity</i>		2.0 kW	1.2 kW
DHW tank		Volume	Electrical supply
		180 l	1.5 kW
Storage tank for space heating		Volume	Electrical supply
		325 l	3.0 kW
			Heat loss coefficient
			2.0 kWh/day

### *10.2.2 OPERATION MODES*

In order to achieve an energy efficient system and to improve the integration between the renewable energy sources, efficient control strategy is crucial. With an efficient control strategy of the solar collector system for instance, solar heat can be utilized for other purposes than domestic hot water production during times with reduced solar irradiation. With well-planned operation modes, an efficient interaction between the different heat sources is obtainable. A suggestion for different operation modes is given in this subchapter.

Mode 1: The solar collectors are used to produce domestic hot water. Heat is produced at high temperatures ( $>50^{\circ}\text{C}$ ), or lower for preheating of the domestic hot water. The GSHP is not in operation and there is no heat extraction from the borehole. The exhaust air heat pump is not in use if set point temperature in the tank is reached due to sufficient heat produced by solar collectors. Being able to shut the exhaust air heat pump off will minimize the stops and starts of the heat pump and improve the operational conditions.

Mode 2: Solar collectors are used to produce heat for the space heating system. If set point temperature in the domestic hot water tank is reached, excessive solar heat can be used to charge the storage tank for space heating. Solar heat produced at lower temperatures ( $20\text{-}50^{\circ}\text{C}$ ) can be utilized for space heating, which will provide the solar collectors with longer operational time and thereby better efficiency. With heat produced at these temperatures the GSHP may be turned off, as solar energy is collected during the day and can be utilized when there is a space heating demand. There will be no heat extraction from the borehole. The exhaust air heat pump will be in operation in order to cover the domestic hot water demand when solar heat is produced at low temperatures.

Mode 3: Solar collectors are used to recharge the borehole. Heat production at lower temperatures ( $5\text{-}20^{\circ}\text{C}$ ) can be utilized to recharge the borehole. Heat is transferred from the solar collector fluid to the antifreeze solution in the brine through a heat exchanger. The heat pump is in operation and heat is extracted from the borehole. The solar collectors are in operation at lower temperatures which increases the efficiency of the system.

With heat production at high temperatures excess solar heat can be dumped in the borehole to obtain thermal balance in the soil and for heat protection of the solar collectors. The heat pump is not in operation – there is no other heating demand and heat is injected to the borehole.

Mode 4: Solar collectors are used to charge the swimming pool. With heat production at high temperatures, excess solar heat will be used to heat the swimming pool if temperatures in the borehole are too high.

### 10.2.3 STEADY STATE CALCULATIONS

A steady state calculation was performed on the system design shown in Figure 27. The calculations were performed in order to get an overview of the possible temperature levels in the different circuits in the system, e.g. the solar heating circuit, the ground-source heat pump circuit and the exhaust air heat pump circuit. The calculations are based on parameters and values received from the manufacturer of the different components in the system. Where parameters were missing, assumed values were used. The results obtained from the calculations can therefore only be regarded as guiding and not as the actual values which will be obtained during operation of the system. To simplify, heat losses were not accounted for.

#### 10.2.3.1 Solar Collectors

The solar collector chosen for this heating system is a flat plate solar collector from Hewalex (Hewalex, 2006). The collector can be seen in Figure 30 and the collector parameters can be seen in Table 6.

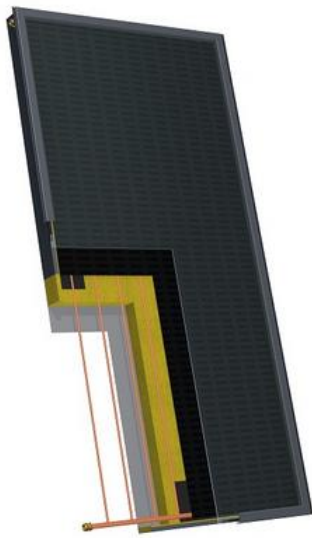


Figure 30 - Hewalex KS2000SLP

Table 6 - Solar collector parameters

Flat plate solar collector - Hewalex KS2000 SLP	
Gross surface	2.09 m <sup>2</sup>
Aperture area	1.82 m <sup>2</sup>
Optical efficiency, $\eta_0$	81.1 %
Heat loss coefficient, $a_1$	4.46 W/m <sup>2</sup> K
Heat loss coefficient, $a_2$	0.0096 W/m <sup>2</sup> K <sup>2</sup>
Concentration glycol	33 %

In order to calculate the inlet and outlet temperatures of the solar collector, the heat transfer fluid's specific heat capacity and density are needed.

The specific heat capacity and density of 33 % glycol-water mixture were calculated by using Equation 8 and Equation 9 (Furbo, 2005).

$$cp = (4255.5 - 958.5 \cdot 10^{-2} \cdot x - 941.7 \cdot 10^{-4} \cdot x^2) + (-168.9 + 843.5 \cdot 10^{-2} \cdot x - 35.0 \cdot 10^{-4} \cdot x^2) \cdot 10^{-2} \cdot T + (146.5 - 79.3 \cdot 10^{-2} \cdot x - 85.3 \cdot 10^{-4} \cdot x^2) \cdot 10^{-4} \cdot T^2 \quad \left[ \frac{J}{kgK} \right] \quad (8)$$

$$\rho = (996.5 + 152.3 \cdot 10^{-2} \cdot x - 96.6 \cdot 10^{-4} \cdot x^2) + (-1.7 - 146.2 \cdot 10^{-2} \cdot x + 76.7 \cdot 10^{-4} \cdot x^2) \cdot 10^{-2} \cdot T + (-38.4 + 62.1 \cdot 10^{-2} \cdot x - 30.8 \cdot 10^{-4} \cdot x^2) \cdot 10^{-4} \cdot x^2 \quad \left[ \frac{kg}{m^3} \right] \quad (9)$$

The x-factor represents the concentration of glycol (weight %), which is 33 % in this case, while T is the mean temperature in the solar collector (weight °C) and was assumed to be 50°C.

The specific heat capacity and density were calculated to be:

**Table 7 - Specific heat capacity and density of 33 % glycol/water mixture**

<b>Specific heat capacity, cp</b>	3917 J/kg·K
<b>Density, ρ</b>	1010 kg/m <sup>3</sup>

The flat plate solar collector efficiency was calculated by using Equation 10 (Morrison, u.d.).

$$\eta = \eta_0 - a_1 \cdot \frac{T_m - T_a}{G} - a_2 \cdot \frac{(T_m - T_a)^2}{G} \quad (10)$$

where,

$\eta_0$  is the optical efficiency of the solar collector

$a_1$  is the first order heat loss coefficient of solar collector [W/m<sup>2</sup>K]

$a_2$  is the temperature dependence of the heat loss coefficient of solar collector [W/m<sup>2</sup>K<sup>2</sup>]

$T_m$  is the mean temperature in the solar collector [°C]

$T_a$  is the ambient temperature [°C]

$G$  is the total solar irradiance [W/m<sup>2</sup>]

The mean temperature in the solar collector was assumed to be 50°C, while the ambient temperature,  $T_a$ , was set to 15°C. The assumption regarding the mean working fluid temperature was based on the fact that flat plate solar collectors may achieve operating temperature up to 80°C. The outlet temperature may be 80°C and the inlet temperature may be 30°C (Morrison, u.d.). The global solar irradiance was assumed to be 800 W/m<sup>2</sup>, which was chosen in accordance with EN 12975 (EN12975, 2006).

By implementing these assumptions, the solar collector efficiency,  $\eta$ , was calculated to be 60 % as seen in Table 8.

**Table 8 - Solar collector efficiency**

<b>Solar collector efficiency, η</b>	60 %
--------------------------------------	------

In order to calculate the useful heating effect produced by the solar collectors, Equation 11 was used.

$$Q = \eta \cdot A \cdot G [W] \quad (11)$$

where,

$\eta$  is the thermal efficiency of the solar collectors

$A$  is the aperture area [m<sup>2</sup>]

$G$  is the total solar irradiance [W/m<sup>2</sup>]

The gross area for one solar collector from Hewalex is 2.09 m<sup>2</sup>. In order to install a solar collector area of 8 m<sup>2</sup> and 16 m<sup>2</sup>, 4 and 8 solar collectors are needed. This gives a total aperture area of 7.28 m<sup>2</sup> and 14.56 m<sup>2</sup> respectively.

The heat effect produced by the solar collectors for each aperture area was then calculated to be:

**Table 9 - Produced useful power according to aperture area**

<b>Aperture area of 7.28 m<sup>2</sup></b>	3494 W
<b>Aperture area of 14.56 m<sup>2</sup></b>	6990 W

In order to calculate the outlet and inlet temperatures of the solar collectors, Equation 12, 13 and 14 were used.

$$Q = \dot{V} \cdot \rho \cdot c_p \cdot \Delta T [W] \quad (12)$$

where,

$\dot{V}$  is the volume flow rate in the solar collector loop [m<sup>3</sup>/s]

$\rho$  is the solar collector fluid density [kg/m<sup>3</sup>]

$c_p$  is the solar collector fluid specific heat capacity [J/kg · K]

$\Delta T$  is the temperature difference between outlet and inlet temperature in the solar collector [K]

$$T_m = \frac{T_{out} + T_{in}}{2} = 50 K \quad (13)$$

$$\Delta T = T_{out} - T_{in} [K] \quad (14)$$

Both the hot water storage tank and the storage tank for space heating are spiral tank systems, as seen in Figure 27. When using spiral tank systems a high flow rate of the working fluid is required. A rule of thumb is to apply 1.0 l/min·m<sup>2</sup> solar collector area (Furbo, 2004). This was used to calculate the volume flow rate for both sizes of solar collector area.

The results are shown in Table 10:

**Table 10 - Solar collector outlet and inlet temperature**

<b>Temperatures</b>	
<b>Aperture area, 7.28 m<sup>2</sup></b>	
<b>T<sub>out</sub></b>	52.94°C
<b>T<sub>in</sub></b>	47.06°C
<b>Aperture area, 14.56 m<sup>2</sup></b>	
<b>T<sub>out</sub></b>	52.95°C
<b>T<sub>in</sub></b>	47.06°C

As seen in Table 10, the outlet and inlet temperature in the solar collector are the same for both aperture areas. This was expected since the produced power with a solar collector area of 8 m<sup>2</sup> is the half of the produced power with a solar collector area of 16 m<sup>2</sup>, and the volume flow rate with 8 m<sup>2</sup> is the half of the volume flow rate for the solar collector of 16 m<sup>2</sup>. The half can then be neglected in the calculation and the results are approximately the same.



### 10.2.3.2 Domestic Hot Water Tank Temperature

In order to estimate the temperature in the storage tank, the heat exchange capacity rate of the solar spiral must be calculated. The heat exchange capacity rate states how much power can be transferred from the solar collector fluid to the heat storage per K temperature difference between the solar collector fluid and the storage (Furbo, 2005). The heat exchange capacity rate,  $H$ , can be calculated by using Equation 15 or Equation 16. In order to find the temperature in the storage tank,  $T_1$ , both equations were used.

$$H = -\dot{V} \cdot c_p \cdot \rho \cdot \ln\left(1 - \frac{T_f - T_r}{T_f - T_1}\right) \left[\frac{W}{K}\right] \quad (15)$$

where,

$T_f$  is the spiral inlet temperature [K]

$T_r$  is the spiral outlet temperature [K]

$T_1$  is the tank temperature [K]

$$H = K_1 + K_2 \cdot \ln(T_f - T_1) + (K_3 + K_4 \cdot \ln(T_f - T_1)) \cdot T_1 \left[\frac{W}{K}\right] \quad (16)$$

where,

$K_1$ ,  $K_2$ ,  $K_3$  and  $K_4$  are constants which depend on the design of the heat exchanger spiral, the solar collector fluid and the volume flow rate.

To calculate the four constants  $K_1$ ,  $K_2$ ,  $K_3$  and  $K_4$ , the computer program VEKSLER was used (Furbo, 2005). VEKSLER calculates the heat exchange capacity rate of a heat exchanger spiral submerged in water in a storage tank, and is developed at the Technical University of Denmark. A short introduction to VEKSLER is found in *Appendix A - VEKSLER*. In order to calculate the heat exchange rate, input such as collector fluid, design of heat exchange spiral and volume flow rate are needed. Assumptions regarding the heat exchange spiral were made in order to perform the calculation. It was assumed that the spiral material was steel with a thermal conductivity of 60 W/m·K, and that the inner and outer diameter of the spiral was 21.6 mm and 26.9 mm respectively. The length of the spiral was calculated based on the rule of thumb stating that the heat exchange spiral should be 2 m per m<sup>2</sup> solar collector (Furbo, 2004).

An illustration of the temperatures in the circuit can be seen in Figure 31.

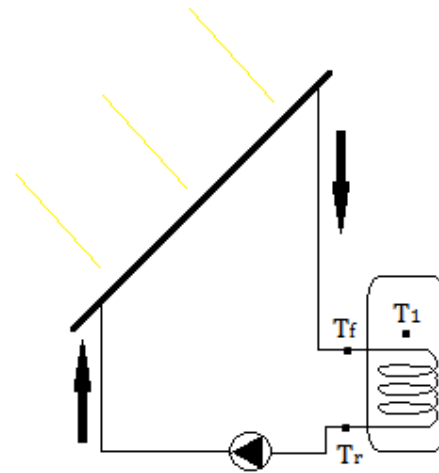


**Figure 31 - Illustration of temperatures in the solar collector heating system**

The power transferred from the solar collector to the tank was assumed to be the same as the useful heating power produced by the solar collectors, found in Table 9. The heat losses from the pipes in the collector loop and in the storage tank were not considered in this steady state calculation. The two equations, Equation 15 and Equation 16, were solved for each aperture area, but since  $T_f$  and  $T_r$  are equal in both scenarios, the tank temperature became approximately the same. The tank temperature can be seen in Figure 32 and Table 11.

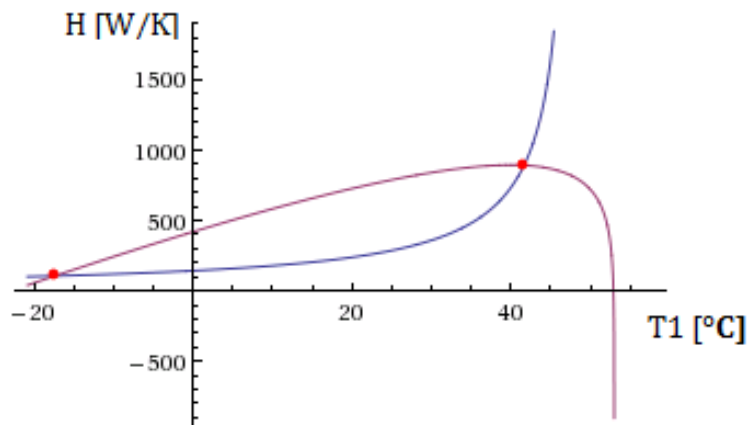


**Figure 32 - Temperature in storage tank**

The blue and red graphs in Figure 32 represent Equation 15 and 16. In order to find the tank temperature, the equations were set equal to each other and in the crossing point, illustrated by the red dot in quadrant 1, the tank temperature was found. Considering that the inlet temperature to the spiral was 52°C and the outlet temperature was 47°C, a tank temperature of 42°C seems realistic.

**Table 11 - DHW tank temperature**

<b>Tank temperature, <math>T_1</math></b>	42°C
---	------

It should be stated that some of the values used in the calculations were assumed values, hence the result values are only guiding. If the total solar irradiance was 700 W/m<sup>2</sup> or if the mean temperature in the solar collector was 60°C, the results would be different as seen in Table 12.

**Table 12 - Changing parameters for solar heating system**

<b>Solar collector area: 8m<sup>2</sup></b>			
	G = 700 W/m <sup>2</sup> T <sub>a</sub> = 15°C, T <sub>m</sub> = 50°C	G = 600 W/m <sup>2</sup> , T <sub>a</sub> = 10°C, T <sub>m</sub> = 50°C	G = 800 W/m <sup>2</sup> T <sub>a</sub> = 15°C, T <sub>m</sub> = 60°C
Collector efficiency, $\eta$	0.57	0.49	0.54
Produced useful heat, Q	2911 W	2182 W	3121 W
T <sub>out</sub>	52.5°C	51.8°C	62.7°C
T <sub>in</sub>	47.4°C	48.1°C	57.3°C
Tank temperature, T <sub>1</sub>	39.6°C	42.0°C	49.9°C
<b>Solar collector area: 16 m<sup>2</sup></b>			
Collector efficiency, $\eta$	0.57	0.49	0.53
Produced useful heat, Q	5822 W	4264 W	6241 W
T <sub>out</sub>	52.5°C	51.8°C	62.7°C
T <sub>in</sub>	47.4°C	48.1°C	57.3°C
Tank temperature, T <sub>1</sub>	39.4°C	41.9°C	49.5°C

As seen in Table 12 there are some differences between the values achieved with changed parameters and the values achieved with the original parameters. Changing the mean temperature in the solar collector resulted in higher temperatures in the tank. A mean temperature of 60°C is a realistic value as well, and the temperature in the tank may get as high as 50°C on a sunny day. With a higher temperature in the storage tank, less auxiliary energy is needed in order to cover the domestic hot water demand.

**10.2.3.3 Ground-Source Heat Pump**

The ground-source heat pump is a Compact P JVP 3kW produced by NILAN (NILAN, u.d.). The heat pump is an invertible heat pump and is able to deliver heat at a minimum of 1.6 kW and a maximum of 3.9 kW. The heat transfer fluid is R410A. An illustration of the ground-source heat pump system can be seen in Figure 33. Figure 33 represents the ground-source heat pump circuit shown in Figure 27.

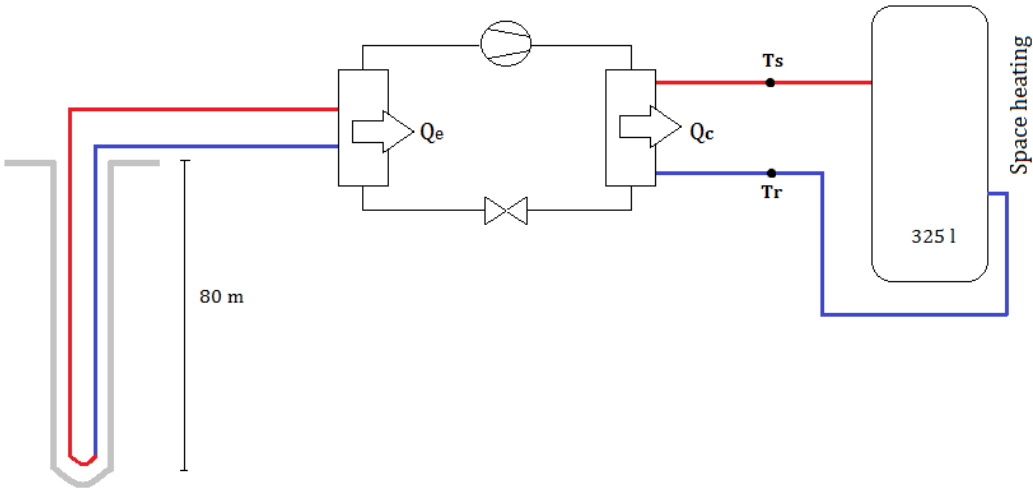


**Figure 33 - Illustration of the ground-source heat pump system**

As seen in Figure 33 the depth of the borehole is 80 m. The power which can be extracted from the borehole is based on the rule of thumb of 35 W/m, which implies a total power extraction of 2.8 kW (Amundsen, 2013). The coefficient of performance, COP, for the heat pump is 4.6 at an outdoor temperature of -10°C.

With a heating effect of 3.0 kW and a COP of 4.6, the required compressor power was calculated to be 0.65 kW, as seen in Equation 17.

$$COP = \frac{Q_c}{W} \rightarrow W = \frac{Q_c}{COP} = \frac{3.0 \text{ kW}}{4.6} = 0.65 \text{ kW} \quad (17)$$

The coefficient of performance indicates how many times more heat is emitted in relation to the electricity supply. A high COP is therefore beneficial.

In order to calculate the supply water temperature entering the accumulation tank,  $T_s$ , as seen in Figure 33, the heating effect transferred from the heat pump to the water in the supply pipe was used. With a heating effect of 3.0 kW, the volume flow rate in the water supply pipe is 0.14 l/s according to NILAN. The heat distribution system in the single-family dwelling is a low temperature floor heating system, and the supply and return temperature of the water should be 35 and 30°C respectively. Assuming a return temperature of 30°C, the supply temperature to the tank was calculated according to Equation 12. The calculation can be seen in Equation 18.

$$T_s = \frac{Q_c}{\rho \cdot c_p \cdot \dot{V}} + T_r = \frac{3.0 \text{ kW}}{1000 \frac{\text{kg}}{\text{m}^3} \cdot 4.2 \frac{\text{kJ}}{\text{kgK}} \cdot 1.4 \cdot 10^{-4} \frac{\text{m}^3}{\text{s}}} + 30^\circ\text{C} = 35.1^\circ\text{C} \quad (18)$$

The water temperature obtained in the storage tank for space heating is additionally depending on the temperatures delivered by the solar collector circuit and by the electrical auxiliary energy. With an inlet temperature from the GSHP to the tank of 35.1°C, the set point temperature of 35°C is reached. It should be noted that in the calculations performed above a heating effect of 3.0 kW was assumed. The maximum heating effect the ground-source heat pump can deliver is however 3.9 kW, and higher temperatures than 35.1°C may be obtained. This may result in less utilization of auxiliary electrical energy.

The results obtained from the calculation are only guiding and are based on assumptions of parameters which may be different in reality. However, the results provide an indication of temperatures which are obtainable in the system.

#### 10.2.3.4 Exhaust Air Heat Pump

The exhaust air heat pump is integrated in Compact P, and is used to heat the supply air and the domestic hot water. The condenser consists of two parts, one which heats the supply air and one which heats the domestic hot water, hence the two different COP values seen in Table 13. An illustration of the system can be seen in Figure 34. The illustration does not take the separation of the condenser into account and the illustrated temperatures are only guiding.

**Table 13 - Coefficient of performance exhaust air heat pump**

Volume flow rate	240 m <sup>3</sup> /s	
	Air/air	Air/water
Coefficient of performance, COP	4.6	3.9

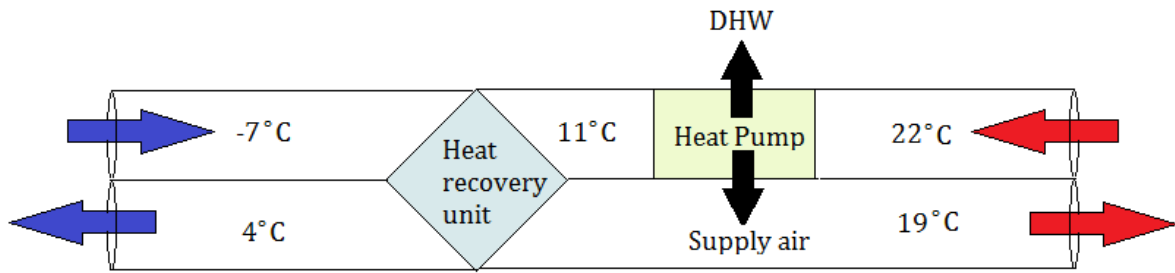


Figure 34 - Illustration of the exhaust air heat pump

The heating effect of the domestic hot water,  $Q_w$ , is given in Figure 35. The heating effect is a function of the volume flow rate at a hot water tank temperature of 41°C, an exhaust air temperature of 20°C and an outdoor temperature of 20°C, in accordance with EN 255-3.

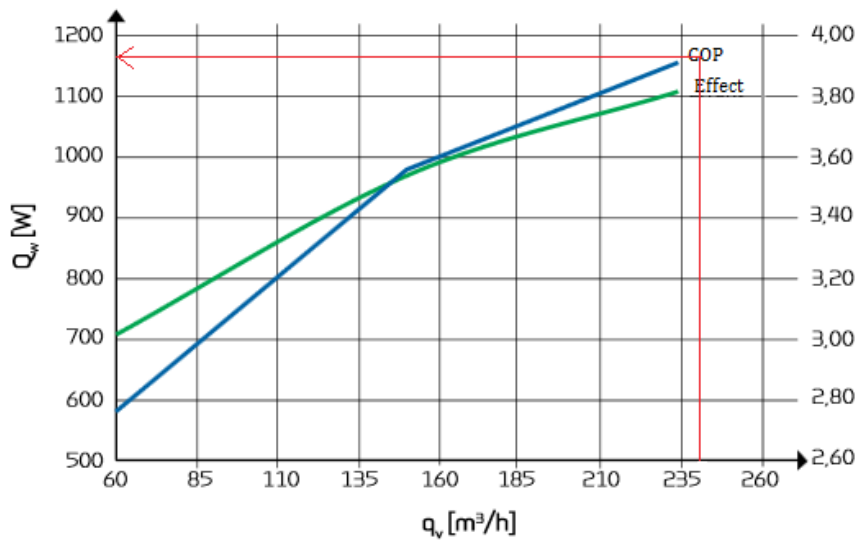


Figure 35 - COP air/water (NILAN, u.d.)

As seen in Figure 35 the heating effect for domestic hot water is approximately 1170 W. Knowing the air/water COP and the heating effect, the power consumption of the heat pump was calculated as seen in Equation 19.

$$COP = \frac{Q_c}{W} \rightarrow W = \frac{1.17 \text{ kW}}{3.9} = 0.30 \text{ kW} \quad (19)$$

With the condenser heating effect and the power consumption of the heat pump, the evaporation heating effect can be calculated assuming that heat loss in the compressor is neglected.

The evaporator heating effect was calculated according to Equation 20.

$$Q_c = Q_e + W \rightarrow Q_e = 1.17 \text{ kW} - 0.30 \text{ kW} = 0.87 \text{ kW} \quad (20)$$

It was assumed that the temperature in the exhaust air, which enters the evaporator, was 22°C and that the volume flow rate was 240 m³/h. The exhaust air temperature at the outlet of the evaporator was calculated based on Equation 12. According to Incropera et al. (2007), the density and specific heat capacity of air at 22°C is 1.1847 kg/m³ and 1.0069 kJ/kg·K. (Incropera,

et al., 2007). The calculation of the outlet temperature can be seen in Equation 21 and Equation 22.

$$\Delta T = \frac{Q_e}{\dot{v} \cdot \rho \cdot c_p} = \frac{0.87 \text{ kW}}{0.0667 \frac{\text{m}^3}{\text{s}} \cdot 1.1847 \frac{\text{kg}}{\text{m}^3} \cdot 1.0069 \frac{\text{kJ}}{\text{kg} \cdot \text{K}}} = 10.9 \text{ K} \quad (21)$$

$$T_{out} = T_{in} - \Delta T = 22.0^\circ\text{C} - 10.9^\circ\text{C} = 11.0^\circ\text{C} \quad (22)$$

In order to calculate the inlet temperature to the domestic hot water storage tank, the Carnot-COP and Carnot efficiency were used since values from the manufacturer were not available. It should be noted that when the Carnot efficiency is used, the calculations become very rough and approximate.

The Carnot-COP is regarded as the ideal COP since it does not consider losses in the compressor, and was calculated according to Equation 23. The Carnot efficiency,  $\eta_c$ , varies between 0.3 and 0.7 depending on refrigerant, temperature differences in the heat exchanger and the efficiency of the compressor (Stene, 2013). A Carnot efficiency of 50 % was chosen in this calculation.

$$COP_c = \frac{COP_{real}}{\eta_c} = \frac{3.9}{0.5} = 7.8 \quad (23)$$

The Carnot-COP can additionally be calculated from the outlet exhaust air temperature from the evaporator and the outlet hot water temperature from the condenser. It is however more common to calculate the Carnot-COP from the condenser temperature,  $T_c$ , and the evaporator temperature,  $T_e$ . When the Carnot-COP is calculated by using the outlet exhaust air temperature and the hot water outlet temperature instead, the heat losses in the heat exchangers (evaporator and condenser) are accounted for. It was decided to do the calculation with these temperatures since it is the outlet hot water temperature which is of interest in this case. An illustration of the exhaust air heat pump with these temperatures can be seen in Figure 36.

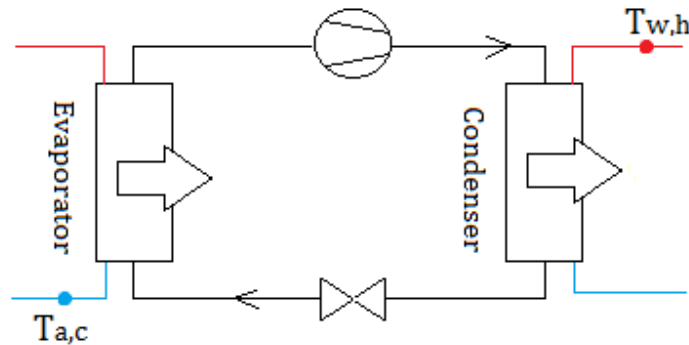


**Figure 36 - Exhaust air heat pump with outlet exhaust air temperature and outlet hot water temperature**

The additional equation used to calculate the Carnot-COP is shown in Equation 24.

$$COP_c = \frac{T_{w,h}}{T_{w,h} - T_{a,c}} \quad (24)$$

where,

$T_{w,h}$  is the hot water temperature at the condenser outlet [°C]

$T_{a,c}$  is the exhaust air temperature at the evaporator outlet [°C]

Equation 24 was used to calculate the outlet hot water temperature from the condenser,  $T_{w,h}$ , as seen in Equation 25. The outlet air temperature from the evaporator,  $T_{a,c}$ , was assumed to be 11.0°C, which was found in Equation 22.

$$T_{w,h} = \frac{7.8 \cdot 284 \text{ K}}{6.8} = 325.8 \text{ K} = 52.8^\circ\text{C} \quad (25)$$

If the Carnot efficiency was 40 % or 60 % instead, the outlet hot water temperature would have been:

**Table 14 - Changing Carnot efficiency**

	$\eta = 40\%$	$\eta = 60\%$
$T_c$	43.5°C	62.6°C

The COP for the air/air part of the exhaust air heat pump is 4.6 and the heating effect is 2.0 kW. From the datasheet describing the Compact P, it is stated that the flat plate heat exchanger may have a temperature efficiency up to 85 %. Assuming the temperatures represented in Figure 34, the temperature of the air exiting the heat recovery unit was calculated according to Equation 26.

$$\eta = \frac{t_t - t_u}{t_a - t_u} \quad (26)$$

where,

$t_t$  is the temperature leaving the heat recovery unit on the supply side [°C]

$t_u$  is the temperature of the supply air entering the heat recovery unit [°C]

$t_a$  is the exhaust air temperature [°C]

With a temperature efficiency of 85 %, the temperature of the supply air leaving the heat recovery unit was calculated to be 8.3°C. With a temperature of 8.3°C entering the condenser and a heating effect of 2.0 kW, the supply air entering the occupant area is close to 30°C. This temperature is too high and would not cause acceptable circulation of the fresh air in the occupant zone. However, this implies that the heat pump is able to deliver a desired supply temperature of approximately 19°C with the earlier assumed temperatures.

## 11 IDA ICE 4.6

IDA Indoor Climate and Energy was chosen as simulation tool for parametric analysis, optimization and evaluation of the heating system designed for the “Multikomfort” dwelling. Settings and input values used to design the model in IDA ICE will be reviewed in this chapter. The “Multikomfort” dwelling designed in IDA ICE is shown in Figure 37.

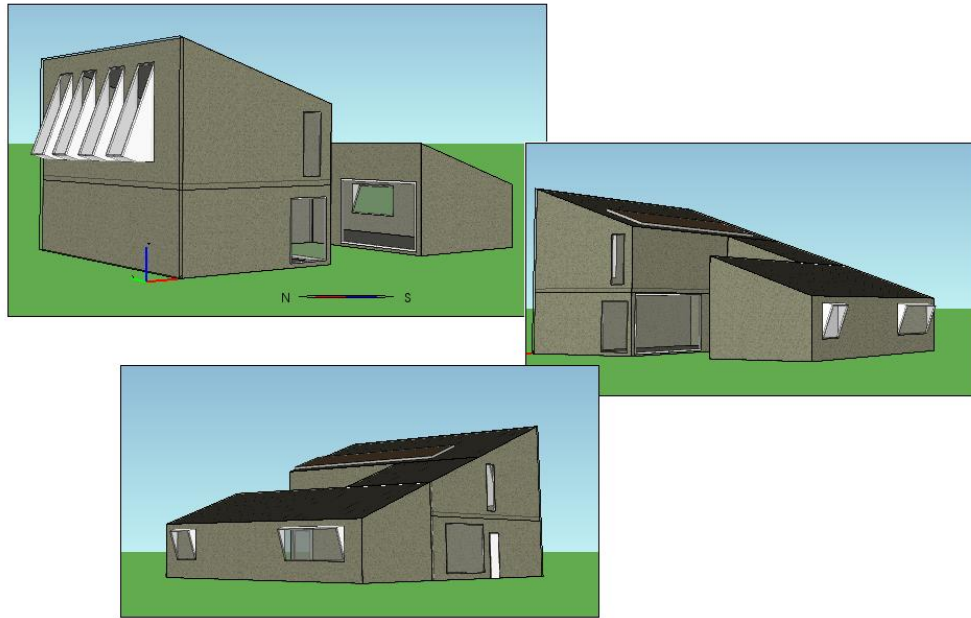


Figure 37 - Building design in IDA ICE 4.6

### 11.1 LOCATION AND CLIMATE SETTINGS

For location and climate settings in IDA ICE, Larvik and Oslo/Fornebu was chosen. Since a climate file for Larvik does not exist in the simulation program, Oslo/Fornebu was chosen even though there may be some deviation from the climate in Fornebu to the climate in Larvik. The direct normal and diffuse horizontal solar radiation for Oslo/Fornebu can be seen in Figure 38, and the dry-bulb temperature through the year can be seen in Figure 39.

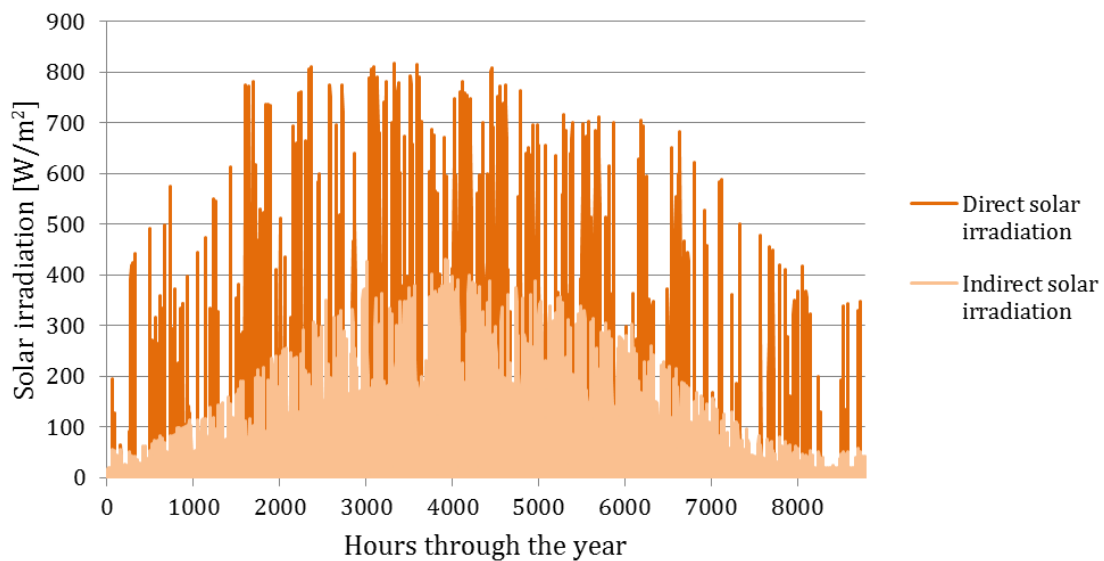


Figure 38 - Direct and diffuse solar radiation Oslo/Fornebu



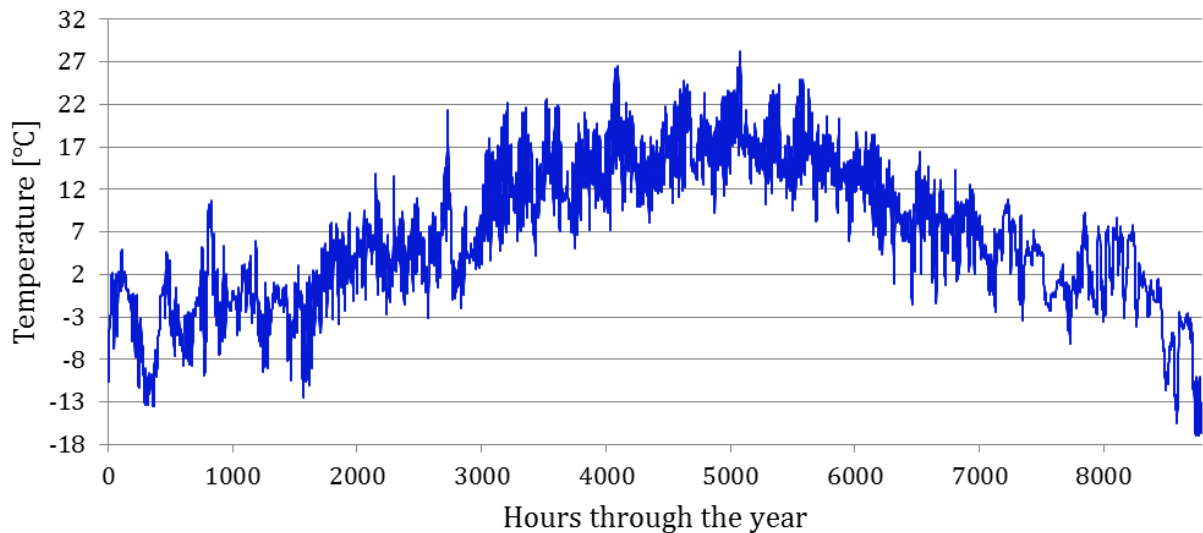


Figure 39 - Dry-bulb temperature Oslo/Fornebu

The coldest days are found in January and December, as seen in Figure 39, and the temperature on those days range between -10 and -17°C.

## 11.2 BUILDING ENVELOPE AND ENERGY USE

The model of the “Multikomfort” dwelling was designed in IDA ICE, and not imported as a DWG- or IFC-file. The designed model is a two story dwelling with floor plans as seen in Figure 40. Compared to the floor plans in the real building, some simplifications were made in IDA ICE in order to reduce the simulation time. For instance, the open space from the ground floor to the first floor with the staircase was not implemented. The bedrooms and hallway on the first floor were simulated as one zone and the ground floor was divided into two zones, one zone representing the kitchen, bathroom and hall and one zone for the living room and office/bedroom. These simplifications were done since only determination of the dwelling’s electricity use, the energy demand and the proportions of utilized free energy are of interest and not detailed information regarding the indoor climate. In order to perform a more detailed study with evaluation of the indoor climate, the dwelling should be divided into additional zones according to usage and orientation.

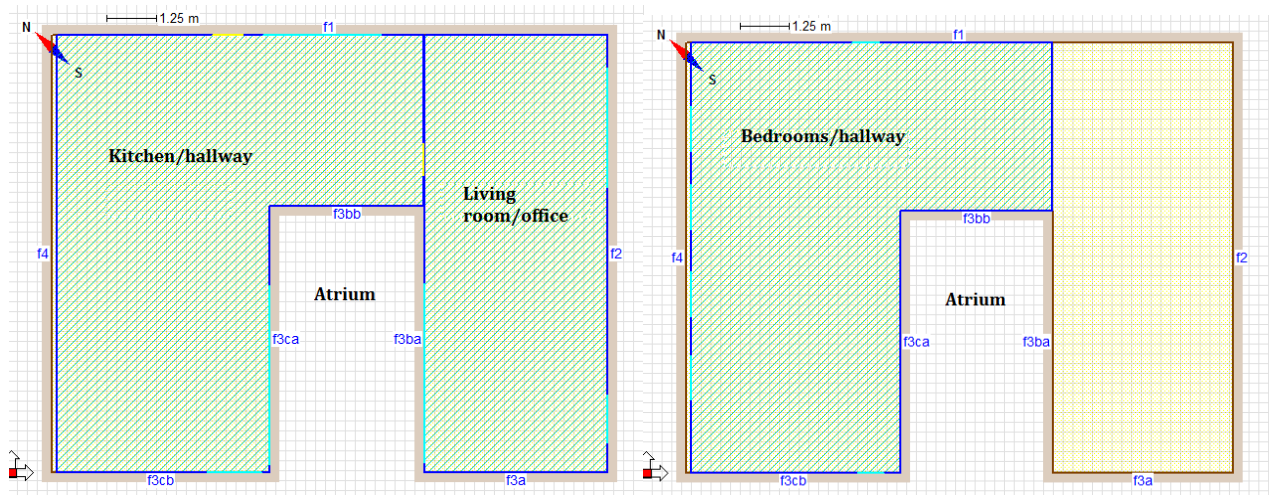


Figure 40 - Ground and first floor in "Multikomfort" building model designed in IDA ICE

The roof was created with a slope of 19° towards south-east, and equipped with thermal solar collectors. Photovoltaic modules are planned to cover the majority of the available roof area on the “Multikomfort” dwelling, but were not included in the model. Modeling the surroundings is important in order to evaluate the impact of solar shading on the PV and thermal solar collectors. However, they were not included in the simulations due to simplifications.

The inside door between the living room and kitchen zone, seen in Figure 40, was scheduled to be “never open”. It was however included in order to create air movements through the zones. In the original drawings of the “Multikomfort” dwelling the north-west and south-east façades are tilted with an angle of 20°. Since it is not possible to tilt external walls in IDA ICE, the windows on the north-west and south-east façade were tilted instead, as seen in Figure 37. This did however not affect the heat demand of the building. External solar blinds with different schedules according to the position of the sun during the day were added to the windows. The schedules can be seen in *Appendix B – Schedules for External Blinds*.

U-values for the external walls, the roof and the external floor were set in accordance with the requirements stated in NS 3700:2013 for dwellings of passive house standard. The U-values and the normalized thermal bridge value can be seen in Table 15 .

**Table 15 - U-values and normalized thermal bridge value according to NS 3700:2013**

	<b>Values</b>
<b>External walls</b>	U = 0.10-0.12 W/m <sup>2</sup> K
<b>External roof</b>	U = 0.08-0.09 W/m <sup>2</sup> K
<b>Slab on ground</b>	U = 0.07 W/m <sup>2</sup> K
<b>Windows</b>	U = 0.65 W/m <sup>2</sup> K
<b>Doors</b>	U = 0.65 W/m <sup>2</sup> K
<b>Normalized thermal bridge value</b>	Ψ = 0.03 W/m <sup>2</sup> K

The materials used were generally low weight concrete and light insulation. It is important to be aware of the specific heat capacity of the materials. A wall with high specific heating capacity may radiate heat to the surroundings during the night, and have a slow absorption of passive solar heat in the morning.

For internal walls, floors and doors default settings in IDA ICE were used. It was decided to use the window type T4-12m two Planitherm Ultra + ar from Saint-Gobain, which has a glazing U-value of 0.6 W/m<sup>2</sup>·K. The Planitherm window from Saint-Gobain represents a new generation of energy saving window glass that uses advanced coatings to retain more internal warmth whilst capturing free energy from natural daylight (Saint-Gobain, u.d.). In order to achieve a window of passive house standard the frame U-value was set to 0.95 W/m<sup>2</sup>·K, and the frame area was calculated according to window and frame dimensions given by Brødrene Dahl. The total U-value of the windows was calculated by IDA ICE to be 0.63 W/m<sup>2</sup>K. In order to reduce simulation time the windows facing the outdoor atrium were simulated as one large window on both the kitchen and living room side, as seen in Figure 37.

The settings for specific fan power (SFP), infiltration and domestic hot water use can be seen in Table 16.

Table 16 - SFP-factor, infiltration and domestic hot water settings in IDA ICE 4.6

	Passive house	Comment
<b>SFP-factor ventilation</b> [kW/m <sup>3</sup> /s]	1.5	NS 3700:2013
<b>Infiltration, 50 Pa, h<sup>-1</sup></b>	0.6	(NS3700, 2013). Wind driven flow
<b>Domestic hot water</b> [kWh/m <sup>2</sup> .year]	29.8	NS 3031: 2007 – single-family dwelling

Infiltration in IDA ICE can either be specified as fixed or as a result of wind driven flow. The fixed infiltration is not accurate, and is mostly used in the design phase. Because of this, wind driven air flow was chosen. Since the pressure coefficients surrounding the building were not known, they were set as default with semi-exposure. Semi-exposure is used when the pressure coefficients are unknown, and when the building is rurally located.

In order to achieve realistic working conditions for the solar thermal collectors a correct schedule for the domestic hot water use is important. Domestic hot water draw-off for a single-family house usually has some peaks during the morning and the evening. As default, the distribution of hot water use in IDA ICE is uniform, indicating a constant draw-off through the day. To achieve correct conditions, schedules for DHW usage in the week days and weekends/holidays were created as seen in Figure 41.

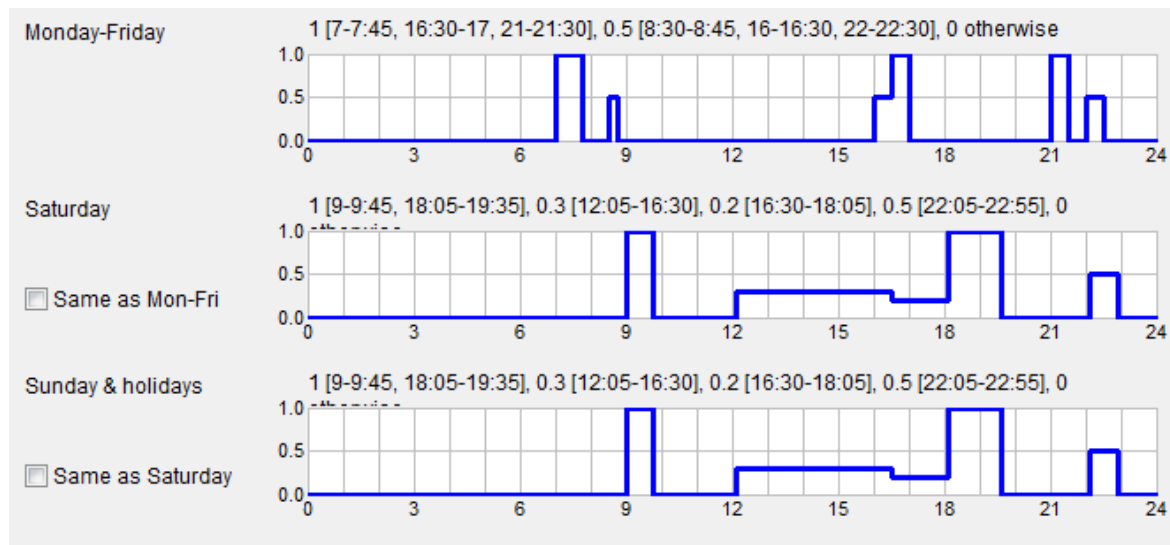


Figure 41 - Distribution of hot water usage

The set point values for the model were set as seen in Table 17.

Table 17 - Control Setpoints for the simulation model

	Minimum	Maximum
<b>Temperature</b>	21°C	25°C
<b>Daylight at workplace</b>	100 lux	10 000 lux

Whenever the temperature in a zone is below 21°C the heating system will activate, and whenever the temperature in a zone is above 25°C, the cooling system will activate. A

temperature throttle of 2.0°C was included. According to NS 3031:2007, the set point temperature for heating of dwellings is 21°C in occupied hours and 19°C in non-occupied hours.

If the daylight intensity at the workplace is below 100 lux, artificial lighting will be turned on, and if the intensity is above 10 000 lux, the artificial lighting is fully off. The controller set points include additional parameters such as CO<sub>2</sub> level, pressure difference over zone envelope etc., but these parameters are only needed when the building is integrated with a VAV system.

### 11.3 INTERNAL LOADS AND HEAT LOSS

Two different schedules for occupant presence in the zones were created, one schedule for the kitchen and living room and one schedule for the bedrooms on the first floor. The schedules can be seen in *Appendix C – Occupant and Equipment/lighting Schedules*. The metabolic rate in each zone was set according to expected activity in the specified zone. Additionally, one schedule for the equipment and lighting was created as seen in *Appendix C – Occupant and Equipment/lighting Schedules*. The heat contribution from equipment, lighting and persons were calculated according to recommended values stated in NS 3700:2013. The values for equipment and lighting in each zone can be seen in Table 18.

**Table 18 - Internal loads, equipment and lighting**

	<b>Equipment</b>	<b>Lighting</b>
<b>NS 3700:2013</b>	1.80 W/m <sup>2</sup>	1.95 W/m <sup>2</sup>
<b>Kitchen/hallway</b>	138 W	150 W
<b>Living room/office</b>	91 W	100 W
<b>Bedrooms</b>	138 W	150 W

The utilization factor for the equipment in each zone was set to 1. It can vary between 0 and 1, 1 meaning that all the heat and emission from the equipment is deposited in the zone and none of it is lost.

The heat losses from the distribution system can either be set as “None”, “Good”, “Typical”, “Poor” or “Very poor” in IDA ICE. They are specified to account for leakage from pipes and ducts that pass through the building, without having to describe their exact path and insulation properties. For the “Multikomfort” model “Good” was chosen. The losses in the DHW circuit and in the supply air duct can be seen in Table 19. Approximately 2 % of the heat delivered by the plant is lost when “Good” was chosen. The losses from the supply air duct include both thermal conduction and air leakage losses, and take the temperature difference between the duct system and the zones into account.

**Table 19 - Distribution system losses**

	<b>System losses</b>
<b>Domestic hot water circuit</b>	0.20 W/m <sup>2</sup> floor area
<b>Supply air duct losses</b>	0.26 W/m <sup>2</sup> floor area

## 11.4 HEAT DISTRIBUTION SYSTEM

A floor heating system was installed in the “Multikomfort” dwelling in order to provide heat to the different zones. In order to size the installed heating effect correctly, a heating load and a cooling load simulation with ideal heaters and ideal coolers was performed. The heating load simulation was performed for the date 15.01.2013, while the cooling load simulation was performed 15.07.2013. The specific heating effect indicates the needed installed effect of the floor heating system in each zone and is given in Table 20.

**Table 20 - Heating effect and specific heating effect**

Zone	Floor area [m <sup>2</sup> ]	Heating effect [W]	Design heating effect [W/m <sup>2</sup> ]
<b>1st floor, bedrooms</b>	75.7	1174	16
<b>Living room/office</b>	50.6	1041	21
<b>Kitchen/hallway</b>	75.7	1006	13

The maximum heat supplied to each zone in the building can be seen in Figure 42.



**Figure 42 - Maximum heat supplied to the dwelling [W/m<sup>2</sup>]**

Maximum heat is supplied to the living room zone as seen in Figure 42. This zone is especially exposed due to the exterior roof and floor and the majority of window area facing north-west.

The heat emission from a floor heating system is primarily radiant heating. A radiant heating system is able to operate with low temperatures which are close to the desired room air temperature. Due to this, the heating source’s coefficient of performance is increased and the distribution losses are decreased, which is beneficial. In order to achieve the desired heat flows at a low temperature difference between the room air and the structure, high thermal conductivity in the slab is needed. The heat flux is increased with increased thermal conductivity; hence a faster heat transfer between the pipes and the surface is achieved.

The floor heating/cooling system which was inserted in IDA ICE divides the floor construction into two parts, one above and one below the heated layer. When inserting a floor heating system,

the floor heating circuit will heat the room below almost as much as the room it is inserted in. The floor heating/cooling system was installed on the first floor and in the living room zone on the ground floor, as seen in Figure 43. Since the floor heating system was installed on the first floor it was not necessary to install a floor heating circuit in the kitchen zone.



**Figure 43 - Floor heating system in the "Multikomfort" dwelling**

The floor construction above the heating/cooling circuit was divided into two layers, one 5 mm floor coating with heat conductivity of  $0.18 \text{ W/m}^2\cdot\text{K}$  and a 20 mm concrete slab with heat conductivity of  $1.7 \text{ W/m}^2\cdot\text{K}$ . The design power of the floor heating was calculated based on ideal heaters and coolers. However, the actual emitted power depends on the resistance in the floor construction, and may be smaller if the resistance is large.

The supply temperature was set to  $35^\circ\text{C}$ , while the return temperature was  $30^\circ\text{C}$ , giving a delta T of  $5^\circ\text{C}$ . The mass flow was chosen to be constant with a maximum coil mass flow temperature difference of  $3^\circ\text{C}$ . The heating/cooling circuit was inserted 2 cm below the surface with a heat transfer rate of  $10 \text{ W/m}^2\cdot\text{K}$ . The recommended heat transfer rate for floor heating and floor cooling is  $11 \text{ W/m}^2\cdot\text{K}$  and  $7 \text{ W/m}^2\cdot\text{K}$  respectively (Higgins & Crocker, 2012). Since the floor in the model functions as both heating and cooling floor, the heat transfer rate of  $10 \text{ W/m}^2\cdot\text{K}$  seems acceptable. The emitted power was set to be controlled by varying the supply water temperature. A PI-controller was selected to control the emitted power according to the air temperature in the corresponding zone.

### 11.5 VENTILATION SYSTEM

The ventilation system in the model is a central air handling unit with balanced and constant air flow rates. The total air flow rate in the aggregate was set to  $240 \text{ m}^3/\text{h}$  with a supply temperature of  $19^\circ\text{C}$  all year. According to NS 3031:2007 the minimum specific air flow rate for a dwelling with floor area above  $110 \text{ m}^2$  is  $1.2 \text{ m}^3/\text{h}\cdot\text{m}^2$  (NS3031, 2007). An air flow rate of  $240 \text{ m}^3/\text{h}$  is in accordance with the requirement set by Brødrene Dahl.

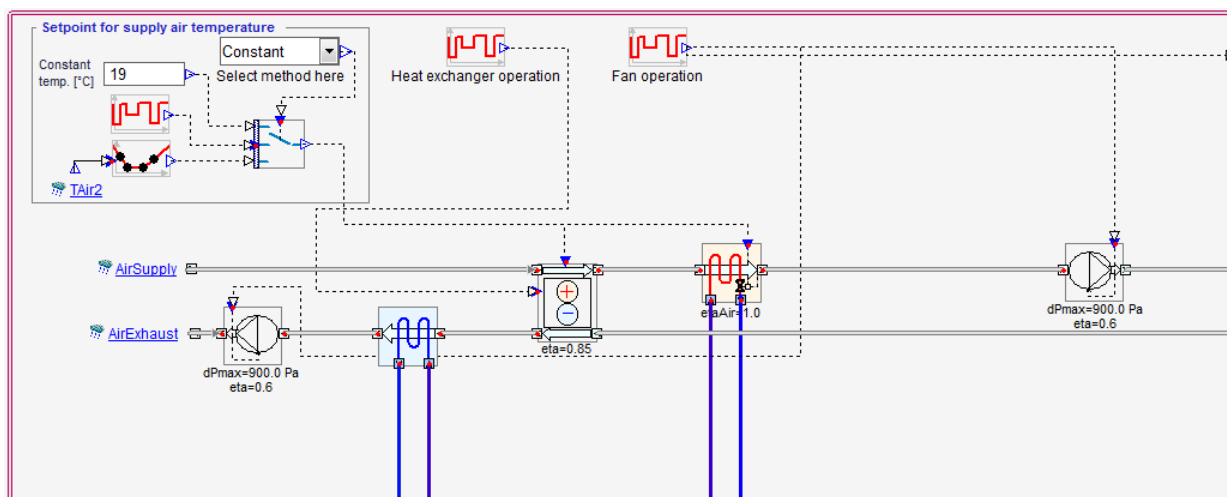


**Figure 44 - The Air handling unit (AHU) for the building model in IDA ICE**

The air handling unit (AHU) shown in Figure 44 was equipped with a highly efficient flat plate heat exchanger with a temperature efficiency of 85 %. The efficiency of the fans was set to 60 % as seen in Figure 44. A heating coil was included in order to reheat the supply air when necessary, and a cooling coil was included in the return air duct after the heat recovery unit. The cooling coil constitutes a part of the exhaust air heat pump which connects the ventilation system to the domestic hot water tank in the plant. It was assumed full mixing of air in each zone, and the displacement degree for gradient calculation was therefore set to 0.

The air flow rates in the model were calculated based on the requirement stated in NS 3031, as seen in Table 21. The air flow rates were balanced for each zone. With additional zones, one for kitchen and one for bathroom, an air handling unit with return air only should have been chosen for those zones. Forced ventilation extract from the bathroom and kitchen should then been compensated with raised supply air flow rate in order to achieve balance in the system. For a more detailed study, the air flows should be based on requirements according to usage of the different rooms. To simplify, it was decided to allocate the ventilation rates based on 1.2 m<sup>3</sup>/h·m<sup>2</sup>, which gives a total of 240 m<sup>3</sup>/h.

**Table 21 - Supply and exhaust air flow rates**

	Supply Air flow rate	Exhaust air flow rate	Comment
		[m <sup>3</sup> /h]	
<b>Kitchen/hall</b>	90 m <sup>3</sup> /h	90 m <sup>3</sup> /h	
<b>Bedrooms</b>	90 m <sup>3</sup> /h	90 m <sup>3</sup> /h	
<b>Livingroom/office</b>	60 m <sup>3</sup> /h	60 m <sup>3</sup> /h	
<b>Total</b>	<b>240 m<sup>3</sup>/h</b>	<b>240 m<sup>3</sup>/h</b>	<b>Gives 1.2 [m<sup>3</sup>/hm<sup>2</sup>]</b>

## 11.6 PLANT

In order to select energy sources and composition of the plant in IDA ICE, the ESBO-plant was selected. With the ESBO-plant, energy sources such as wind power, solar heating, PV, ground-source or air can be chosen. The base heating can either be brine to water heat pump, air to water heat pump or CHP, while the top heating can be selected as fuel boiler, electrical boiler or oil boiler. Solar thermal collectors and a ground-source heat pump were chosen as the main energy suppliers in the system design. Electrical boilers were chosen as auxiliary energy to cover the peak loads.

When the ESBO-plant is chosen, with the desired energy sources, a standard system solution designed by IDA ICE is created. This system deviates a lot from the system designed for the “Multikomfort” dwelling shown in Figure 27, and modifications had to be done in order for the two systems to be similar. In the “Multikomfort” system both vertical and horizontal ground-source heat exchangers are included and grey water is used to preheat both the water in the tank for space heating and the water in the tank for domestic hot water production. Even though the system in IDA ICE can be modified, there are limitations to the energy sources that can be selected, and grey water is not an option. The ground-source heat exchanger can be selected to be either vertical or horizontal, but including both is not possible. It was therefore difficult to design a system identical to the “Multikomfort” system. The swimming pool, which is included in the “Multikomfort” system for utilizing excess solar heat, was not possible to select in IDA ICE. The excess solar heat was instead only utilized to recharge the borehole. Designing the storage tanks similar to the tanks in the original system was very complicated, and modifications were done. In the “Multikomfort” system a combination unit which includes ventilation and domestic hot water preparation is included. The exhaust air heat pump supplies energy to the DHW storage tank and cooperates with solar energy in order to prepare domestic hot water. An exhaust air heat pump which connects the air handling unit to the plant in IDA ICE is not a setting which can be chosen, and in order to include this solution a self-composed exhaust air heat pump was created. For simplifications, the exhaust air heat pump does not heat the supply air, which is the intention in the “Multikomfort” system design. Additionally, in the “Multikomfort” system, the ventilation air is heated directly from the ground-source heat exchanger. In the system created in IDA ICE a heating coil was included in the air handling unit, and heat was supplied directly from the storage tank for space heating.

The flat plate solar collectors were provided with the same parameters as the Hewalex solar collector, and should theoretically obtain the same performance. It is decided in the “Multikomfort” design that the tilt angle of collectors should be 19°, facing the south-east and that the heat-transfer fluid is a 33 % mixture of glycol-water. The brine to water ground-source heat pump has a heating effect of 3 kW and a COP of 4.6, which is the same as for the Nilan Compact JWP 3 kW. The heating effect of the exhaust air heat pump was set to 1.2 kW and the COP was set to 3.9, which corresponds to the parameters given for the heat pump in the compact unit intended for the “Multikomfort” system. Additionally, only one borehole with a depth of 80 m was included with properties as shown in Table 22



Table 22 - Borehole properties

Properties		
Thermal resistance, $R_b$ [ $m^2 \cdot K/W$ ]	0.039	
Mass flow rate [ $kg/s$ ]	1.0	
	Ground	Grout
Specific heat capacity, $c_p$ [ $J/kg \cdot K$ ]	840	4180
Thermal conductivity, $k$ [ $W/m \cdot K$ ]	3.8	0.6
Density, $\rho$ [ $kg/m^3$ ]	288	1000

A sketch of the modified system design created in IDA ICE can be seen in Figure 45, and how the layout of the system looks in IDA ICE can be seen in *Appendix D – System Design in IDA ICE 4.6*.

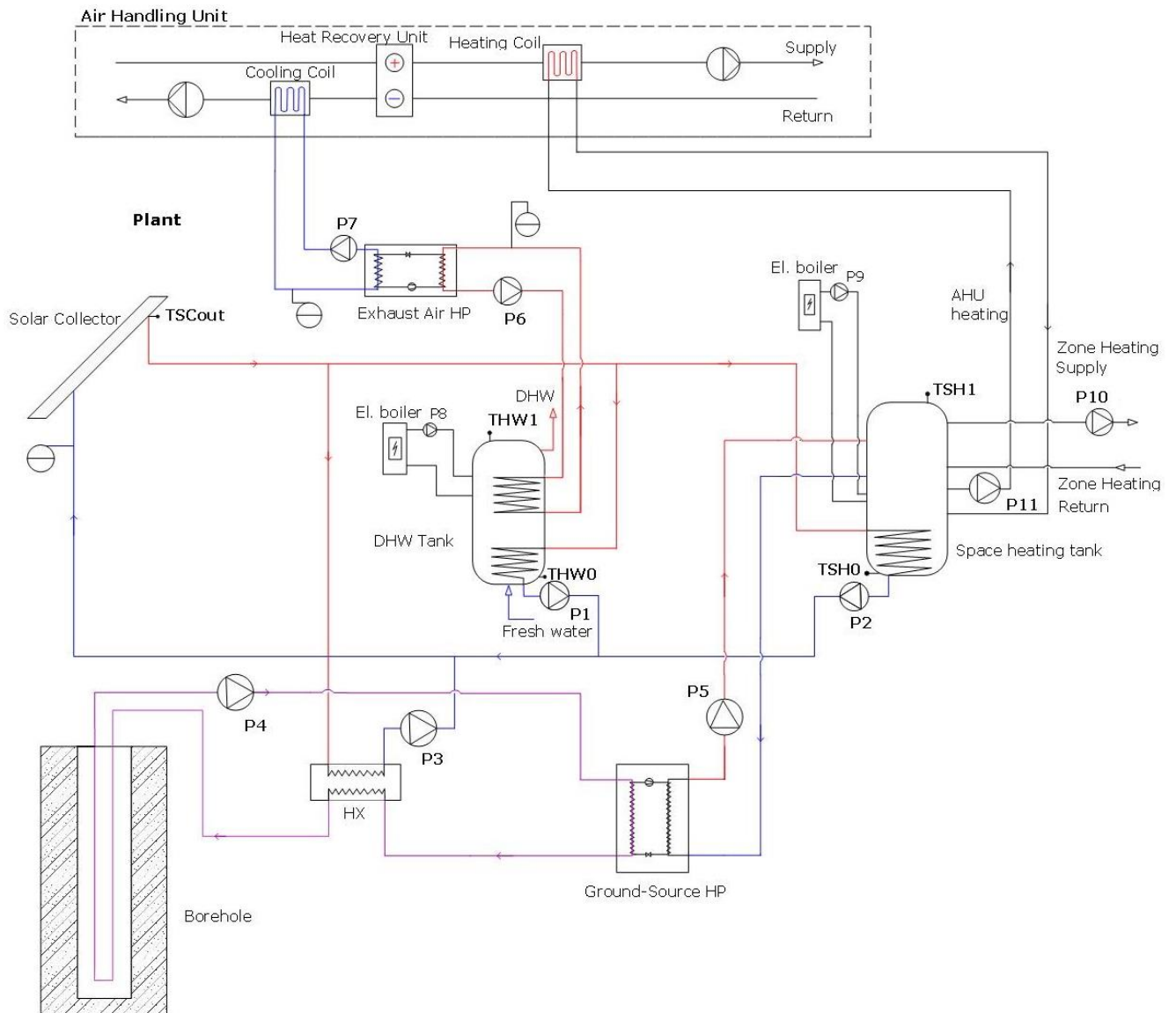


Figure 45 - System solution designed in IDA ICE

The system presented in Figure 45 consists of three main circuits: the solar circuit, the ground-source heat pump circuit and the exhaust air heat pump circuit. This system was designed based on the standard system created by IDA ICE, and some of the components found in the IDA ICE

system were reused in this system design. The control of the solar circuit and the exhaust air heat pump circuit was self-composed. How the system is intended to operate theoretically will be discussed in the next subchapters.

### *11.6.1 THE SOLAR CIRCUIT*

Solar energy is transported from the solar collectors to the DHW tank and the space heating tank through integrated solar spiral heat exchangers, or to the ground through a counter flow heat exchanger, as seen in Figure 45. A difference between the solar circuit in this system and the “Multikomfort” system seen in Figure 27 is the use of three-way valves. Including three-way valves was first tried, but it led to problems and complications and the system would not run. Trillat-Berdal et al. (2006), which performed a study on a similar system, found three-way valves to generate higher maintenance costs and complicate the control system. Circulation pumps were used instead (Trillat-Berdal, et al., 2006). The system created in IDA ICE worked better with circulation pumps, and even though the electricity consumption may be increased compared to the use of three-way valves, circulation pumps with an efficiency of 80 % were used instead.

The operating mode of the solar collectors is a function of the temperature registered at the solar collector outlet (TSCout) and the temperature registered at the integrated solar heat exchanger outlet in both tanks (THW0 and TSH0). THW0 is the temperature sensor located near the integrated solar heat exchanger outlet in the DHW tank, while TSH0 is the temperature sensor located near the integrated solar heat exchanger outlet in the space heating tank. The location of each temperature sensor is illustrated in Figure 45.

Domestic hot water preparation is the priority in the solar circuit and the circulation pump, P1, can be regarded as the main circulation pump in the solar circuit. The heat transfer fluid is circulated from the solar collectors through the DHW tank by P1, as seen in Figure 45. Circulation pump P1 is activated if  $(TSCout - THW0) > 5^{\circ}C$  and if  $THW0 < 60^{\circ}C$  as seen in Figure 46. The first temperature control setting ensures that solar heat is not transferred to the tank when the temperature difference between the solar collector and the DHW tank is minimal. This ensures that solar heat is not transferred to the tank when the tank temperature already is sufficient for DHW use, and when the solar collector temperature is too low to be utilized for DHW production. The temperature at the bottom of the tank is generally very low during the heating season, as is the temperature in the solar collector due to low solar insolation. The temperature difference  $(TSCout - THW0)$ , which is most likely lower than  $5^{\circ}C$  in this period, ensures that the energy provided by the solar collector is not utilized for domestic hot water as the temperature in the collectors are not adequate. During spring, summer and early autumn the temperature in the solar collectors will increase to up to  $60-70^{\circ}C$  due to the increased solar irradiation. The temperature difference,  $(TSCout - THW0)$ , will as a consequence of this, increase as well. Solar energy can therefore be utilized for domestic hot water production. Additionally, a temperature difference of  $5^{\circ}C$  ensures that the circulation pumps do not consume more electricity than necessary. The second temperature control setting ensures that the circulation pump will be turned off when the temperature registered by THW0 exceeds  $60^{\circ}C$ . When the temperature near the bottom of the tank is  $60^{\circ}C$ , the temperatures at the top of the tank will be higher due to the thermal stratification in the tank. The circulation pump is turned off to make sure that the temperature in the tank does not exceed the boiling point of the storage water.

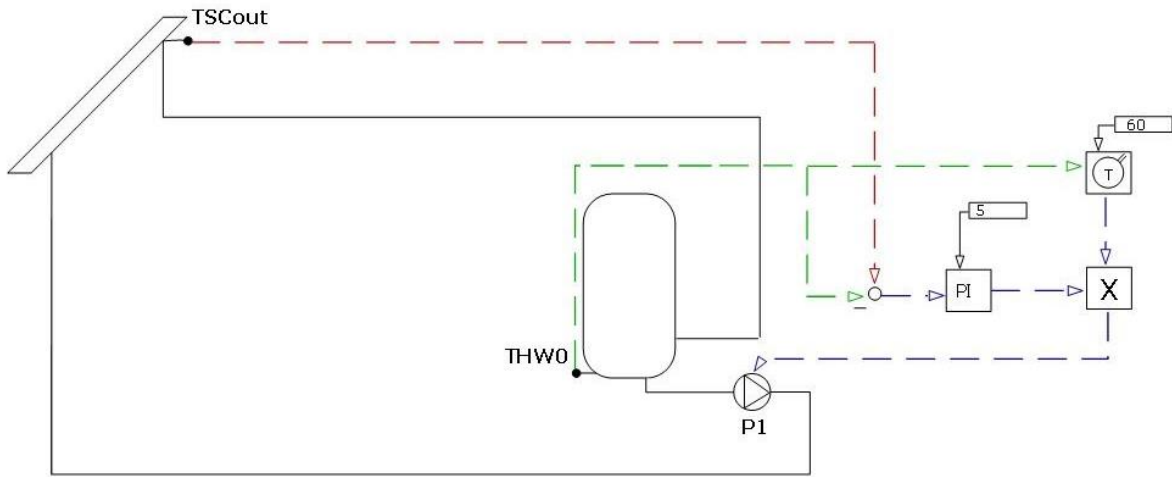


**Figure 46 - Control of circulation pump P1, DHW preparation**

Using solar energy for space heating purposes is the second priority in the system. Circulation pump P2, which circulates the heat transfer fluid from the solar collector to the space heating tank, is activated when  $(TSCout - TSH0) > 5^{\circ}\text{C}$  and when  $T_{indoor} < (T_{setting} + 3^{\circ}\text{C})$ , otherwise it is turned off. The control is illustrated in Figure 47.  $T_{indoor}$  is the measured air temperature in the dwelling, while  $T_{setting}$  is the zone set point temperature, which is  $21^{\circ}\text{C}$ . The indoor setting is increased with  $3^{\circ}\text{C}$  in order to utilize solar energy to cover parts of the space heating demand and as a result, to decrease the operating time of the ground-source heat pump. With these settings, solar energy should not be supplied to the building (or space heating tank) during the summer months since the measured indoor air temperature is likely to be above  $24^{\circ}\text{C}$ . As for the control of P1, the temperature difference between the solar collector outlet and TSH0 has to be sufficiently large in order for the contribution of solar energy to make a difference to the temperature in the space heating storage tank.

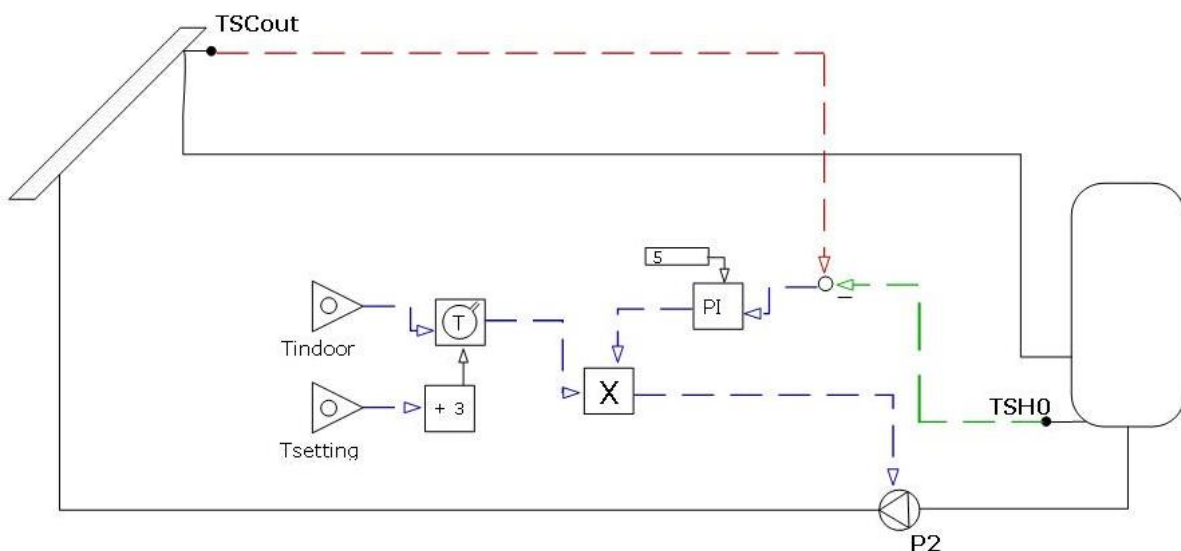


**Figure 47 - Control of circulation pump P2, space heating preparation**

When the temperature registered by THW0 exceeds  $60^{\circ}\text{C}$ , P1 is turned off and P3 is activated. Circulation pump P3 is utilized to circulate heat transfer fluid from the solar collector to the ground when excess solar heat is produced. The control can be seen in Figure 48. When the

temperature near the bottom of the DHW tank exceeds 60°C, solar heat is utilized to recharge the borehole. It is desirable to recharge the borehole in order to enhance the operation of the heat pump, but this control setting may also be regarded as a heat protection initiative for the solar collectors. When the DHW tank storage water exceeds the maximum allowable temperature, the heat transfer fluid is sent to the ground in order to prevent overheating of the solar collectors.

For optimizing the system it would be interesting to see if recharging the borehole during heating season as well would have an effect. P3 would in that case be activated when  $(T_{SCout} - THW0) < 5^\circ\text{C}$  as well, resulting in additional operating time for the thermal solar collectors, which would enhance the collector performance.

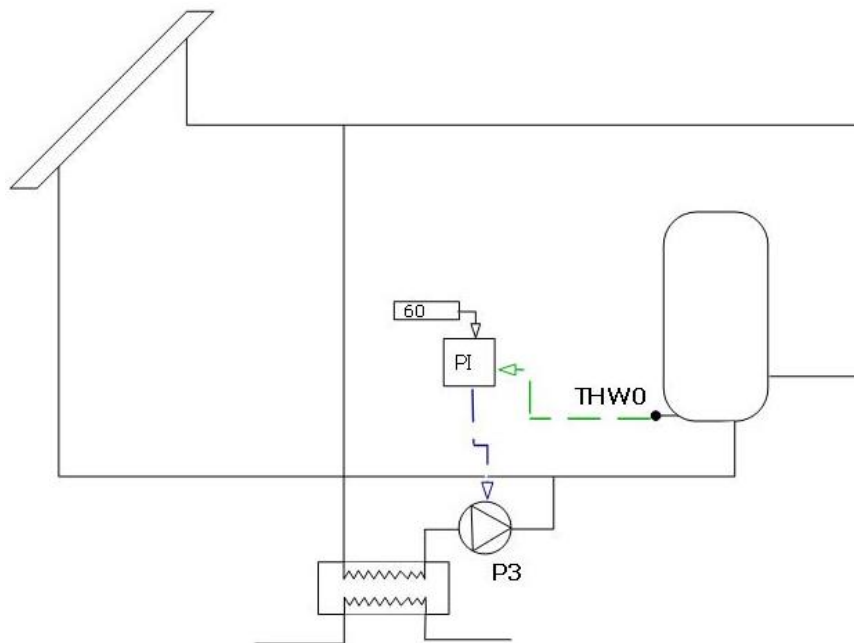


**Figure 48 - Control of circulation pump P3, recharging the borehole**

As seen in Figure 46, Figure 47 and Figure 48, all circulation pumps in the solar circuit are controlled by a PI-controller. The PI-controller was set to cooling type control mode, which means that the controller will only send an ON-signal when the measured in-signal is higher than the set point of 5°C or 60°C respectively. In Figure 46 and Figure 47 an ON/OFF thermostat is included as well. The thermostat will only send an ON-signal when the measured in-signal is lower than the set point of 60°C and 24°C respectively.

### 11.6.2 THE GROUND-SOURCE HEAT PUMP CIRCUIT

Energy collected from the ground is transferred to the space heating tank by a ground-source heat exchanger and a ground-source heat pump. The control system of the heat pump is created by IDA ICE for the standard system. The heat pump and the belonging circulation pump, P5 shown in Figure 45, are controlled by a PI-controller, and are activated when the measured temperature at the top of the space heating tank, TSH1, is lower than the set point temperature of 35°C. Additionally, the PI-controller attempts to keep the *fill ratio* of the space heating tank at a constant level of 0.2. "The fill ratio is defined as the degree at which the tank is filled with water at the highest required set point, i.e. if all water is heated to the highest set point, the fill

ratio is 1, while if the whole tank holds the ambient temperature (20°C), the fill ratio is zero” (Equa, 2013).

### 11.6.3 THE EXHAUST AIR HEAT PUMP CIRCUIT

An exhaust air heat pump is included in the system in order to utilize energy in the exhaust air for DHW production. When solar energy is not sufficient for this purpose the energy supplied by the exhaust air heat pump ensures that the required DHW temperature is reached. Energy is collected from the return air in the air handling unit by a cooling coil, and transferred to the DHW tank by a water to water heat pump as seen in Figure 45. The exhaust air heat pump in the “Multikomfort” system is an air to water heat pump, and not a water to water heat pump, as in this system. Creating an air/water heat pump in IDA ICE was challenging. It was therefore decided to simplify and use a water to water heat pump instead.

The exhaust air heat pump and the belonging circulation pumps, P6 and P7 which can be seen in Figure 45, are controlled by a PI-controller which attempts to keep the temperature at the upper part of the tank at 60°C. The exhaust air heat pump is activated when the temperature registered by temperature sensor THW1, seen in Figure 49 is lower than 60°C.

### 11.6.4 THE DOMESTIC HOT WATER TANK

Hot water storage tanks are generally considered to be the most important components in a solar heating system. Two storage tanks are included in this system design, one for DHW preparation, and one buffer tank for space heating. An illustration of the tank layers, inlets, outlets and location of the temperature sensors in the DHW tank is shown in Figure 49.

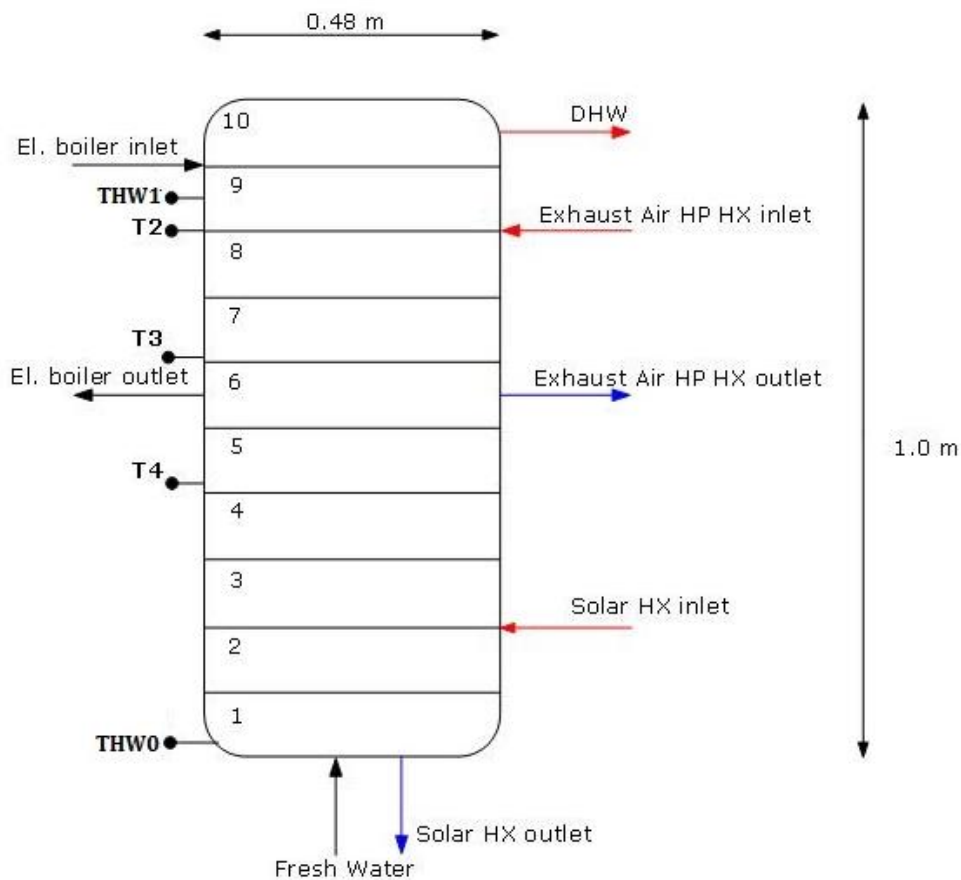


Figure 49 - DHW Tank

In order to calculate the thermal performance of solar heating system it is necessary to be able to calculate the temperatures everywhere in the tank. As seen in Figure 49 the tank is divided into 10 layers, which makes it possible for the simulation program to calculate the vertical thermal stratification in the tank. Achieving thermal stratification is important for the thermal performance of the system. This is discussed in more detail in chapter 7.2 *Design of the Storage Tank*.

A good thermal stratification relies on an appropriate tank design. The storage tank shown in Figure 49 holds approximately 180 liters of hot water, and has a height/diameter (h/d) ratio of 2.08, which is satisfying considering that the tank is a spiral tank. The solar heat exchanger inlet is located at Layer 2, near the bottom of the tank which is common with a high-flow spiral tank. When solar energy is transferred from the heat exchanger to the tank, a temperature rise in all the layers will occur, especially from Layer 3 and upwards. Connecting the exhaust air heat pump to the upper part of the tank ensures that the thermal stratification is maintained, since the temperature at this level in the tank corresponds to the inlet temperature from the exhaust air heat pump. Unlike the inlet temperatures from the solar circuit, the inlet temperatures from the exhaust air heat pump are relatively constant through the year due to the more stable energy source.

An electrical boiler is connected to the upper part of the tank as seen in Figure 45. With an increase in domestic hot water demand, which cannot be met by the supplied solar or exhaust air energy, the electrical boiler ensures that the peak loads are covered. Hot water, which holds a temperature of 65°C, is supplied to the tank by the electric boiler.

The boiler is also installed as a security if the solar collectors and/or the exhaust air heat pump fail. In order to cover the domestic hot water demand, the auxiliary electrical volume in the tank should be in the 60–100 liter range (Furbo, 2005). The auxiliary electrical volume in the DHW tank is approximately 60 liters. It is however desirable that the volume heated by the auxiliary electrical energy is as small as possible in order to increase the thermal performance of the system. The boiler circulation pump, P8, is activated when the temperature registered by temperature sensor THW1, seen in Figure 49, is lower than the set point temperature of 55°C. It is desirable that the exhaust air heat pump is activated before the electrical boiler in order to decrease the operating time of the boiler. This may be done if the temperature sensor connected to the operation of the exhaust air heat pump is located lower than the temperature sensor for the electrical boiler. Both the exhaust air heat pump and the boiler are connected to the same temperature sensor in the system design presented in Figure 45. A better solution may be to connect them to separate temperature sensors in order to achieve a better result.

The heat loss coefficient of the tank top, bottom and coat as well as the height/diameter ratio of the DHW storage tank is given in Table 23.

**Table 23 - Main characteristics of DHW Tank**

<b>Main characteristics of DHW tank</b>	
<b>U<sub>Coat</sub> [W/m<sup>2</sup>K]</b>	0.4
<b>U<sub>Top</sub> [W/m<sup>2</sup>K]</b>	0.4
<b>U<sub>Bottom</sub> [W/m<sup>2</sup>K]</b>	0.4
<b>Height/diameter ratio</b>	2.08

### 11.6.5 THE SPACE HEATING STORAGE TANK

An illustration of the space heating tank with its pipe connection points, layers and temperature sensor locations, is shown in Figure 50.

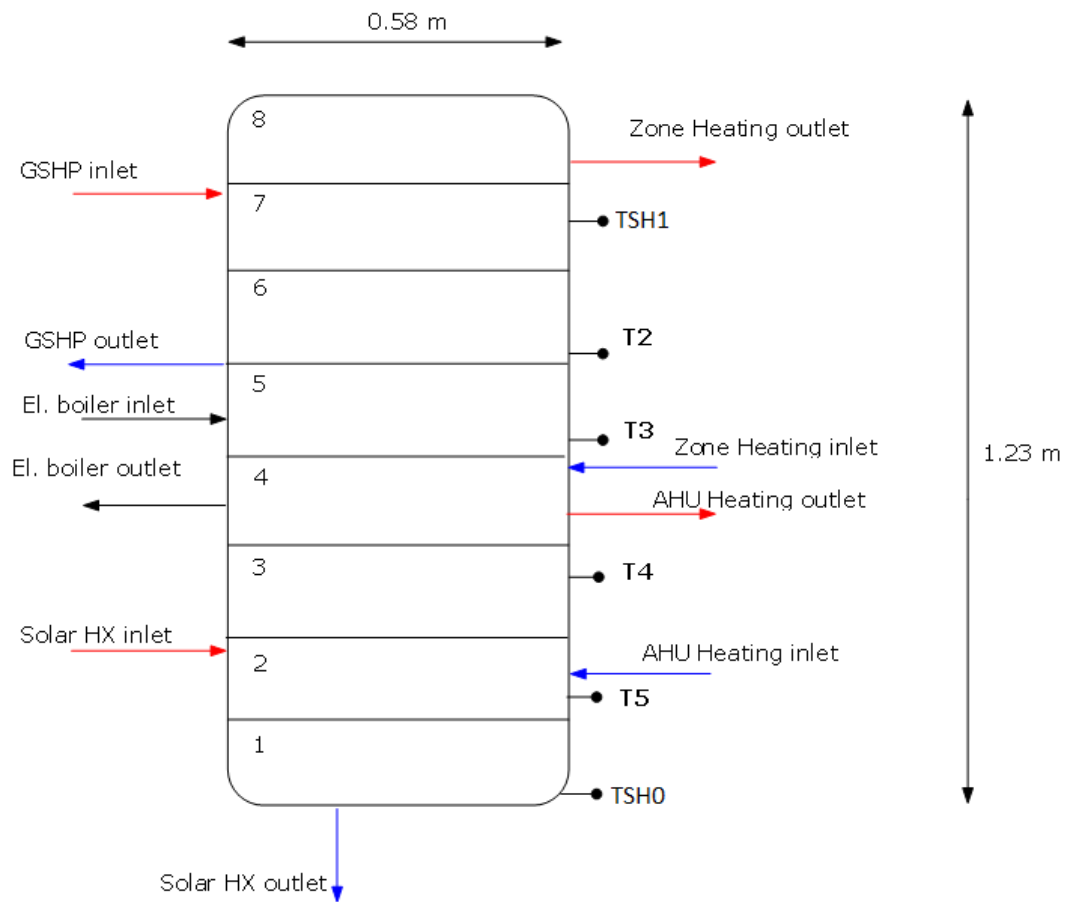


**Figure 50 - Space heating Tank**

The space heating tank (SH tank) holds 325 l of hot water, and has a h/d ratio of 2.12, which is a bit higher than for the DHW tank. The tank is divided into 8 layers in order for the simulation program to calculate the temperature at each layer and the vertical thermal stratification. Due to the control settings of circulation pump P2, found in the subchapter *11.6.1 The Solar Circuit* in Figure 47, a temperature rise will most likely occur in April/May and September/October when the solar irradiation is adequate, and the outside temperature is lower than during the summer months.

Hot water for the zone heating (ZH) system and the air handling unit heating coil is drawn from the tank at different locations according to desired hot water temperature. The zone heating outlet is located near the top where the highest temperatures are found, while the AHU heating outlet is located at the middle of the tank.

Energy is supplied to the tank by three sources: ground-source, solar heat and electricity by the electrical boiler. As for the DHW tank, the integrated solar spiral is located near the bottom of the tank, and the ground-source heat pump inlet is located at the upper part of the tank, as seen in Figure 50. The ground-source heat pump supplies reliable and constant temperatures to the tank through the year due to a more reliable energy source. When connected to the upper part of

the tank, the set point temperature of 35°C is likely to be met by the ground-source heat pump through the year, resulting in shorter operating time of the auxiliary electrical boiler. However, the electrical boiler is included to cover peak loads and as a security if failures in the system occur. The temperature supplied to the tank from the electric boiler holds 45°C.

Circulation pumps P10 and P11 shown in Figure 45, which ensures circulation of hot water to the zone heating circuit and the AHU heating circuit respectively, are controlled by an ON/OFF thermostat. When the outside air temperature is lower than 18°C, the circulation pumps are activated and hot water is supplied to the heating system in the single-family dwelling and to the heating coil in the air handling unit.

The heat loss coefficient of the tank top, coat and bottom as well as the height/diameter ratio of the SH tank are given in Table 24.

**Table 24 - Main characteristics of SH Tank**

<b>Main characteristics of SH tank</b>	
<b>U<sub>Coat</sub> [W/m<sup>2</sup>K]</b>	0.3
<b>U<sub>Top</sub> [W/m<sup>2</sup>K]</b>	0.3
<b>U<sub>Bottom</sub> [W/m<sup>2</sup>K]</b>	0.3
<b>Height/diameter ratio</b>	2.12



## 12 SYSTEM PERFORMANCE

The system illustrated in Figure 45 was simulated in IDA ICE 4.6 with a solar collector area of 16 m<sup>2</sup> and floor heating as heating system in the dwelling. With an oversized solar collector area, excess solar heat is produced and can be utilized to recharge the borehole during the summer months. It was chosen to perform the simulation with an oversized collector area since this seemed to be of more interest. An energy simulation for the year 2013 was performed.

This chapter is included in order to show that the system created in IDA ICE is operating as desired, and therefore can be used as a reference system when the further optimization of the system is performed.

It should be noted that all temperatures in the system is registered by IDA ICE even though the respective components in the system are not in operation. For instance, even though the ground-source heat pump is inactive during the cooling season, temperatures from the heat pump to the storage tank are presented. When this is the case, the power consumption of the component or the heat input is presented for better understanding of the components' operation.

In order to get a better understanding of the system as a whole, results such as the incoming solar radiation, the collected solar heat through the year, the mass flow rates in the system and the inlet and outlet temperatures of the solar collector are included. Results related to the subjects discussed in chapter 11.6 *Plant* are presented.

### 12.1 THE SOLAR CIRCUIT

#### 12.1.1 INCOMING RADIATION PER SOLAR COLLECTOR AREA AND COLLECTED HEAT

The incoming solar radiation per m<sup>2</sup> of solar collector area is shown in Figure 51.

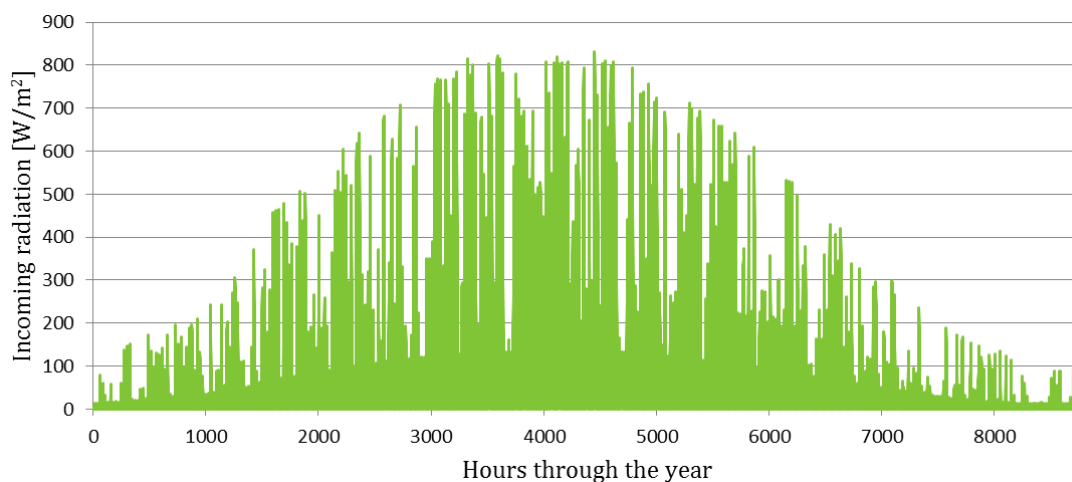


**Figure 51 - Annual incoming solar radiation per solar collector area**

The incoming solar radiation is mainly affected by the local weather, and is divided into both direct and diffuse radiation. The incoming radiation is normally measured as it hits a surface perpendicular to the sun. On a sunny day during the summer time in the south of Norway the incoming radiation may get as high as 1000 W/m<sup>2</sup> collector area, but on a cloudy day it may be as low as 300 W/m<sup>2</sup> (Zijdemans, 2012). During winter, the incoming solar radiation can be as low as 100 W/m<sup>2</sup>, which seems to agree well with the result presented in Figure 51.

The annual solar energy collected by the installed solar collectors is shown in Figure 52.

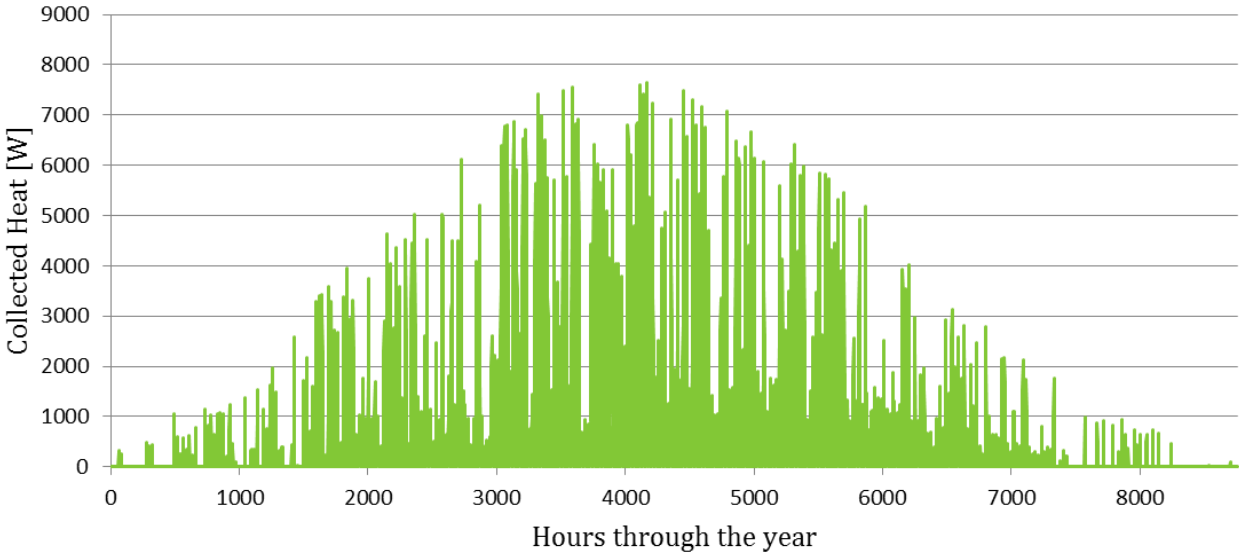


**Figure 52 - Annual collected heat**

The collected heat is dependent of the solar collector efficiency and thereby the design of the solar collector. According to the steady state calculations performed in chapter 10.2.3 *Steady State Calculations*, the collected heat was calculated to be approximately 7000 W with a collector aperture area of 14.56 m<sup>2</sup> and an incoming radiation of 800 W/m<sup>2</sup>. During the summer months the incoming radiation is approximately 800 W/m<sup>2</sup> as seen in Figure 51, and the collected heat during the same period is approximately 7000 W as seen in Figure 52. These results support the performed calculations.

**12.1.2 TEMPERATURE DIFFERENCE**

The temperature difference between the outlet and inlet heat transfer fluid circulating through the solar collector is of great importance to the collector thermal performance. It is desirable to have low inlet temperatures in order to collect as much heat as possible. A temperature difference of 10 K is sensible to use when calculating the theoretical collector thermal performance (DGS, 2005).

The solar collector outlet temperature is shown in Figure 53.

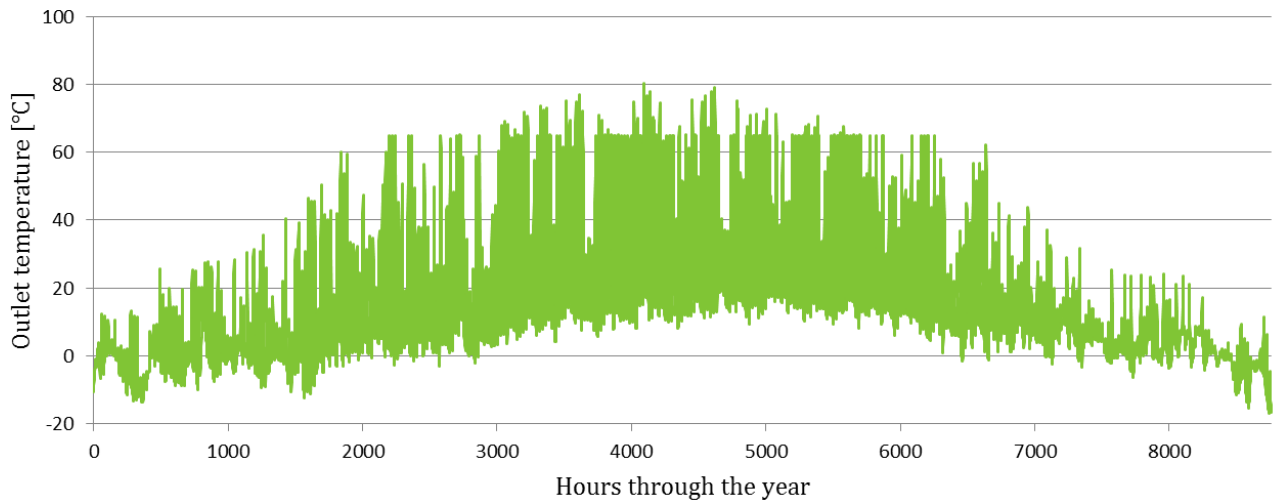


**Figure 53 - Outlet temperature solar collector**

As seen from Figure 53, the outlet temperatures from the solar collector are close to 80°C during the summer months, while during the winter the temperature is just below 20°C.

Due to the high heat losses, which are experienced with flat plate solar collectors, the operating temperature is usually limited to less than 80°C. It is possible to achieve higher operating temperature if the flat plate collector is installed with vacuum insulation or convection suppression (Morrison, u.d.).

The temperature difference between the outlet and inlet temperature of the solar collector through the year is illustrated in Figure 54.

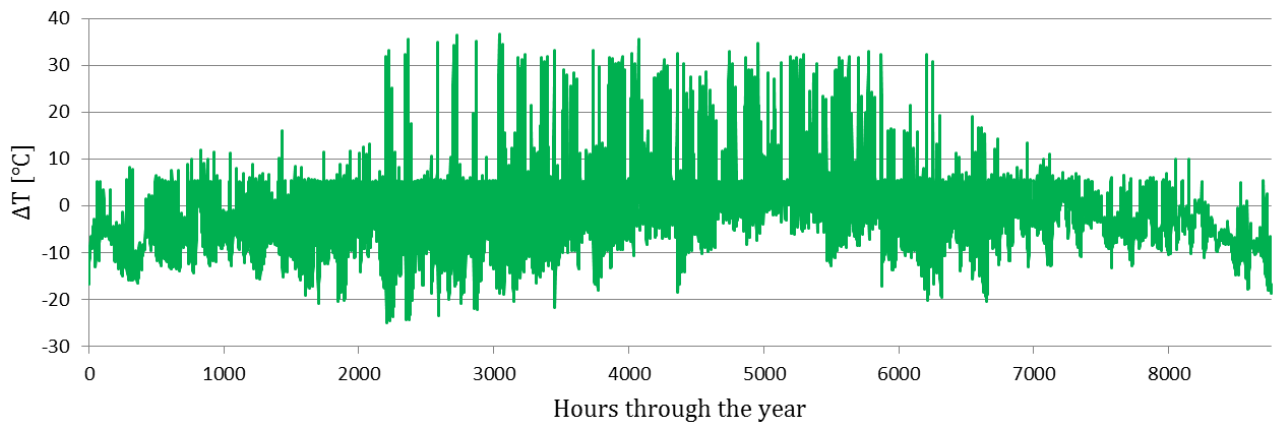


**Figure 54 - Temperature difference, outlet and inlet solar collector temperature**

The temperature difference during the summer months is approximately 30°C, which is desirable. On sunny days during the winter months it can be seen that the temperature difference is at least 5°C, which means that adequate solar heat can be collected and utilized for DHW preparation or to preheat the hot water for space heating. It can be seen from Figure 54 that useful heat can be collected in March, which is represented by the hours ranging from 1400-2100. This is also case in the period 5800-7000, which represents September/October.

### 12.1.3 MASS FLOW RATE

The mass flow rate through the solar collectors depends on the system design and the choice of hot water tanks for short-time storage. In this system design the storage tanks are both spiral tanks. According to Furbo (2004) the flow rate through the solar collector, and thereby through the integrated spiral heat exchanger, should be about 1.0 l/min·m<sup>2</sup> solar collector area (Furbo, 2004). This corresponds to a mass flow rate of 0.016 kg/s per solar collector area, when considering the density of the water-glycol mixture. Zijdemans (2012) operates with an equation in order to calculate an adequate mass flow rate, which is given in Equation 27.

$$\dot{V} = \frac{\varphi}{\rho \cdot c_p \cdot \Delta T} \left[ \frac{m^3}{s} \right] \quad (27)$$

where,

$\varphi$  is the maximum collected heat [W]

$\rho$  is the heat transfer fluid density [kg/m<sup>3</sup>]

$c_p$  is the fluid specific heat capacity [J/kg·K]

$\Delta T$  is the temperature difference

By using the maximum collected heat of 7000 W given in Figure 52, the calculated density and heat capacity given in Table 7 and a temperature difference of 10 K, the volume flow rate for this system should be approximately 0.17 kg/s and 0.012 kg/s·m<sup>2</sup> solar collector area.

The mass flow rate through the solar collectors is shown in Figure 55. During the summer months when the solar collectors have longer operational time, the mean mass flow rate is approximately 0.16 kg/s, which agrees with the flow rate calculated by Equation 27.

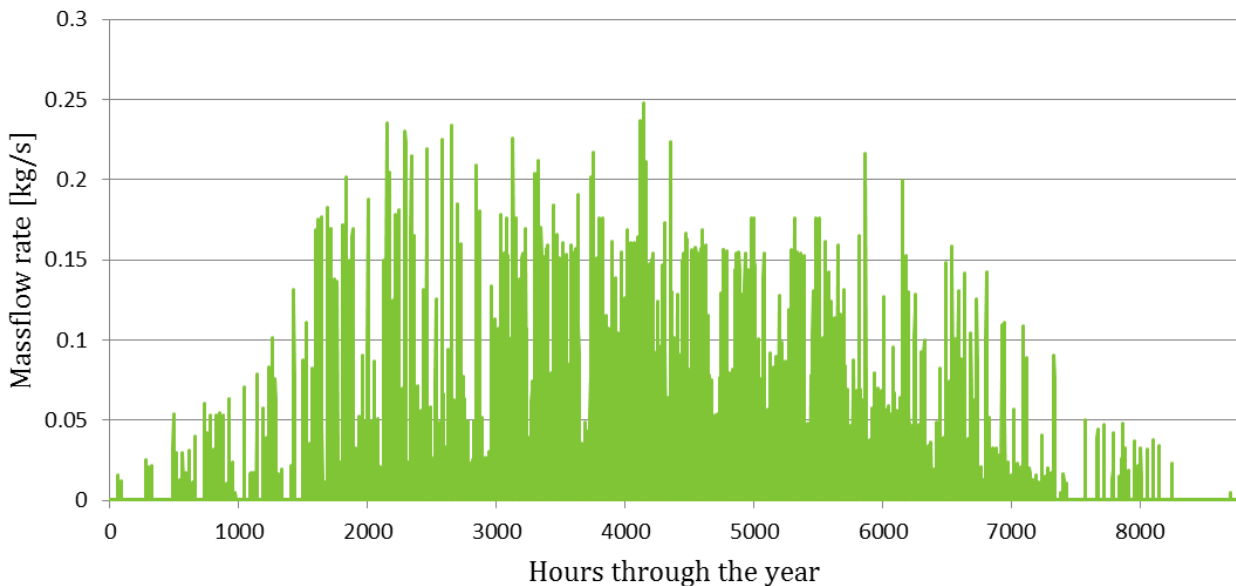
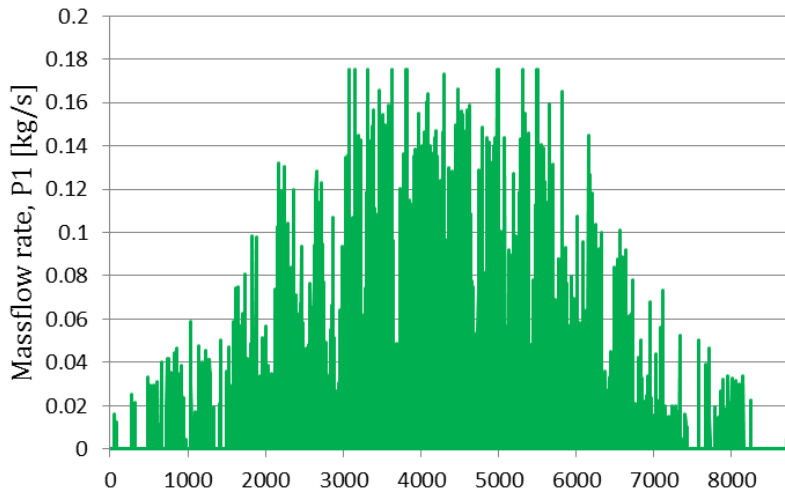
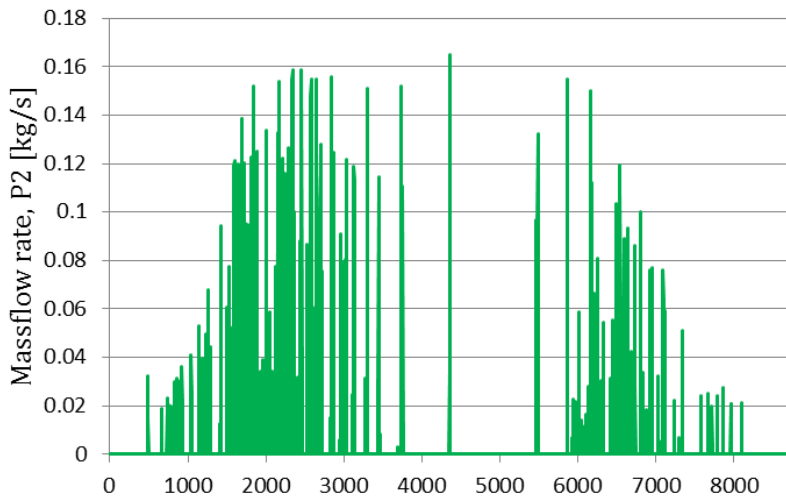


Figure 55 - Mass flow rate through the solar collectors

The mass flow rate through each of the circulation pumps in the solar circuit is shown in Figure 56-Figure 58.



**Figure 56 - Mass flow rate, circulation pump P1, DHW circuit**



**Figure 57 - Mass flow rate, circulation pump P2, space heating circuit**

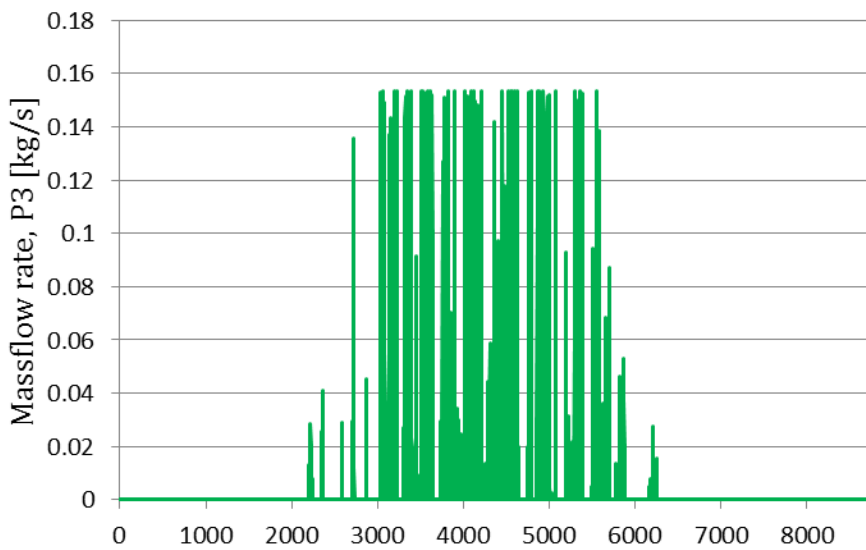


**Figure 58 - Mass flow rate, circulation pump P3, recharging the borehole**

The mass flow rate through each of the circulation pumps indicates when each pump is in operation. Circulation pump P1, which operates through the year in order to provide or preheat

domestic hot water, has the highest flow rate during the summer months when the majority of solar irradiation is available. Circulation pump P2 is controlled to operate when the indoor temperature is lower than 24°C and when the temperature difference between the bottom of the SH tank and the solar collector outlet temperature is higher than 5°C. As seen in Figure 57, P2 is in operation in the heating season and not during the summer months. However, a peak can be seen in July between the hours 4000 and 5000. The temperature inside the building is higher than 24°C at this point, and the peak is therefore regarded as a miscalculation by IDA ICE. Circulation pump P3 is only activated when excess solar heat is produced and dumped to the borehole for storage. Excess solar heat is produced during the summer months, and as seen in Figure 58, circulation pump P3 is only activated in this period when the solar insolation is high.

#### 12.1.4 CONTROL OF THE CIRCULATION PUMPS

How the circulation pumps P1, P2 and P3 are intended to be controlled has been discussed in the chapter 11.6.1 *The Solar Circuit* and shown in Figure 46-Figure 48. How well the control seems to work is presented in this chapter.

The operation of circulation pump P1, which circulates the heat transfer fluid from the solar collector to the DHW tank, is shown for a day in June in Figure 59.

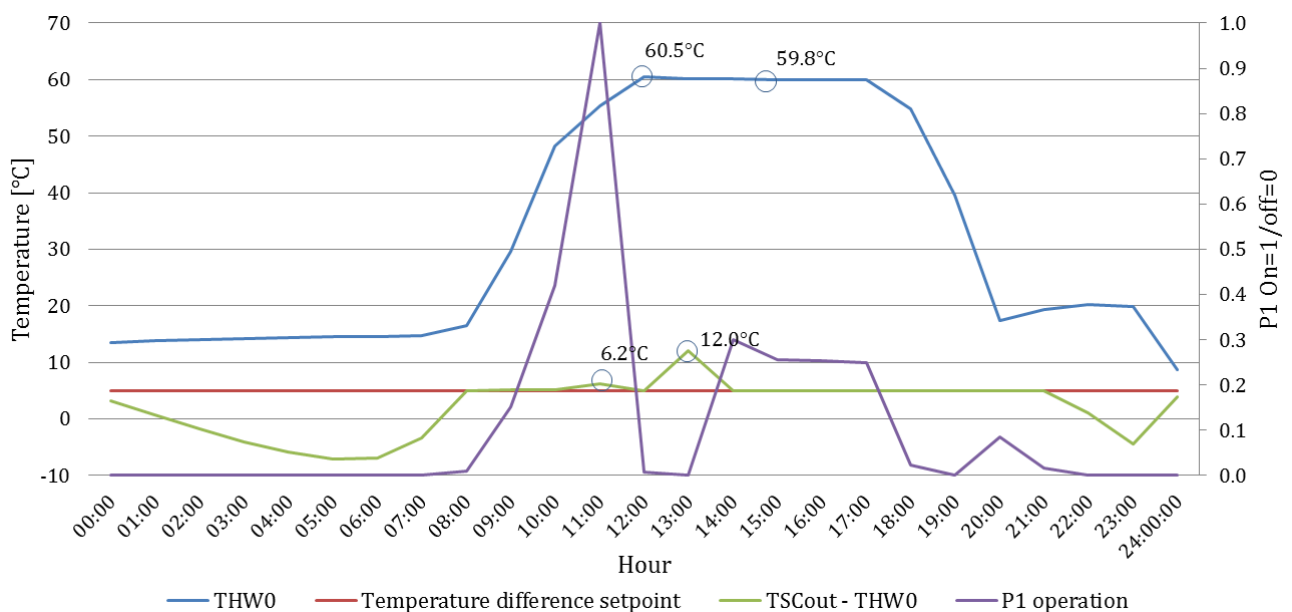


Figure 59 – Operation of circulation pump P1 2013-06-01

P1 is controlled by a PI-controller which turns the pump off when the temperature difference between TSCout and THW0 is below 5°C and when THW0 is above 60°C. The operation of the pump is illustrated by the purple line in Figure 59. The blue line is the temperature which is measured near the bottom of the DHW tank where the outlet of the solar heat exchange spiral is located. It can be seen from Figure 59 that the temperature at the bottom of the tank increases throughout the day when solar irradiation is high. Maximum temperature is reached at 12:00 pm and is as high as 60.5°C. The temperature difference between the solar collector outlet temperature and the temperature measured at the solar heat exchanger outlet is represented by the green line in Figure 59. This temperature difference is compared to the constraint of 5°C, which is represented by the red line. When the temperature difference is close to 5°C, P1 starts to operate as illustrated between 08:00 pm and 10:00 pm. The temperature near the bottom of

the tank increases, and when it exceeds 60°C, the pump is turned off even though the temperature difference is above 5°C. This is illustrated at approximately 12:00 pm in Figure 59. The pump starts to operate again when the temperature at the solar heat exchanger outlet decreases and when the temperature difference is above 5°C. After 21:00 pm, the temperature difference decreases to below 5°C, and the pump is turned off. The circulation pump is variable-speed regulated, which means that if the temperature difference is slightly below 5°C or if THW0 registers temperatures slightly above 60°C, the pump will not be shut completely off. Instead the volume flow rate is regulated according to the input signal. With this control, rapid on/off operation is avoided, which in addition to increase the electricity consumption, can harm the pump itself.

The operation of circulation pump P2, which ensures that the solar heat transfer fluid circulates through the SH tank, is shown in Figure 60 for a day in the middle of April.

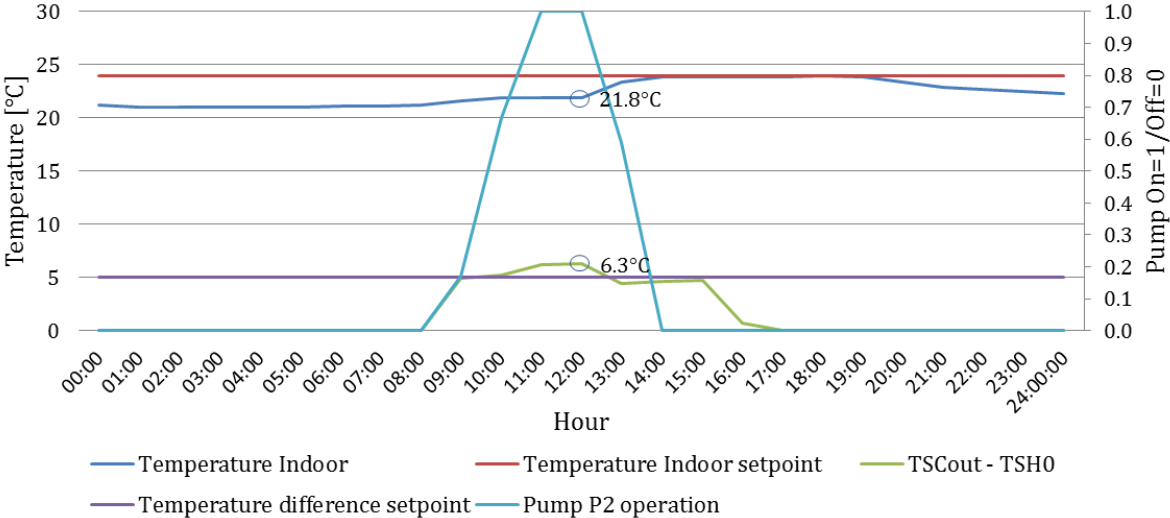


Figure 60 - Operation of circulation pump P2 2013-04-18

The operation of circulation pump P2 is also shown in Figure 61, but this time for a day in July.

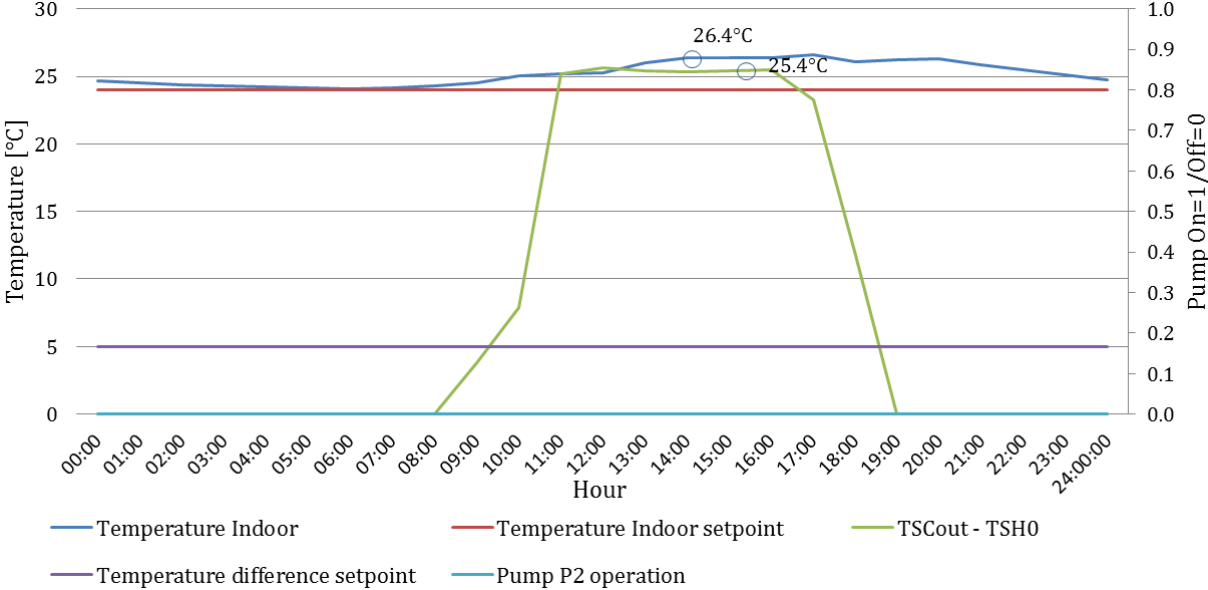


Figure 61 - Operation of circulation pump P2 2013-07-06

The operation of P2 is represented by the turquoise line in both Figure 60 and Figure 61, while the temperature difference between the solar collector outlet and the bottom of the SH tank is given by the green line. The purple line is the temperature difference constraint of 5°C. The indoor air set point temperature of 24°C is represented by the red line, and the actual indoor air temperature measured is represented by the blue line.

In Figure 60 it can be seen that the indoor temperature never exceeds the set point temperature of 24°C, which means that a positive signal is sent to the PI-controller. The pump is then only activated when the temperature difference between the outlet temperature from the solar collector and the outlet temperature from the integrated solar heat exchanger is higher than 5°C, as seen between 09:00 pm and 13:00 pm in Figure 60.

Figure 61 represents a summer scenario when the indoor temperature exceeds the set point temperature. Even though the temperature difference between the outlet collector temperature and the outlet heat exchanger temperature exceeds the set point temperature of 5°C most of the day, the pump is never activated since there is no need for space heating during the summer day.

The operation of circulation pump P3, which ensures that excess solar heat is dumped to the borehole, is shown in Figure 62 for a day in June.

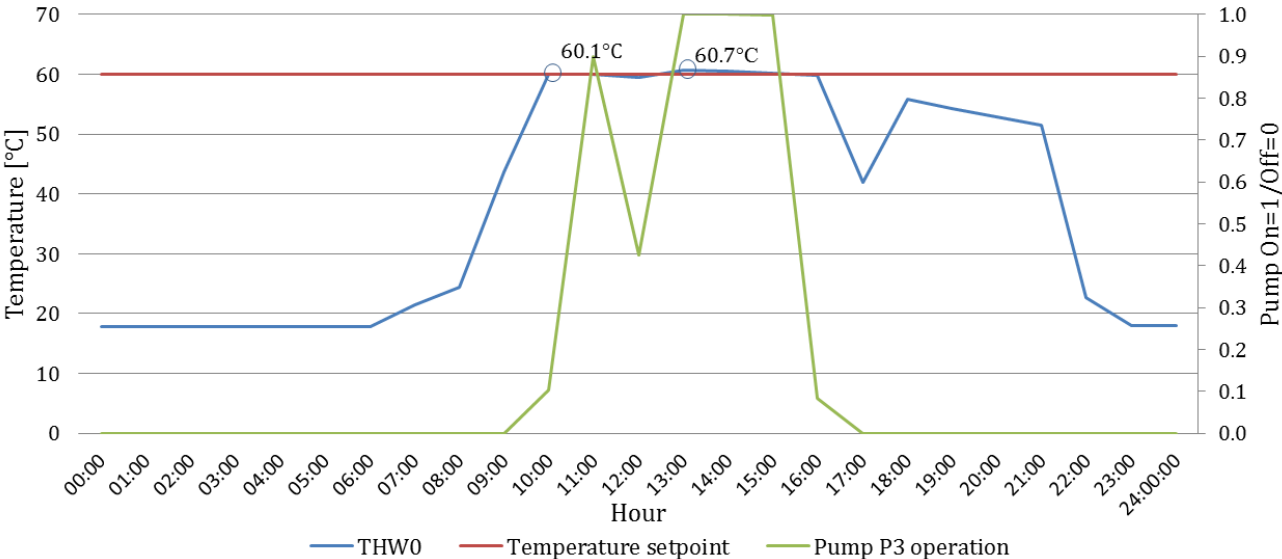


Figure 62 - Operation of circulation pump P3 2013-06-20

The operation of P3 is represented by the green line in Figure 62, while the temperature registered at the bottom of the DHW tank, THW0, is represented by the blue line. The temperature constraint of 60°C is represented by the red line.

It is illustrated in Figure 62 that the circulation pump is only activated when the temperature at the solar heat exchanger outlet exceeds 60°C. When the storage water near the bottom of the tank reaches the set point temperature, there is no longer need to utilize solar energy for domestic hot water production as the temperatures in the tank are high enough. If the system was an ordinary domestic hot water solar heating system, the solar collectors would not be in operation at this point. However, by utilizing the excess heat to recharge the borehole, the collectors have longer operational time and thereby better thermal performance.



### 12.1.5 SOLAR ENERGY IN THE SOLAR CIRCUIT

How the collected solar heat is distributed between the DHW tank, the SH tank and the borehole through the year is shown in Figure 63.

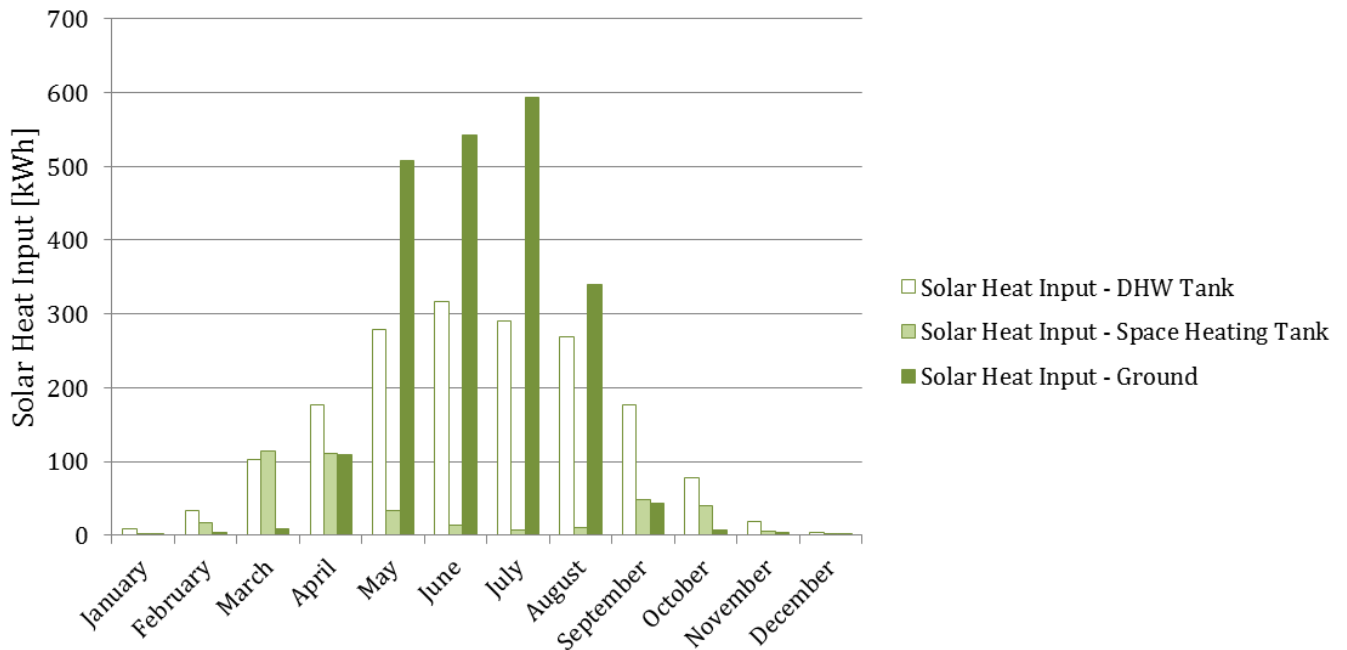


**Figure 63 - Heat flow from solar circuit to DHW tank, SH Tank and to ground**

Solar heat is transferred to the DHW tank from January to November, and the highest heat input is found during the summer months. Approximately 300 kWh is transferred to the DHW tank in June. Since circulation pump P1 is not in operation when the temperatures near the bottom of the tank exceeds 60°C due to the control setting, excess solar heat is transferred to the ground as seen in Figure 63. The borehole is recharged with solar heat from April to September, and the highest heat input is found from May to August, which is expected. Approximately 600 kWh of solar heat is transferred to the ground in July, which is twice as much as the heat transferred to the DHW tank in the same month. By increasing the control setting of 60°C, more solar heat would probably be utilized for DHW production instead of recharging the borehole. However, when increasing the temperature set point at the bottom of the DHW tank, the temperature at the top of the tank may exceed its maximum allowable temperature.

A simulation was performed where excess solar energy was not utilized for recharging the borehole as well. By comparing the results it was proven that recharging the borehole with excess solar heat resulted in a slight increase in evaporator brine inlet temperature from April to October. Due to the increase in brine inlet temperature, a slight increase in the GSHP COP was observed as well.

Transferring solar heat to the SH tank is the second priority in the solar heating system. As seen in Figure 63, solar heat is transferred to the SH tank during the heating season. The highest solar heat input is found in March and April, and approximately 100 kWh of solar energy is transferred to the SH tank in these months. It can be seen that solar heat is also utilized for space heating in September and October. Detailed graphs which visualize the solar heat transfer to the storage tanks are found in the subchapters *12.4 The DHW Tank* and *12.5 The Space Heating Tank*.

## 12.2 THE GROUND-SOURCE HEAT PUMP

The entering brine evaporator temperature and the temperature from the ground-source heat pump to the SH tank are illustrated in Figure 64. The dark green line represents the entering evaporator temperature from the ground, while the lighter green represents the leaving condenser temperature from the GSHP.

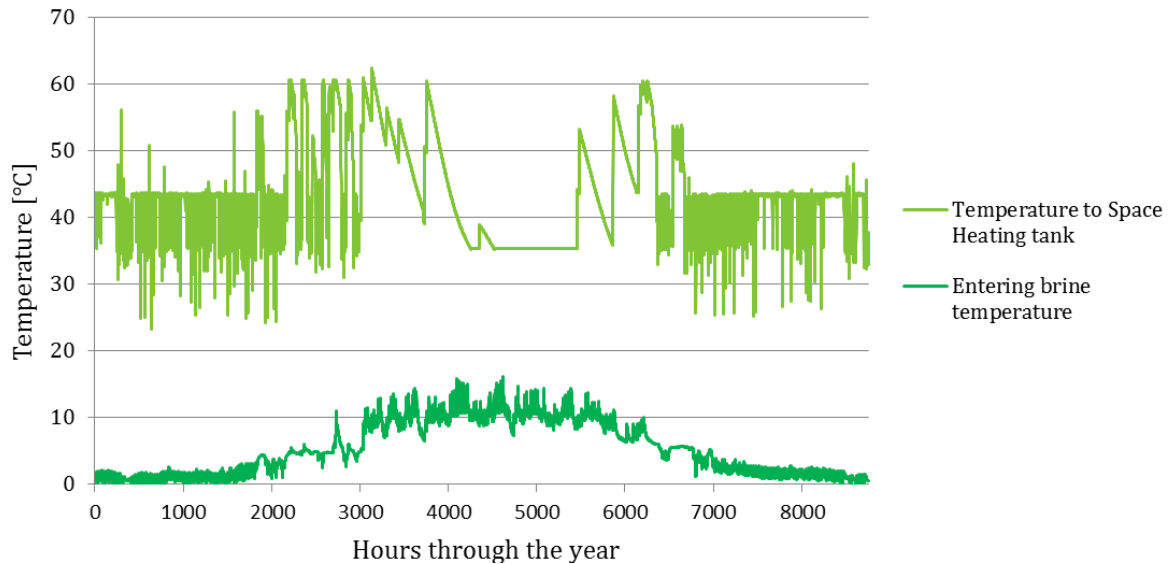


Figure 64 - Entering brine and leaving water temperature GSHP

As seen in Figure 64 the temperature rise from the evaporator to the condenser is approximately 30-40°C. A gap in temperature is registered from about 3000-6000 hours, which is during the summer months. In this period, the GSHP is turned off since there is no heating demand, and the temperatures are therefore relatively irregular. The operation of the GSHP can be seen in Figure 67. The temperature entering the SH tank lies between 35 and 45°C, which is sufficient to meet the space heating temperature requirement of 35°C. Some temperature drops are however registered during the heating season, as seen in Figure 64. The temperature drops are a consequence of the heat pump being turned off, which indicates that the temperature in the tank has reached an adequate value, as seen in Figure 65 and Figure 66.

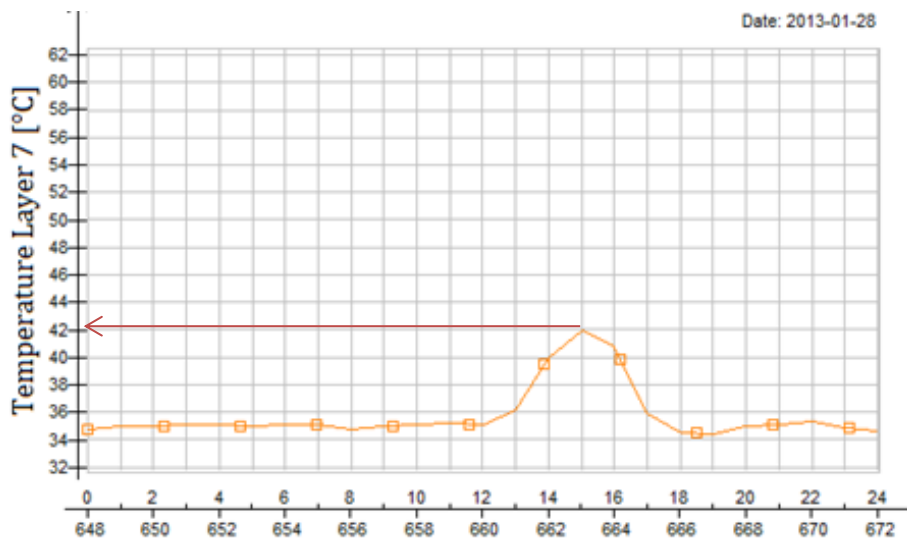
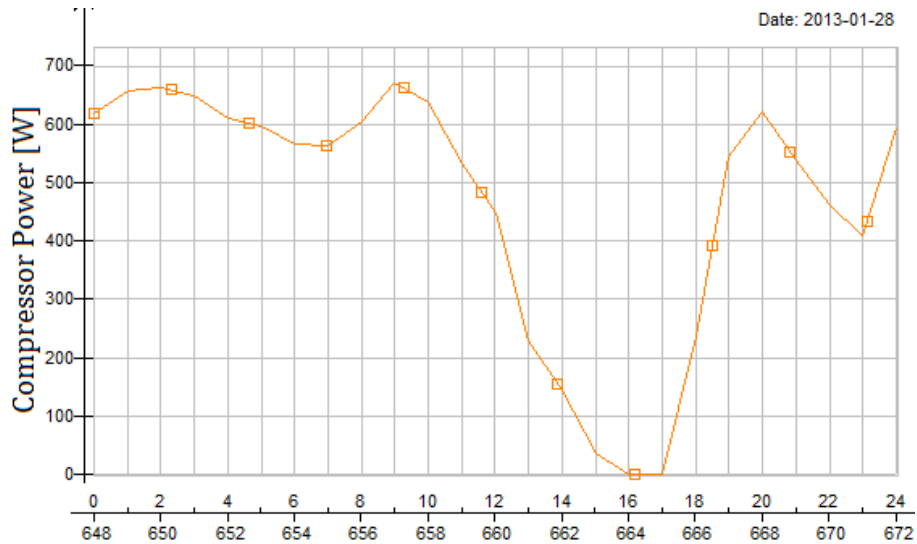


Figure 65 - Temperature Layer 7 SH tank



**Figure 66 - Ground-source heat pump compressor power**

The temperature at the upper part of the tank, which is represented by the temperature in Layer 7 in Figure 65, reaches 42°C at 15:00 pm. This temperature is registered by the GSHP controller, and the heat pump is turned completely off at 16:00 pm, as seen in Figure 66. When the temperature in the tank drops to 34°C at 18:00, the heat pump is again in operation.

The compressor energy consumption, the condenser energy and the energy gained from the ground through the year can be seen in Figure 67.

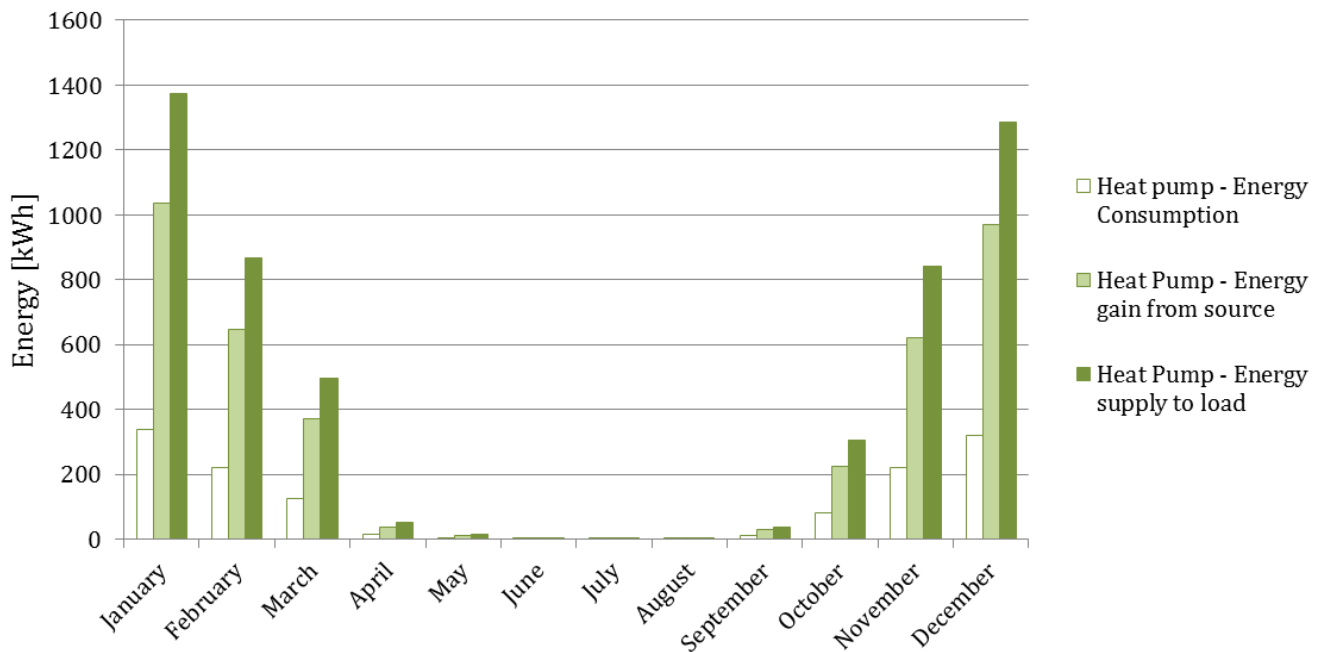


**Figure 67 - Annual performance ground-source heat pump**

Figure 67 illustrates that the ground-source heat pump is not in operation during the summer months when there is no heating demand.

The Nilan ground-source heat pump has a theoretical COP of 4.6. How the COP varies through the heating season can be seen in Figure 68.

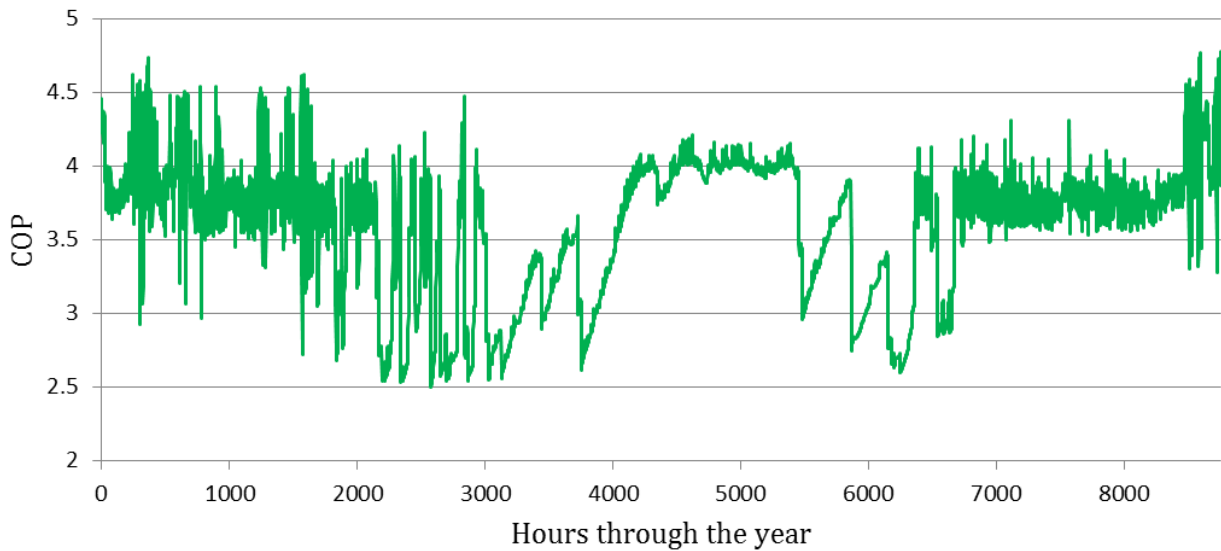


**Figure 68 - Ground-source heat pump COP**

The COP is dependent of the condenser power and the compressor power. When the share of compressor power constitutes a larger part of the condenser power, the COP decreases. The condenser power varies through the year depending on the demand and the temperatures in the tank, and thus the compressor power and the COP vary as well. It can be seen that the COP varies between 3.5 and 4.5, which is considered to be sufficient.

### 12.3 THE EXHAUST AIR HEAT PUMP

The yearly performance of the exhaust air heat pump is shown in Figure 69, where the compressor energy consumption, the source energy and the supplied energy are illustrated.

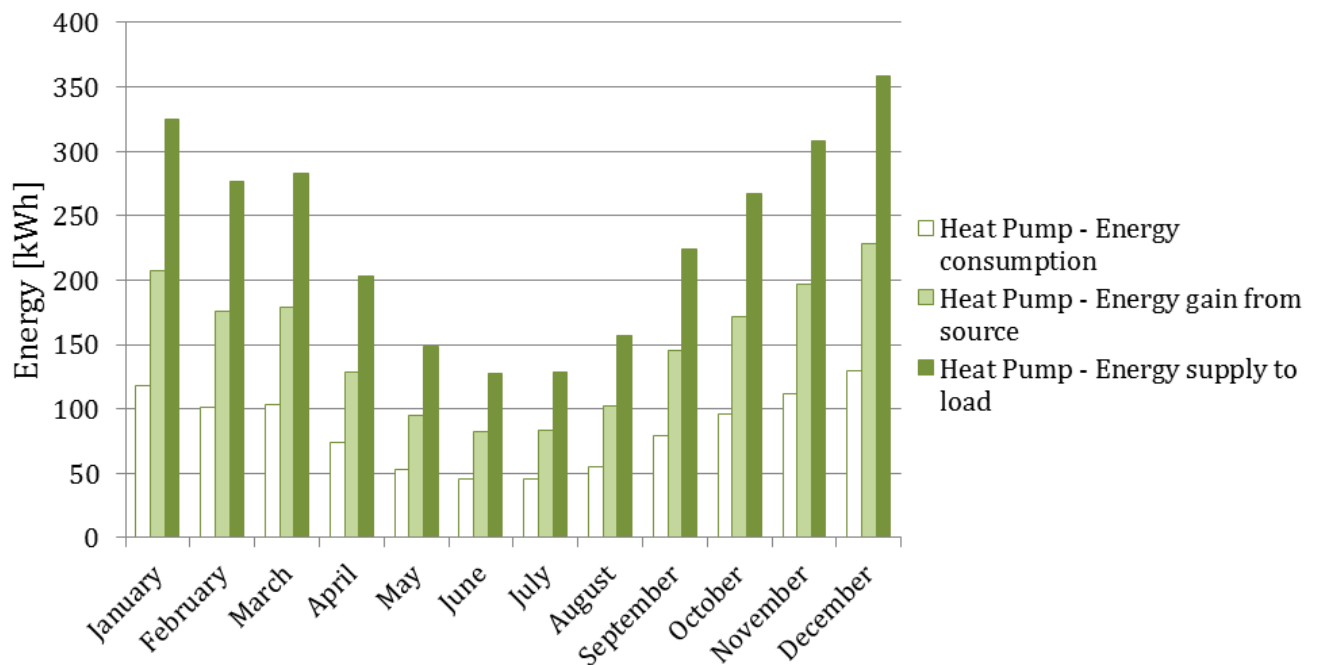


**Figure 69 - Annual performance exhaust air heat pump**

The exhaust air energy demand is reduced towards the summer months as seen in Figure 69. From January to June, the demand is reduced with approximately 50 %, which indicates that a greater proportion of the DHW demand is covered by solar heat in the summer month.

The inlet brine temperature entering the evaporator and the outlet temperature leaving the condenser are shown in Figure 70. The inlet brine evaporator temperature is represented by the dark green line, while the outlet condenser temperature is represented by the lighter green line.

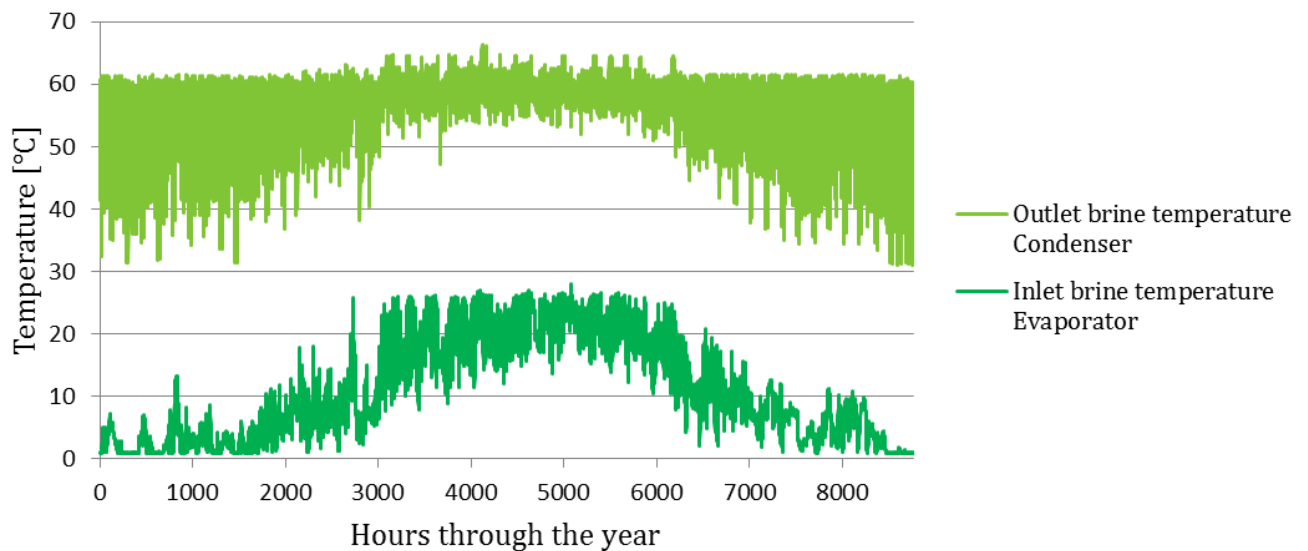


**Figure 70 - Evaporator inlet temperature and condenser outlet temperature**

The maximum temperature leaving the condenser and entering the DHW tank is approximately 62°C, as seen in Figure 70. It can be seen that the outlet condenser temperature constantly drops from maximum temperature to about 35°C. This is mainly caused by the DHW draw-off pattern, and will be discussed later.

The inlet brine evaporator temperature varies between 2 and 26°C through the year, as seen in Figure 70. From Figure 45 it can be seen that the cooling coil, which absorbs the energy in the exhaust air, is located after the heat recovery unit in the air handling unit. During the winter the heat recovery unit is active and the cooling coil inlet temperature is therefore very low, explaining the low inlet brine temperatures during heating season. During the summer months, the need for heat recovery is not equally important, and the inlet brine temperature increases as seen in the hours 3000-6000 in Figure 70.

A more detailed graph showing the operation of the exhaust air heat pump is presented by the compressor power consumption in Figure 71.

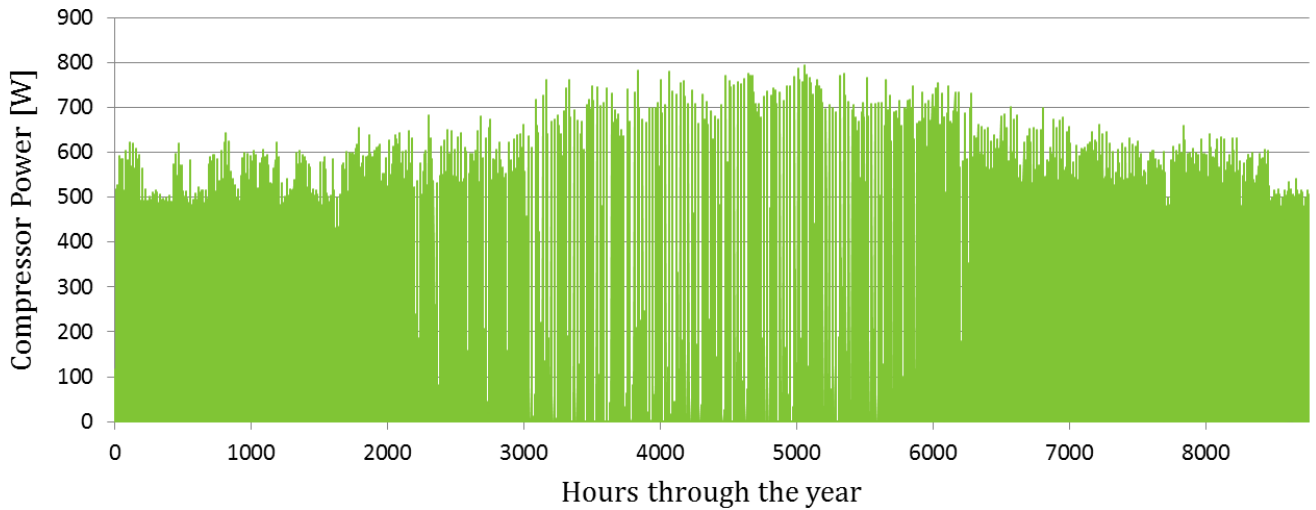


**Figure 71 - Compressor power exhaust air heat pump**

The exhaust air heat pump is constantly in operation all year, except during some periods in the summer months. During these periods the solar irradiation is high and the collected heat is at its maximum as seen in Figure 51 and Figure 52. This implies that the solar heat transferred from the solar circuit to the DHW tank is sufficient for domestic hot water production. The exhaust air heat pump can therefore be turned off when adequate temperatures are reached at the top of the tank.

In Figure 72 the correlation between the compressor power and the temperature in the tank is illustrated for a day at the start of January. The compressor power is illustrated by the light green line, while the inlet condenser temperature is represented by the darker green line in Figure 72.

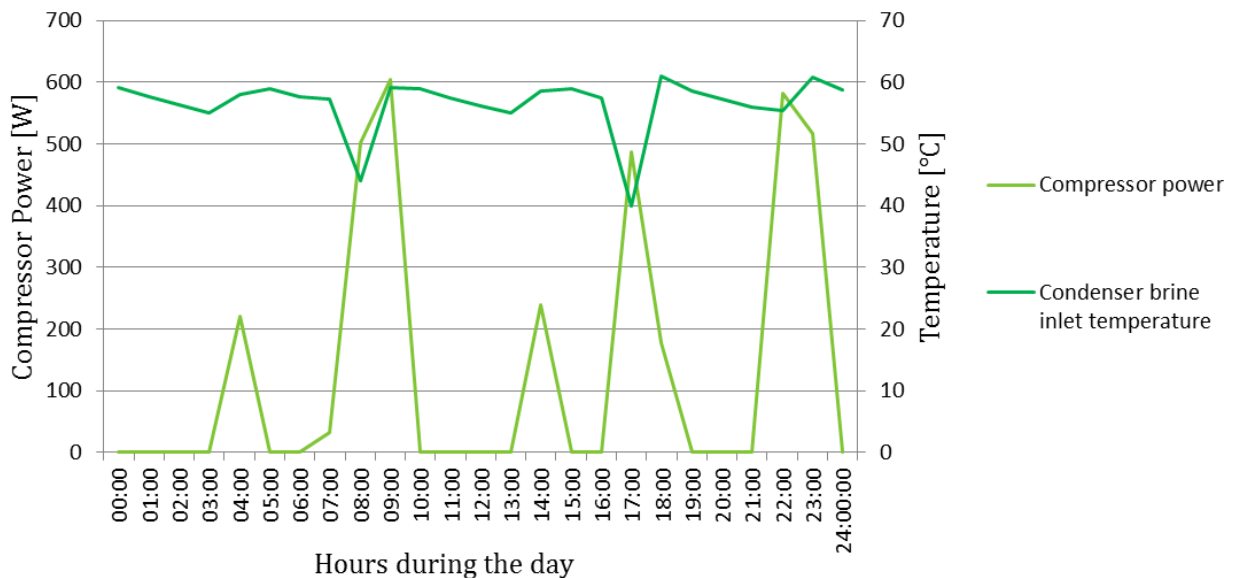


**Figure 72 - Correlation between compressor power and inlet temperature to EAHP condenser 2013-01-04**

It is evident from Figure 72 that the exhaust air heat pump suffers from on/off operation through the day. The temperature sensor, THW1, which sends signals to the heat pump controller, is located between Layer 8 and Layer 9 in the DHW tank, as seen in Figure 49. The temperature in between these layers fluctuates between 55 and 60°C, causing the controller to

send rapid on and off signals to the heat pump compressor and belonging circulation pumps P6 and P7. Placing the temperature sensor further down in the tank may help to reduce this undesired operation. The temperature drops seen in Figure 72 is highly affected by the domestic hot water pattern, which is illustrated for a regular day in Figure 73.

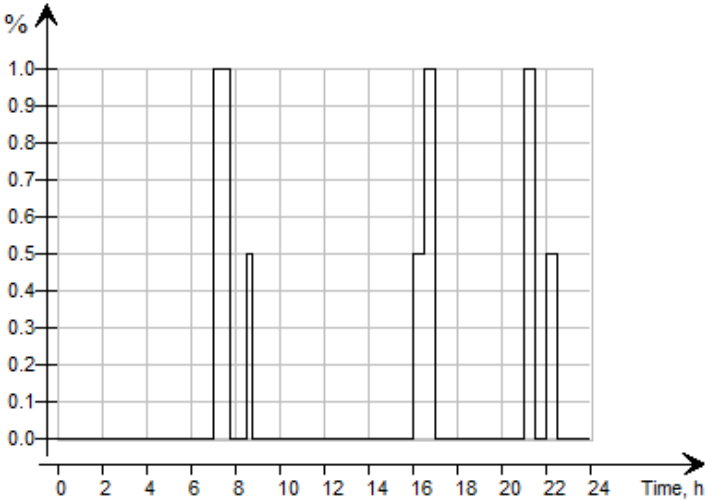


Figure 73 - DHW draw-off pattern a regular day

The maximum draw-off is at 07:00 am, and the decrease in temperature in the tank, due to this draw-off, is illustrated in Figure 72 with the drop in temperature at 08:00 am. The same can be seen for the draw-off at 16:00 pm and 21:00 pm.

### 12.4 THE DHW TANK

The mean temperature registered at each layer in the DHW tank each month can be seen in Figure 74.

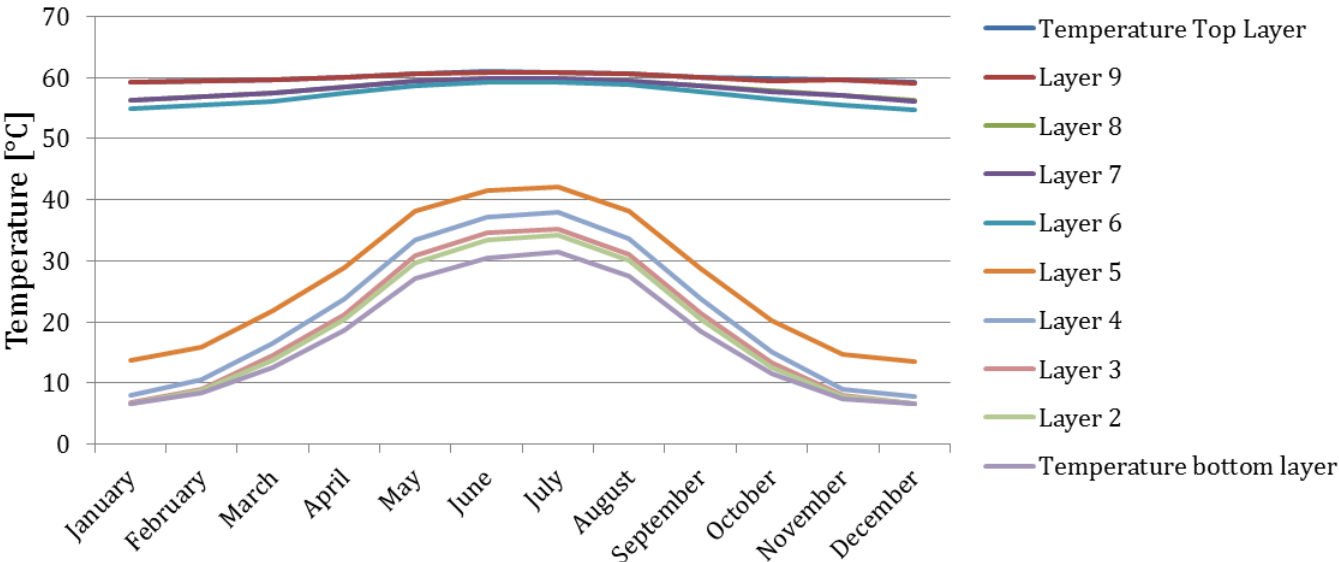


Figure 74 - Tank temperature layers, DHW tank

From Figure 74 it can be seen that thermal stratification is more or less achieved in the tank, as the temperature decreases towards the bottom. The temperature layers are strongly dependent of the location of the internal heat exchangers from both the solar circuit and from the exhaust

air heat pump. The inlet of the solar circuit heat exchanger is located at Layer 2, while the inlet of the exhaust air heat exchanger is located at Layer 8 with the outlet between Layer 5 and 6, as seen in Figure 49. It is clearly shown that the temperatures in the tank are dependent of the solar irradiation as they increase remarkably during the summer months.

The upper 6 layers in the tank hold a temperature which ranges from 55–60°C. This is considered adequate to cover the domestic hot water temperature requirement of 55°C.

The temperature drawn from the DHW tank for DHW purpose is shown in Figure 75. The temperature is stable throughout the year, which indicates that the domestic hot water demand is met at all time.

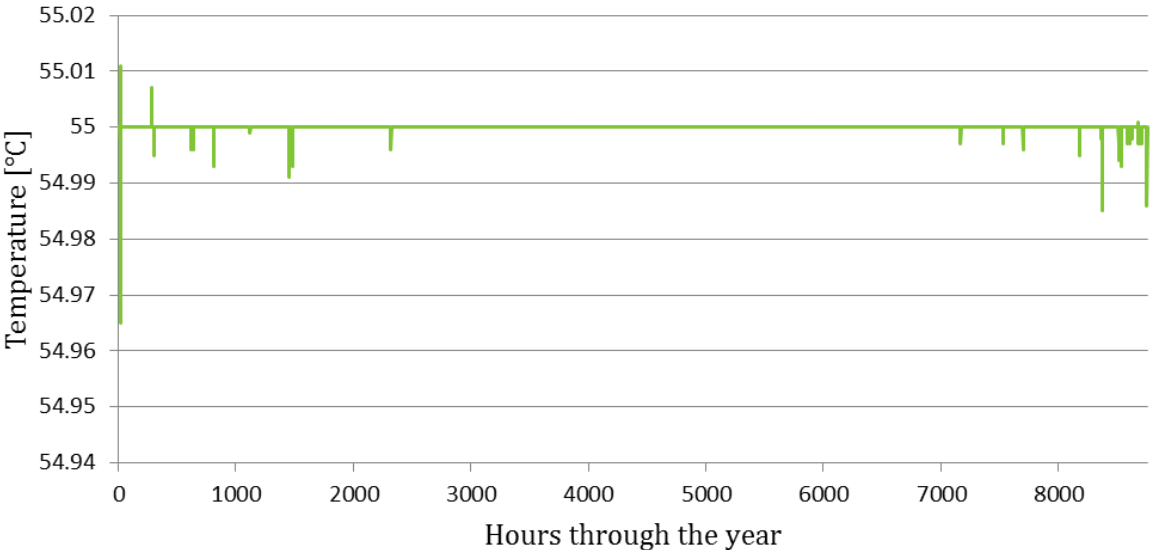


**Figure 75 - Domestic hot water draw-off temperature**

The inlet temperature from the exhaust air heat pump to the domestic hot water tank through the year can be seen in Figure 76.

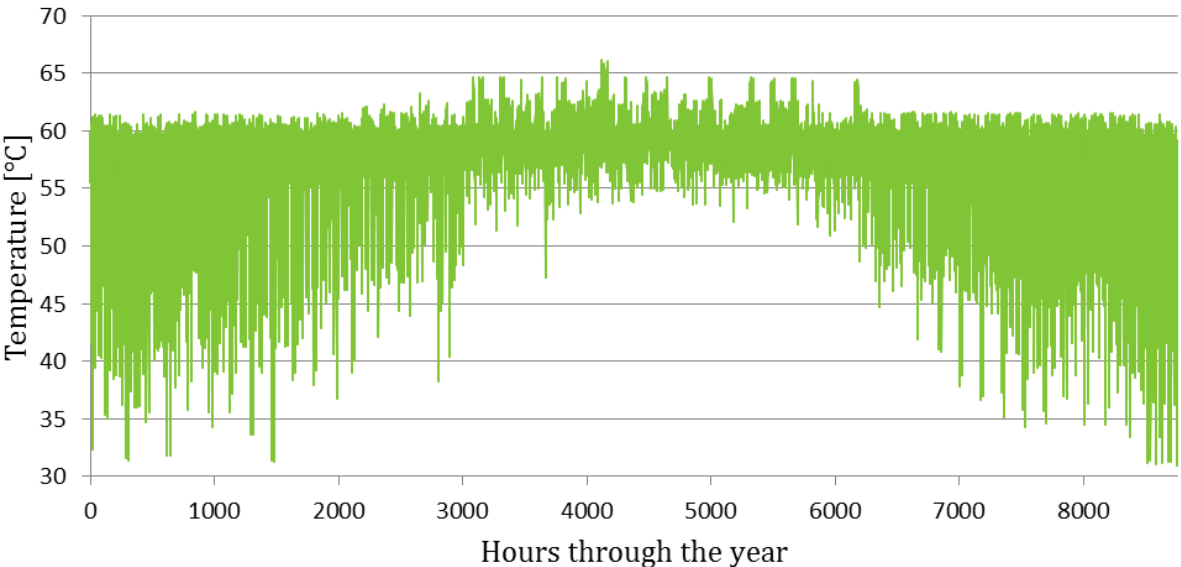


**Figure 76 - Inlet temperatures to tank from exhaust air HP**



The inlet tank temperatures supplied by the exhaust air heat pump are not constant through the day, but vary from 35-60°C. They are greatly affected by the domestic hot water draw-off pattern, illustrated in Figure 73.

The brine inlet evaporator temperature is constantly very low during the winter, as seen in Figure 70, and since the desired outlet temperature from the EAHP is close to 60°C, the temperature rise in the heat pump is rather high. After a large domestic hot water draw-off the temperature in the tank decreases, and the EAHP is not able to supply the DHW tank with adequate temperature immediately. The electrical boiler is therefore activated to ensure that the required temperature of 55°C is maintained in the tank. This is illustrated in Figure 77-Figure 79. A large drop in the tank inlet temperature from the EAHP is registered between 18:00-19:00 pm, and as a consequence, the boiler is activated and the temperature in the tank (illustrated by Layer 9) is kept at 55°C. When the boiler is activated the electricity consumption in the system will increase. The electricity consumption may be reduced if the temperature sensor, which sends operational signals to the EAHP controller, is lowered and the EAHP is activated before the electrical boiler.

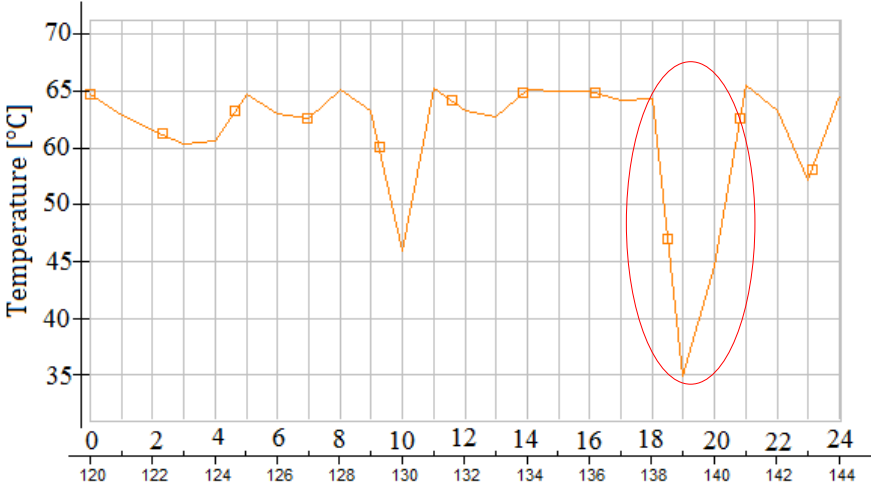


Figure 77 - Inlet temperature to tank from EAHE, 2013-01-06

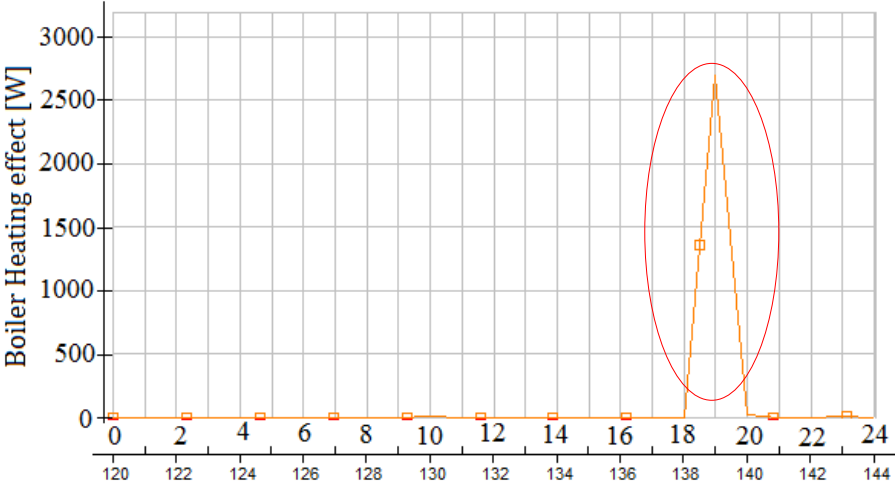
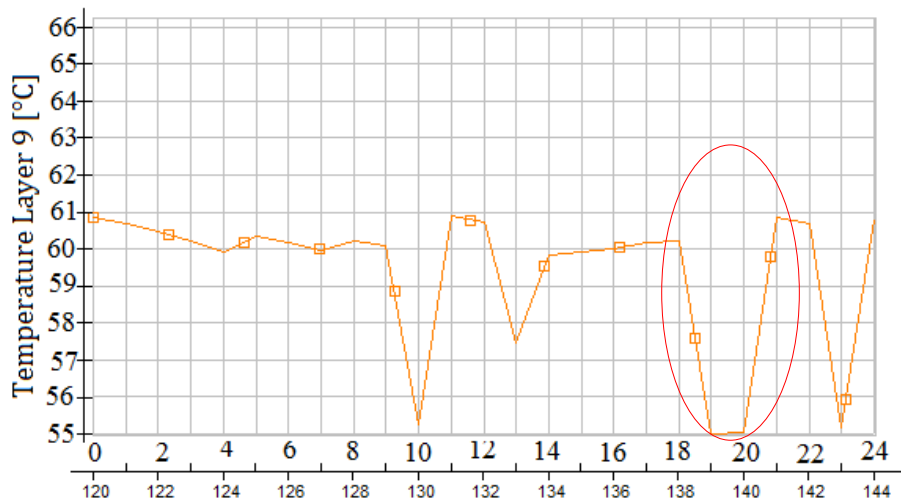
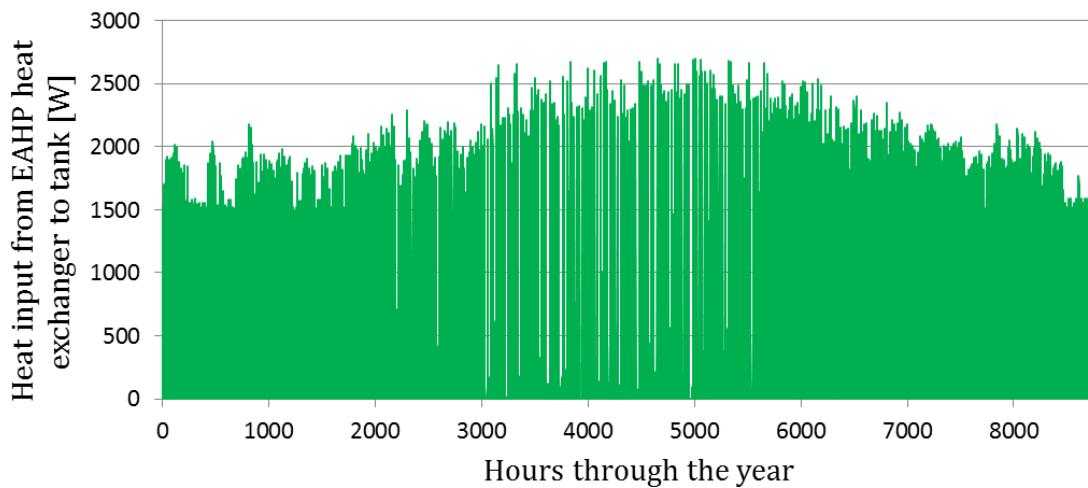


Figure 78 - Electrical boiler heating effect, 2013-01-06



**Figure 79 - Temperature Layer 9 DHW tank, 2013-01-06**

The total heating effect from the integrated exhaust air heat exchanger, the electrical boiler and the integrated solar heat exchanger are shown in Figure 80-Figure 82. The inlet temperature from the solar circuit to the DHW tank is shown in Figure 83.



**Figure 80 - Heat input from exhaust air heat pump to DHW tank**

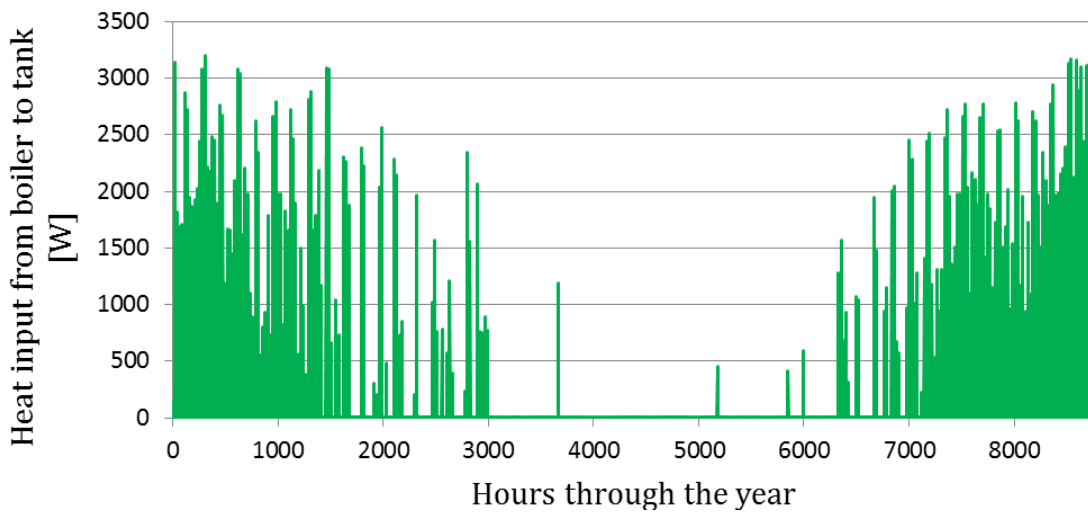


**Figure 81 - Heat input form electric boiler to DHW tank**

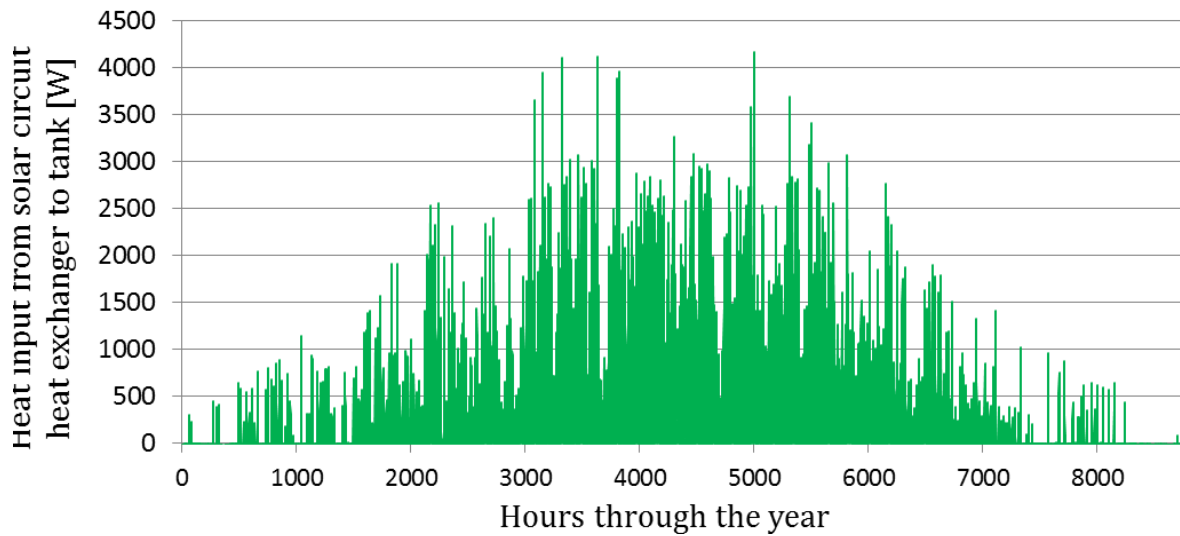


**Figure 82 - Heat input from solar circuit to DHW tank**

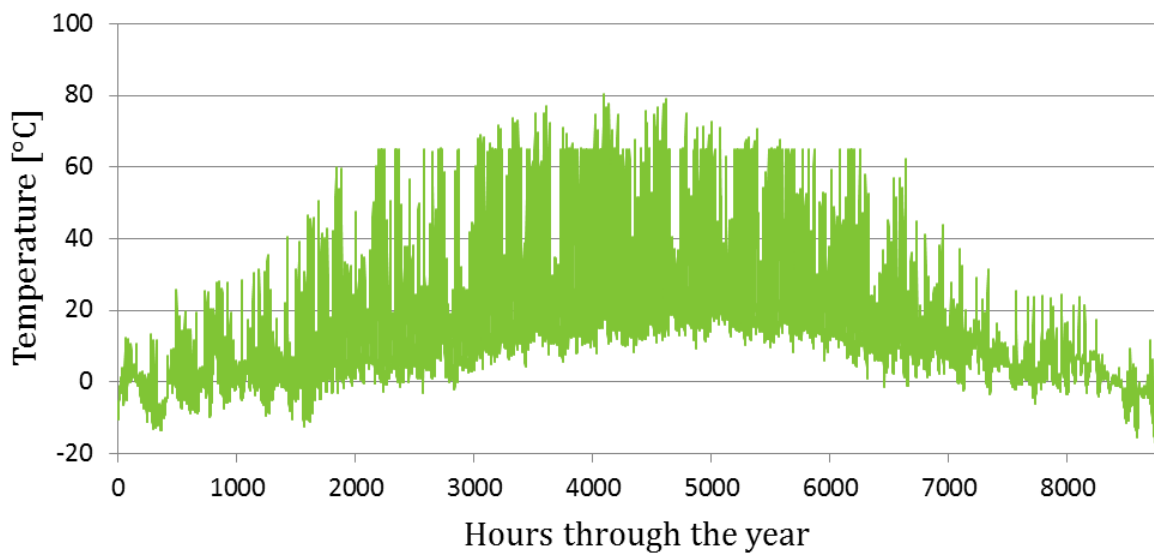


**Figure 83 - Inlet temperature to tank from solar circuit**

Figure 80 shows that the heat input from the exhaust air heat pump varies strongly from May to September, and is nearly zero at some periods during June, July and August. The electrical boiler is not in operation during this period, as seen in Figure 81. This implies that the domestic hot water demand is almost completely covered by solar heat in these periods. The heat input from the solar circuit to the tank is illustrated in Figure 82, and has its maximum during June, July and August. During these months the inlet temperature from the solar circuit holds a temperature of approximately 65°C, which is sufficient for domestic hot water production.

However, when comparing Figure 82 with the collected solar heat shown in Figure 52, the heat transferred to the DHW tank is nearly halved. Due to the temperature control setting of circulation pump P1, shown in Figure 46, a large amount of collected solar heat is transferred to the ground when the temperature near the bottom of the DHW tank exceeds 60°C. As seen in Figure 83 the temperatures from the solar collector to the tank exceed 60°C during the summer months, which implies that available solar energy is transferred to the ground instead. By increasing the temperature setting, more solar energy may be utilized for domestic hot water production, and as a consequence, the system's electricity consumption may be reduced. The top

tank temperature never exceeds 60°C, and since the temperature limit of the tank is 100°C, higher inlet temperatures can be allowed.

Additionally, the heat transfer from the integrated solar heat exchanger to the tank can be affected by the mass flow rate through the heat exchange spiral, the heat transfer area and/or the heat exchange capacity rate from the spiral to the tank. As a rule of thumb the heat exchange capacity rate should be 50 W/K·m<sup>2</sup> solar collector area (Furbo, u.d.). With a collector area of 16 m<sup>2</sup>, the heat exchange capacity rate should in theory be 800 W/K. It is however important to make sure that the capacity of the heat exchanger is sufficiently large. How changing the capacity rate affects the transferred heat will be investigated in the subchapter *13.1.7 Effect of Spiral Heat Exchanger Capacity Rate and Spiral Length*.

### 12.5 THE SPACE HEATING TANK

The mean temperature registered at each layer in the SH tank is shown in Figure 84. An illustration of the SH tank can be seen in Figure 50.

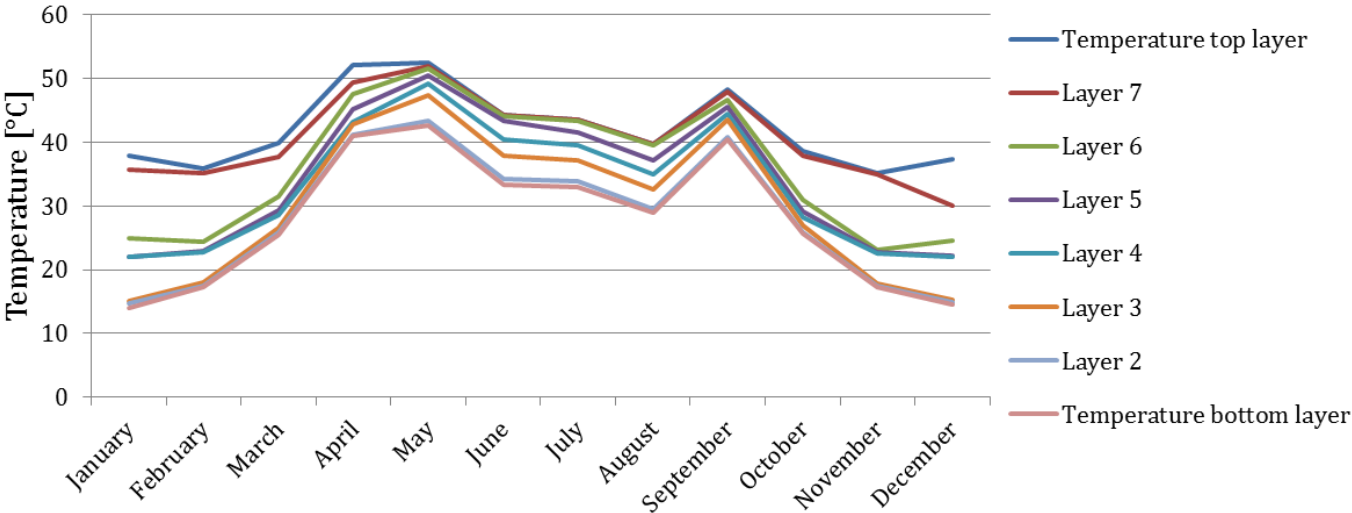
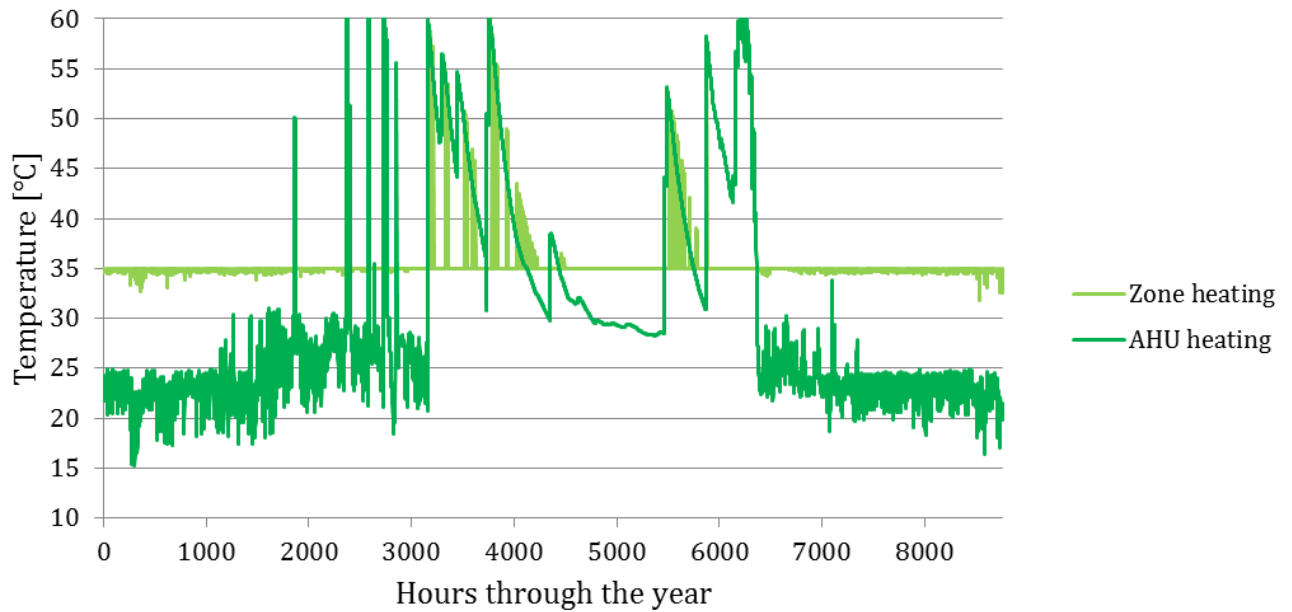


Figure 84 - Layer temperatures in space heating tank

Thermal stratification also occurs in the storage tank for space heating, as seen in Figure 84. The effect of the solar energy is clearly illustrated by the increase in temperature in April/May and September/October. The integrated solar spiral inlet is located at Layer 2, while the inlet from the ground-source heat pump is located at Layer 7. The top layers hold a temperature of 35-55°C which is sufficient for zone heating demand.

The temperatures drawn from the space heating tank to the heating system and to the heating coil in the AHU can be seen in Figure 85. The temperatures for the heating system are represented by the light green line, while the temperatures drawn for the heating coil is represented by the darker green line.



**Figure 85 - Outlet temperature to zone heating and AHU heating**

The zone heating temperature is stable during the heating season, except for some drops in temperature seen in January and December. The drops are never below 32°C, but in order to ensure that the temperature stays at 35°C at all time, the connection point between the tank and the zone heat supply pipe can advantageously be positioned higher. The temperature supplied to the heating coil drops to below 20°C during the winter months, as seen in Figure 85, but the minimum air temperature registered in the dwelling is however not lower than 20.4°C. The connection point between the tank and the AHU heating pipe can be located higher in order to ensure higher temperatures from the tank.

From Figure 85 it can be seen that there are several peaks in temperature during the summer months, both for the zone heating and the AHU heating. However, the circulation pumps, P10 and P11, which ensures circulation of hot water to the heating system in the dwelling and to the AHU, are not in operation in this period since there is no space heating demand. The circulation pumps P10 and P11 are controlled the same way, and the operation of P10 can be seen in *Appendix E – Operation of P10 and P11*.

The heat transferred from the integrated solar heat exchanger and the electrical boiler is shown in Figure 86 and Figure 87.

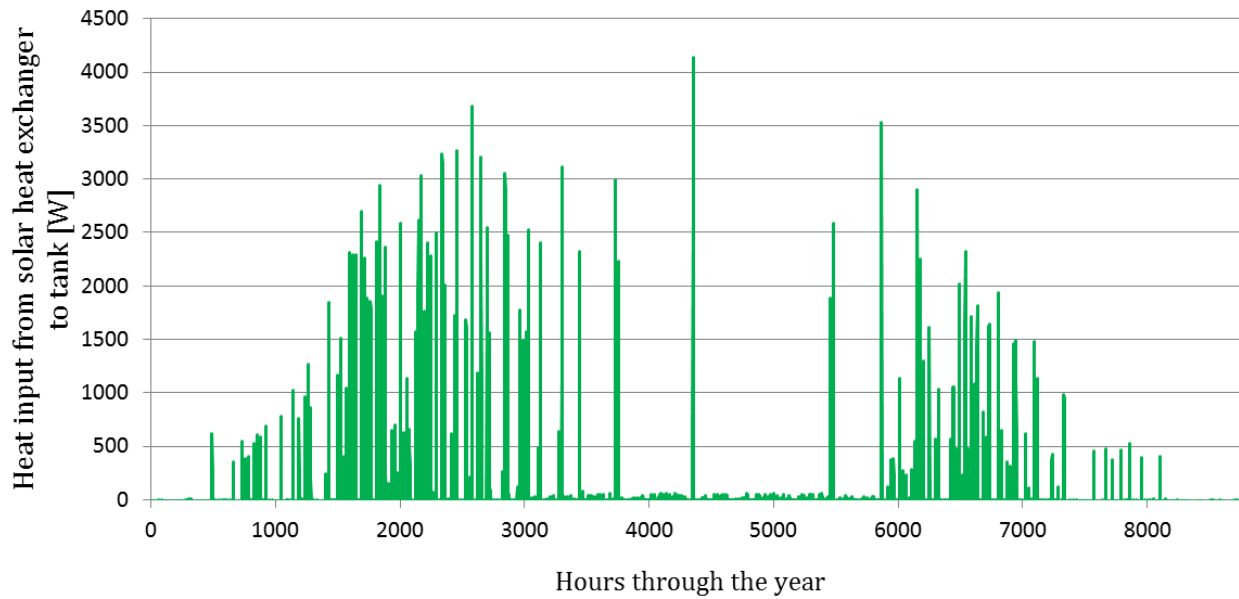


**Figure 86 - Heat input to space heating tank from solar heat exchanger**

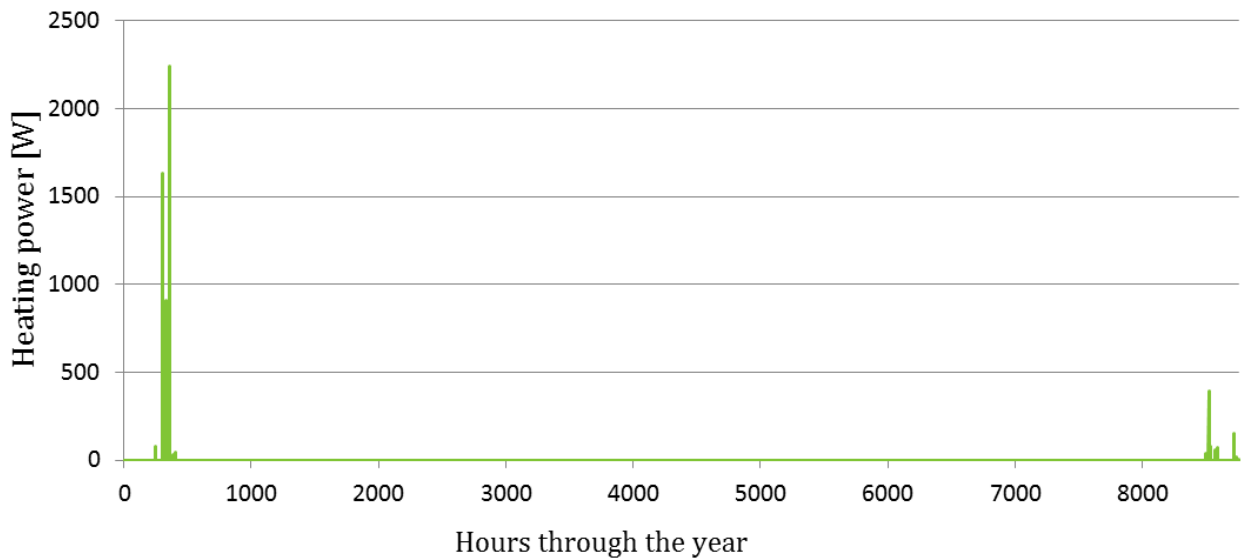


**Figure 87 - Heating power from electrical boiler to space heating tank**

As seen in Figure 86, solar energy is utilized for space heating from February to April (1000-3000) and from September to November (6000-7500). A peak is shown between hour 4000 and 5000, which is in the middle of July. As earlier discussed in *12.1.3 Mass Flow Rate* this peak is regarded as a miscalculation by IDA ICE. With the increase in solar heat transferred to the SH tank, the operation time of the GSHP is reduced, and a reduction in electricity use is achieved.

The ground-source heat pump condensing power, which is transferred to the space heating tank, and the accompanying water inlet temperature are shown in Figure 67 and Figure 64. The figures show that sufficient temperatures are supplied to the tank during heating season, and that the ground-source heat pump is not in operation during cooling season.

The top heater (electrical boiler) is only in operation during a few days in January and a few days in December as seen in Figure 87. This implies that the zone heating demand is covered almost entirely by renewable energy.

## 12.6 ENERGY DEMAND, UTILIZED FREE ENERGY AND SOLAR FRACTION

The system's delivered energy, the energy demand and the amount of utilized free energy will be presented in this chapter.

Delivered energy is defined as the total energy which has been purchased for (or generated within) the building. It includes electricity for lighting and equipment, power for the top heating electrical boilers, electricity for fans and pumps as well as the needed compressor power for the ground-source heat pump and the exhaust air heat pump.

In order to determine the thermal performance of the system, the annual solar fraction is calculated. The solar fraction is defined as the energy supplied by the solar part of the system divided by the total system load (EN9488, 1999), and is calculated according to Equation 28.

$$\text{Annual solar fraction} = \frac{\text{Net utilized solar energy}}{\text{Total heating demand}} \quad (28)$$

The solar fraction is a good indicator of the system performance since it establishes the overall performance of the entire system, not just for one component.

The total delivered energy is presented in Figure 88. The "Electrical heating" column represents the electrical energy utilized by the electrical boilers, and the compressors in both the ground-source heat pump and the exhaust air heat pump. HVAC Aux covers the electricity consumption of the fans and pumps in the system.

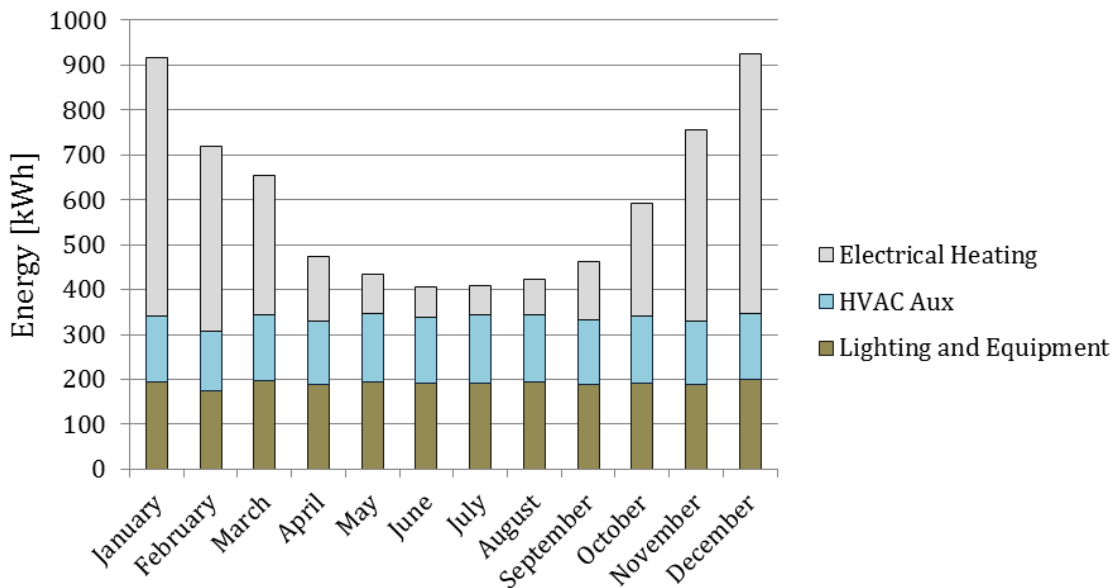


Figure 88 - Delivered energy

The total specific delivered energy for the single-family dwelling is 35.5 kWh/m<sup>2</sup>.

The monthly energy balance between the energy demand and the amount of utilized free energy is illustrated in Figure 89. Both space heating demand and the DHW demand are included in the "Energy demand" columns. The obtained monthly solar fractions are represented by the orange line in Figure 89, and it can be seen that the solar fractions from May to August is 100 %. This indicates that excess solar heat is produced.

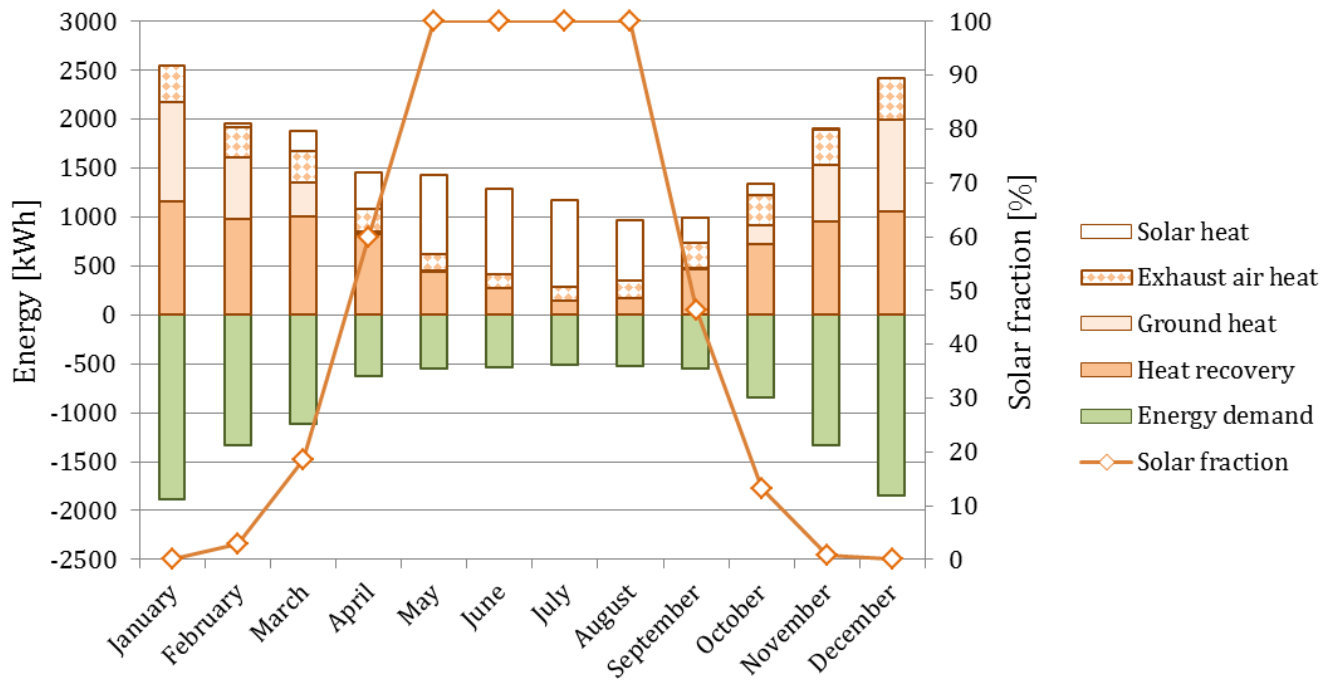


Figure 89 - Energy demand, utilized free energy and solar fraction

The system's total annual solar fraction for the simulated year is 35.9 %.

The specific heating demand for the single-family dwelling is 27.1 kWh/m<sup>2</sup>, which is higher than the required 17.6 kWh/m<sup>2</sup> stated in NS 3700.

The most important factors for determining the system performance are summarized in Table 25.

Table 25 - Specific delivered energy, specific heating demand and annual solar fraction

<b>Total specific delivered energy</b>	35.5 kWh/m <sup>2</sup>
<b>Specific heating demand</b>	27.1 kWh/m <sup>2</sup>
<b>Annual solar fraction</b>	35.9 %

From the results presented in this chapter it is concluded that the system seems to work apparently well. However, the system is far from optimized and as seen, several settings can be changed in order to achieve a better system performance. How the system can further be optimized by changing both design and operation parameters will be presented in the next chapter.



## 13 OPTIMAL SYSTEM DESIGN AND OPERATION

This chapter addresses the optimization process of the system's design and operating parameters. Firstly, a parametric study of the most important design and operating parameters are presented. A summary of the optimal design and operating parameters with the greatest effect on the system's electricity use is presented in the subchapter *13.3 Summary of the Design and Operation Parameter Optimization*. In the subchapter *13.4 Optimized Scenarios*, different scenarios composed of different optimized parameters are presented with corresponding obtained electricity use. A sensitivity analysis is performed on the scenario with the lowest use in electricity and is presented in *13.5 Sensitivity Analysis*. Finally, the electricity use, domestic hot water, space heating demand and the amount of utilized free energy are presented for two of the scenarios which are considered to represent optimal solutions.

The values of the parameters which have been elucidated and utilized in the parametric study are based on information and recommendations found in the literature, see chapter 7. In order to find the optimum design and operational parameters, simulations where only one parameter was changed at a time were performed. During the simulations all other parameters in the system were kept at initial settings. In order to evaluate the system performance and the effect of each change in design or operation parameter, the specific delivered energy and the total system annual solar fraction will be presented. The net utilized solar energy will be presented instead of the annual solar fraction when this result is considered to be more appropriate to present. The specific delivered energy is the amount of utilized electric energy in the system, and the annual solar fraction is the amount of net utilized solar energy divided by the total system energy demand and is calculated according to Equation 28.

It should be noted that when performing simulations on a solar combi-system it is very easy to achieve rough approximations on the system's performance, and very difficult to get close to how the system performance will be in reality due to the complex nature of combi-systems (Weiss, 2003). Details, such as design of hot water storage and how heat is transferred to and from the tank can result in difference to the overall system performance. With a bad design the system performance can be reduced drastically. A good system design is therefore crucial for achieving an energy efficient system.

### 13.1 STUDY OF OPTIMAL DESIGN PARAMETERS

The results which are not presented by figures or tables in this subchapter, due to insignificant impact on the system performance, are presented by figures in *Appendix F – Design Parameter Study*. All results are however commented on in this chapter.

#### 13.1.1 EFFECT OF SOLAR COLLECTOR AREA

Initially the reference system has a solar collector area of 16 m<sup>2</sup>. Investigating how the system performance and system electricity use is affected by installing 8 m<sup>2</sup> instead has been a general desire, but in order to optimize the system, solar collector areas between 8 and 16 m<sup>2</sup> have to be investigated as well. The model was therefore simulated with collector areas of 10, 12 and 14 m<sup>2</sup> as well. All other system parameters were kept at initial settings.

The total monthly solar fraction for each solar collector area is illustrated in Figure 90. It should be noted that the solar fractions presented are the total system's solar fraction and includes the solar energy utilized to recharge the borehole.

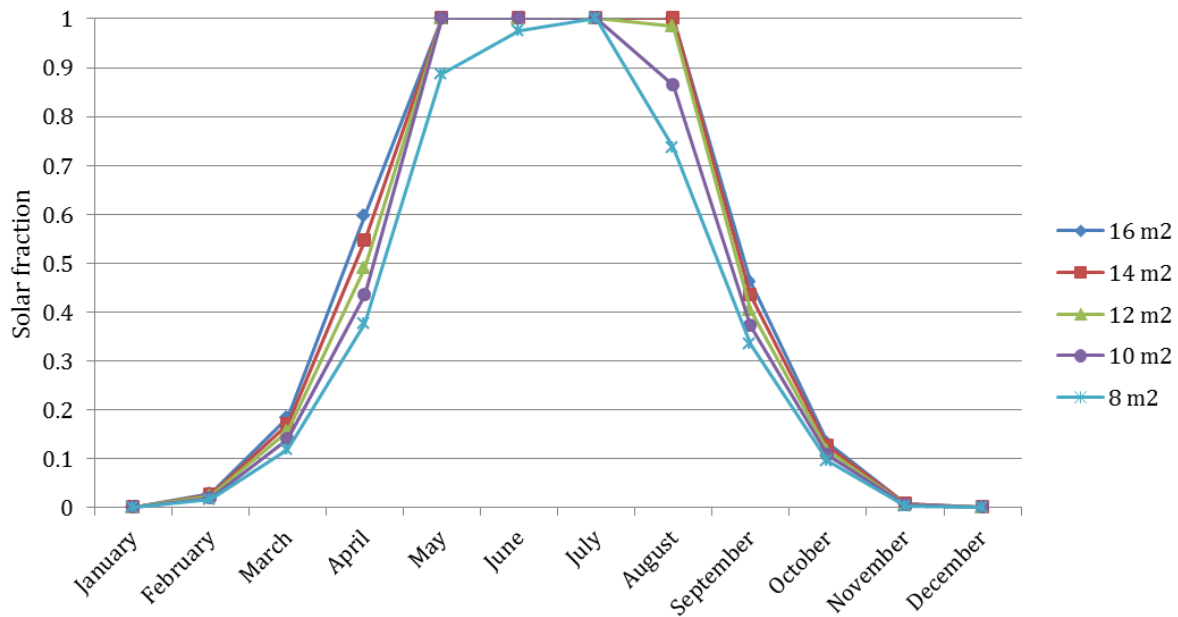


**Figure 90 - Monthly solar fractions for different solar collector areas**

The results show that the highest monthly solar fractions are obtained with a solar collector area of 16 m<sup>2</sup>. The difference in solar fraction between 16, 14 and 12 m<sup>2</sup> of solar collector area is however not particularly large, and excess solar heat is produced from May to July, as seen in Figure 90. The solar fraction is reduced by 7 % and 8 % in March and April respectively, by decreasing the collector area from 16 to 14 m<sup>2</sup>. The reduction in solar fraction in September and October is 6 % and 5 %. During the summer months approximately 50 and 60 % of the DHW demand is covered by solar energy when 14 and 16 m<sup>2</sup> of solar collector area is installed.

With a collector area of 8 m<sup>2</sup>, 45-50 % of the domestic hot water demand is covered by solar energy from May to August. Compared to a solar collector area of 16 m<sup>2</sup>, the solar fraction is reduced by 37 % and 12 % in April and May respectively and a reduction of 27 % is found in August.

The total annual solar fraction and the total annual electric energy consumption for each solar collector area can be found in Table 26.

**Table 26 - Annual solar fraction and specific delivered energy for different solar collector areas**

	16 m <sup>2</sup>	14 m <sup>2</sup>	12 m <sup>2</sup>	10 m <sup>2</sup>	8 m <sup>2</sup>
<b>Total annual solar fraction [%]</b>	35.9	32.8	29.5	25.9	22.3
<b>Total annual specific delivered energy [kWh/m<sup>2</sup>]</b>	35.5	35.6	35.7	35.9	36.1

From Table 26 it can be seen that the decrease in annual solar fraction is steeper than the increase in electricity consumption when the solar collector area is reduced. This is due to the temperature control setting which ensures that solar energy is transferred to the ground when the temperature near the bottom of the DHW tank exceeds 60°C. When the solar collector area is reduced, a significantly higher percentage reduction of solar heat transferred to the ground is obtained compared to the percentage reduction of solar heat transferred to the DHW tank. This

implies that the amount of supplied electrical energy to the DHW tank is hardly affected by the difference in solar collector area. Increasing the set point temperature near the bottom of the DHW tank as well and thus allowing more solar energy into the tank will probably result in a greater reduction of the electricity use in the system.

A solar collector area of 16 m<sup>2</sup> has the lowest amount of utilized electric energy and the highest annual solar fraction. However, the difference between 16 m<sup>2</sup> and 14 m<sup>2</sup> is relatively small and when considering the cost, space requirements and reliability of large solar collector areas, a collector area of 14 m<sup>2</sup> may be a better solution. Additionally, when considering the coverage of domestic hot water demand during the summer, the difference is negligible between the two collector areas.

**13.1.2 EFFECT OF SOLAR COLLECTOR ORIENTATION AND TILT ANGLE**

The solar collectors installed on the “Multikomfort” dwelling rooftop have a tilt angle of 19° from the horizontal surface, and are orientated towards the south-east. With this position, the majority of the collected solar heat is during the summer when the sun has a high position on the sky. Available solar energy which could have been collected during spring, autumn and winter is lost due to the tilt angle. Because of the south-east orientation the solar collectors produce useful heat during the morning and the midday, and solar energy available on the afternoon is not included. With an orientation towards the south, solar energy available from late morning to early evening could have been collected.

The model was simulated with a south-east orientation, a south orientation and a south-west orientation with tilt angles 19°, 40°, 55° and 60° in order to evaluate and determine the better solution which would enhance the system performance and reduce the amount of used electricity. The simulations were performed with a collector area of 16 m<sup>2</sup> and all other system parameters at initial settings.

The system’s monthly solar fractions with tilt angles of 19°, 40°, 55° and 60° orientated towards the south-east, the south and the south-west are shown in Figure 91-Figure 93.

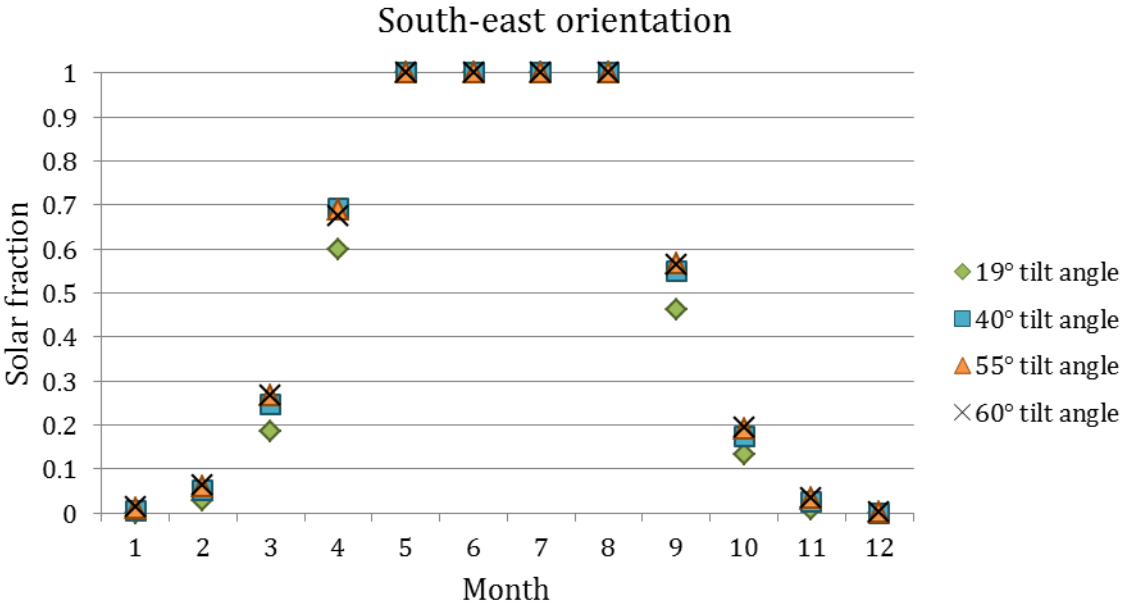


Figure 91 - Tilt angles 19°, 40°, 55° and 60° towards the south-east

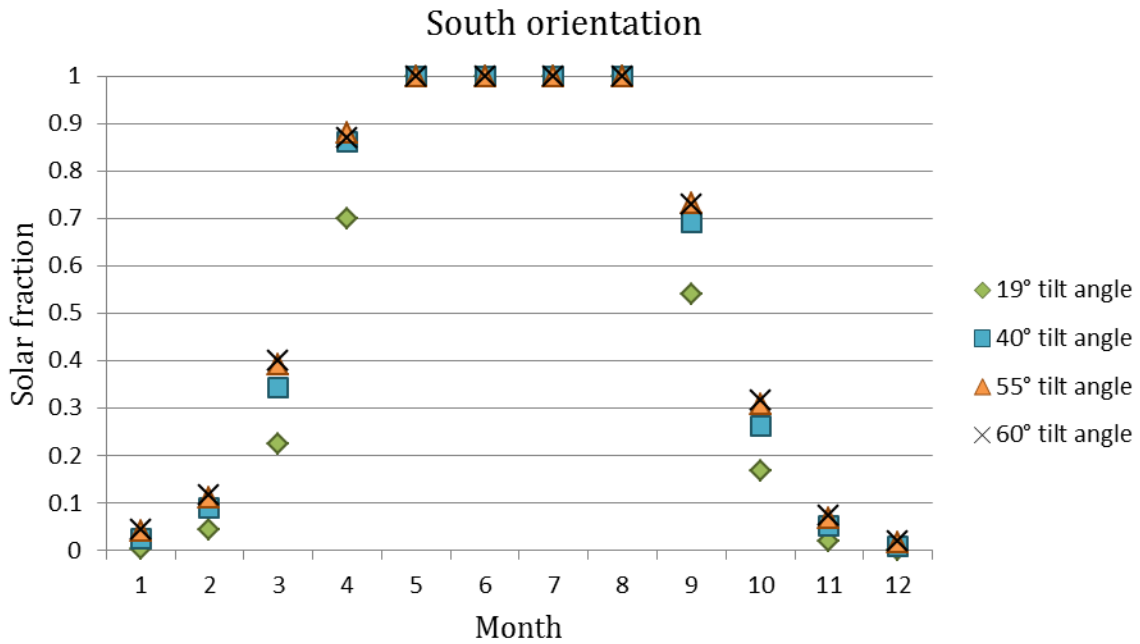


Figure 92 - Tilt angles 19°, 40°, 55° and 60° towards the south

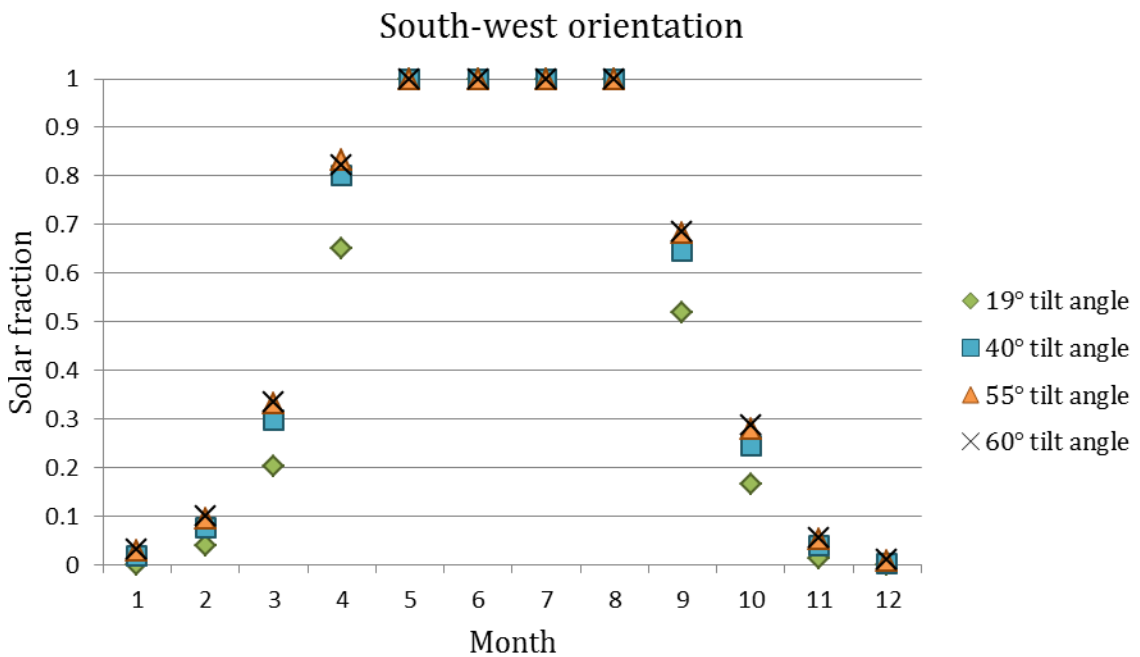
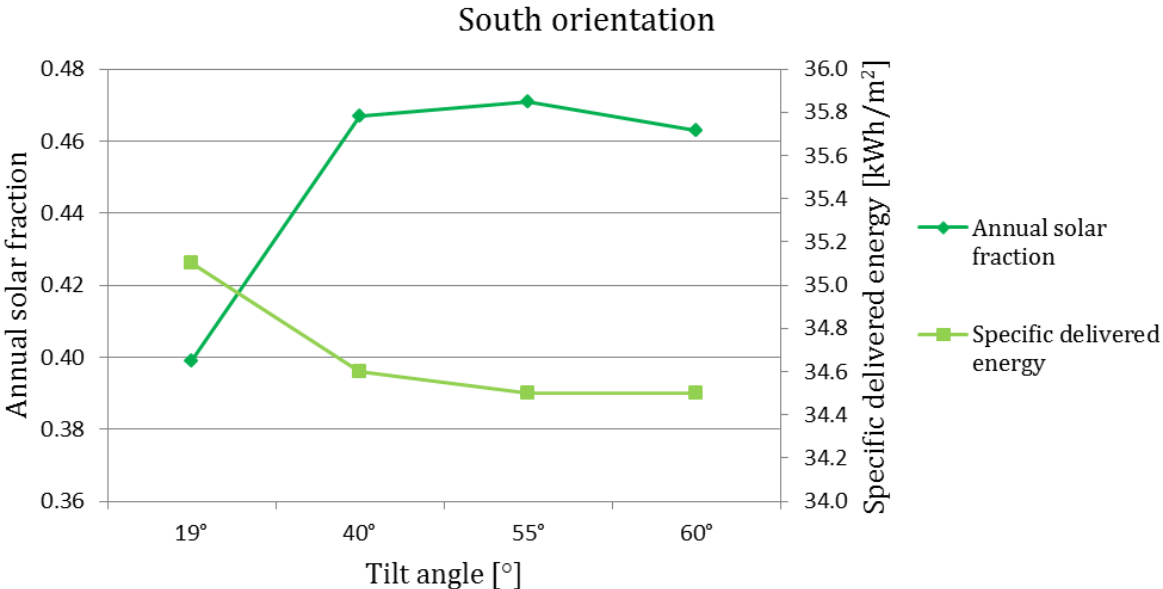


Figure 93 - Tilt angles of 19°, 40°, 55° and 60° towards the south-east

Figure 91-Figure 93 show that by orientating the solar collectors from the south-east to the south, the monthly solar fraction for the original tilt angle of 19° increases noticeably, especially in April and September. By orientating the solar collectors towards the south, more solar energy is collected, and with a tilt angle as low as 19° more solar energy is collected during late spring, summer and early autumn due to the high position of the sun. With a collector area of 16 m<sup>2</sup>, excess solar heat is produced for every tilt angle from May to August where the solar fraction is 100 %, as seen in Figure 91-Figure 93. This means that a steeper tilt angle is possible without affecting the amount of solar energy collected during the summer months. A steeper tilt angle is considered beneficial since more solar energy can be collected during the heating season when the sun's position on the sky is lower.

From Figure 91-Figure 93 it can be seen that a tilt angle of 55-60° results in higher solar fractions, with the highest found in Figure 92 where the collectors are oriented towards the south. It can be seen that tilt angles as high as 55° and 60° does not affect the amount of utilized solar energy during the summer months, as excess solar heat is still produced. By comparing the initial tilt angle and orientation with a tilt angle of 55° and orientation towards the south, a considerable increase in the monthly solar fractions is observed. The system is able to utilize solar energy every month, and a substantial increase is observed in March where the solar fraction increases from 18.4 % (19° and south-east orientation) to 39.2 % (55° and south orientation). The annual solar energy transferred from the solar circuit to the DHW tank is increased by approximately 30 % with an optimized tilt angle and orientation.

The system’s annual solar fraction and the annual specific delivered energy for tilt angles of 19°, 40°, 55° and 60° with an orientation towards the south are shown in Figure 94. It was chosen to focus on the south orientation since the highest monthly solar fractions were achieved with this orientation.



**Figure 94 - Annual solar fraction and annual specific delivered energy - south orientation**

By orientating the solar collectors with a tilt angle of 19° towards the south instead, the annual solar fraction is increased by 11 % and the specific delivered energy is decreased by 1.1 %. From Figure 94 it can be seen that by increasing the tilt angle to 40° and 55°, the annual solar fraction is increased by 17.0 % and 18.0 % respectively. A decrease in annual solar fraction is shown from 55° to 60°, indicating that a tilt angle of 55° results in a better system performance. The specific delivered energy is decreased with approximately 1.4 % and 1.7 % by changing the tilt angle to 40° and 55° respectively.

From the obtained results it is perceived that a tilt angle of 55° and an orientation towards the south is the optimum solution. An annual solar fraction of 47.1 % and an electrical energy use of 34.5 kWh/m² are obtained with this tilt angle and orientation. It should be noted that by changing the tilt angle and orientation of the solar collectors, the aesthetic expression of the single-family dwelling is changed as well. The solar collectors can no longer be an integrated part of the roof construction and they become more visible.

### 13.1.3 EFFECT OF SOLAR COLLECTOR HEAT LOSS

The model was simulated with different types of flat plate solar collectors in order to investigate the effect of the solar collector heat loss on the total system performance. It is not possible to change the insulation type and insulation thickness on the solar collector casing in IDA ICE. The same applies to the absorber emittance and absorption coefficient. However, the solar collector's first and second order heat loss coefficients can be changed. The flat plate collector chosen for the "Multikomfort" dwelling is a product from Hewalex called KS2000 SLP with heat loss coefficients as seen in Table 27. The solar collector is shown in Figure 30. In order to investigate the effect of installing a solar collector with better thermal performance, two additional flat plate solar collectors, also from Hewalex, with lower heat loss coefficients were simulated. The solar collector area, tilt angle, orientation and all other parameters in the system were kept at initial settings. The heat loss coefficients and coating material for each of the simulated solar collectors are found in Table 27.

**Table 27 - Characteristics of different solar collectors from Hewalex**

	<b>KS2000 SLP</b>	<b>KS2000 TLP</b>	<b>KS2000 TLP ACR</b>
<b>Absorber</b>	Copper	Copper	Aluminum
<b>Coating</b>	Black chrome	Blue Tec	Blue Tec
<b>a<sub>1</sub> [W/m<sup>2</sup>K]</b>	4.46	3.80	3.79
<b>a<sub>2</sub> [W/m<sup>2</sup>K<sup>2</sup>]</b>	0.0096	0.0067	0.0118

The absorption coefficient of Blue Tec is 0.95 and the emittance is 0.05, while for black chrome, the absorption coefficient ranges from 0.90- 0.95 and the emittance may be as high as 0.11 (Morrison, u.d.). A high absorption factor and low emittance is desirable, as discussed in chapter 7.

The monthly solar fractions for each solar collector type are given in Figure 95.

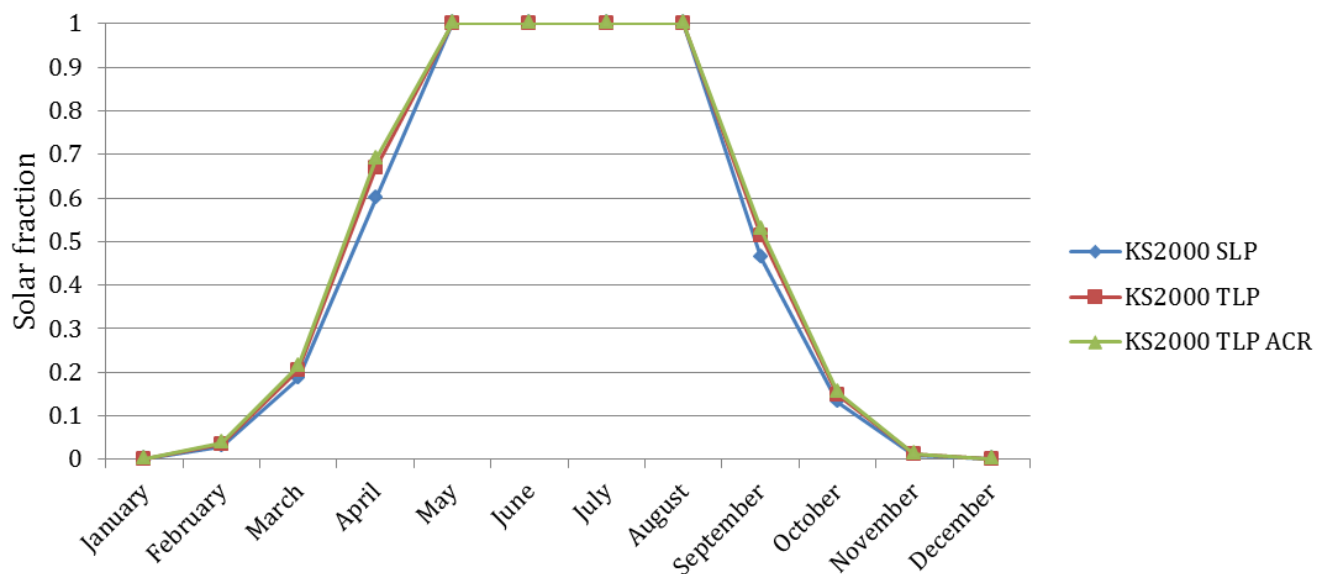


**Figure 95 - Monthly solar fractions for each solar collector type**

By installing solar collectors with less heat loss to the surroundings, a greater amount of the collected solar heat is utilized through the year as seen in Figure 95. Higher solar fractions are

obtained especially in March, April and September. In April, the solar fraction is increased by 12.0 % and 15.4 % by changing the collector to a KS2000 TLP and a KS2000 TLP ACR respectively.

With a lower solar collector heat loss, a greater amount of solar energy is utilized for domestic hot water production. The DHW coverage with the initial solar collector is, for instance, 19.0 % in March, while with KS2000 TLP and KS2000 TLP ACR the coverage is 20.7 % and 21.3 % respectively. During the summer months the DHW coverage varies from 52.0-59.3 % with KS2000 SLP, while with KS2000 TLP and KS2000 TLPACR it varies from 53.7-60.7 % and 54.4-61.8 % respectively. As seen in Figure 95, excess solar heat is produced from May -August for all solar collector types as the solar fractions exceed 100 %.

The total annual solar fraction and the specific annual delivered energy obtained with the different solar collector types are shown in Table 28.

**Table 28 - Total annual solar fraction and specific delivered energy for different solar collector types**

	<b>KS2000 SLP</b>	<b>KS2000 TLP</b>	<b>KS2000 TLP ACR</b>
<b>Total annual solar fraction [%]</b>	35.9	39.0	40.1
<b>Specific delivered energy [kWh/m<sup>2</sup>]</b>	35.5	35.3	35.2

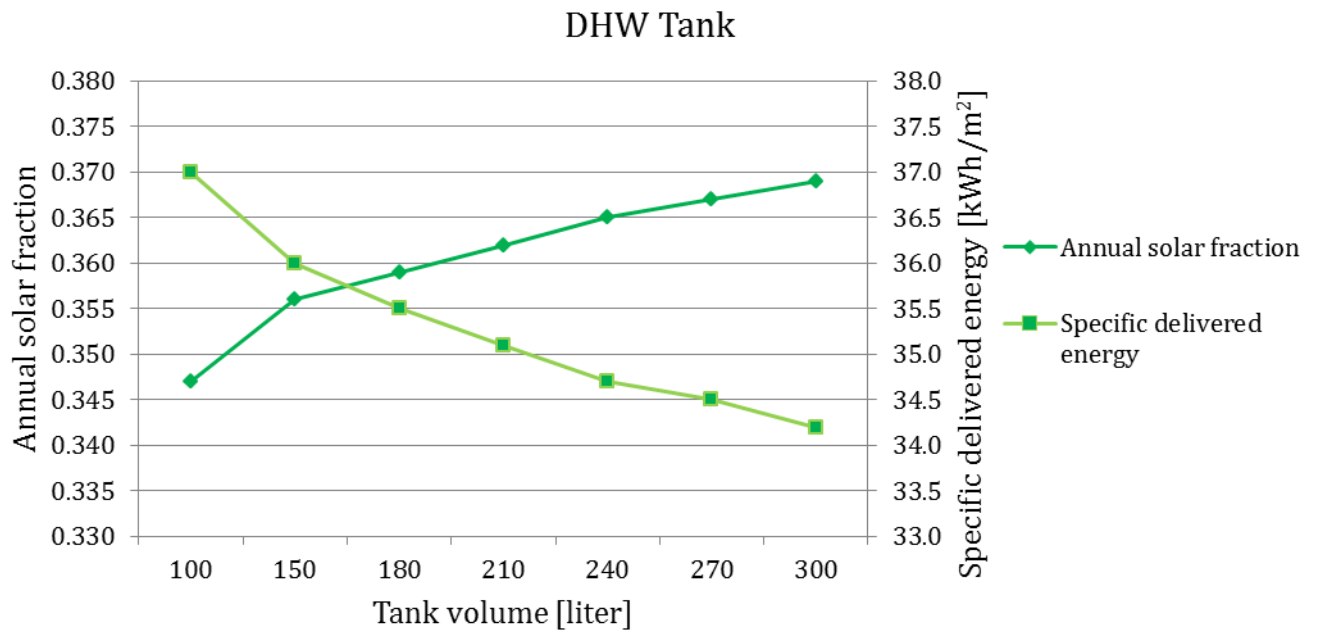
As seen in Table 28, the total annual solar fraction is increased by 8.6 % and 11.7 % by installing a solar collector with better thermal performance. The electric energy consumption is decreased by correspondingly 0.6 % and 0.9 %. The KS2000 TLP ACR is considered to be the optimum collector. Again, a higher percentage increase in transferred solar heat to the ground is obtained compared to the percentage increase of solar heat transferred to the DHW tank. This is due to the temperature control setting of maximum 60°C near the bottom of the DHW tank, and explains why the increase in annual solar fraction is steeper than the decrease in annual specific delivered energy as seen in Table 28.

#### *13.1.4 EFFECT OF THE TANK VOLUME*

In order to investigate the effect of changing the storage tank volume, simulations with different tank volumes were performed both for the DHW tank and the space heating tank. The height/diameter ratios were kept constant for all tank volumes, and the pipe connection points and temperature sensor locations were placed corresponding to the positions of the initial tank volumes of 180 l and 325 l as seen in Figure 49 and Figure 50. All other system parameters were kept at the initial settings.

As mentioned in the subchapter 7.2 *Design of the Storage Tank*, the tank volume for the DHW tank should be 1-2 times the daily hot water consumption. Assuming a consumption of 100-150 l/day gives a total DHW tank volume of 100-300 liters. The space heating tank volume should be approximately 100-200 l per kW heating load. For the “Multikomfort” dwelling a space heating effect of 2.8 kW was calculated by Brødrene Dahl. This results in a tank volume of approximately 280-560 liters.

How the total annual solar fraction and the specific delivered energy are affected by the difference in DHW tank volume is shown in Figure 96.



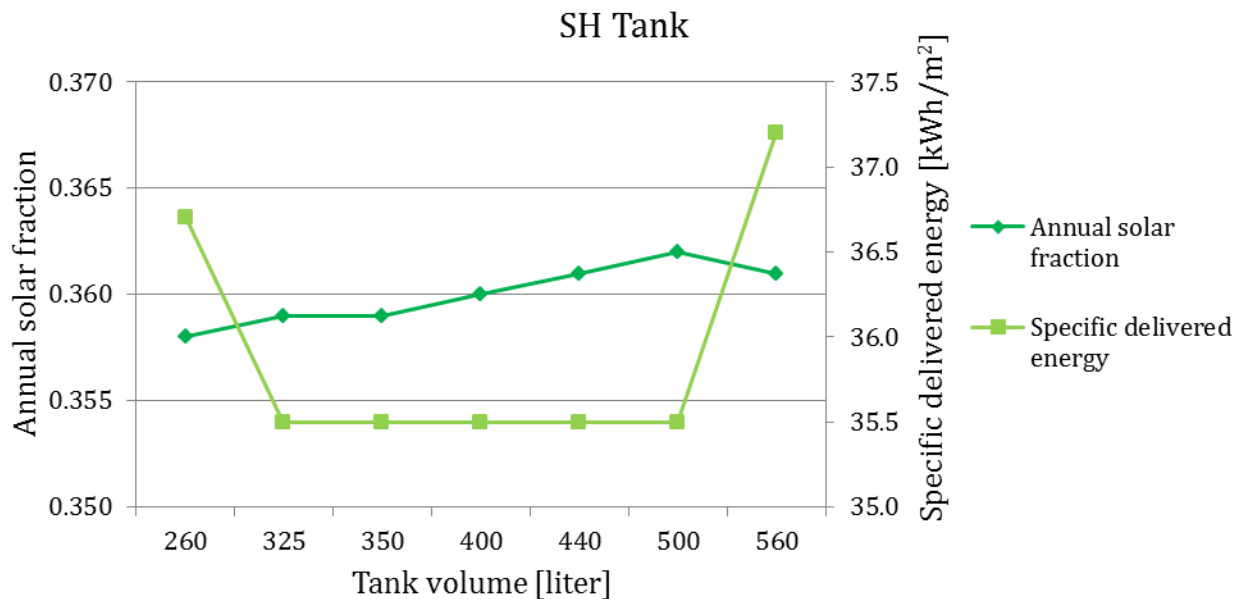
**Figure 96 - Annual solar fraction as a function of the volume of the DHW tank**

Figure 96 shows the annual solar fraction and the specific delivered energy as a function of the volume of the DHW tank. It can be seen that by increasing the tank volume, the thermal performance of the system is increased accordingly. With a larger tank volume, the solar volume increases and more solar energy can be stored and used when the demand occurs. Additionally, a larger tank volume results in diminished effect from the other heat sources on the solar volume and a lower temperature is maintained at the lower part of the tank. This results in decreased inlet temperatures to the solar collectors, which increases the collector efficiency. A decrease of 3-4°C in inlet collector temperature is observed when increasing the tank volume from 180 l to 300 l. The annual solar fraction is increased by approximately 3.0 % and the specific delivered energy is decreased by 3.7 % by increasing the tank volume from 180 l to 300 l.

It is observed that with an increasing tank volume, more solar heat can be utilized during the heating season since the available solar volume in the storage tank is increased. The net utilized solar energy in March and October are, for instance, approximately 10 % and 16 % higher with a tank volume of 300 l compared to a tank volume of 180 l. The increase in utilized solar energy during the summer months are minimal, and only an increase of 0.5 % is observed in July. If the tank volume is reduced to 150 l on the other hand, the annual solar fraction is decreased by 0.84 % and the specific delivered energy increases by 1.4 %. From Figure 96 it can be seen that a tank volume of 300 l gives the best system performance with an annual solar fraction of approximately 37 % and an annual specific delivered energy of 34.2 kWh/m<sup>2</sup>.

The annual solar fraction and the specific delivered energy for the space heating tank are shown as a function of the storage tank volume in Figure 97.





**Figure 97 - Annual solar fraction and specific delivered energy as a function of SH tank volume**

Storing solar energy in the space heating tank is only the second priority in the system. It is visualized, by comparing Figure 96 and Figure 97 that changing the storage tank volume has a greater effect on the DHW tank, where storing solar energy is the priority. The effect on the annual solar fraction and specific delivered energy in the space heating tank is not as striking as for the DHW tank. It can be seen in Figure 97 that the annual solar fraction has a very gentle slope from a volume of 325 l to 500 l, and that the specific delivered energy is constant. It is evident from Figure 97 that a SH tank volume of 560 l is insufficient since a noticeable increase in specific delivered energy is obtained. Increasing the tank volume to 560 l results in a higher heat loss to the surroundings, and as a consequence more electricity is used to cover the space heating demand.

Less solar energy is stored in the SH tank compared to the DHW tank, which makes the importance of a good solar storage tank design less crucial. In the DHW tank where solar energy dominates, the dependency between storage tank volume and utilized solar energy is greater, which is visualized in Figure 96.

### *13.1.5 EFFECT OF THE HEIGHT/DIAMETER RATIO*

Investigations performed on storage tanks in solar heating systems show that good thermal stratification is obtained for spiral tanks when the height/diameter ratio is 2 or higher (Furbo, 2004). A good thermal stratification in the tank enhances the system performance. The height/diameter ratios for the storage tanks in this system are initially 2.08 and 2.12 for the DHW tank and the SH tank respectively, and are thus equal to the recommended value. However, how increasing the height/diameter ratio would affect the system performance was investigated. The model was simulated with increasing h/d-ratios for both the DHW tank and SH tank. The tank volumes and all other system parameters were kept at initial settings.

The annual solar fraction and the annual specific delivered energy are shown as a function of the h/d - ratio for the DHW tank in Figure 98.

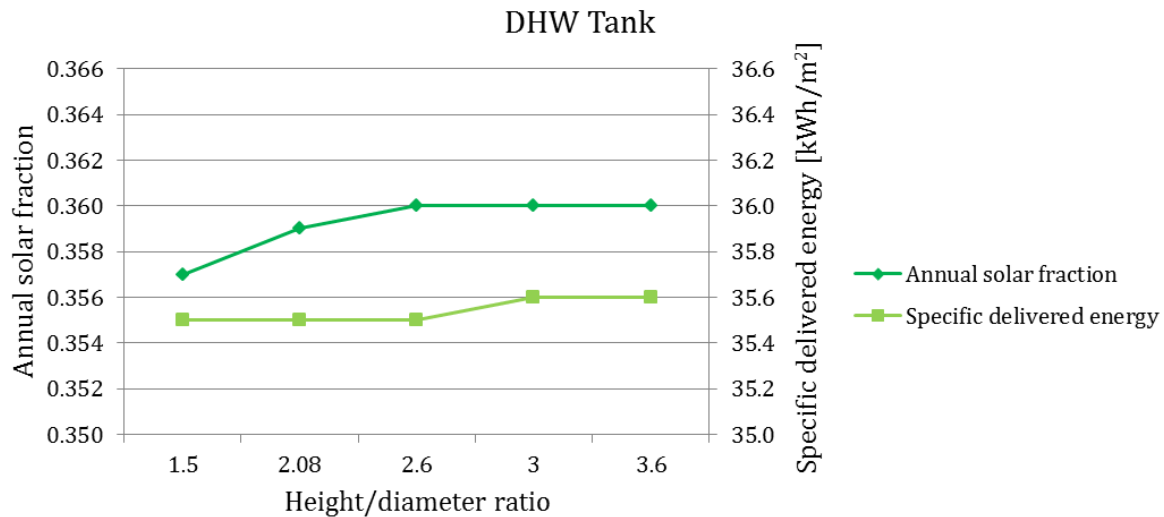


**Figure 98 - Annual solar fraction and delivered energy as a function of h/d ratio, DHW Tank**

Increasing the h/d-ratio further has no severe effect on the system performance, as seen in Figure 98. A dependency between the annual solar fraction and the h/d ratio is however observed. By reducing the h/d-ratio to 1.5 the annual solar fraction is decreased by 0.6 %, and by increasing the h/d-ratio to 2.6, the increase in annual solar fraction is 0.3 % compared to the initial h/d-ratio of 2.08. The specific delivered energy, on the other hand, is not affected by the change in h/d-ratio, as seen in Figure 98. This may be due to the fact that the difference in utilized solar energy is marginal when the h/d-ratio is changed from 1.5 to 2.6, and does not reduce the auxiliary electrical energy needed to cover the peaks. When the h/d-ratio is increased to 3.0, the annual solar fraction is constant, while the specific delivered energy is increased to 35.6 kWh/m<sup>2</sup>. The increase is not significant, but indicates that increasing the h/d-ratio further does not improve the system performance, which underlines the fact that spiral tanks should have an h/d-ratio around 2. From Figure 98 it can be seen that an h/d-ratio of around 2.6 provides the optimum system performance.

The annual solar fraction and the annual specific delivered energy are shown as a function of the height/diameter-ratio for the SH tank in Figure 99.

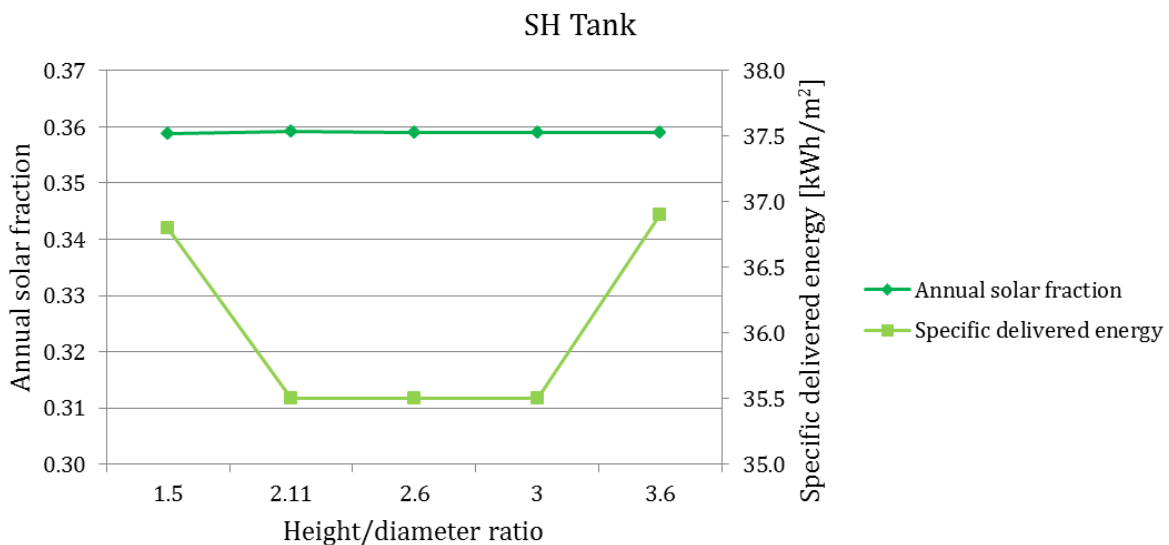


**Figure 99 - Annual solar fraction and specific delivered energy as a function of h/d-ratio, SH tank**

The annual solar fractions obtained for the SH tank are not equally affected by the change in h/d-ratio as the DHW tank, as seen in Figure 99. Less solar energy is transferred to the SH tank compared to the DHW tank, and the system performance, when considering the solar fraction, is therefore not as affected by the SH tank design as it is by the DHW tank design. The same phenomenon was observed when the tank volumes were increased, as seen in Figure 96 and Figure 97. The results presented in Figure 96-Figure 99 underline that a storage tank, where solar heat constitutes a large part of the heat input to the tank, is dependent of the tank design in order to enhance the system performance. Additionally, Figure 50 shows that the pipe inlet from the AHU heating coil to the SH tank is located below the solar heat exchanger inlet. This may affect the thermal stratification at the lower part of the tank and increase the outlet temperature returning to the solar collectors. This means that even though the h/d-ratio is changed in order to increase the thermal stratification, the thermal stratification in the lower part of the tank may be deteriorated by the inlet temperatures from the AHU heating coil. To which extent this affects the system performance will be investigated in *13.1.8 Effect of Tank Pipe Inlet and Outlet Locations*.

The specific delivered energy is clearly affected by the change in h/d-ratio, especially when the h/d ratio is less than or above 2. This indicates that the initial h/d-ratio of 2.12 is sufficient for the SH tank.

**13.1.6 EFFECT OF AUXILIARY ELECTRICAL VOLUME**

The effect of changing the auxiliary electrical volume in the DHW tank was investigated by performing simulations with auxiliary electrical volume ranging from 30-100 l. It is recommended that the volume heated by the auxiliary electrical supply system is 60-100 l in order to cover the DHW demand if needed. The auxiliary volume in the DHW tank is approximately 60 liters initially, but it may be reduced advantageously since the heat supplied by the exhaust air heat pump is relatively stable throughout the year. When reducing the electrical auxiliary volume, it is important to make sure that the DHW demand is met at all time.

The annual net utilized solar energy and the annual specific delivered energy are shown as functions of the auxiliary electric volume in the DHW tank in Figure 100.

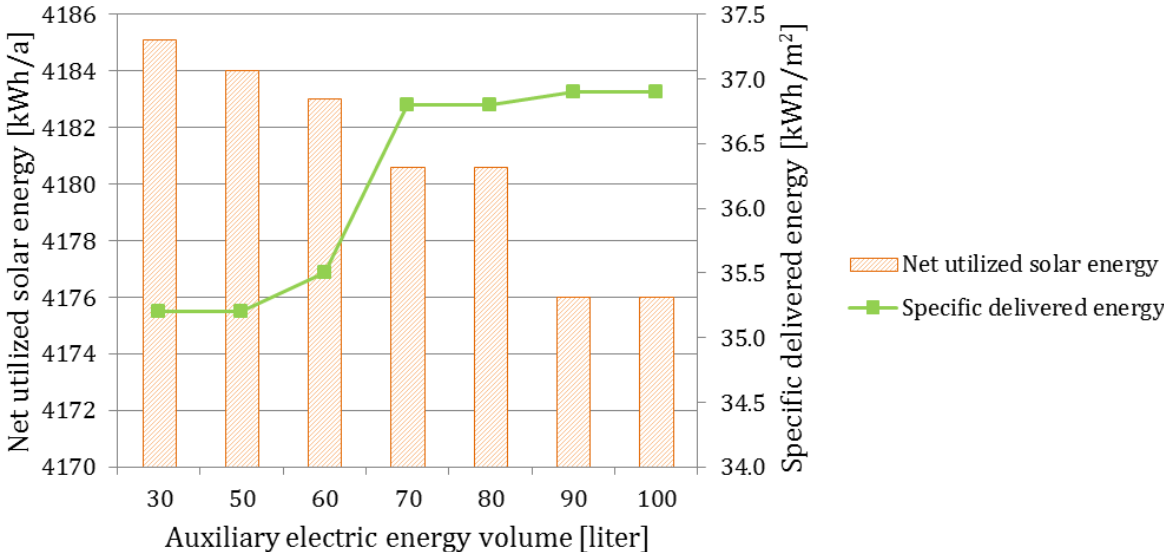


**Figure 100 - Net utilized solar energy and specific delivered energy as a function of auxiliary electric volume in DHW tank**

From Figure 100 it can be seen that the electrical energy consumption is greatly reduced as a result of decreased electrical auxiliary volume. By decreasing the electrical volume, more solar energy can be supplied to the tank and the annual net utilized solar energy increases.

By increasing the auxiliary electrical volume from 60 l to 70 l, a particularly large increase in specific delivered energy is observed, as seen in Figure 100. If the volume is decreased from 60 l to 50 l, on the other hand, a decrease in electrical energy consumption of 0.85 % is obtained. By increasing the auxiliary volume to 100 l, from 60 l, the electrical energy consumption is increased by 3.9 %.

Heat is supplied to the DHW tank from an electrical boiler, an exhaust air heat pump and from the solar circuit. As the energy supplied by the exhaust air heat pump is relatively stable throughout the year, it may be possible to reduce the electrical auxiliary volume to 50 l. However, if a failure in the exhaust air heat pump should occur, the DHW demand would not be covered completely. It should be noted that the DHW demand is covered with an auxiliary volume of 50 l when the exhaust air heat pump is operating correctly.

### 13.1.7 EFFECT OF SPIRAL HEAT EXCHANGER CAPACITY RATE AND SPIRAL LENGTH

The model was simulated with different heat exchange capacity rates for the integrated solar heat exchangers in both storage tanks. The heat exchange capacity rate must be sufficiently large according to Furbo (u.d.), and a rate of 50 W/K·m<sup>2</sup> collector area is recommended (Furbo, u.d.). Laughton (2010) recommends a heat exchange capacity rate of 100 W/K·m<sup>2</sup> collector area (Laughton, 2010), and IDA ICE uses a capacity rate of 170 W/K·m<sup>2</sup> collector area. The model was therefore simulated with heat exchange capacity rates ranging from 50-200 W/K·m<sup>2</sup> collector area. All other system parameters were kept at the initial settings.

The effect of changing the integrated spiral heat exchangers capacity rate is shown in Figure 101. Both the annual solar fraction and the specific delivered energy are plotted as a function of the change in heat exchange capacity rate.

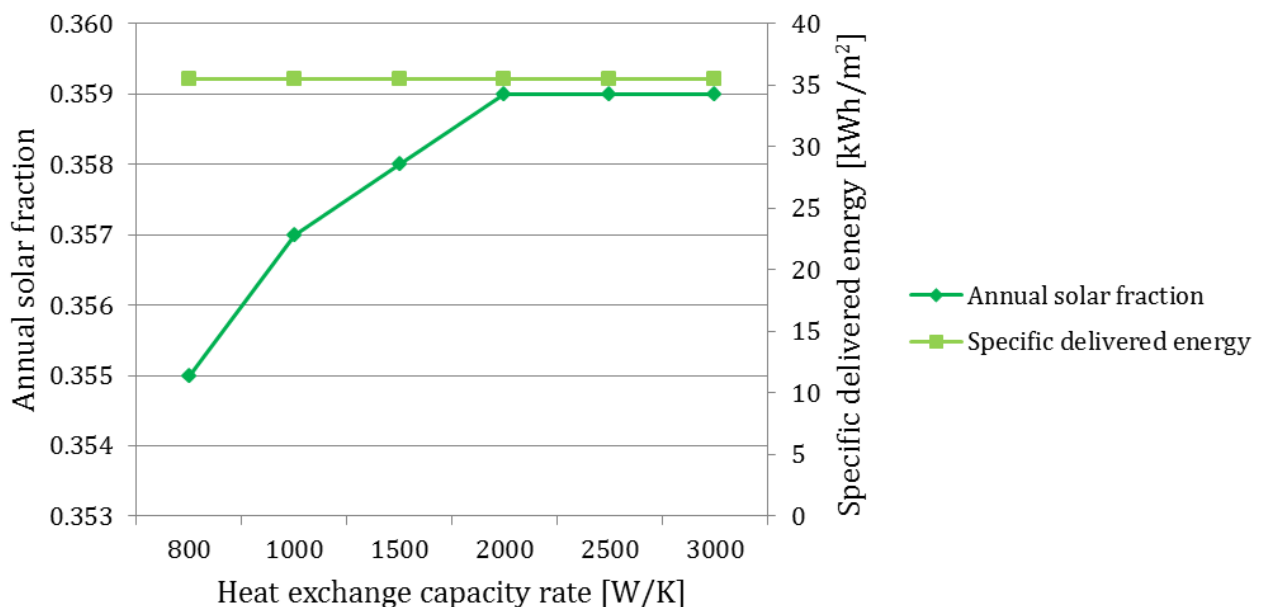


Figure 101 - Annual solar fraction and specific delivered energy as a function of heat exchange capacity rate

From Figure 101 it can be seen that the electric energy consumption is unaffected by the change in heat exchange capacity rate, and is constant at 35.5 kWh/m<sup>2</sup> for all simulated capacity rates. An increase in annual solar fraction is achieved by increasing the capacity rate from 800 W/K to 2000 W/K. The increase is however only 1.1 %, which indicates that the system performance is barely affected by the change in capacity rate. This explains why the electrical energy consumption is relatively constant. The effect of changing the heat exchange capacity rate may be more effective if the mass flow rate through the heat exchanger and/or the heat exchanger design is changed as well.

The length of integrated solar heat exchange spirals are dimensioned based on a rule of thumb, which recommends a length of 2 m/m<sup>2</sup> collector area (Furbo, 2004). This gives a total length of approximately 30 m with a collector area of 16 m<sup>2</sup>. It was assumed that the inner diameter of the heat exchanger is 21.6 mm, which gives a heat exchange volume of 0.04 m<sup>3</sup>. The integrated solar heat exchanger in the IDA ICE system has a volume of 0.01 m<sup>3</sup>. It was therefore decided to simulate the model with different heat exchange volumes ranging from 0.01 to 0.04 m<sup>3</sup> for both the integrated solar heat exchanger in the DHW tank and in the SH tank. It should be noted that it is only the volume that can be changed in IDA ICE, and not the heat exchanger inner diameter or length. The heat exchange capacity rate was kept at the IDA ICE setting of 170 W/K·m<sup>2</sup> during the simulations. All other parameters were kept at initial settings.

Increasing the integrated solar heat exchanger volume did not have any effect on the system performance. The annual net utilized solar energy and the annual specific delivered energy are presented in *Table F. 1* in *Appendix F – Design Parameter Study*.

### 13.1.8 EFFECT OF TANK PIPE INLET AND OUTLET LOCATIONS

The model was simulated with different pipe inlet and outlet locations for both the DHW tank and the SH tank in order to investigate if another composition would enhance the system performance. Simulations with changes made to the DHW tank and the SH tank were performed separately in order to get a better understanding of the effect of the changes performed. Several scenarios were simulated for both tanks, but only the scenarios which provided interesting results are presented.

The different scenarios simulated for the DHW tank are presented in Figure 102. The reference tank with the initial pipe inlet and outlet locations is shown to the upper left.

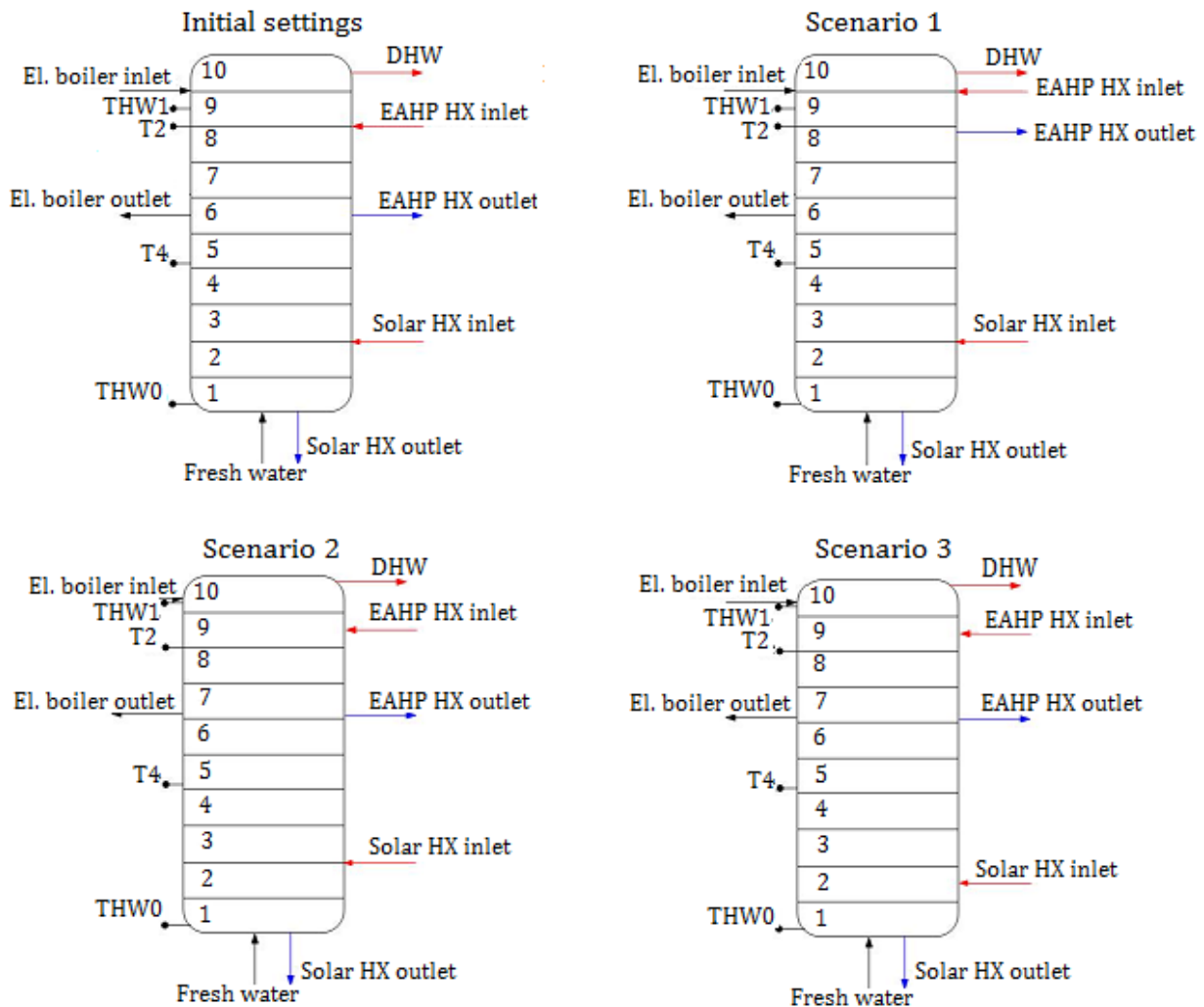
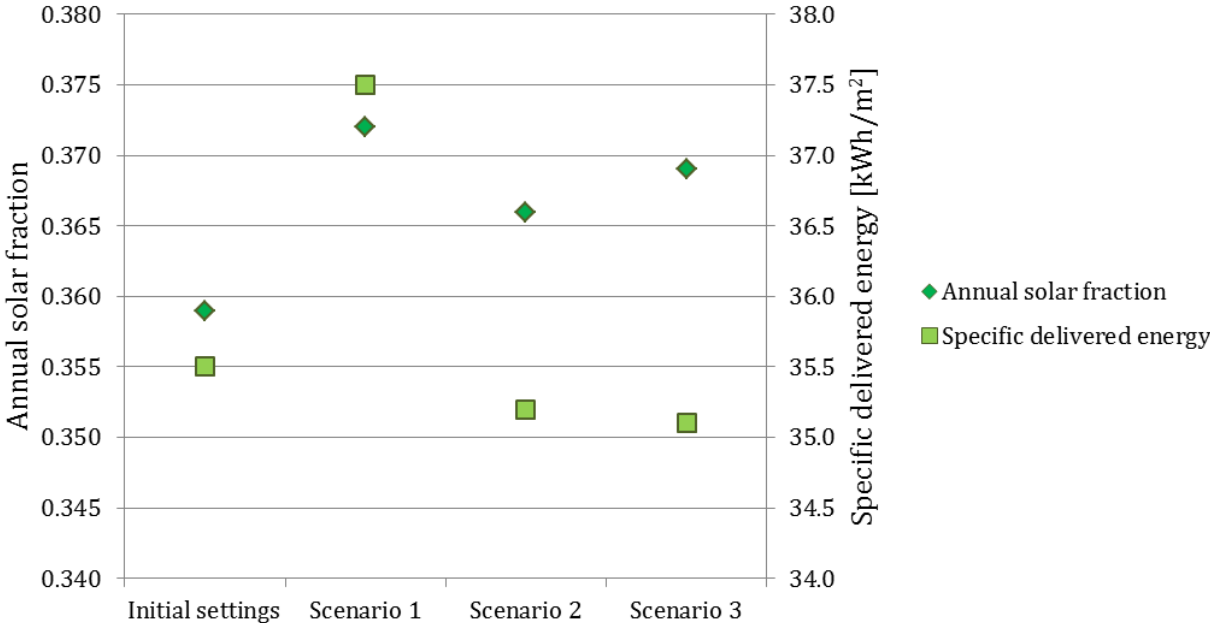


Figure 102 - Different pipe inlet and outlet locations, DHW Tank

In Scenario 1, the EAHP heat exchanger is located closer to the top of the tank, while in Scenario 2 and 3 the heat exchanger is located just a bit higher than in the reference tank. In Scenario 2 and 3 the location of temperature sensor, THW1, is located higher than in the reference tank and Scenario 1. Even though changing the location of the temperature sensor was not the purpose of this simulation, it had to be done since too high electrical energy consumption was observed when changes to the pipe inlets and outlets were performed without taking the location of the temperature sensor into account. As described earlier, both the operation of the electrical boiler and the exhaust air heat pump are controlled by signals sent from THW1. In Scenario 3, the

location of the solar heat exchanger inlet is lowered by 4 cm compared to the reference tank and the other scenarios. The DHW outlet is put even higher in Scenario 2 and 3 to ensure that the highest temperatures in the tank are utilized.

The annual solar fractions and the specific delivered energy obtained with the different scenarios are presented in Figure 103.



**Figure 103 - Annual solar fraction and specific delivered energy for different pipe inlet and outlet locations, DHW Tank**

The results show that the amount of utilized net solar energy is highly dependent on the available solar volume in the tank. Figure 103 shows that when EAHP heat exchanger is relocated higher in the tank (from reference tank to Scenario 1), the annual solar fraction is increased by 3.5 %. The colder the water in the lower part of the tank is, the more solar energy can be utilized and better solar collector efficiency is obtained. However, as seen in Figure 103, the electrical energy consumption is increased by 5.3 % from the reference tank to Scenario 1. Since the EAHP heat exchanger outlet is located at the upper part of the tank in Scenario 1, the volume covered by the EAHP is decreased and in order to cover the DHW demand, more electrical energy is consumed. Additionally, as seen in Figure 102, THW1 is located below both the EAHP heat exchanger and the electrical boiler, which results in worse control of these components. The temperature sensor should be located at the same height or higher than the components it controls.

A simulation with settings equal to Scenario 2, except for the location of THW1, which was at its initial height, was performed and resulted in an electrical energy use of 37.7 kWh/m². The volume covered by the EAHP was equally large as the volume in the reference tank and no extra electrical energy was needed to cover the DHW demand. The high electrical energy consumption was therefore due to the location of THW1.

In Scenario 2 the location of THW1 is increased to the same height as the electrical boiler and higher than the EAHP heat exchanger, as seen in Figure 102. This results in a decrease in electrical energy consumption to 35.2 kWh/m², as seen in Figure 103. The solar heat exchanger

inlet was lowered in Scenario 3 in order to make sure that the other heat suppliers in the tank did not affect the available solar volume. Figure 103 shows that this results in an increase in annual solar fraction of 0.6 % from Scenario 2 to Scenario 3.

During all simulations the DHW tank volume was kept at 180 l. With a larger tank volume, the EAHP heat exchanger could have been located higher in the tank, resulting in lower temperatures at the lower part of the tank. This would result in better system performance since more solar heat could have been supplied to the tank. From the results presented in Figure 103, Scenario 3 provides the best system performance with an electrical energy consumption of 35.2 kWh/m<sup>2</sup> and an annual solar fraction of 36.9 %. It should be noted that when several heat sources are utilized in a solar storage tank, the tank volume should range from 300-500 liters. If solar heat is the only energy supply, the tank volume may range from 140-300 liters (Laughton, 2010).

The different scenarios simulated for the SH tank are presented in Figure 104. The initial location for the pipe inlets and outlets is shown in the tank to the upper left, which is referred to as the reference tank.

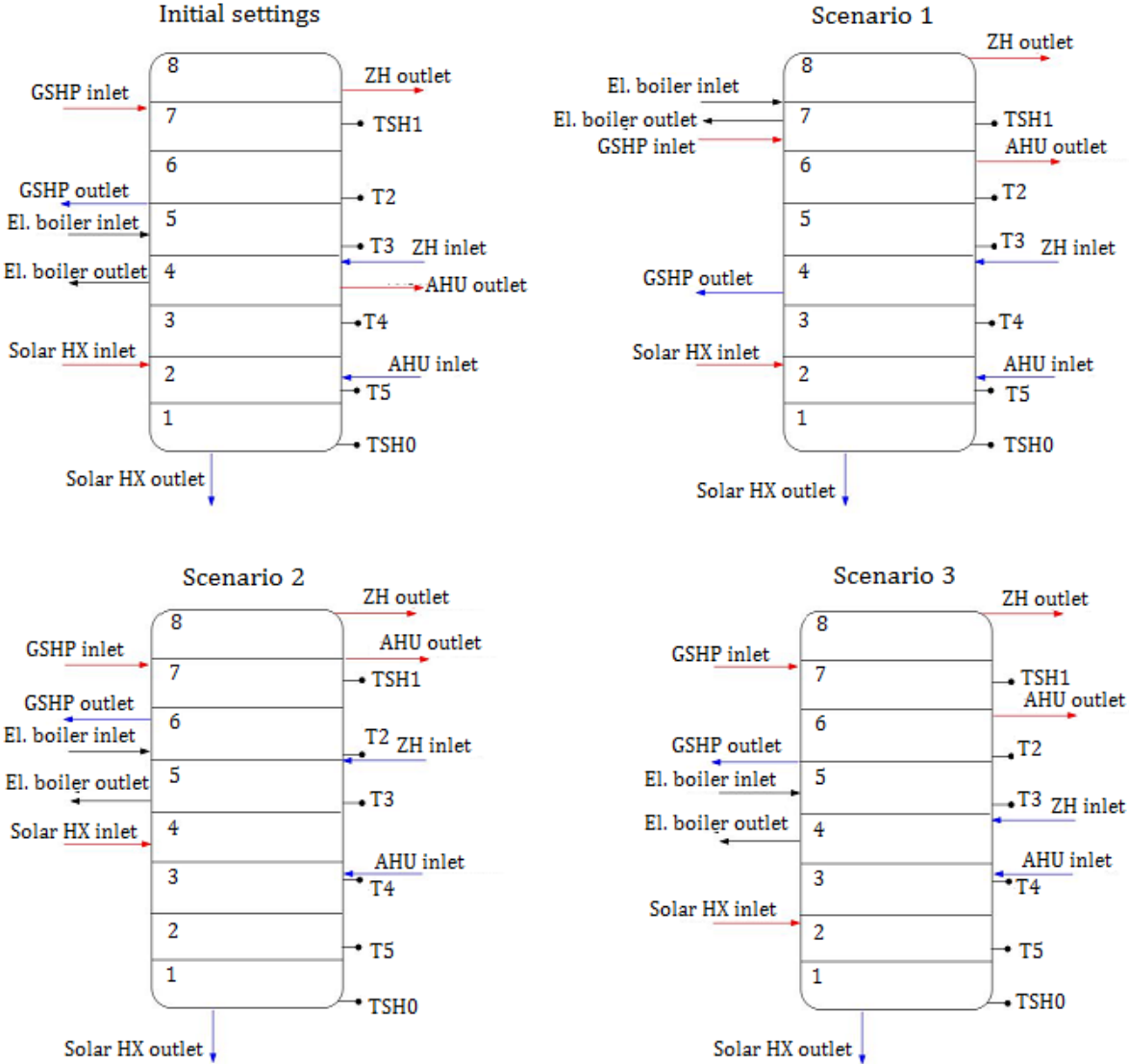
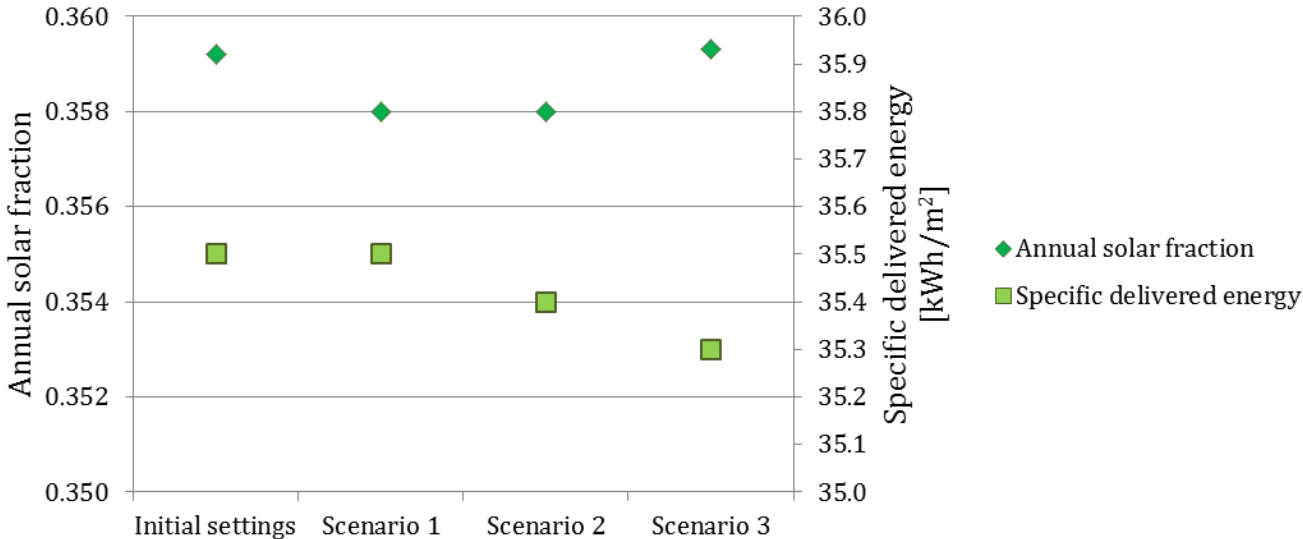


Figure 104 – Inlet and outlet locations, SH tank



As seen in Figure 104, Scenario 1 is the scenario which differs the most from the other scenarios since the position of the GSHP and the electrical boiler is switched. As opposed to the initial locations, the ZH and AHU outlets are located higher in the other scenarios in order to ensure that sufficient temperatures are supplied to the dwelling heating system and the heating coil in the air handling unit. In Scenario 2, the solar heat exchanger inlet is located higher than in the other scenarios, the ground-source volume is decreased and the auxiliary electrical boiler connections are positioned higher in the tank. In Scenario 3, the ground-source and electrical boiler pipe connections are at the initial locations, but the AHU outlet is located above the solar heat exchanger inlet.

The resulting annual solar fractions and the specific delivered energy for the reference system and each scenario are given in Figure 105.



**Figure 105 - Annual solar fraction and specific delivered energy for different pipe inlet and outlet locations, SH tank**

As seen in Figure 105, Scenario 3 results in enhanced system performance. By locating the AHU inlet above the integrated solar heat exchanger, the specific delivered energy is reduced by 0.6 %. Solar heat transferred to the tank increases slightly from the reference system to Scenario 3, which indicates that better system performance is achieved when other heat sources/sinks are located above the solar volume. The inlet temperatures from the AHU pipeline has a better match with the temperatures in Layer 3 compared to Layer 2, which is where the AHU pipe inlet is located in the reference tank. With a better temperature match, a better thermal stratification in the tank is achieved. The temperatures drawn to the zone heating system and the AHU heating coil with Scenario 3 are presented in *Figure F. 1 in Appendix F – Design Parameter Study*.

Switching the location of the GSHP and the electrical boiler does not affect the system positively since the annual solar fraction decreases as seen in Figure 105.

**13.1.9 EFFECT OF VERTICAL BOREHOLE DEPTH**

The effect of changing the borehole depth was investigated by simulating the model with depths ranging from 60–140 m. The depths were calculated based on the rule of thumb recommendations given in Table 3 and the required space heating effect of 2.8 kW calculated by Brødrene Dahl.

The specific delivered energy and the annual solar fraction obtained with each borehole depth is shown in Figure 106. It can be seen that with borehole depths shorter than 70 m, the specific delivered energy is increased, which indicates that the borehole is undersized. With depths ranging from 70–95 m, the specific delivered energy is constant. By increasing the depth further, a small reduction in electricity consumption is achieved as seen in Figure 106. The brine inlet temperature to the GSHP evaporator is increased due to a deeper borehole, resulting in decreased compressor electricity consumption.

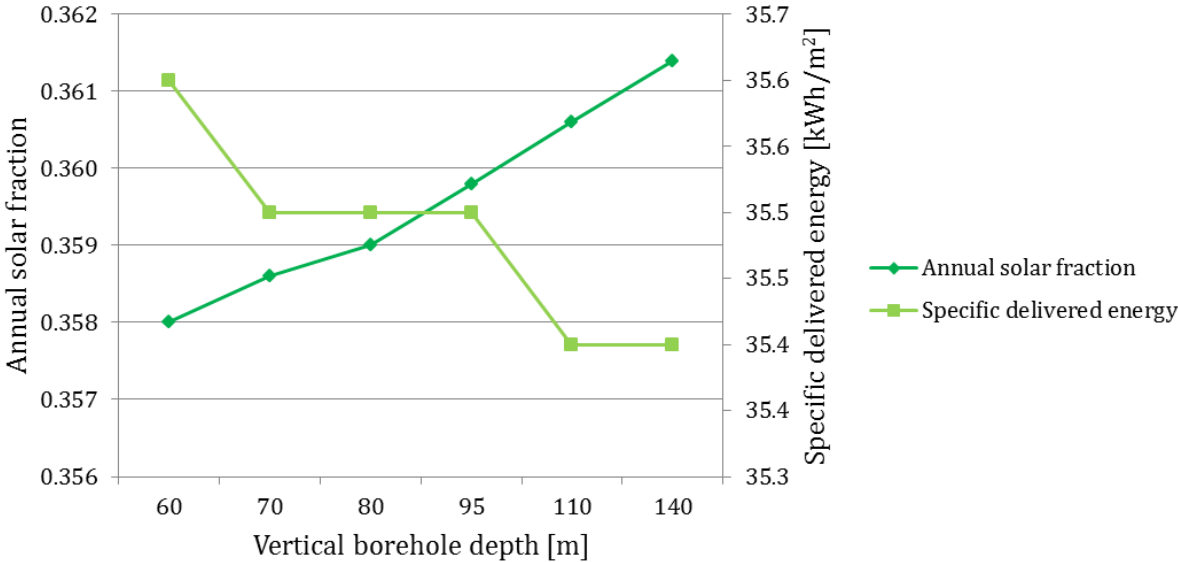


**Figure 106 - Annual solar fraction and specific delivered energy as a function of the borehole depth**

The results show that changing the borehole depth has a minor influence on the system’s electricity use. However, it is shown that the borehole depth can be as short as 70 m and still cover the space heating demand with the same use of electricity as the original depth of 80 m. This means that the initial costs of the system may be reduced due to a shorter borehole depth.

From Figure 106 it can be seen that the annual solar fraction increases from a borehole depth of 60 m to a borehole depth of 140 m. Compared to the initial borehole depth of 80 m, the maximum increase in annual solar fraction is approximately 0.7 %. With a deeper borehole, more solar energy is transferred to the ground, which explains the increase in annual solar fraction.

**13.1.10 EFFECT OF VERTICAL BOREHOLE DIAMETER**

The model was also simulated with different borehole diameters in order to investigate the effect on the system performance. Simulations with borehole diameters ranging from 11–16 cm were performed, and the results are presented in Table 29. The initial borehole diameter is 11.5 cm.

**Table 29 - Annual solar fraction and specific delivered energy for each borehole diameter**

	11.5 cm	12.5 cm	13.5 cm	14.5 cm	15.5 cm
<b>Net utilized solar energy [kWh/a]</b>	4183.5	4184.2	4184.7	4185.0	4186.8
<b>Specific delivered energy [kWh/m²]</b>	35.5	35.5	35.5	35.5	35.5

As seen in Table 29, the amount of net utilized solar energy is the only result affected by the change in borehole diameter. By increasing the diameter from the original setting of 11.5 cm to 15.5 cm the net utilized solar energy increases by 3.3 kWh/a, which only constitutes a minor difference and may be regarded as negligible. Decreasing the borehole diameter from 11.5 cm results in a slightly higher electricity consumption.

#### *13.1.11 EFFECT OF HORIZONTAL HEAT EXCHANGER LENGTH*

It was desired to investigate the difference in system performance with a horizontal ground heat exchanger installed instead of a vertical borehole. The model was therefore simulated with a horizontal GHE with different lengths ranging from 140-180 m. The lengths were calculated based on the required space heating effect of 2.8 kW, and the rule of thumb heat extraction rates for a horizontal loop, which are given in Table 3.

The results showed no difference in electrical energy consumption with the different horizontal ground heat exchanger lengths. However, by installing a horizontal loop instead of a vertical borehole, a reduction in electrical energy consumption was obtained. The results showed that the inlet brine temperature to the GSHP evaporator increased by 2°C, by installing a horizontal loop, even during winter. The actual temperatures registered in the ground with a vertical loop were lower compared to the temperatures with the horizontal loop, again even during the winter months. It was however expected that the actual temperatures in the ground would be higher further down in the ground than the temperatures at the upper soil layers. The ground is much more affected by the ambient air temperatures at the upper soil layers, than further down in the ground. As a consequence of the higher brine inlet temperature to the GSHP evaporator, the consumed compressor power was reduced when installing the horizontal loop.

The results obtained are considered unreliable due to the unreasonable temperature difference between the upper layers of the soil and the deeper layers in the ground. It was confirmed by the IDA ICE producers that the program does not work as well with horizontal ground heat exchangers as with vertical ground heat exchangers. It was therefore decided not to proceed with simulations regarding the horizontal ground heat exchanger.

#### *13.1.12 EFFECT OF GROUND-SOURCE HEAT EXCHANGER DIAMETER AND THICKNESS*

The effect of the heat exchanger diameter and thickness were investigated by simulating the model with a heat exchanger diameter ranging from 32–40 mm, and a thickness ranging from 2.0–3.7 mm. The ground heat exchanger material is normally plastic (PEM) with a thermal conductivity ranging from 0.3–0.5 W/m·K, depending on the density of the plastic material. In IDA ICE the thermal conductivity of the ground heat exchanger is initially 0.42 W/m·K. This seemed realistic and it was therefore decided not to change the thermal conductivity of the material in the performed simulations. The simulations were performed with an 80 m deep vertical borehole.

The results show that changing the heat exchanger diameter and the thickness of the heat exchanger pipe does not have any impact on the system performance. The specific annual delivered energy is presented in *Figure F. 2* in *Appendix F – Design Parameter Study*.

## 13.2 STUDY OF OPTIMAL OPERATION PARAMETERS

The results that are not presented by figures or tables in this subchapter, due to insignificant impact on the system performance, are presented by figures in *Appendix G – Operation Parameter Study*. The results are however commented on in this chapter.

### 13.2.1 EFFECT OF HEAT TRANSFER FLUID IN SOLAR CIRCUIT

The initial concentration of glycol in the solar circuit heat transfer fluid is 33 % for the “Multikomfort” system. The specific heat of glycol-water mixtures depends on and varies according to the fluid’s temperature and the volumetric percentage of glycol in the water. With a glycol-water mixture of 33 % the corresponding freezing point of the liquid is approximately -17°C, and the specific heat capacity varies from 3800-4100 J/kg·K. The recommended concentration is however 40-50 %, which allows temperatures down to -29°C. The specific heat capacity of 40-50 % glycol in water varies from 3474-3999 J/kg·K.

The model was simulated with glycol-water mixtures ranging from 25-45 %, in order to investigate the effect on the system performance. With a low glycol concentration, more heat may be transferred to the system since the specific heat capacity of water is higher. However, the fluid’s freezing point is then increased, which may be damaging to the solar collectors.

The results show that changing the glycol concentration has a minor impact on the system performance. It is observed that a slight increase in net utilized solar energy and a slight decrease in delivered energy are obtained when the fluid concentration is increased from 33 % to 45 %. This may be due to the freezing point of the fluid. The climate file utilized in the simulations contains outdoor air temperatures as low as -17°C. A better system operation is probably achieved when the freezing point of the liquid is decreased further. However, the differences are minor and changing the fluid concentration from 33 % to 45 % results in a decrease of only 0.02 % in electric energy consumption. The monthly solar fractions, annual net utilized solar energy and the specific annual delivered energy are presented in *Figure G. 1-Figure G. 2* in *Appendix G – Operation Parameter Study*.

### 13.2.2 EFFECT OF THE COLLECTOR MASS FLOW RATE

The effect of the collector’s mass flow rate on the system performance was simulated for mass flow rates ranging from 0.003 kg/s·m<sup>2</sup> to 0.014 kg/s·m<sup>2</sup> solar collector area. The initial mass flow rate through the solar circuit is approximately 0.010 kg/s·m<sup>2</sup> as seen in *12.1.3 Mass Flow Rate*. All other parameters were kept at the initial settings during the simulations.

In IDA ICE it is not possible to adjust the mass flow rate circulating through the collectors just by changing a parameter in the solar collector. The nominal mass flow rate as well as the pressure head in the circulation pumps in the solar circuit have to be adjusted in order to get appropriate mass flow rates through the collectors.

The obtained annual solar fraction and the annual specific delivered energy for each mass flow rate are plotted in *Figure 107*.

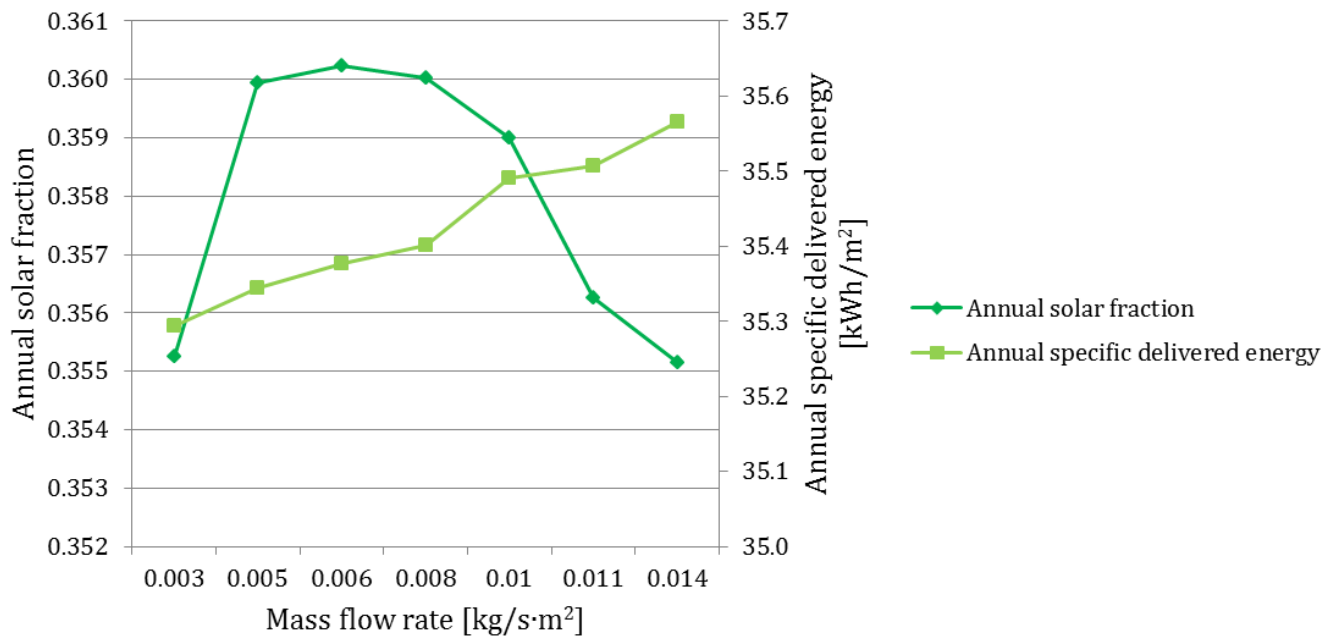


**Figure 107 - Annual solar fraction and annual specific delivered energy as a function of the collector mass flow rate**

Figure 107 shows that by increasing the mass flow rate in the solar circuit, higher electric energy consumption and lower annual solar fractions are obtained. The system's electric energy consumption increases since more electricity is used to circulate the enlarged flow rate through the solar circuit. By using too large mass flow rates through the solar collectors, usable flow temperatures may not be generated, which negatively affects the amount of usable solar heat transferred to the storage tanks in the system. This can be seen in Figure 107 where the annual solar fraction is decreased by 1.1 % from a mass flow rate of 0.010 kg/s·m<sup>2</sup> to 0.014 kg/s·m<sup>2</sup>. When the amount of solar heat transferred to the DHW tank, for instance, is decreased, the operation time of the electrical boiler and the EAHP compressor is increased in order to cover the DHW demand. This results in increased system electricity consumption as well.

If mass flow rates of 0.003 kg/s·m<sup>2</sup> or smaller are used in the system, the amount of collected heat is considerably reduced and low annual solar fractions are obtained as seen in Figure 107. Too high flow temperatures are obtained in the solar collector, and as a consequence the amount of collected solar heat is significantly reduced. As pointed out earlier, low collector temperature results in good collector efficiency.

As seen in Figure 107, mass flow rates ranging from 0.005–0.008 kg/s·m<sup>2</sup> enhance the system performance. Compared to the initial mass flow rate of approximately 0.010 kg/s·m<sup>2</sup>, the maximum increase in annual solar fraction within this range is 0.33 %, while the maximum decrease in annual specific delivered energy is 0.56 %. The differences are not major but noteworthy. The mass flow rates considered as optimum are however smaller than the mass flow rates which are recommended in the literature for solar heating systems with high-flow spiral tanks. As found in the subchapter *12.1.3 Mass Flow Rate*, the mass flow rates at maximum solar irradiation should be approximately 0.17 kg/s, which is 0.07 kg/s higher than the mass flow rate considered optimum for this system. However, solar heating systems are complex and a system configuration can vary significantly from one system to another. The design and operation parameters which may be considered optimum for one system may not be optimum

for another. It is also common that results from a computer simulation program differ from results obtained in a laboratory or when a full-size system is tested in reality.

### 13.2.3 EFFECT OF BRINE LIQUID IN THE GROUND-SOURCE HEAT EXCHANGER

The model was studied with different types of brine liquid circulating through the ground-source heat exchanger in order to investigate the effect on the system performance. As found in 7.3.2 *Ground Heat Exchanger Fluid*, the recommended and most commonly used brine liquid is a 30 % mixture of ethanol and water. The model was simulated with three different brine liquids with properties as shown in Table 30.

**Table 30 - Brine liquid in ground-source heat exchanger**

<b>Brine</b>	<b>Freezing point [°C]</b>	<b>Heat conductivity [W/m·K]</b>
<b>Ethylene-glycol</b>	-25	0.42
<b>Propylene-glycol</b>	-15	0.445
<b>Ethanol</b>	-20	0.399

Among these three brine liquids, the ethanol mixture has the highest specific heat capacity of approximately 4170 J/kg·K. During the simulations, all other parameters were kept at the initial settings.

The results show that the system performance is not notably affected by the change of brine liquid in the ground-source heat exchanger. The specific delivered energy obtained for each of the brine liquids can be seen in *Figure G. 3* in *Appendix G – Operation Parameter Study*.

### 13.2.4 EFFECT OF THE GROUND-SOURCE HEAT EXCHANGER MASS FLOW RATE

The system performance was investigated by changing the borehole mass flow rate. As discussed earlier, a mass flow rate of approximately 0.5 kg/s is commonly used. The initial mass flow rate in the borehole is 1.0 kg/s as seen in Table 22. The model was simulated with mass flow rates ranging from 0.3-1.2 kg/s. All other parameters were kept at initial settings.

The results show that lowering the mass flow rate to 0.3 and 0.5 kg/s increases the electricity consumption. This increase indicates that not enough heat is transferred in the circuit, and as a consequence, the operation time of the electrical boiler is increased in order to ensure that the set point temperature in the tank is maintained. The results show that with a mass flow rate of 0.7 kg/s the system's lowest electricity consumption is achieved. However, the difference in obtained specific delivered energy is minor, and a decrease of 0.06 % is achieved by changing the mass flow rate from 1.0 kg/s to 0.7 kg/s. The delivered energy for each simulation is shown in *Figure G. 4* in *Appendix G – Operation Parameter Study*.

### 13.2.5 EFFECT OF CONTROL SETTINGS

The model was simulated with different set point temperatures for the maximum allowable temperature near the bottom of the DHW tank. Initially the maximum allowable temperature is 60°C, as seen in Figure 46. With this temperature setting, available solar energy is transferred to the ground when the temperature at the lower part of the DHW tank reaches 60°C. By increasing this temperature, more solar energy may be utilized for domestic hot water preparation. The model was therefore simulated with maximum set point temperatures ranging from 60-85°C, in order to investigate the effect on the system's electrical energy consumption. All other parameters were kept at initial settings.

The results, both annual solar fraction and annual specific delivered energy, are presented in Figure 108.

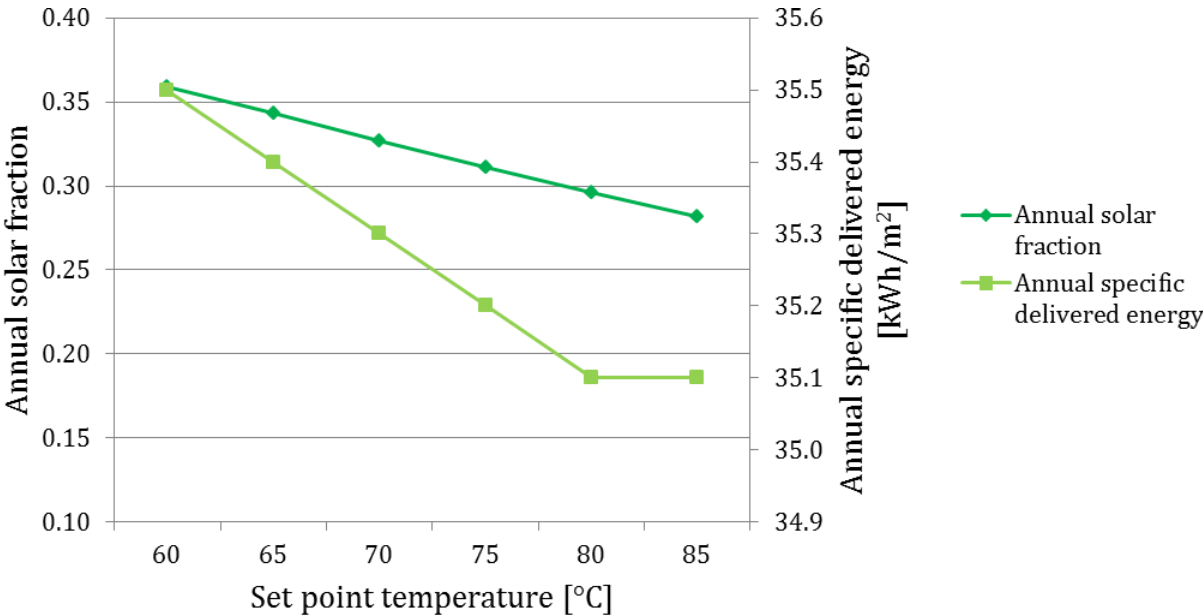


Figure 108 - Set point temperature DHW tank

It can be seen from Figure 108 that by increasing the set point temperature, the specific delivered energy is reduced. By increasing the temperature from 60 to 80°C, a reduction of 1.13 % in specific delivered energy is obtained. Figure 108 also indicates that the annual solar fraction is reduced, which is theoretically undesirable. However, by increasing the set point temperature, more solar energy is transferred to the DHW tank and not to the ground. The results show that the reduction of solar energy to the ground is higher than the increase in solar energy transferred to the tank, which explains why the solar fraction is reduced even though more solar energy is used for DHW preparation.

By increasing the set point temperature from 60 to 85°C, the DHW demand covered by solar energy in May, June, July and August is increased, as seen in Figure 109.

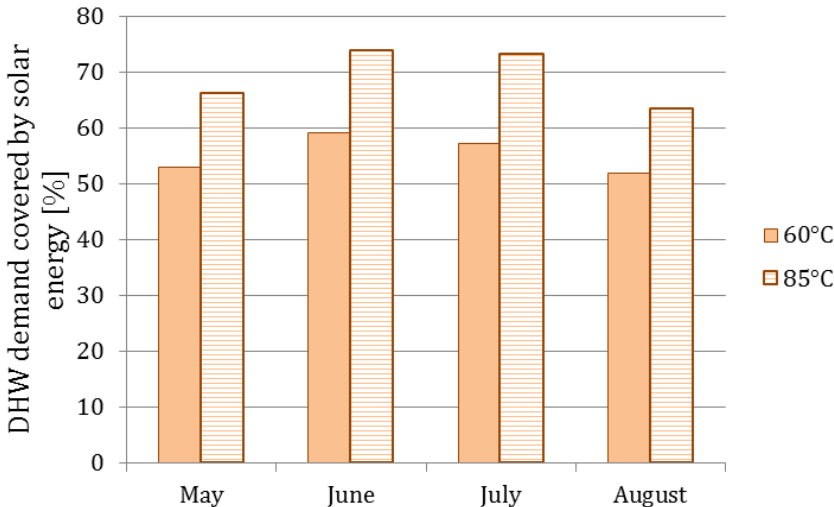


Figure 109 - DHW demand covered by solar energy during the summer months

By increasing the bottom set point temperature to 85°C, approximately 18 % more solar energy is transferred to the DHW tank through the year.

It should be noted that increasing the maximum allowable temperature near the bottom of the tank to 85°C did not result in overheating. The maximum temperature registered at the top of the tank did not exceed 90°C.

A simulation was also performed with additional control of circulation pump P3, which circulates the heat transfer fluid from the solar collectors to the ground. P3 is initially only in operation when the temperature at the bottom of the tank exceeds 60°C. However, solar energy is not utilized when the temperature difference between TSCout and THW0 is less than 5°C. By letting P3 be in operation when  $THW0 > 60^\circ$ ,  $(TSCout - THW0) < 5^\circ$  and when  $TSCout > 5^\circ$ , more solar energy can be utilized. With this control setting, the borehole is recharged during winter as well, which may result in higher brine inlet temperatures to the GSHP evaporator. Utilizing more of the solar energy increases the operation time of the solar collectors, which is beneficial.

The results show that by recharging the borehole during winter as well as summer, the annual solar fraction increases to 42.9 %, which is an increase of approximately 19 % compared to the initial annual solar fraction. Transferring solar heat to the borehole during the winter months results in a minor increase in inlet evaporator temperature and consequently a minor increase in the GSHP COP. This increase is of a small caliber and has therefore only an insignificant impact on the amount of utilized electrical energy. Since there was no noteworthy change in electricity consumption the results are not presented. The effect of recharging during winter would probably have been greater if there were several boreholes instead of only one due to the natural recovery of the ground.

In order to investigate the effect of the temperature sensor location in the DHW store, simulations with different sensor locations were performed. According to the German section of the International Solar Energy Society (2005), the temperature sensors should be located at the same height as the auxiliary heat exchanger or higher, but never below it (DGS, 2005). As seen in Figure 49, the temperature sensor which provides both the electrical boiler and the exhaust air heat pump with operational information, THW1, is located between Layer 8 and 9. THW1 is initially located below the inlet of the electrical boiler, and a simulation where THW1 was set at the same height as the electrical boiler was performed. Further, a simulation where THW1 was located above both the electrical boiler and the EAHP heat exchanger was also performed. An additional simulation where THW1 only provided information to the electrical boiler controller and T2 provided information to the exhaust air heat pump controller was performed. THW1 was located at the same height as the electrical boiler and T2 was located at the same height as the exhaust air heat pump.

The obtained annual specific delivered energy for each simulation is presented in Figure 110.





**Figure 110 - Temperature sensor location in DHW store, annual specific delivered energy**

As seen in Figure 110, locating the temperature sensor, THW1, at the same height as the electrical boiler inlet does not have any effect on the specific delivered energy compared to the initial setting. Changing the location to above the electrical boiler results in higher electrical energy consumption, as seen in Figure 110. The specific delivered energy decreases to 35.4 kWh/m<sup>2</sup> when the electrical boiler and the exhaust air heat pump are controlled by signals from separate temperature sensors. According to the results, lowering the temperature sensor connected to the operation of the EAHP improves the operation of the heat pump. When the temperature sensor was located between Layer 8 and Layer 9 the heat pump suffered from rapid on/off operation, as seen in *12.3 The Exhaust Air Heat Pump*. With the new location of temperature sensor T2, the operation is enhanced. The operation of the EAHP 2013-01-04 can be seen in *Figure G. 5 in Appendix G – Operation Parameter Study*.

### *13.2.6 EFFECT OF SUPPLY AIR AND ZONE SET POINT TEMPERATURE*

The specific delivered energy of 35.5 kWh/m<sup>2</sup> obtained with the initial parameter settings was calculated based on a zone set point temperature of 21°C and a supply air temperature of 19°C. If these temperatures were to be decreased within reasonable limits, the system electricity consumption may be reduced. In order to investigate the effect of this, the model was simulated with zone set point temperatures ranging from 19-21°C and supply air temperatures ranging from 17-20°C.

The results are shown in Figure 111-Figure 113.

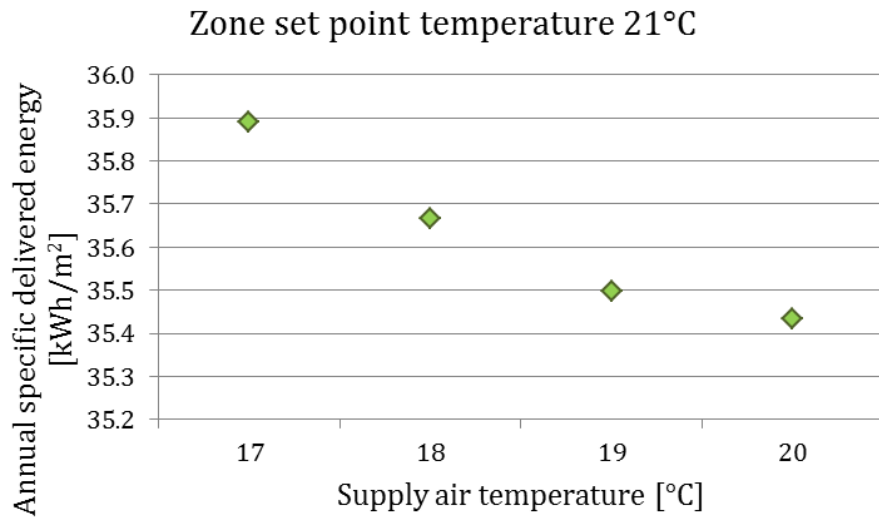


**Figure 111 - Annual specific delivered energy, zone set point temperature of 21°C and varying supply air temperature**

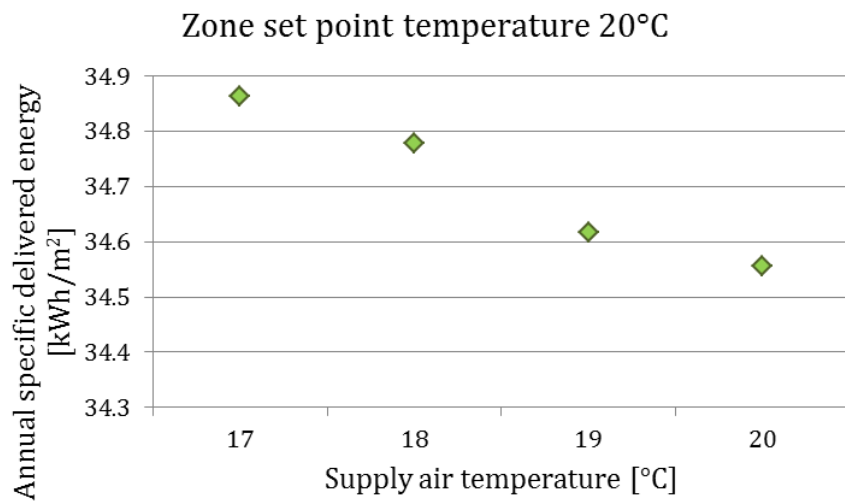


**Figure 112 - Annual specific delivered energy, zone set point temperature of 20°C and varying supply air temperature**

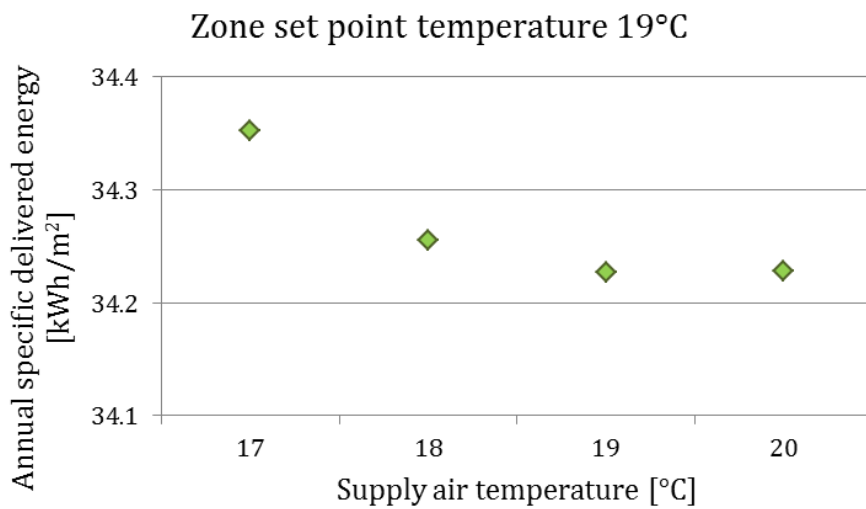


**Figure 113 - Annual specific delivered energy, zone set point temperature of 19°C and varying supply air temperature**

As seen in Figure 111-Figure 113, the specific delivered energy is greatly reduced from the initial value of 35.5 kWh/m<sup>2</sup> when the supply air and zone set point temperatures are reduced. A supply air temperature and a zone set point temperature of 19°C give the lowest electrical energy use. The specific delivered energy is reduced by approximately 3.6 %. With these temperature settings, the minimum indoor air temperature is reduced from 20.8°C to 18.5°C. However, the minimum air temperature is registered during the night in the winter months. During the day the air temperature lies between 19 and 20°C. With supply air and zone set point temperatures of 19 and 20°C respectively, the minimum temperature registered is 18.5°C as well, and the indoor air temperature during the day lies between 19 and 20°C. With both a supply air and zone set point temperature of 20°C, the minimum indoor air temperature is increased to be just below 20°C during the night in winter, and between 20.5 and 21.5°C during the day. A reduction of 2.8 % in specific delivered energy is obtained with temperature settings of 20°C compared to the initial temperature settings of 19°C for the supply air and 21°C for the zone set point temperature. The indoor air temperatures registered with a supply air and a zone set point temperature of 19°C may be perceived as too low. It is stated in NS 3031 that a set point temperature of 21°C should be maintained in order to provide a comfortable indoor climate. A supply air and zone set point temperature of 20°C thus appears to be the better solution.

**13.2.7 EFFECT OF NIGHT SETBACK CONTROL**

The model was initially simulated with a zone set point temperature of 21°C at all hours. In order to investigate what the effect of a night setback control would be, the model was simulated with set point temperatures of 17°C, 18°C and 19°C during the night and 21°C during the day. All other parameters were kept at the initial settings.

The results can be seen in Table 31.

**Table 31 - Specific delivered energy with night setback control**

<b>Night set point temperature</b>	<b>17°C</b>	<b>18°C</b>	<b>19°C</b>	<b>21°C (initial setting)</b>
<b>Specific delivered energy [kWh/m<sup>2</sup>]</b>	36.4	36.2	36.0	35.5

The specific delivered energy is increased by 1.4-2.5 % when a night set back control is used. The results show that there is a peak load in the morning when the zone set point temperature increases from for instance 17°C to 21°C. This peak is covered by the electrical boiler and as a consequence, more electrical energy is utilized compared to the model where a set point temperature of 21°C is maintained at all hours.

A simulation where the transition from the night set back temperature to the desired indoor air temperature was extended was also performed in order to investigate how it would affect the results. The result shows that the specific electrical energy is still higher than the result obtained with the initial set point temperature setting of 21°C. It should also be noted that the operation of the GSHP is smoother when a set point temperature of 21°C is maintained at all hours compared to the simulations where night setback control is used.

### 13.2.8 EFFECT OF AIR VOLUME FLOW RATE

The supply air flow rate in the dwelling is initially based on the minimum permitted average air volume flow rate stated in NS 3031, which is  $1.2 \text{ m}^3/\text{h}\cdot\text{m}^2$ . The model was simulated with different air volume flow rates in order to investigate the effect on the amount of utilized electrical energy in the system.

The annual specific delivered energy obtained from the simulations, as well as the annual average  $\text{CO}_2$ -concentration registered in the dwelling are presented in Figure 114.

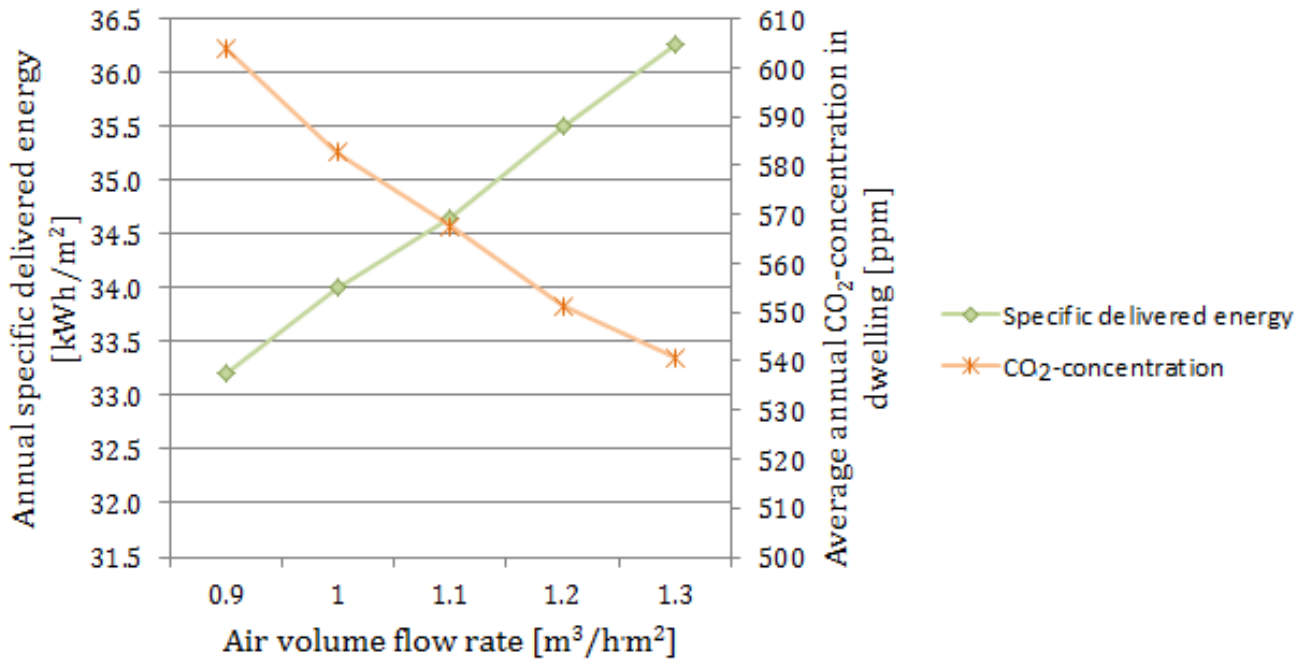


Figure 114 - Annual specific delivered energy as a function of air volume flow rate

The electrical energy use is considerably reduced when the air volume flow rate is decreased, as seen in Figure 114. The annual average  $\text{CO}_2$ -concentration registered in the dwelling is included in Figure 114 in order to provide an indication of the indoor air quality. It can be seen that the  $\text{CO}_2$ -concentration increases as the supply air flow rate decreases, which is expected. The  $\text{CO}_2$ -concentration presented in Figure 114 is the total  $\text{CO}_2$ -concentration and includes the outdoor concentration, which is assumed to be 350-400 ppm in Norway (Novakovic, et al., 2007). For dwellings with indoor air quality class 1 (high), the indoor  $\text{CO}_2$ -concentration should not exceed 350 ppm above outdoor concentration. For dwellings with indoor air quality class 2 (medium), the  $\text{CO}_2$ -concentration should not exceed 500 ppm above outdoor concentration. The general recommendation in Norway is a total  $\text{CO}_2$ -concentration below 1000 ppm in order to secure sufficient indoor air quality. In order to have an acceptable air quality, it is recommended that the supply air flow rate is 7 l/s per person in the respective room (Novakovic, et al., 2007). This roughly coincides with a volume flow rate of  $1.2 \text{ m}^3/\text{h}\cdot\text{m}^2$ . Figure 114 shows that the average  $\text{CO}_2$ -concentration never exceeds 1000 ppm. However, on a daily basis the registered  $\text{CO}_2$ -concentration is higher, and with a volume flow rate of  $0.9 \text{ m}^3/\text{h}\cdot\text{m}^2$ , concentrations up to 1000 ppm are found. As the volume flow rate decreases, the local age-of-air in each room increases and the air may be perceived as “heavy” and uncomfortable.

By decreasing the air volume flow rate from 1.2 to 1.0 m<sup>3</sup>/h·m<sup>2</sup>, the specific delivered energy is reduced by 4.2 %, and the increase in average CO<sub>2</sub>-concentration is just 5 %. By reducing the amount of available free energy in the exhaust air duct, the heat supplied by the electrical boiler to the DHW tank is increased. However, the increase is relatively small compared to the reduction in utilized fan power and a reduction in the system's total electrical use is achieved. It should be considered if it is desired to save electrical energy at the expense of high quality indoor air.

### 13.2.9 EFFECT OF HEATING SYSTEM SUPPLY TEMPERATURE

The model was simulated with different heat distribution system supply temperatures in order to investigate the effect on the electrical energy consumption. The supply temperature is initially set to 35°C, which ensures that the heating demand is met at all hours. Supply temperatures ranging from 28–35°C were simulated. All other parameters were kept at the initial settings.

The results can be seen in Table 32.

**Table 32 - Specific delivered energy with different heating system supply temperatures**

<b>Supply temperature heating system</b>	<b>28°C</b>	<b>30°C</b>	<b>32°C</b>	<b>35°C (initial setting)</b>
<b>Specific delivered energy [kWh/m<sup>2</sup>]</b>	34.9	35.1	35.2	35.5

By decreasing the supply temperature, the specific delivered energy decreases as seen in Table 32. Decreasing the supply temperature to 30°C results in 700 hours of unmet heating. Several days in the winter months have temperatures below 19°C, which is considered to be too low. With a supply temperature of 32°C, the lowest indoor air temperature registered is a day in January and is 19.6°C, which is considered acceptable. The specific delivered energy is reduced by 0.8 % when the supply zone heating temperature is decreased from 35 to 32°C, shown in Table 32. By decreasing the supply temperature from 35 to 32°C, an increase in GSHP COP is observed, which enhances the system performance.

### 13.3 SUMMARY OF THE DESIGN AND OPERATION PARAMETER OPTIMIZATION

The design and operation parameters with the greatest effect on the system electricity use are summarized and presented in this chapter.

In Figure 115 the change in utilized electrical energy,  $\Delta E$ , from the reference model with initial settings to the model with either optimized design or operation parameter, is shown in %. The optimized design parameters are presented by the green columns, and the optimized operation parameters are presented by the orange columns. The intention with Figure 115 is to elucidate the parameters with the greatest impact on the system electricity use, and thereby provide an indication of which parameters to focus on in order to optimize and enhance the system.

The column representing the change in solar collector area is derived from the difference in installing a suitable collector area of approximately 8 m<sup>2</sup> to an oversized collector area of 16 m<sup>2</sup>. The column which represents the auxiliary electrical volume in the DHW tank is derived from the difference in using an auxiliary volume of 100 l, which is recommended in the literature, and an auxiliary volume of 50 l.

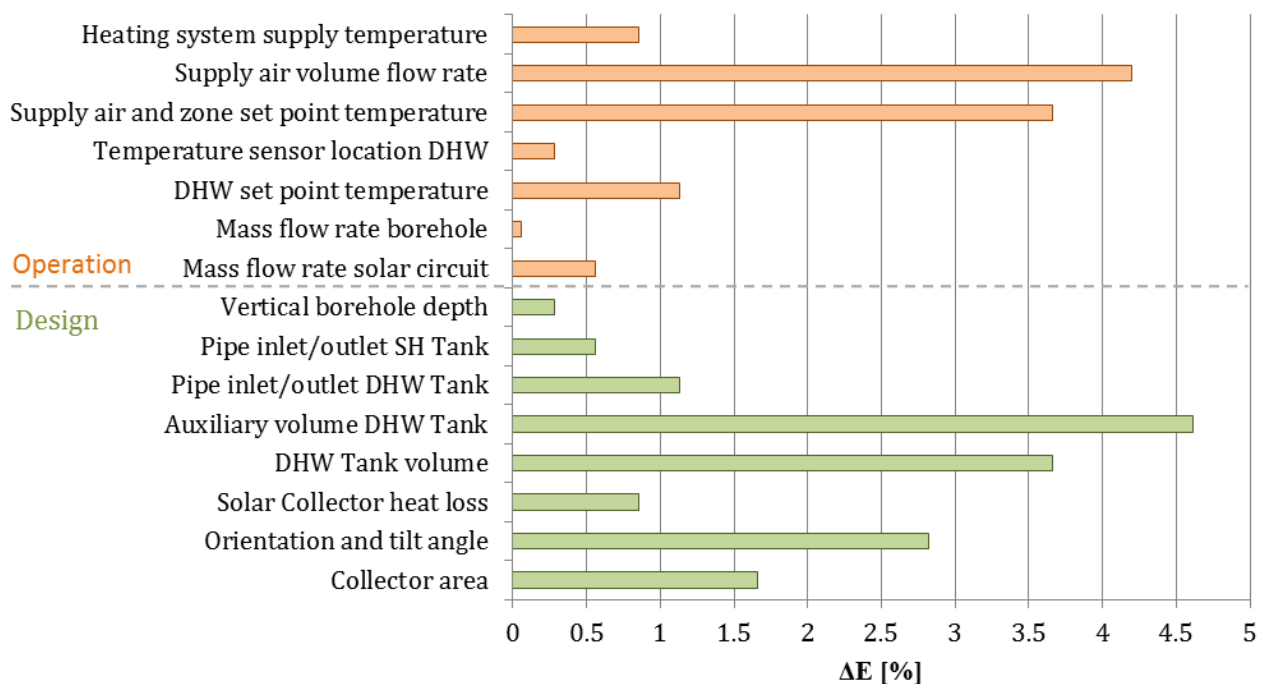


**Figure 115 - Design and operation parameters which gave the greatest reduction in electric energy use**

It is evident from Figure 115 that a good storage tank design is crucial as well as the orientation and tilt angle of the solar collectors. With an oversized solar collector area, approximately 1.6 % of the electricity use can be saved. Approximately 3.6 % of electrical energy can be saved by reducing the supply air and zone set point temperature from 19 and 20°C to 19°C. From Figure 115 it can be seen that the supply air volume flow rate has a great impact on  $\Delta E$ . Approximately 4.2 % of the electricity use is decreased just by reducing the supply air flow rate from 1.2 to 1.0 m<sup>3</sup>/h·m<sup>2</sup> floor area.

The changes that constitute the greatest difference in electricity use are the changes made to the supply air volume, supply air and zone set point temperatures, auxiliary electrical volume, volume of the DHW tank, orientation and tilt angle and the collector area. By comparing the

relative change for each of these parameters, the parameters with the greatest impact can be identified. The change in collector orientation and tilt angle has a great impact on the electricity use, but finding the percentage change from south-east to south is rather difficult. This change is therefore not included in the calculation.

The relative change is calculated according to Equation 29.

$$k = \frac{\Delta E}{\Delta X} \cdot 100 \% \tag{29}$$

where,  
 $\Delta E$  is the percentage change in used electricity  
 $\Delta X$  is the percentage change in parameter

The relative change for each of the parameters in question is listed in Table 33.

**Table 33 - Relative change in parameter**

	<b>Supply air volume</b>	<b>Supply temperature</b>	<b>Auxiliary volume</b>	<b>DHW tank volume</b>	<b>Collector area</b>
<b>Relative change [%]</b>	25.2	38.5	4.6	5.5	1.7

From Table 33 it can be seen that the operation parameters supply air volume, supply air and zone set point temperatures have the greatest impact on the system’s electricity use when taking the percentage change in parameter into account. The relative change obtained for the DHW tank volume and solar collector area are rather small, due to the percentage change in parameter. When the change results in increased component size, the amount of energy saved must be evaluated in context with the cost of installing enhanced solar collectors and/or larger storage tanks, for instance. A large change in parameter accompanied with a small change in saved energy may be regarded as unprofitable.

### 13.4 OPTIMIZED SCENARIOS

In this chapter, different optimized scenarios are created. When creating the scenarios, the design and/or operation parameters which resulted in the best system performance are included. The parameters which provided the lowest electricity use are prioritized. However, parameters where the electricity use did not change, but the annual solar fraction increased, are included as well. All the optimized design parameters for the solar collector are, for instance, gathered in one scenario. The same is done for the system storage tanks and the vertical borehole. A scenario where all the optimized operation parameters are gathered is created as well.

As seen in Table 34, scenarios which contain different compositions of the optimized system components are presented. By creating these scenarios it is possible to investigate the effect of optimizing few or several of the components in the system. The scenario number is given to the left in Table 34, while the belonging optimized system components can be found in the middle. The optimized parameters or the composition of optimized scenarios are shown to the right.

**Table 34 - Optimized scenarios**

	<b>Components</b>	<b>Parameters</b>
<b>Scenario 1</b>	Solar collectors	Solar collector area: $16 \text{ m}^2$ Orientation and tilt angle: <i>south, <math>55^\circ</math></i> Heat loss coefficients: $a_1 = 3.79 \text{ W/m}^2\text{K}$ , $a_2 = 0.0118 \text{ W/m}^2\text{K}^2$
<b>Scenario 2</b>	DHW storage tank	Tank volume: $300 \text{ l}$ Height/diameter ratio: $2.6$ Auxiliary electrical energy volume: $27 \%$ of tank volume Solar spiral heat exchanger effectiveness: $2000 \text{ W/K}$ Pipe inlet and outlet locations: <i>Scenario 3</i>
<b>Scenario 3</b>	SH storage tank	Tank volume: $500 \text{ l}$ Solar spiral heat exchanger effectiveness: $2000 \text{ W/K}$ Pipe inlet and outlet locations: <i>Scenario 3</i>
<b>Scenario 4</b>	Vertical ground heat exchanger	Depth: $110 \text{ m}$
<b>Scenario 5</b>	Operation	Collector mass flow rate: $0.006 \text{ kg/s}\cdot\text{m}^2$ Max. temp. DHW tank: $85^\circ\text{C}$ Temperature sensor: <i>THW1 at el.boiler, T2 at EAHP HE</i> Supply air/zone temp.: $20^\circ\text{C}$ Supply air volume flow rate: $1.0 \text{ m}^3/\text{h}\cdot\text{m}^2$ Zone supply temp.: $32^\circ\text{C}$
<b>Scenario 6</b>	Storage tanks	Scenario 2 and Scenario 3
<b>Scenario 7</b>	Solar collectors and DHW tank	Scenario 1 and Scenario 2



<b>Scenario 8</b>	Solar collectors and SH tank	Scenario 1 and Scenario 3
<b>Scenario 9</b>	Solar collectors and storage tanks	Scenario 1 and Scenario 6
<b>Scenario 10</b>	Solar collectors, DHW tank and vertical GHE	Scenario 1, Scenario 2 and Scenario 4
<b>Scenario 11</b>	Solar collectors, SH tank and vertical GHE	Scenario 1, Scenario 3 and Scenario 4
<b>Scenario 12</b>	Solar collectors, storage tanks and vertical GHE	Scenario 1, Scenario 4 and Scenario 6
<b>Scenario 13</b>	Solar collectors, DHW tank, vertical GHE and operation	Scenario 1, Scenario 2, Scenario 4 and Scenario 5
<b>Scenario 14</b>	Solar collectors, SH tank, vertical GHE and operation	Scenario 1, Scenario 3, Scenario 4 and Scenario 5
<b>Scenario 15</b>	Solar collectors, storage tanks, vertical GHE and operation	Scenario 1, Scenario 4, Scenario 5 and Scenario 6
<b>Scenario 16</b>	Storage tanks and operation	Scenario 5 and Scenario 6
<b>Scenario 17</b>	Storage tanks, vertical GHE and operation	Scenario 4, Scenario 5 and Scenario 6
<b>Scenario 18</b>	Solar collectors and operation	Scenario 1 and Scenario 5
<b>Scenario 19</b>	Solar collectors, storage tanks, vertical GHE and operation	Scenario 15 (with initial air volume flow rate)

Simulations with all the scenarios presented in Table 34 were performed, and the resulting specific delivered energy for each scenario is presented in Figure 116.

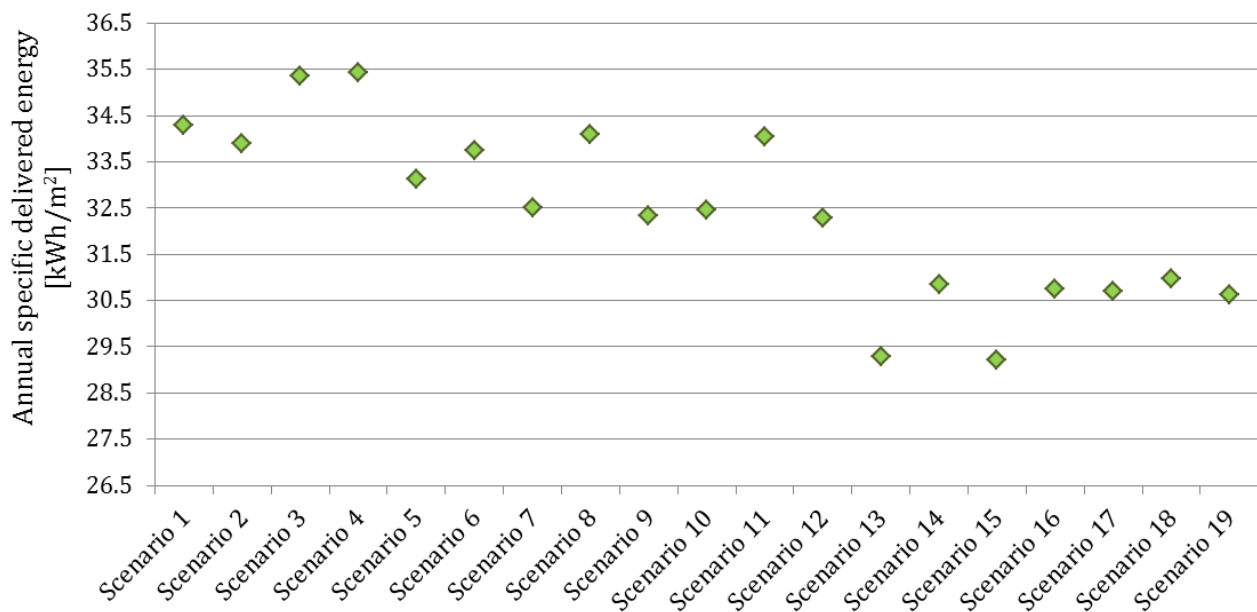


**Figure 116 - Optimized Scenarios, specific delivered energy**

Figure 116 shows that by optimizing only the solar collectors the annual specific delivered energy is decreased by 3.7 %. By optimizing the operation of the system (Scenario 5) and the storage tanks (Scenario 6), the annual solar fraction is decreased by 6.8 % and 5.1 % respectively.

The minimum annual specific delivered energy is obtained with Scenario 15, where the solar collectors, the storage tanks, the operation and the vertical borehole are optimized. The annual

specific delivered energy is decreased by 17.8 % compared to the reference system. A simulation where the air volume flow rate was kept at its initial value of 1.2 m<sup>3</sup>/h·m<sup>2</sup> (Scenario 19) was simulated in order to compare with the result obtained with Scenario 15. By keeping the initial air volume flow rate, a decrease in annual specific delivered energy of 13.8 % is obtained, which is 4 % lower than the obtained result in Scenario 15.

In Scenario 17, the solar collectors are not optimized, only the storage tanks, the operation of the system and the vertical borehole. Without taking the possibility of optimizing the solar collectors into account, the annual specific delivered energy is reduced by 13.5 % compared to the reference system.

### 13.5 SENSITIVITY ANALYSIS

A sensitivity analysis was performed on Scenario 15 in order to investigate how the result would be influenced by variations in input parameters. Parameters such as the solar collector efficiency, the efficiency of the circulations pumps and the fans in the system as well as the U-value of the storage tanks, the conductivity of the ground and the efficiency of the heat recovery unit, were modified by ± 10 %. The heat loss coefficients of the storage tanks were modified by ± 20 %.

The diagram showing the variations in obtained annual specific delivered energy can be seen in Figure 117.

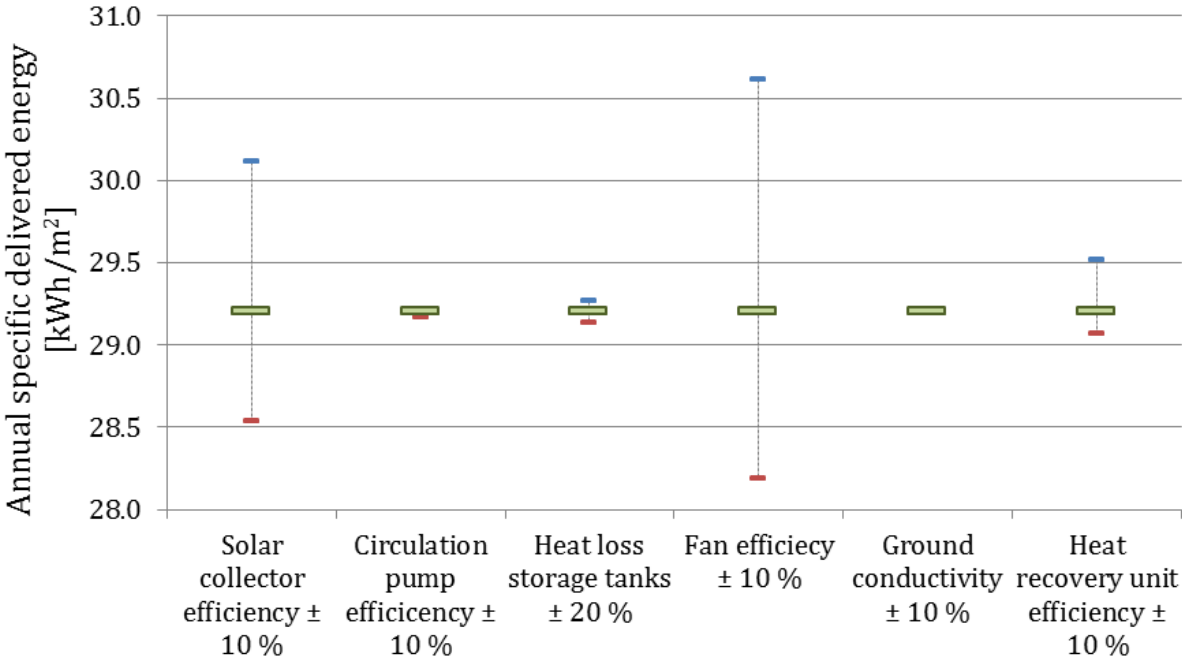


Figure 117 - Sensitivity analysis, Scenario 15

With improved solar collector efficiency the annual specific delivered energy could have been 28.5 kWh/m<sup>2</sup>, which represents a reduction of 2.4 % from the initial electricity use in Scenario 15 and 19.7 % compared to the reference system.

From Figure 117 it can be seen that variations in the circulation pump efficiency, the storage tank U-values and the ground conductivity have minor effect on the result. With better tank insulation and/or tank material, the result could have been enhanced by 0.24 %. It is evident

that the efficiency of the fans in the air handling unit has considerable impact on the result. By increasing the efficiency by 10 %, the specific delivered energy could have been reduced by 3.5 % from Scenario 15 which would give a total reduction of 20.6 % from the reference system. If a less efficient heat recovery unit was installed, the system's electricity use could have increased with about 1.1 %.

### 13.6 SYSTEM WITH OPTIMIZED DESIGN AND OPERATION PARAMETERS

Electrical energy use, energy demand and utilized free energy for both Scenario 15 and Scenario 17 will be presented in this chapter. The parameters which are optimized in these scenarios can be found in Table 34. It is chosen to include Scenario 17, where the solar collectors are not optimized, since it is decided that the solar collectors ought to be an integrated part of the roof construction in the "Multikomfort" dwelling. The collector orientation and tilt angle is therefore south-east and 19° in Scenario 17. Additionally, the solar collector heat loss is not optimized in Scenario 17. It is desired to investigate the difference between installing 16 m<sup>2</sup> and 8 m<sup>2</sup> of solar collector area even though the previous results show that a collector area of 16 m<sup>2</sup> is more favorably energetically.

#### 13.6.1 ELECTRICITY USE AND ENERGY DEMAND

The specific delivered energy, the specific heating demand and the total heating demand for Scenario 15 and Scenario 17, both with 16 m<sup>2</sup> and 8 m<sup>2</sup> of installed solar collector area, are presented in Table 35. The specific heating demand is the energy needed to cover the space heating demand, while the total heating demand includes the energy needed for domestic hot water preparation. The obtained results from the optimized scenarios are compared to the reference system in Table 35.

**Table 35 - Specific delivered energy, specific heat demand and total heat demand for Scenario 15 and 17**

	<b>Specific delivered energy [kWh/m<sup>2</sup>]</b>	<b>Specific heating demand [kWh/m<sup>2</sup>]</b>	<b>Total heating demand [kWh/m<sup>2</sup>]</b>
<b>Reference system</b>	35.5	27.1	57.7
<b>Scenario 15, 16 m<sup>2</sup></b>	29.2	23.4	54.0
<b>Scenario 15, 8 m<sup>2</sup></b>	30.4	23.4	54.0
<b>Scenario 17, 16 m<sup>2</sup></b>	30.7	23.4	54.0
<b>Scenario 17, 8 m<sup>2</sup></b>	31.6	23.4	54.0

Compared to the reference system with the initial settings, the specific delivered energy is considerably reduced in the optimized scenarios with 16 m<sup>2</sup> of installed solar collector area. A reduction of 13.5 % is achieved from the reference system to Scenario 17. By optimizing the solar collectors as well, an additional 4 % of the electrical energy can be saved.

As seen in Table 35, the specific heating demand is reduced to 23.4 kWh/m<sup>2</sup> in the optimized scenarios. This constitutes a reduction of 13.6 % compared to the reference system. The reduction is primarily obtained by reducing the indoor zone set point temperature to 20°C. It was decided to use a zone set point temperature of 20°C instead of 19°C in order to ensure that the indoor air temperature is maintained at a comfortable level. A graph showing the indoor air temperature for the different zones in the "Multikomfort" dwelling can be seen in *Appendix H – Indoor Air Temperatures*.

### 13.6.2 UTILIZED FREE ENERGY – SCENARIO 17

In Figure 118 the total heating demand, the AHU heat recovery, the total utilized free energy as well as electrical heating is presented for Scenario 17, with both 16 m<sup>2</sup> and 8 m<sup>2</sup> of installed solar collector area.

The total heating demand includes the required energy for space heating and domestic hot water, while the utilized free energy includes solar energy, ground source energy and energy from the exhaust air. The electrical heating includes required electrical energy needed to cover the peaks and the electricity utilized by the heat pump compressors in the system.

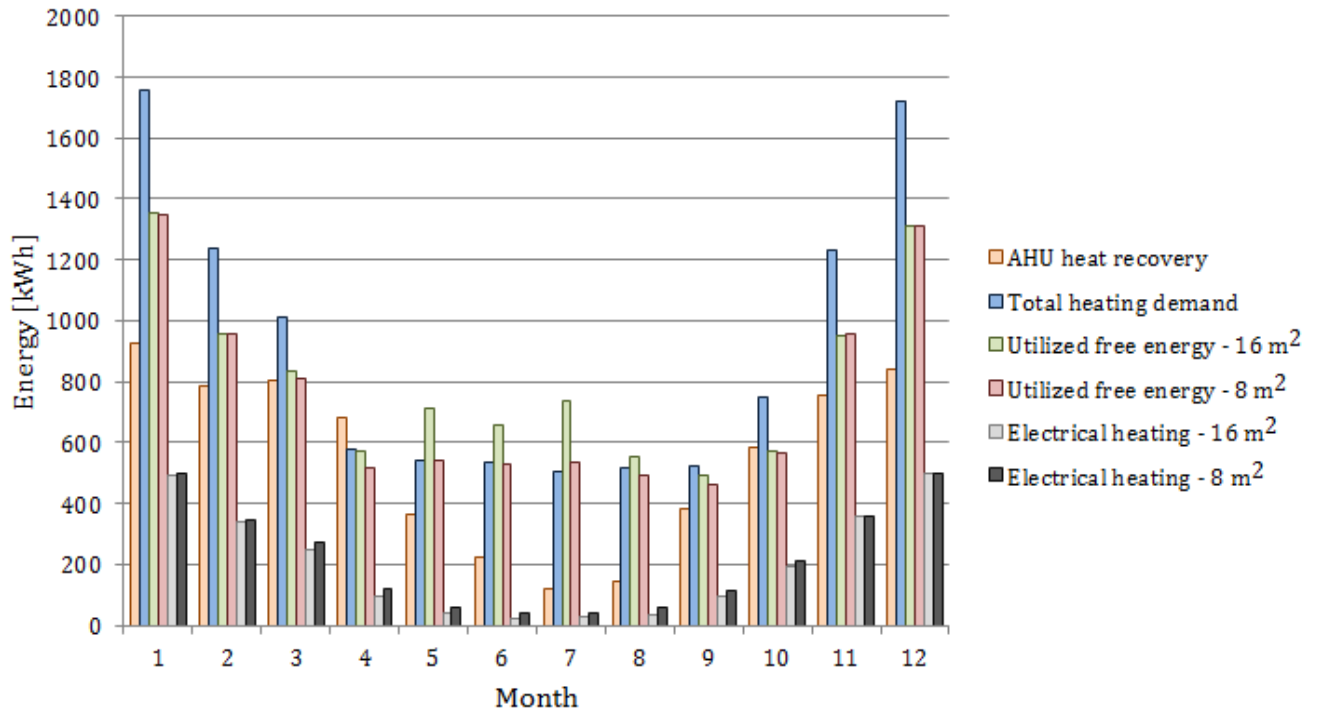


**Figure 118 - Total heating demand, AHU heat recovery, utilized free energy and electrical heating for Scenario 17, 16 and 8 m<sup>2</sup> collector area**

The total annual heating demand for the “Multikomfort” dwelling is 10 900 kWh/year and the total annual AHU heat recovery is 6 600 kWh/year. It can be seen in Figure 118 that heat recovery of the supply air is needed in all months. With 16 m<sup>2</sup> of solar collectors installed, a larger amount of free energy is utilized in March, April and September compared to a solar collector area of 8 m<sup>2</sup>. The noticeable increase in utilized free energy seen in May, June, July and August, indicates that excess solar heat is produced. As the monthly heating demand decreases and a larger part of the demand can be covered by free energy, the need for electrical heating is reduced as seen in Figure 118. By installing 8 m<sup>2</sup> of solar collectors less solar energy is collected, which results in an increased electricity use through the year. It can be seen that no excess solar heat is produced with 8 m<sup>2</sup> of solar collectors installed.

The total amount of utilized free energy for a collector area of both 16 m<sup>2</sup> and 8 m<sup>2</sup> is compared to the total heating demand in Table 36. The excess solar energy utilized to recharge the borehole is not included in the calculations.

**Table 36 - Amount of utilized free energy, Scenario 17**

	<b>Total</b>	<b>Fraction</b>
<b>Heating demand</b>	10 900 kWh/year	-
<b>Scenario 17, 16 m<sup>2</sup></b>	9 120 kWh/year	83.7%
<b>Scenario 17, 8 m<sup>2</sup></b>	8 050 kWh/year	73.9 %

If 16 m<sup>2</sup> of solar collectors are installed, approximately 84 % of the annual heating demand is covered by free energy. This constitutes approximately 10 % more than if 8 m<sup>2</sup> of solar collectors are installed.

### 13.6.3 DHW DEMAND

How the utilized free energy is distributed in the domestic hot water tank is illustrated in Figure 119. The DHW demand as well as the transferred solar heat and exhaust air heat with both 16 m<sup>2</sup> and 8 m<sup>2</sup> of solar collector area are presented.

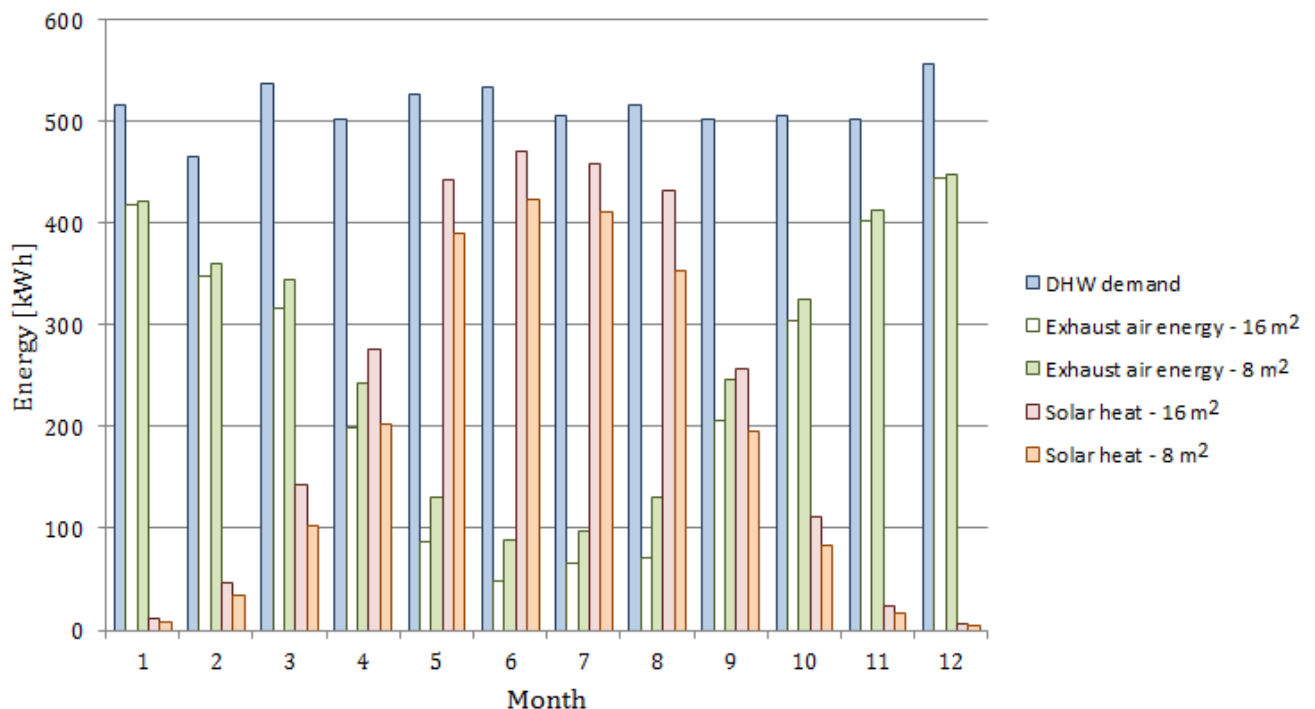


**Figure 119 - Amount of utilized free energy in DHW Tank, Scenario 17**

The DHW demand is relatively constant through the year, and is approximately 500 kWh per month. From Figure 119 it can be seen that less exhaust air energy is transferred to the DHW tank towards the summer months, when more solar energy is available and can be utilized for DHW production. It is evident from Figure 119 that a large part of the DHW demand is covered by solar energy during the summer months with both a solar collector area of 16 m<sup>2</sup> and 8 m<sup>2</sup> installed. Due to the temperature control setting of the DHW tank, not all of the collected solar energy is utilized for DHW production during the summer months. The maximum allowable temperature near the bottom of the DHW tank is 85°C, and when this temperature is exceeded, available solar energy is transferred to the ground instead. As a consequence, the EAHP is in operation during the summer months in order to cover the DHW demand. Even with an oversized solar collector area, the DHW demand is not 100 % covered, as seen in Figure 119.

The temperature control setting is necessary in order to protect the tank from overheating. Without this restriction, 100 % coverage of the DHW demand would probably have been achieved, especially with a collector area of 16 m<sup>2</sup>.

The monthly fractions of DHW demand covered by solar heat, with both 16 m<sup>2</sup> and 8 m<sup>2</sup> of solar collector area, can be seen in Figure 120.

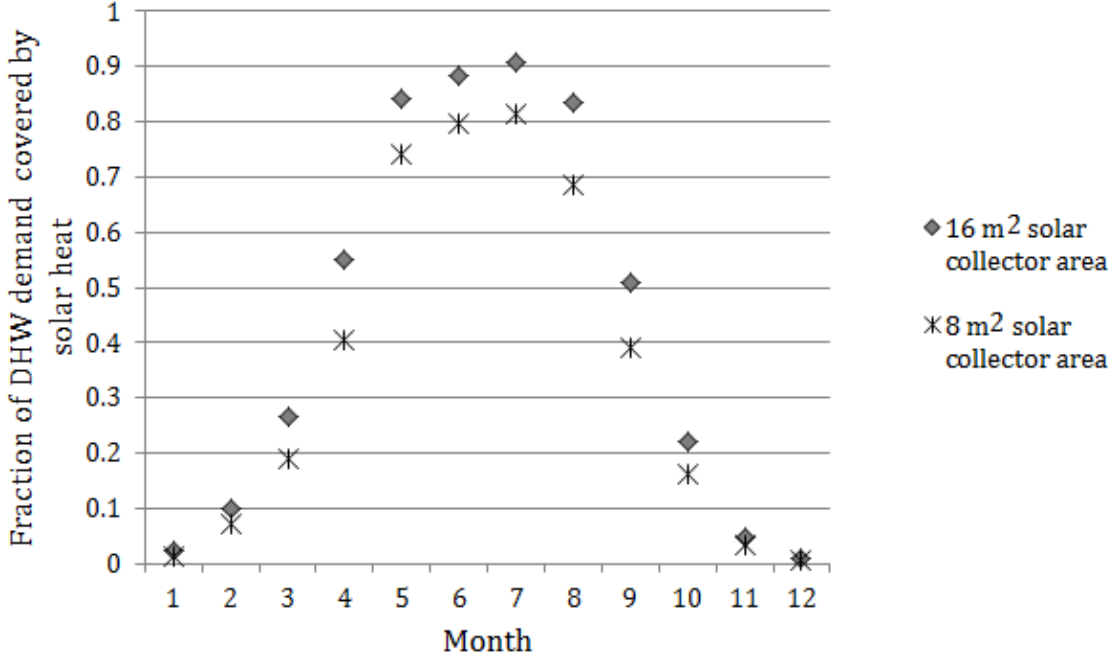


Figure 120 - Fraction of monthly DHW demand covered by solar heat, Scenario 17

By installing 16 m<sup>2</sup> of solar collectors a larger fraction of the total domestic hot water demand is covered by solar heat through the year. In March, for instance, approximately 30 % of the DHW demand is covered by solar energy, compared to only 20 % with a solar collector area of 8 m<sup>2</sup>. About 50 % of the demand is covered by solar heat in September with a collector area of 16 m<sup>2</sup>. Between 80 and 90 % of the DHW demand is covered by solar heat in May, June, July and August when 16 m<sup>2</sup> of solar collectors are installed.

### 13.6.4 SPACE HEATING DEMAND

The amount of utilized free energy for space heating, both with 16 m<sup>2</sup> and 8 m<sup>2</sup> collector area installed, can be seen in Figure 121. The blue column represents the space heating demand, which includes both the zone heating demand and AHU heating demand.

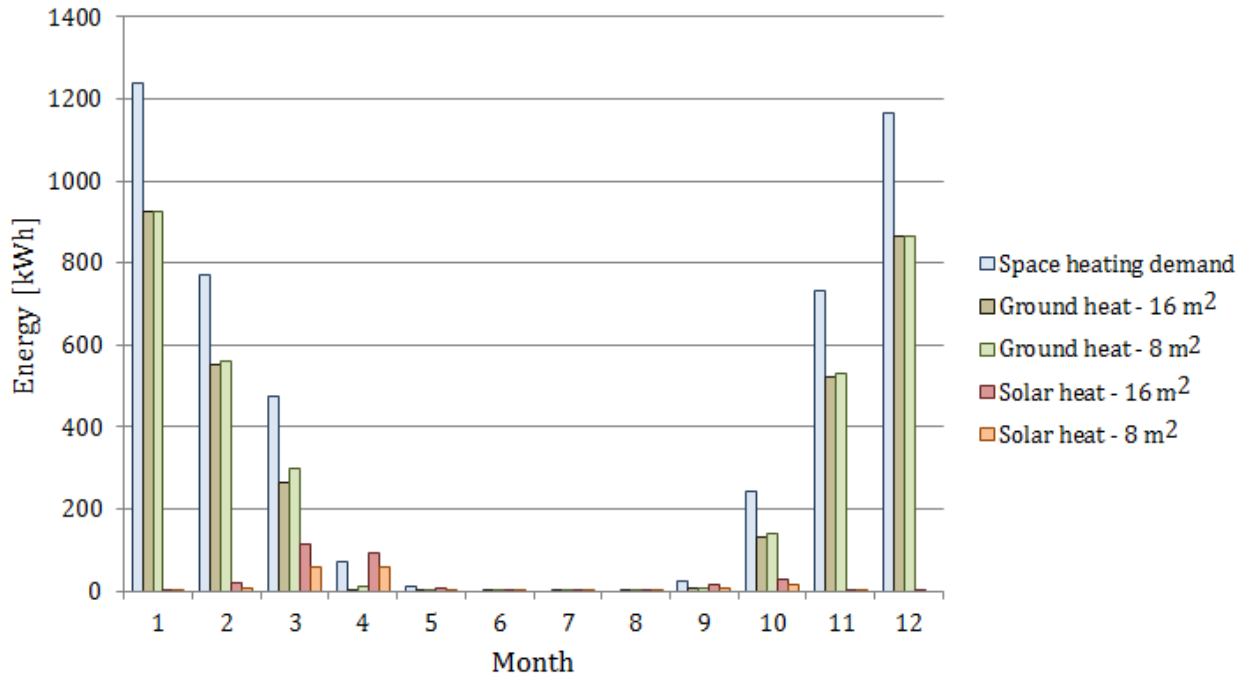


Figure 121 - Amount of utilized free energy for space heating, Scenario 17

As seen in Figure 121, the highest space heating demand is found in January and is approximately 1200 kWh. The lowest heat demand is found in May and is approximately 10 kWh. Figure 121 shows that there is almost no heating demand in the “Multikomfort” dwelling from May to September. Approximately 75 % of the space heating demand is covered by ground heat in the coldest winter months, January and December. Solar energy is utilized for space heating from February to October, and with 16 m<sup>2</sup> of solar collectors installed, the space heating demand in April is covered 100 % by solar energy.

The amount of space heating demand covered by solar energy, with both 16 m<sup>2</sup> and 8 m<sup>2</sup> of collector area, is listed in Table 37.

Table 37 - Space heating demand covered by solar energy, Scenario 17

Month	16 m <sup>2</sup> collector area	8 m <sup>2</sup> collector area
February	2.4 %	0.9 %
March	24.0 %	12.7 %
April	100 %	79.1 %
May	72.2 %	41.2 %
September	74.0 %	36.0 %
October	12.1 %	5.9 %

Approximately 70 % of the space heating demand is covered by solar heat in May and September with a collector area of 16 m<sup>2</sup>, as opposed to only 40 % with 8 m<sup>2</sup> of installed solar collector area.

### 13.6.5 SOLAR ENERGY TRANSFERRED TO THE GROUND

The amount of solar heat utilized to recharge the borehole is illustrated in Figure 122 for both a collector area of 16 and 8 m<sup>2</sup>.

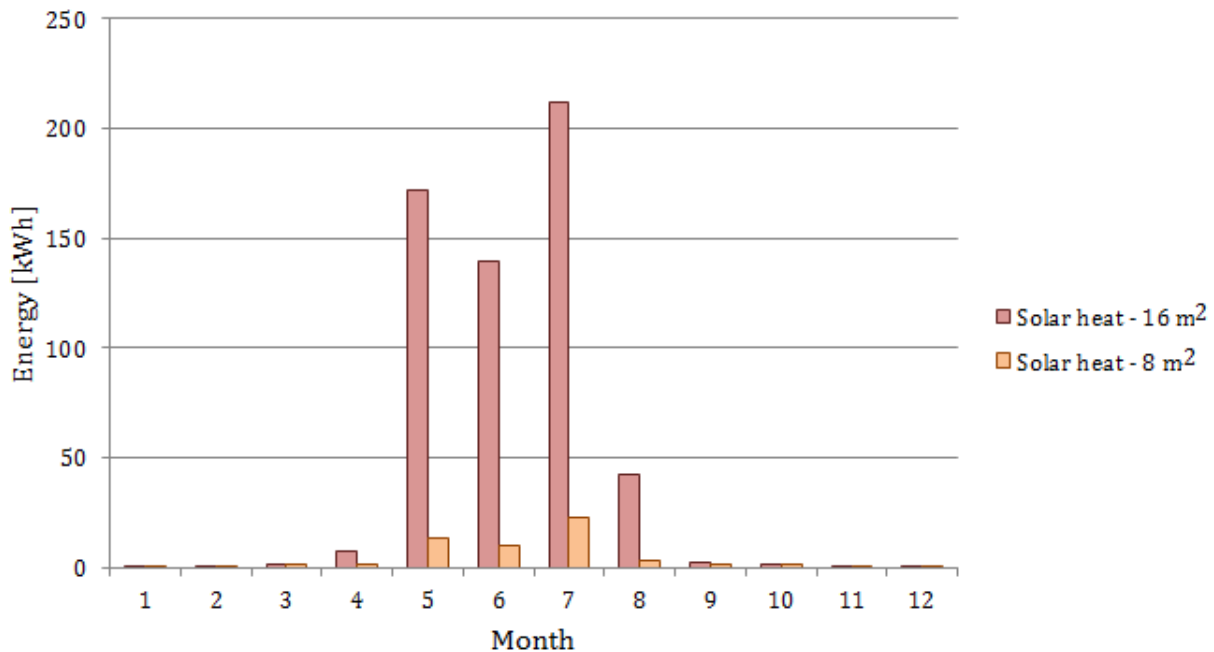


Figure 122 - Amount of utilized solar energy for recharging of borehole, Scenario 17

As pointed out earlier, excess solar heat is produced when 16 m<sup>2</sup> of solar collector area is installed. This excess heat can be utilized to recharge the borehole or a swimming pool if desired. The results showed that recharging the borehole with excess solar heat during the summer had minor effect on the GSHP COP and entering brine temperature during winter. Since only one borehole is needed in this system, the ground recovers naturally without any need for excess energy. However, utilizing the borehole for heat protection is advantageous and both the solar collectors and the storage tanks are protected against too high temperatures. Figure 122 indicates that solar heat is transferred to the ground also with 8 m<sup>2</sup> of solar collectors installed. This is due to the maximum allowable temperature at the bottom of the tank of 85°C, which is needed for heat protection as earlier discussed.

The system's annual solar fraction, simulated with both 16 m<sup>2</sup> and 8 m<sup>2</sup> of installed solar collector area for Scenario 17 can be seen in Table 38.

Table 38 - Annual solar fraction, Scenario 17

	16 m <sup>2</sup> solar collector area	8 m <sup>2</sup> solar collector area
<b>Solar fraction [%]</b>	32.3	22.3

By installing 16 m<sup>2</sup> of solar collector area instead of 8 m<sup>2</sup>, 10 % more solar energy is utilized to cover the energy demand of the "Multikomfort" dwelling.



### 13.7 UTILIZED FREE ENERGY – SCENARIO 15

The total heating demand, the AHU heat recovery, the utilized free energy and electrical heating demand with both 16 m<sup>2</sup> and 8 m<sup>2</sup> of solar collectors installed for Scenario 15 are presented in Figure 123. The solar collectors are optimized in Scenario 15, and have an orientation towards the south and a tilt angle of 55°.

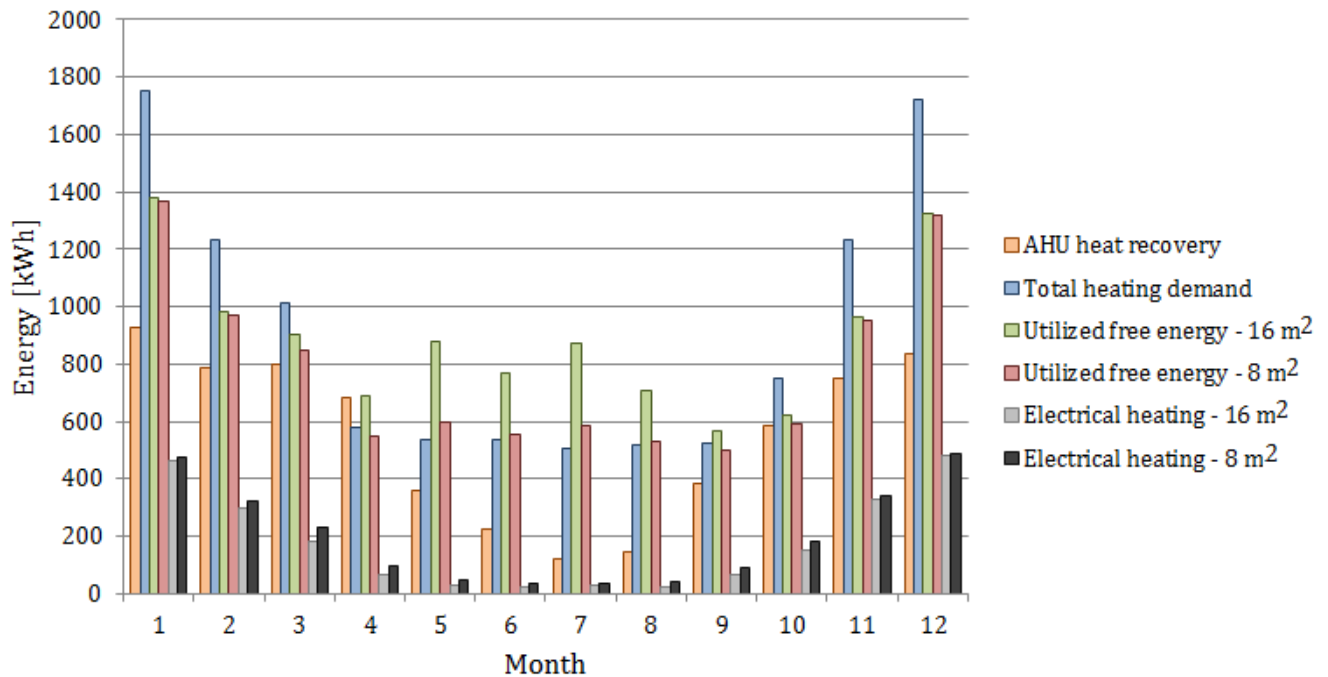


Figure 123 - Total heating demand, AHU heat recovery, utilized free energy and electrical heating for Scenario 15, 16 and 8 m<sup>2</sup> collector area

As for Scenario 17, the annual total heating demand is 10 900 kWh/year and the heat recovered in the air handling unit is 6 600 kWh/year. The electrical heating demand is reduced by approximately 40 kWh per month during the winter, compared to Scenario 17. This applies to both a solar collector area of 16 and 8 m<sup>2</sup>. With optimized orientation and tilt angle, more solar energy can be collected and utilized to cover the demand and as a consequence, a reduction in electricity use is obtained. The monthly amount of utilized free energy is increased with 40 kWh per month during the winter and approximately 100 kWh per month during summer when 16 m<sup>2</sup> of collector area is installed. With 8 m<sup>2</sup>, the amount of utilized free energy is increased with 20 kWh per month during the winter and 50 kWh per month during summer. This is partly due to the enhanced orientation, but also due to the lower share of solar collector heat loss. From Figure 123 it can be seen that the amount of utilized free energy exceeds the energy demand during the summer months with both 16 and 8 m<sup>2</sup> of collector area. This implies that excess solar heat is produced with both solar collector areas.

The total amount of utilized free energy for both 16 m<sup>2</sup> and 8 m<sup>2</sup> solar collector areas, are compared to the total heating demand in Table 39. The excess solar heat, which is utilized to recharge the borehole, is not included in the calculations.

**Table 39 - Amount of utilized free energy, Scenario 15**

	<b>Total</b>	<b>Fraction</b>
<b>Heating demand</b>	10 900 kWh/year	-
<b>Scenario 15, 16 m<sup>2</sup></b>	9 312 kWh/year	85.4 %
<b>Scenario 15, 8 m<sup>2</sup></b>	9 150 kWh/year	83.9%

When the excess solar energy is not taken into consideration, the amount of utilized free energy is nearly the same for a collector area of 16 m<sup>2</sup> and 8 m<sup>2</sup>. This result shows that a collector area of 8 m<sup>2</sup>, when orientated and tilted correctly, is sufficient for a single-family dwelling with a solar combi-system, as recommended in the literature by Zijdemans (2012). However, if it is desired to heat an outdoor swimming pool with excess solar heat, a collector area of 16 m<sup>2</sup> is more suitable.

### 13.7.1 DHW DEMAND

The amount of free energy transferred to the DHW tank is presented in Figure 124. The DHW demand, as well as the monthly solar and exhaust air energy which are transferred to the tank, are presented.

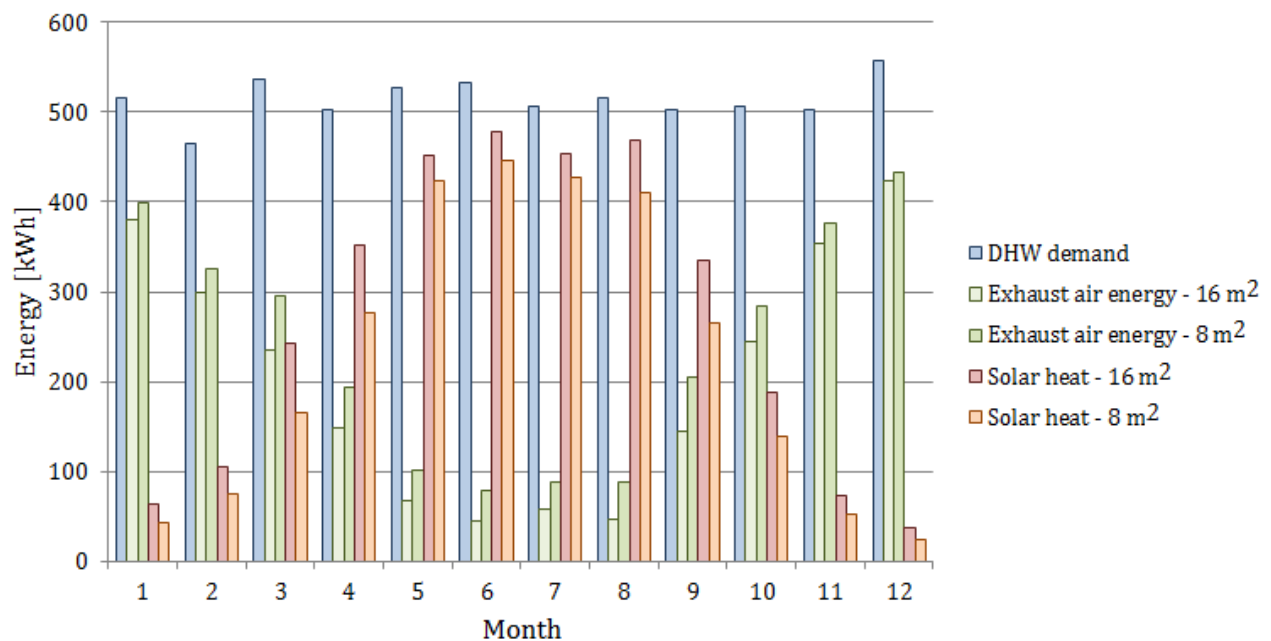


**Figure 124 - Amount of utilized free energy in DHW Tank, Scenario 15**

The monthly amount of utilized energy from the exhaust air is decreased in Scenario 15 compared to Scenario 17. This is due to the increase in collected solar energy, and thereby the increase in solar energy transferred to the DHW tank. By comparing Figure 124 with Figure 119 it can be seen that a larger part of the monthly DHW demand is covered by solar energy during the winter months in Scenario 15 than in Scenario 17. With optimized collector orientation and tilt angle, a larger fraction of the DHW demand is covered by solar energy with 8 m<sup>2</sup> solar collectors installed than with a collector area of 16 m<sup>2</sup> where the tilt angle and orientation are at initial settings, as in Scenario 17.

The amount of the DHW demand covered by solar energy in each month, both with 16 and 8 m<sup>2</sup> of installed solar collector areas is shown in Figure 125.

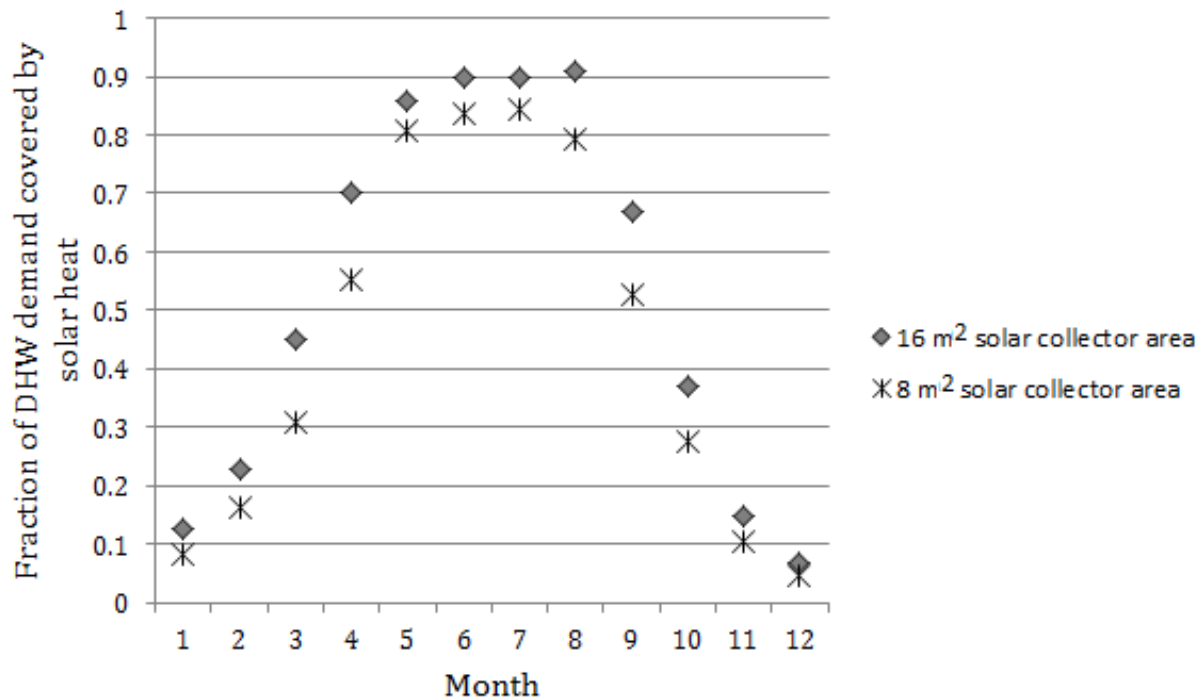


**Figure 125 - Fraction of monthly DHW demand covered by solar heat, Scenario 15**

Approximately 90 % of the DHW demand is covered in June, July and August when a solar collector area of 16 m<sup>2</sup> is installed. In April and September, 70 % is covered, which is about 20 % higher compared to Scenario 17. If 8 m<sup>2</sup> of solar collectors are installed instead, the DHW coverage ranges between 80 and 90 % from May to August. With both 16 m<sup>2</sup> and 8 m<sup>2</sup> of solar collector area, about 10 % of the demand is covered in the coldest winter months, January and December. By comparing the coverage of DHW demand obtained with 8 m<sup>2</sup> of solar collectors installed in Scenario 15 with 16 m<sup>2</sup> of solar collectors installed in Scenario 17, it can be seen that the difference is not particularly large. However, a higher fraction of the DHW demand is covered with 8 m<sup>2</sup> of collector area in Scenario 15 during the coldest months in heating season. Approximately 18 % of the demand is covered in February with 8 m<sup>2</sup> collector area in Scenario 15 opposed to only 10 % coverage with 16 m<sup>2</sup> of collector area in Scenario 17. Since the tilt angle is steeper in Scenario 15, more of the available solar energy during the winter months can be collected.

### 13.7.2 SPACE HEATING DEMAND

In Figure 126 is the monthly solar and ground-source energy utilized to cover the space heating demand presented for both a solar collector area of 16 m<sup>2</sup> and 8 m<sup>2</sup>. The monthly amount of utilized free energy is compared to the actual space heating demand of the dwelling.

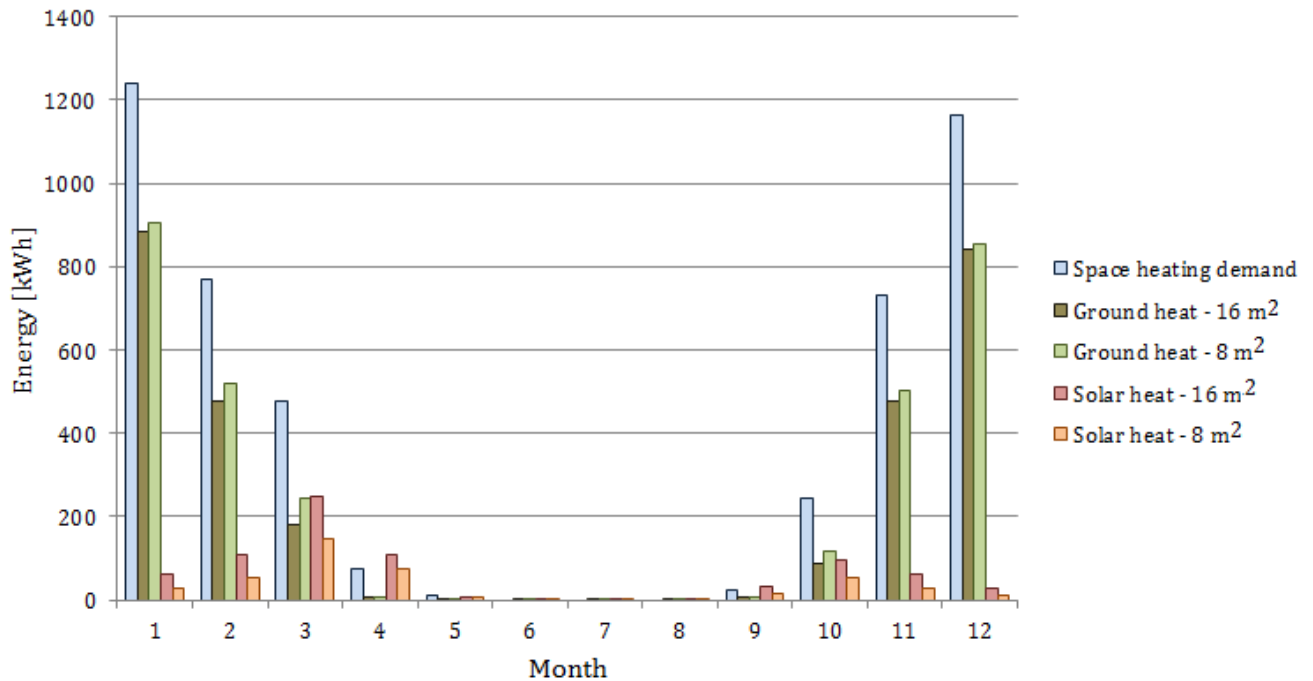


Figure 126 - Amount of utilized free energy for space heating, Scenario 15

Comparing Figure 126 with Figure 121 show that the monthly utilized ground heat is reduced and that more solar energy is utilized for space heating. With optimized orientation and tilt angle, solar energy can be utilized for space heating in January, November and December as well. Even though the solar fraction is not significant, the operation time of the GSHP can be reduced and more electrical energy can be saved.

The amount of space heating demand covered by solar energy in the winter months is listed in Table 40.

Table 40 - Space heating demand covered by solar energy, Scenario 15

Month	16 m <sup>2</sup> collector area	8 m <sup>2</sup> collector area
January	4.8 %	2.3 %
February	14.0 %	6.7 %
March	52.6 %	30.7 %
April	100 %	100 %
September	100 %	70.3 %
October	40.0 %	22.3 %
November	8.6 %	3.7 %
December	2.5 %	1.1 %

As seen in Table 40, 50 % of the space heating demand is covered by solar energy in March, while 100 % is covered in April and September with a solar collector area of 16 m<sup>2</sup>. Even in October, 40 % is covered. With 8 m<sup>2</sup> of collector area installed, 30 % of the space heating

demand is covered in March, while 100 and 70 % is covered in April and September. This is comparable to the results obtained with 16 m<sup>2</sup> collector area in Scenario 17. But again, a higher fraction of the space heating demand is covered by solar energy in the coldest winter months with 8 m<sup>2</sup> in Scenario 15 compared to 16 m<sup>2</sup> of solar collectors in Scenario 17.

**13.7.3 SOLAR ENERGY TRANSFERRED TO THE GROUND**

The amount of solar energy utilized to recharge the borehole for both 16 m<sup>2</sup> and 8 m<sup>2</sup> of solar collector area installed, can be seen in Figure 127.

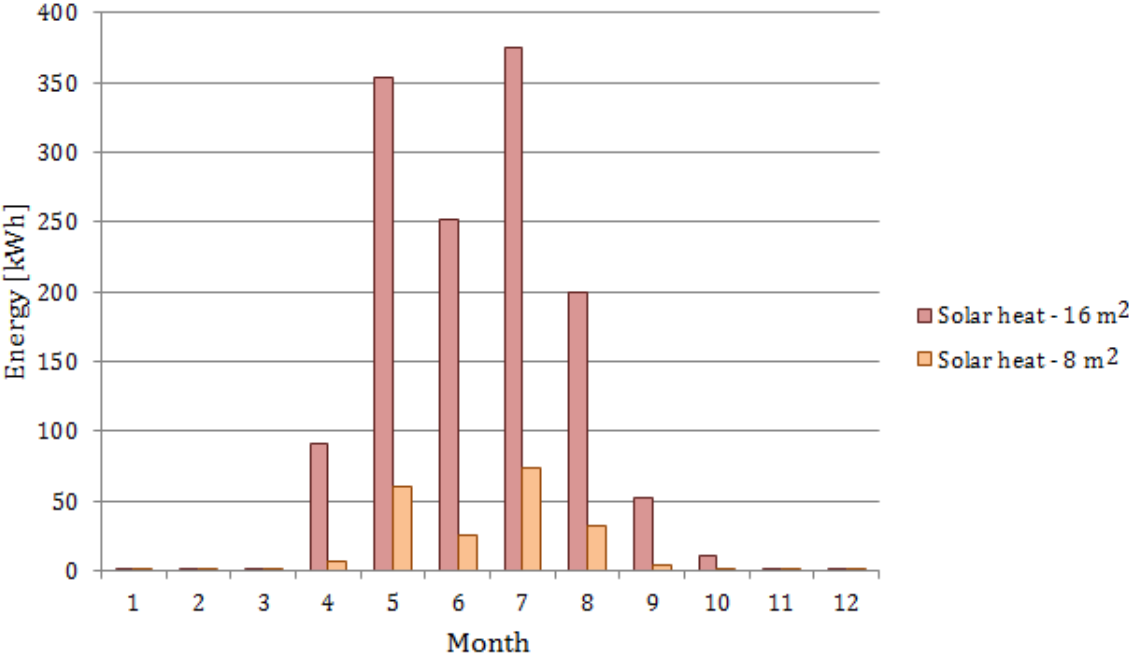


**Figure 127 - Amount of utilized solar energy for recharging of borehole, Scenario 15**

With collector orientation towards the south and with a tilt angle of 55°, a larger share of excess solar heat is produced through the year. Compared to Figure 122, it can be seen in Figure 127 that excess solar heat is produced from April to October and not only from April to August. Even though recharging the borehole in this system has minor impact on the GSHP COP, it is useful to dump excess solar energy into the borehole for heat protection. If an outdoor swimming pool is considered to be heated by solar energy, more solar energy is available in Scenario 15 than in Scenario 17.

The system’s annual solar fraction, both with 16 m<sup>2</sup> and 8 m<sup>2</sup> of installed solar collector area, is given in Table 41.

**Table 41 - Annual solar fractions for 16 and 8 m<sup>2</sup> collector area, Scenario 15**

	16 m <sup>2</sup> solar collector area	8 m <sup>2</sup> solar collector area
<b>Solar fraction [%]</b>	48.1	30.6

If 16 m<sup>2</sup> of solar collector area is installed and orientated towards the south with a tilt angle of 55°, the annual solar fraction is 48.1 %. This is about 18 % higher than if 8 m<sup>2</sup> of solar collector area is installed. Compared to Scenario 17, the obtained solar fraction is approximately 16 % higher in Scenario 15 when 16 m<sup>2</sup> of solar collector area is installed.

## 14 DISCUSSION

As seen in 13.6.1 *Electricity Use and Energy Demand*, the annual specific heat demand is higher than the required 17.6 kWh/m<sup>2</sup> stated in NS 3700:2013. The deviation may be explained by the architectural design of the building which results in increased envelope area. In order to design a single-family dwelling which can be categorized as a dwelling of passive house standard, limitations are set on room height and consequently, building envelope area. It is stated in the guidance for design of passive house dwellings, published by Sintef Byggforsk (2012), that the room height should not exceed 2.4 m in order to reach passive house standard with a Norwegian climate (Myhre, et al., 2012). If the room height exceeds 2.4 m, the total heat loss due to infiltration increases. The “Multikomfort” dwelling has a room height of 2.6 m on the ground floor, while the maximum room height is 4.5 m on the first floor. This may explain the higher heat demand compared to the requirements. In addition, due to the outdoor atrium the total envelope area increases and a higher heating demand must be expected.

It is however challenging to achieve the requirements of passive house standard, especially with a Norwegian climate. A study performed by Husbanken in 2009 showed that for a single-family dwelling of passive house standard with 200 m<sup>2</sup> floor area located in Oslo, the yearly heating demand was calculated to be 21.7 kWh/m<sup>2</sup> and the specific heating effect was 15.6 W/m<sup>2</sup> (Våge, et al., 2009). NorOne, the first Norwegian passive house constructed according to the German PHPP-standard (Passive House Planning Package) built in 2007 in Sørumsund in Akershus, had an annual heating demand of 21 kWh/m<sup>2</sup> in 2011. The heating demand was however calculated to be 15 kWh/m<sup>2</sup> if the temperature set point for space heating had been 20°C (NorONE, 2011). The EU-funded demonstration project CEPHEUS (Cost Efficient Passive Houses as European Standards) includes 221 housing units built with passive house standard in five European countries. Heating demand measurements performed on the projects revealed that some housing units achieved roughly the predicted space heating consumption of 15 kWh/m<sup>2</sup>, while others were significantly above this. For instance, a detached dwelling located in Horn in Austria had an annual heating demand of 27.9 kWh/m<sup>2</sup> (Feist, et al., 2001). The specific heating demand for the “Multikomfort” model must therefore be assumed adequate, even though a lower heating demand would be desirable.

The heating system designed in IDA ICE represents a simplified version of the “Multikomfort” heating system, and the results obtained and presented in this report may therefore deviate from the result obtained with the original “Multikomfort” system. Since it is not possible to include both a vertical and a horizontal ground loop as well as grey water as energy source in IDA ICE, the proportions of utilized free energy may be a bit smaller than what they could have been. As seen in Figure 45, the space heating tank designed in IDA ICE is relatively simplified compared to the space heating tank in the “Multikomfort” system. It is however not possible to include an integrated buffer tank in the storage tank in IDA ICE, and due to this the operation and system performance may differ. As discussed earlier, the three-way valves found in the solar circuit in the “Multikomfort” system design were not included in the system designed in IDA ICE. Circulation pumps were used instead in order for the system to work properly. Due to this the system’s electricity use may be a bit higher than what it would have been if three-way valves were used instead.

It should also be noted that some of the parameters used in the system design are based on assumptions, and by changing these parameters a deviation from the presented results may

occur. In the subchapter *13.5 Sensitivity Analysis*, parameters such as the efficiency of the fans in the air handling unit and the solar collector efficiency was changed with  $\pm 10\%$ , and as a result the system's electricity use was affected. This demonstrates that if other assumptions were made during the design of the system, the results presented would have been somewhat different.

From the control of circulation pump P1, which circulates the heat transfer fluid from the collectors to the DHW tank, and P2, which circulates the heat transfer fluid from the collectors to the SH tank, it can be seen that these are operated simultaneously during some periods through the year. The intention was to create a control system which ensured that the operation of P1 was prioritized and that P2 was only activated when the set point temperature in the DHW tank was reached. However, designing a control system in IDA ICE is rather complicated and challenging. It was therefore decided to design a simpler control system, as the one presented in this report, which proved to work satisfactorily.

During the parametric study, the DHW tank volume was increased from 180 l to 300 l. However, when utilizing multiple energy sources in one storage tank, it is recommended that the tank volume is even larger. With a DHW tank volume of 300 l it is evident that the system performance is significantly enhanced and increasing the tank volume further may result in even better system performance, especially if a solar collector area of 16 m<sup>2</sup> is installed. Installing a larger storage tank will at some point result in too high heat losses to the surroundings which is undesirable. A larger tank is also space consuming, and the cost of increasing the tank volume should be considered in correlation to the energy saved.

From the parametric optimization study it was found that reduction in supply air volume as well as reduction in supply air and zone set point temperature resulted in a notable decrease in electricity consumption. However, maintaining a comfortable indoor climate is crucial and it is important to ensure that the indoor climate is not compromised at the expense of saving energy.

When all the simulations were performed it was informed by the IDA ICE producers that the pressure head in the circulation pumps in the solar circuit should be of magnitude 30 kPa in order for the energy in the system to be correct. However, the obtained system energy with a lower pressure head seemed realistic and satisfactory. By changing the pressure head to 30 kPa the only change in system performance was an increase in electricity use of 0.5%. It was therefore decided to present the results with the initial pressure head setting of 3 kPa.

## 15 CONCLUSION

In this report a suggestion to a system design for a single-family dwelling, which includes the combination of solar thermal collectors and ground-source heat pump, has been presented. A collector area of 16 m<sup>2</sup> and an 80 m deep borehole is considered. The combination of solar thermal collectors and ground-source heat pump makes it possible to alleviate many of the disadvantages which appear if a solar collector heating system or a ground-source heat pump system operates separately. Optimal design and operation of the system will result in new operational conditions which provide better efficiency, better use of renewable energy and minimize the energy costs. The combination makes it possible to utilize solar heat at lower insolation and thereby increase the operation time of the solar collectors which results in better efficiency of the system. By introducing a heat pump with high COP in the system solution, a significant reduction of greenhouse gases is achieved. However, the combination represents a rather complex solution and the more complex a system is the more expensive and difficult to control it becomes. It is therefore crucial to find an optimal design and control which assures high coverage with renewable energy in order for the system to be beneficial. Another possibility is to connect additional single-family dwellings to the same borehole (or extend to a borehole field).

The marginal cost of extending the solar collector area is relatively small compared to the system cost, and due to overproduction of solar heat the possibility of thermal energy storage was investigated. By introducing the possibility to store solar energy in a borehole from summer to winter, the heat pump COP may increase and result in a more efficient system. However, for a single-family dwelling only one borehole is needed and recharging the borehole with excess solar heat may be unnecessary due to fast natural recovery. The results from the simulations showed that by recharging the borehole with excess solar heat during the summer months, a slight increase in the ground-source heat pump COP was obtained from April to October. By recharging the borehole with solar heat during the winter months when the solar insolation is too low to be utilized for DHW preparation or space heating, a minor increase in COP was observed as well. However, the increase had minor impact on the performance of the heat pump and thereby the total system's electricity use. Recharging the borehole is beneficial as it protects the solar collectors from overheating, but in the long run it may lead to overheating of the ground which results in reduced possibility to utilize free cooling. For a single-family dwelling it may be more efficient to utilize the excess solar heat for other purposes, e.g. heating of a swimming pool.

A parametric study of the main design and operating parameters was performed in order to optimize and enhance the system performance. The study showed that the design of the short time storage tank is crucial as well as the tilt angle and orientation of the solar collectors. With an optimized storage tank design a reduction of approximately 5 % in electricity use was obtained. Tilting and orientating the solar collectors towards the recommended directions and reducing the heat loss resulted in a reduction of 4 %. The parametric study also revealed that the operating parameters: supply air and zone set point temperature as well as the supply air volume flow rate had the greatest impact on the system's electricity use when taking the percentage change in parameter into account. A reduction of 2.8 % in electricity use was obtained by reducing the zone set point temperature from 21°C to 20°C and still maintaining a comfortable indoor climate. By optimizing the system's main operating parameters a reduction of 6.8 % in electricity use was achieved.



By optimizing the heating system's main design and operating parameters a total reduction of 17.8 % in electricity use was obtained with 16 m<sup>2</sup> of solar collectors installed. A simulation of the optimized system was performed with 8 m<sup>2</sup> of solar collector area as well in order to investigate the difference. This resulted in an electricity use reduction of 14.3 %. Additionally, an optimized system with the initial collector heat loss coefficients, tilt angle and orientation was performed with both 8 and 16 m<sup>2</sup> of solar collector area. Without optimizing the design of the solar collectors a total reduction of 13.5 % in electricity use was achieved with 16 m<sup>2</sup> of collector area installed.

The simulations showed that the highest percentage of renewable energy coverage of the total heating demand was achieved with 16 m<sup>2</sup> installed solar collector area tilted and orientated towards optimum directions. Approximately 85 % of the total heating demand was covered by renewable energy. The highest proportion of domestic hot water demand and space heating demand met by solar energy during the winter months was achieved with this scenario. Approximately 20 % and 45 % of the domestic hot water demand and 14 % and 50 % of the space heating demand in February and March respectively was covered by solar energy. Without optimizing the solar collectors, only 10 % and 28 % of the domestic hot water demand and 2.4 % and 14 % of the space heating demand was covered in February and March respectively.

It was found that if only 8 m<sup>2</sup> of solar collector area was installed, but tilted and orientated towards the optimum directions with minimum heat loss, approximately the same results were achieved as if 16 m<sup>2</sup> of solar collector area was installed without optimizing the collectors. It can be concluded that only half the solar collector area is needed as long as the tilt angle and orientation are optimized in order to obtain the same system performance. Optimizing the tilt angle and orientation will influence the possibility of using the solar collector area as part of the roof construction and the benefit must be considered in coherence with the cost of the extra roof construction.

## 16 FUTURE WORK

The results in this report suggest that by optimizing the main design and operating parameters in the heating system, it is possible to reduce the system's total electricity consumption by approximately 18 %. The system designed in IDA ICE represents a simplification of the original system, and by designing a system which is even more identical to the original system a more exact reduction of the electricity use may be achieved. Spending more time developing the configuration of pipelines and three-way valves in the system could reduce the electricity use even further.

Traditional spiral tanks are utilized as short time storage tanks in the system design presented in this report. Research has shown that low-flow solar heating systems with mantle tanks for small systems and storage tanks with a built-in inlet stratifier for larger systems result in better system performance than when spiral tanks are installed. With mantle tanks or tanks with a built-in inlet stratifier, a stronger thermal stratification is built up in the tank which enhances the operation of the solar collectors. It may therefore be interesting to investigate the effect on the electricity use by installing mantle tanks or tanks with an inlet stratifier instead of spiral tanks.

The effect of recharging the borehole with solar energy both during the summer months and the winter months were investigated in this report. Performing simulations for more than one year should be emphasized in order to get a better impression of how recharging the borehole affects the operation of the ground-source heat pump after several years. Additionally, the thermal balance in the ground, and how it is affected by the thermal exploitation and recharge should be investigated.

The model was simulated with ideal settings regarding internal loads and occupational behavior. It would be interesting to simulate the model with different scenarios of occupational behavior and to investigate the resulting effect on the total electricity use of the dwelling.

In order to really evaluate the heating system suggested for the "Multikomfort" dwelling, a cost-benefit analysis should be performed. As the results showed, installing the solar collectors towards the south with optimum tilt angle resulted in the lowest use of electricity. What is more profitable of utilizing more of the available solar energy through the year or utilizing the solar collectors as a part of the roof construction should be examined through a cost-benefit analysis.

## 17 BIBLIOGRAPHY

- Alonso, M. & Stene, J., 2013. *State-of-the-Art Analysis of Nearly Zero Energy Buildings - Country Report IEA HPP Annex 40 Task 1 - NORWAY*, s.l.: International Energy Agency.
- Amundsen, H., 2013. *Email correspondence with Harald Amundsen from Brødrene Dahl*. Trondheim: s.n.
- Andresen, I., 2008. *Planlegging av solvarmeanlegg for lavenergiboliger og passivhus. En introduksjon.*, s.l.: Sintef Byggforsk.
- Chiasson, A. D. & Yavuzturk, C., 2003. *Assessment of the Viability of Hybrid Geothermal Heat Pump Systems with Solar Thermal Collectors*, s.l.: ASHRAE Transactions 109.
- Crawley, D. B. et al., 2001. *EnergyPlus: creating a new-generation building energy simulation program*, USA: Elsevier.
- Curtis, R. et al., 2005. *Ground Source Heat Pumps - Geothermal Energy for Anyone, Anywhere: Current Worldwide Activity*, s.l.: s.n.
- Danielewicz, J., Fidorow, N. & Szulgowska-Zgrzywa, M., 2013. *A ground source heat pump with heat exchanger regeneration - simulation of the system performance in a single-family house*, Wroclaw, Poland: Taylor & Francis.
- Dehghan, A. & Barzegar, A., 2010. *Thermal performance behavior of a domestic hot water solar storage tank during consumption operation*, s.l.: Elsevier.
- DGS, 2005. *Planning and Installing Solar Thermal Systems - A guide for installers, architects and engineers*. Berlin: James & James Ltd.
- Dokka, T. & Hermstad, K., 2005. *Fremtidens energieffektive boliger*, Trondheim: Skipnes Trykkeri.
- Dokka, T. H. et al., 2013. *A zero emission concept analysis of a single family house*, s.l.: The Research Centre on Zero Emission Buildings.
- Dokka, T. H., Wigenstad, T. & Lien, K., 2009. *Fremtidens energiløsning i større boligutviklingsprosjekter - Jåtten Øst 2 som case*, s.l.: Sintef.
- EC-JRC, 2014. *European Commission JRC - Photovoltaic Geographical Information System*. [Online] Available at: <http://re.jrc.ec.europa.eu/pvgis/apps4/pvest.php> [Accessed 26 February 2014].
- EN12975, 2006. *Thermal solar systems and components. Solar Collectors. Part 2: Test methods*, Brussels: European committee for standardization.
- EN9488, 1999. *Solar energy Vocabulary*, Brussels: European committee for standardization.
- ENOVA, 2012. *Solfanger*. [Online] Available at: <http://www.enova.no/radgivning/privat/rad-om-produkter-og-losninger/oppvarmingsalternativ/solfanger/solfanger-/116/138/> [Accessed 16 November 2013].

- ENOVA, n.d. *Luft/vann-varmepumpe*. [Online]  
Available at: <http://www.enova.no/radgivning/privat/rad-om-produkter-og-losninger/oppvarmingsalternativ/luftvann-varmepumpe/luftvann-varmepumpe-/113/135/>  
[Accessed 18 November 2013].
- Equa, 2013. *IDA Early Stage Building Optimization (ESBO) User guide*, s.l.: EQUA Simulation Technology Group.
- Equa, n.d. *IDA Indoor Climate and Energy*. [Online]  
Available at: <http://www.equa-solutions.co.uk/en/software/idaice>  
[Accessed 12 November 2013].
- Esen, H., Inalli, M. & Esen, Y., 2009. *Temperature distributions in boreholes of a vertical ground-coupled heat pump system*, s.l.: Elsevier.
- Eslami-nejad, P. & Bernier, M., 2011. *Coupling of geothermal heat pumps with thermal solar collectors using double U-tube boreholes with two independent circuits*, Montreal: Elsevier.
- European Commission, J. R. C., 2013. *Photovoltaic Geographical Information System - Interactive Maps PVGIS*. [Online]  
Available at: <http://re.jrc.ec.europa.eu/pvgis/apps4/pvest.php>  
[Accessed 25 October 2013].
- Feist, W., Peper, S. & Görg, M., 2001. *CEPHEUS-Projectinformation No. 36*, Hanover: Stadtwerke Hanover AG.
- Fonkalsrud, J. et al., 2003. *Utredning om energitiltak og tiltak mot kimagassutslipp i Larvik kommune*, Larvik: Larvik Kommune.
- Fornybar, 2007. *Solenergiressursen i Norge, Fornybar*. [Online]  
Available at: <http://fornybar.no/solenergi/ressursgrunnlag/solenergiressursen-i-norge>  
[Accessed 28 August 2013].
- Furbo, S., 2004. *Hot water tanks for solar heating systems*, Kongens Lyngby: Department of Civil Engineering, DTU.
- Furbo, S., 2004. *Low Flow Solar Heating Systems*, Kongens Lyngby: DTU.
- Furbo, S., 2005. *Heat Storage for Solar Heating Systems*, Kongens Lyngby: BYG DTU.
- Furbo, S., 2013. *Education Notes Course 11117 Solar Heating Systems*. Kongens Lyngby: Technical University of Denmark.
- Furbo, S., n.d. *Present and Future SDHW System Technology*, Kongens Lyngby: Technical University of Denmark.
- Halvorsen, U. M. et al., 2011. *Mulighetsstudie Solenergi i Norge*, Oslo: Sintef, KanEnergi.
- Hansen, P. E., 2013. *Email correspondance with representative from Nilan Norway*. Trondheim: s.n.
- Hausner, R. & Fink, C., 2002. *Stagnation behaviour of solar thermal systems*, Gleisdorf: IEA.

- Hepbasli, A. & Kalinci, Y., 2008. *A review of heat pump water heating systems*, s.l.: Elsevier Ltd.
- Hewalex, 2006. *Hewalex Solar Collectors*. [Online]  
Available at: <http://www.hewalex.eu/en/offer/flat-plate-collectors/solar-collector-ks2000-slp.html>  
[Accessed 7 December 2013].
- Higgins, J. & Crocker, C., 2012. *Radiant heating & cooling systems: a theoretical discussion, literature review*, s.l.: University of British Columbia.
- Incropera, DeWitt, Bergman & Lavine, 2007. *Fundamentals of Heat and Mass transfer*. s.l.: John Wiley & sons.
- Kalogirou, S. A., 2004. *Solar thermal collectors and applications*, Nicosia: Elsevier .
- Kjellsson, E., 2009. *Solar Collectors Combined with Ground-Source Heat Pumps in Dwellings. Analyses of System Performance*, Lund: Lund University.
- Kjellsson, E., Hellström, G. & Bengt, P., 2009. *Optimization of systems with the combination of ground-source heat pump and solar collectors in dwellings*, s.l.: Elsevier.
- Kragh, J., Rose, J., Nielsen, T. R. & Svendsen, S., 2006. *New counter flow heat exchanger designed for ventilation systems in cold climates*, Lyngby: Technical University of Denmark.
- Laughton, C., 2010. *Solar Domestic Water Heating - The earthscan expert handbook for planning, design and installation*. s.l.: Earthscan.
- Mauthner, F. & Weiss, W., 2013. *Solar Heat Worldwide*, s.l.: IEA-SHC.
- Midttømme, K. et al., 2008. *Ground-Source Heat Pumps and Underground Thermal Energy Storage - Energy for the future*, s.l.: s.n.
- Morrison, G. L., n.d. *Solar Collectors*, Sydney: University of New South Wales.
- Morrison, G. L., n.d. *Solar water heating*, Sydney: University of New South Wales.
- Myhre, L. et al., 2012. *Veileder for prosjektering av passivhus - småhus. Prosjektrapport 105*, Oslo: Sintef Akadmeisk foralg.
- NGU, 2008. *Norges geologiske undersøkelse - Bergvarme*. [Online]  
Available at: <http://www.ngu.no/no/hm/Georessurser/Grunnvarme/Bergvarme/>  
[Accessed 10 September 2013].
- NILAN, 2013. *NILAN Outstanding Indoor Climate*. [Online]  
Available at: [http://www.nilan.dk/da-dk/forside/loesninger/boligloesninger/kompaktloesning/compact-p.aspx#.UjmU-D\\_hcYI](http://www.nilan.dk/da-dk/forside/loesninger/boligloesninger/kompaktloesning/compact-p.aspx#.UjmU-D_hcYI)  
[Accessed Wednesday 18th September 2013].
- NILAN, n.d. *Compact P*. [Online]  
Available at: [http://www.nilan.dk/da-dk/forside/loesninger/boligloesninger/kompaktloesning/compact-p.aspx#.UqQ4sOKAo\\_M](http://www.nilan.dk/da-dk/forside/loesninger/boligloesninger/kompaktloesning/compact-p.aspx#.UqQ4sOKAo_M)  
[Accessed 8 December 2013].

NILAN, n.d. *Compact P GEO*. [Online]  
Available at: [http://www.nilan.dk/da-dk/forside/loesninger/boligloesninger/kompaktloesning/compact-p-geo.aspx#.UqMca-KAo\\_M](http://www.nilan.dk/da-dk/forside/loesninger/boligloesninger/kompaktloesning/compact-p-geo.aspx#.UqMca-KAo_M)  
[Accessed 7 December 2013].

NorONE, 2011. *NorOne - Norges første PHPP sertifisert passivhus*. [Online]  
Available at: <http://www.norone.info/static.php?page=M%E5leresultater>  
[Accessed 11 November 2013].

NorthernLights, n.d. *How do Solar Vacuum Tubes Work*. [Online]  
Available at: <http://www.solartubs.com/how-do-solar-vacuum-tubes-work.html>  
[Accessed 8 December 2013].

Novakovic, V. et al., 2007. *ENØK i Bygninger - Effektiv energibruk*. 3 ed. Trondheim: Gyldendal Norsk Forlag AS.

NS3031, 2007. *Calculation of energy performance of buildings. Method and data.*, s.l.: Norsk Standard.

NS3700, 2013. *Criteria for passive houses and low energy buildings. Residential buildings*, s.l.: Norsk Standard.

NVE, 2011. *Energibruk*. [Online]  
Available at:  
<http://www.nve.no/Global/Publikasjoner/Publikasjoner%202011/Rapport%202011/rapport9-11.pdf>  
[Accessed 10 December 2013].

Olesen, B. W. & Pavlov, G. K., 2012. *Thermal energy storage - A review of concepts and systems for heating and cooling applications in Buildings: Part 1 - Seasonal storage in the ground*, Kgs. Lyngby, Denmark: Taylor & Francis.

Olesen, B. W. & Pavlov, G. K., n.d. *Seasonal solar thermal energy storage through ground heat exchangers - Review of system applications*, Kgs. Lyngby, Denmark: International Centre for Indoor Environment and Energy.

Oljefri.no, n.d. *Væske/vann varmepumpe*. [Online]  
Available at: <http://oljefri.no/bolig/vaeske-vann-varmepumpe/category1531.html>  
[Accessed 16 November 2013].

Omer, A. M., 2006. *Ground-source heat pump systems and applications*, Nottingham: Elsevier Ltd.

OSOHOTwater, 2014. *Optima Triple Coil*. [Online]  
Available at: <http://www.osohotwater.no/boligprodukter/optima-triple-coil.html>  
[Accessed 26 May 2014].

Prenøk, 3., 2011. *Energibrønner i fjell*, Oslo: Skarland Press.

Ramlow, B. & Nusz, B., 2006. *Solar water heating - A comprehensive guide to solar water and space heating systems*. Canada: New Society Publishers.

- Ramstad, R. K., 2011. *Grunnvarme i Norge - Kartlegging av økonomisk potensial*, Oslo: NVE.
- Ramstad, R. K., 2013. *E-mail correspondence regarding solar seasonal storage in boreholes*. Trondheim: s.n.
- Rindal, L. B. & Salvesen, F., 2008. *Solenergi for varmeformål - snart lønnsomt?*, Oslo: NVE.
- Saint-Gobain, n.d. *Planitherm*. [Online]  
Available at: <http://www.planitherm.com/>  
[Accessed 12 December 2013].
- Sakellari, D. & Lundqvist, P., 2004. *Energy analysis of a low-temperature heat pump heating system in a single-family house*, Stockholm: Wiley and Sons.
- Sanner, B., Karytsas, C., Medrinos, D. & Rybach, L., 2003. *Current status of ground source heat pumps and underground thermal energy storage in Europe*, s.l.: Elsevier Ltd.
- Shariah, A. M., Rousan, A., Rousan, K. K. & Ahmad, A. A., 1999. *Effect of thermal conductivity of absorber plate on the performace of a solar water heater*, Jordan: Pergamon.
- Sintef, 2011. *Grunnvarmebaserte varmepumpesystemer for oppvarming og kjøling*. [Online]  
Available at: <http://www.sintef.no/Projectweb/Annex29/Grunnvarme/>  
[Accessed 3 April 2014].
- Solaris, V., 2007. *User Manual Polysun 4.0*, s.l.: Vela Solaris AG.
- Solaris, V., 2013. *Photovoltaics, Solar Thermal and Geothermal - with Polysun you get everything in one tool!*. [Online]  
Available at: <http://www.polysun.ch/english/product/overview.html>  
[Accessed 12 November 2013].
- Southface, 2013. *How solar thermal works*. [Online]  
Available at: <http://www.southface.org/learning-center/library/solar-resources/how-solar-thermal-works>  
[Accessed 16 November 2013].
- Stene, J., 1997. *Varmepumper Bygningsoppvarming*. 3. utgave ed. Trondheim: Sintef.
- Stene, J., 2004. *IEA HPP Annex 29 - Ground-Source Heat Pumps Overcoming Technical and Market Barriers. Status Report NORWAY*, s.l.: Sintef.
- Stene, J., 2008. *Oppvarmingssystemer for boliger av lavenergi- og passivhusstandard*, Trondheim: Sintef.
- Stene, J., 2013. *Lecture notes from the course TEP 16 Heat Pump Technology*. Trondheim: Jørn Stene.
- Stene, J., 2013. *Lecture notes in the course TEP4260 - Varmepumper for bygningsklimatisering*. Trondheim: Stene.
- Trillat-Berdal, V., Souyri, B. & Achard, G., 2006. *Numerical simulations of ground-coupled heat pumps combined with thermal solar collectors*, Geneva: PLEA2006.

Trillat-Berdal, V., Souyri, B. & Fraisse, G., 2006. *Experimental study of a ground-coupled heat pump combined with thermal solar collectors*, France: Elsevier Ltd.

TRNSYS, 2013. *TRNSYS Transient System Simulation Tool, What is TRNSYS*. [Online]  
Available at: <http://www.trnsys.com/#1>  
[Accessed 12 November 2013].

Våge, M., Marrable, H., Burgvold, J. & Nielsen, H. K., 2009. *Kurs i planlegging og bygging av passivhus*, s.l.: Husbanken.

Wang, H. & Qi, C., 2007. *Performance study of underground thermal storage in a solar-ground coupled heat pump system for residential buildings*, Tianjin: Elsevier .

Weiss, W., 2003. *Solar heating systems for houses - a design handbook for solar combisystems*. London: James & James.

Xiao Wang, M. Z. W. Z. S. Z. T. Y., 2010. *Experimental study of a solar-assisted ground-coupled heat pump system with solar seasonal thermal storage in severe cold areas*, Harbin: Harbin Institute of Technology.

Xi, C. et al., 2011. *Experimental studies on a ground coupled heat pump with solar thermal collectors for space heating*, China: Science Direct.

ZEB, 2013. *About The Research Centre on Zero Emission Buildings - ZEB*. [Online]  
Available at: <http://www.zeb.no/index.php/about-zeb>  
[Accessed 12 November 2013].

Zijdemans, D., 2012. *Vannbaserte oppvarmings- og kjølesystemer*. Oslo: SkarlandPress.



# APPENDIX A - VEKSLER

## A. 1 VEKSLER

### Short Introduction to the Computer Program VEKSLER

#### 1. Background

The computer program VEKSLER calculates the heat exchange capacity rate of a heat exchanger spiral submerged in water in a storage tank. The heat transfer medium in the heat exchanger spiral can either be water or a propylene glycol/water mixture.

The heat exchange capacity rate  $H$  [W/K] is used as a measure of how well the heat exchanger spiral transfers the heat from the fluid in the spiral to the surrounding fluid. As heat exchanger spirals frequently form part of hot water tanks both for the auxiliary heating and the solar heat, it is important to be able to determine the heat transfer precisely under different operation conditions.

#### 2. The Output of the Program

When you have run a program, the following expression will appear on the screen:

$$H=A(DT)+B(DT)*TL$$

$$A(DT)=K1+K2\cdot\ln(DT)$$

$$B(DT)=K3+K4\ln(DT)$$

$$DT=TI-TL$$

In these expressions

$H$	is the heat exchange capacity rate of the heat exchanger spiral	[W/K]
$A(DT)$	is an ancillary quantity	[W/K]
$B(DT)$	is an ancillary quantity	[W/K <sup>2</sup> ]
$TI$	is the inlet temperature to the heat exchanger spiral	[°C]
$TL$	is the mean storage temperature on a level with the heat exchanger spiral	[°C]
$DT$	is the mean storage temperature – the inlet temperature	[°C]
$K1-K4$	are constants	

#### 3. In this Way You Make the Input File

The input file consists of 3 lines: Line 1 states the properties of the heat exchanger spiral. In line 2, 5 different temperatures are to be typed in, and in line 3 the volume flow rates in the heat exchanger spiral matching the temperatures are to be typed in. These temperatures and volume flow rates can e.g. come from some measurements. The values are used for a regression to find  $H$  as a function of the heat storage temperature.

The following are to be typed in:

In line 1	The propylene glycol rate (weight%)	[%]
	The inner diameter of the heat exchanger spiral	[m]
	The outer diameter of the heat exchanger spiral	[m]
	The length of the heat exchanger spiral	[m]
	The thermal conductivity of the heat exchanger spiral material	[W/mK]
In line 2	Heat storage temperature 1	[°C]
	Heat storage temperature 2	[°C]
	Heat storage temperature 3	[°C]
	Heat storage temperature 4	[°C]
	Heat storage temperature 5	[°C]
In line 3	Volume flow rate 1	[l/min]
	Volume flow rate 2	[l/min]
	Volume flow rate 3	[l/min]
	Volume flow rate 4	[l/min]
	Volume flow rate 5	[l/min]

#### 4. When you run the program

- different questions appear on the screen:

- 1) *Ønsker du at indtaste dataene via skærmet (j/n)? Do you want to type in the data via the screen?*

Here you answer “n” (for no) if you want to use an input file. Otherwise, answer “j”. If you answer “n” to question 1, the following question appears:

- 2) *Indtast filnavn – (ENTER bruger “INPUT.DAT”) Type in file name (ENTER uses “INPUT.DAT”):*

Here you write the name of the input file. If you just press ENTER, the program thinks that the input data file is called INPUT.DAT.

If you answered “j” to question 1, you have to type in the data of the spiral and the temperatures continuously.

## APPENDIX B – SCHEDULES FOR EXTERNAL BLINDS

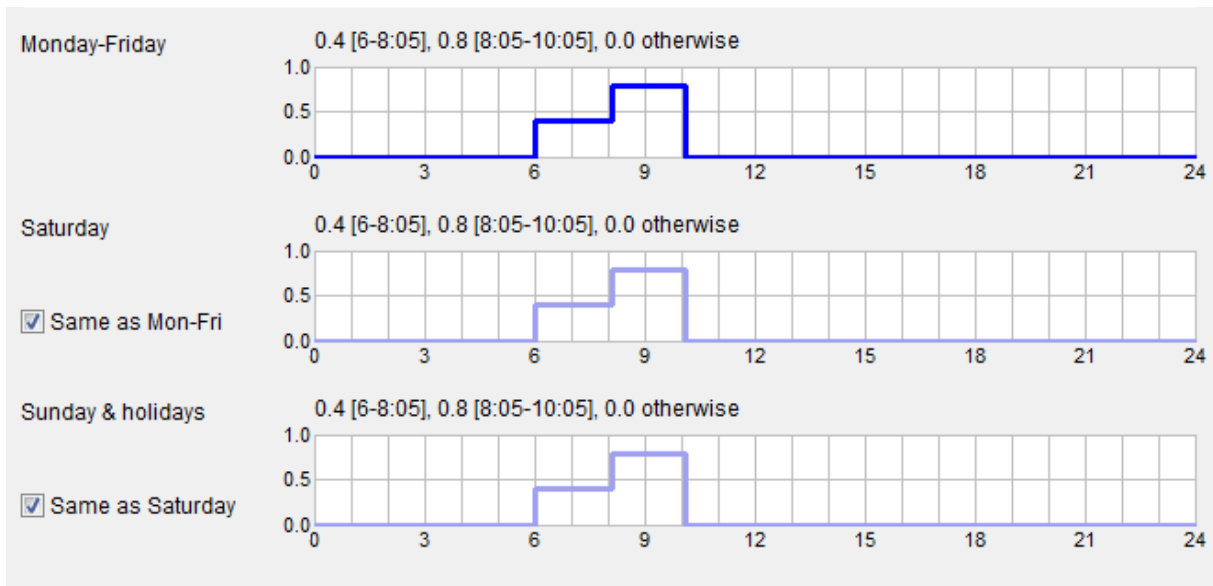


Figure B. 1 - External blinds schedule north-east

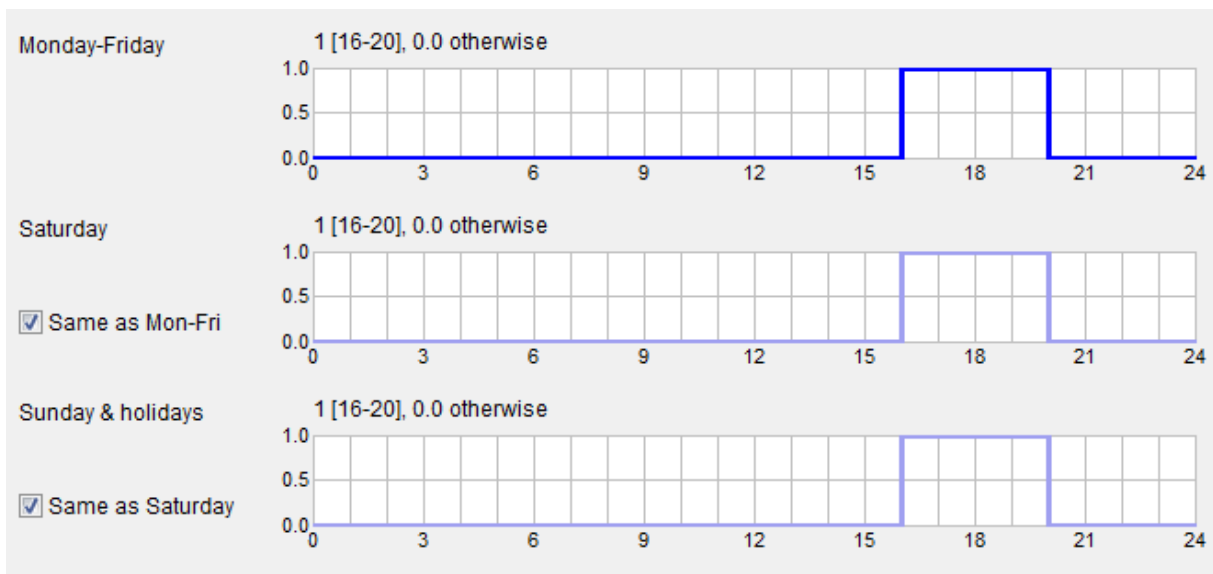


Figure B. 2 - External blinds schedule north-west

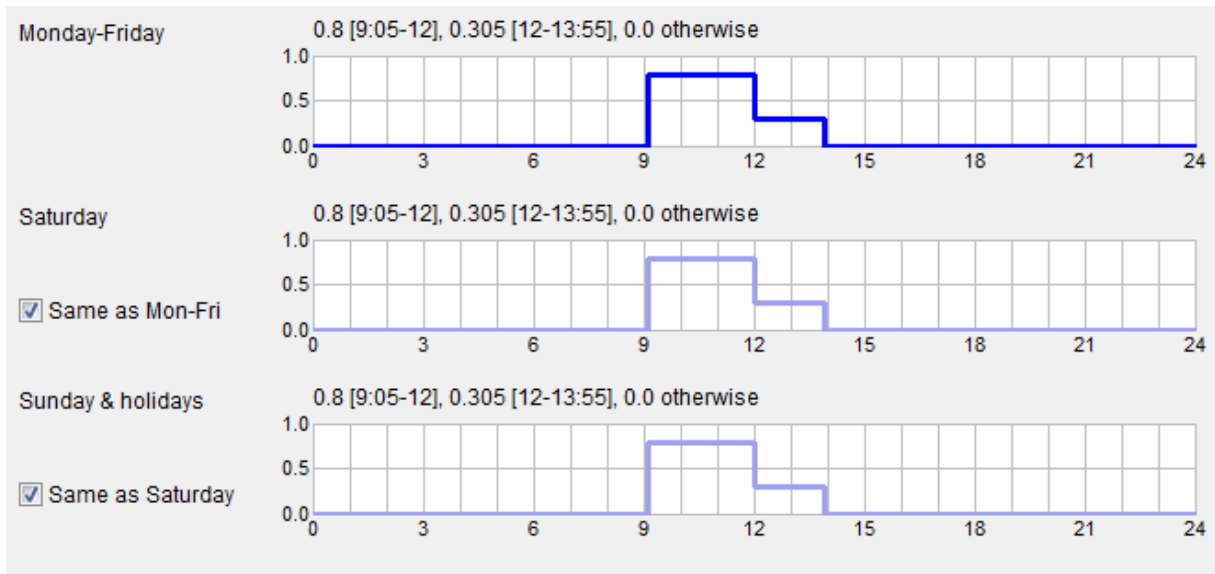


Figure B. 3 - External blinds schedule south-east

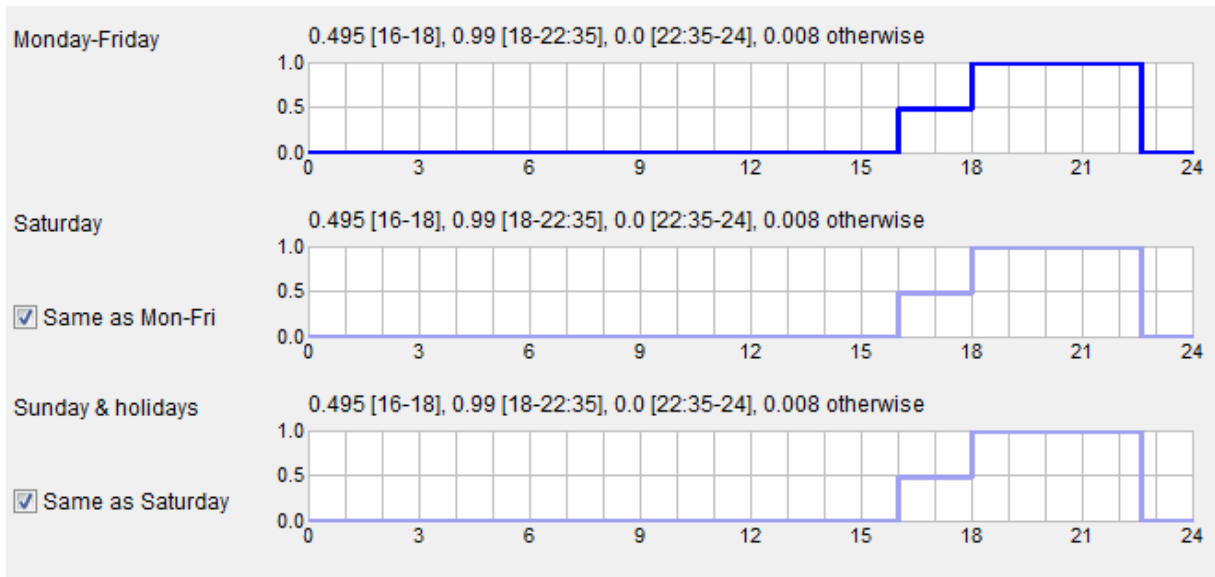


Figure B. 4 - External blinds schedule south-west

# APPENDIX C – OCCUPANT AND EQUIPMENT/LIGHTING SCHEDULES

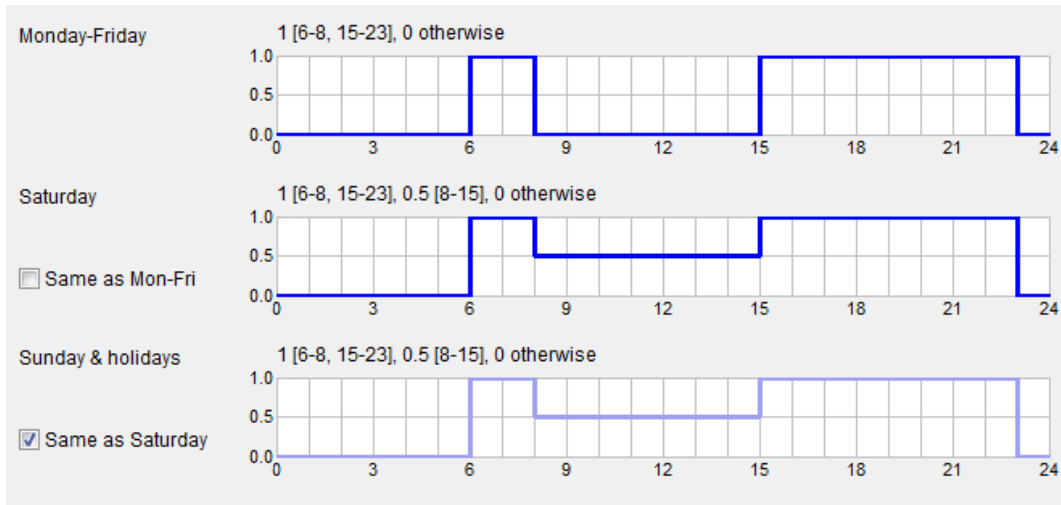


Figure C. 1 - Schedule for equipment and lighting

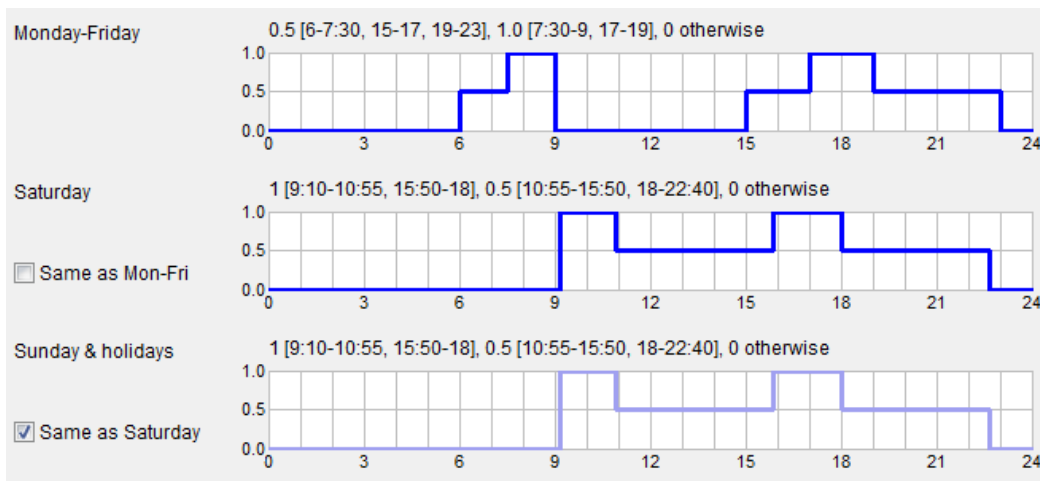


Figure C. 2 - Presence occupants kitchen and living room (Number of occupants = 4)

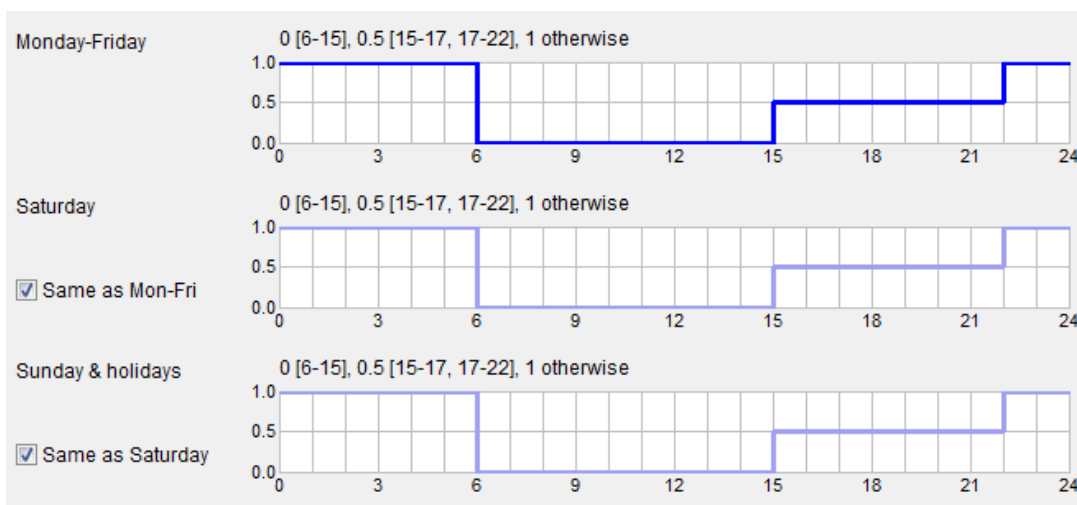


Figure C. 3 - Presence occupants bedroom (Number of occupants = 4)

# APPENDIX D – SYSTEM DESIGN IN IDA ICE 4.6

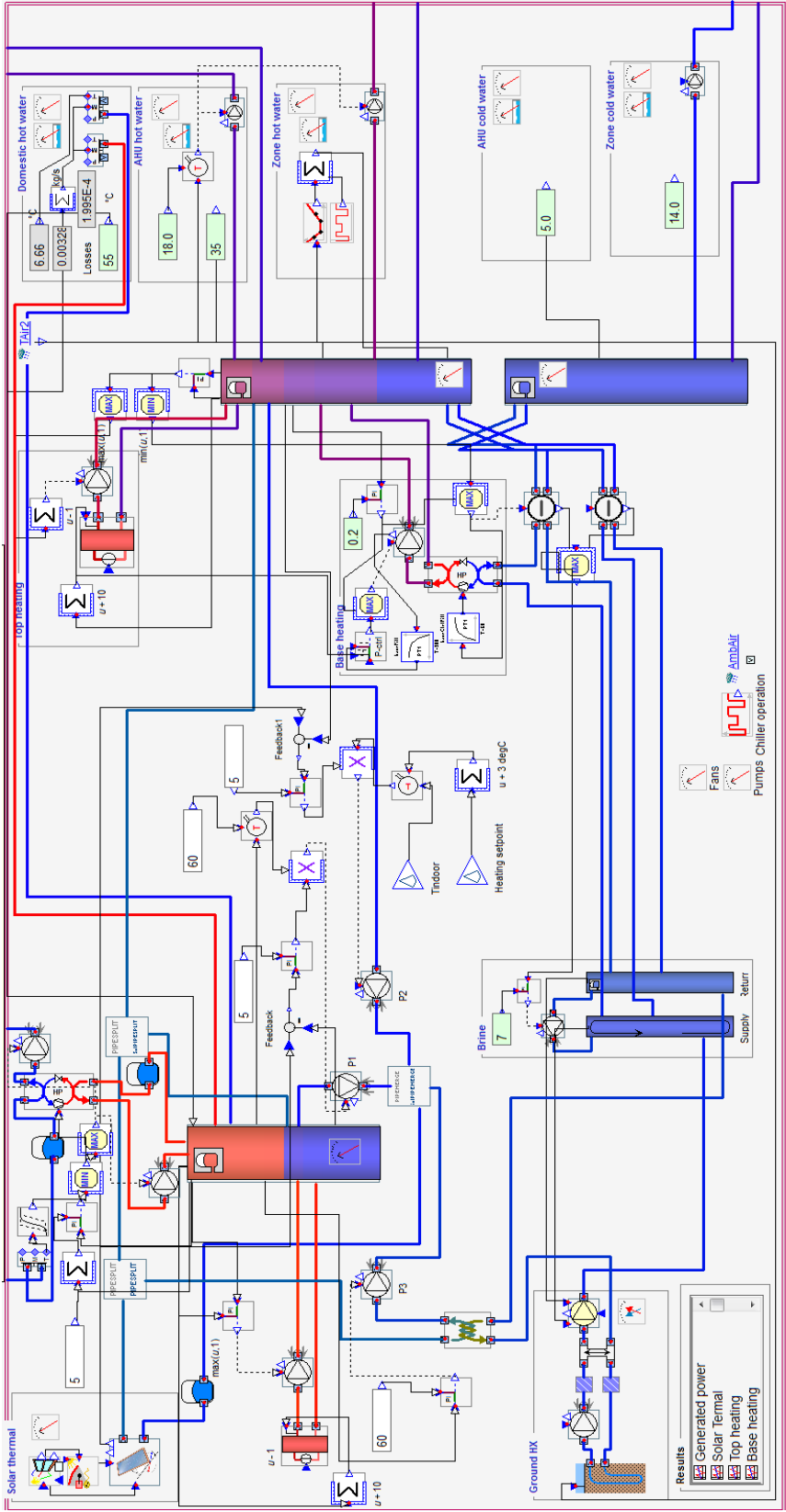


Figure D. 1 - System design in IDA ICE 4.6

# APPENDIX E – OPERATION OF P10 AND P11

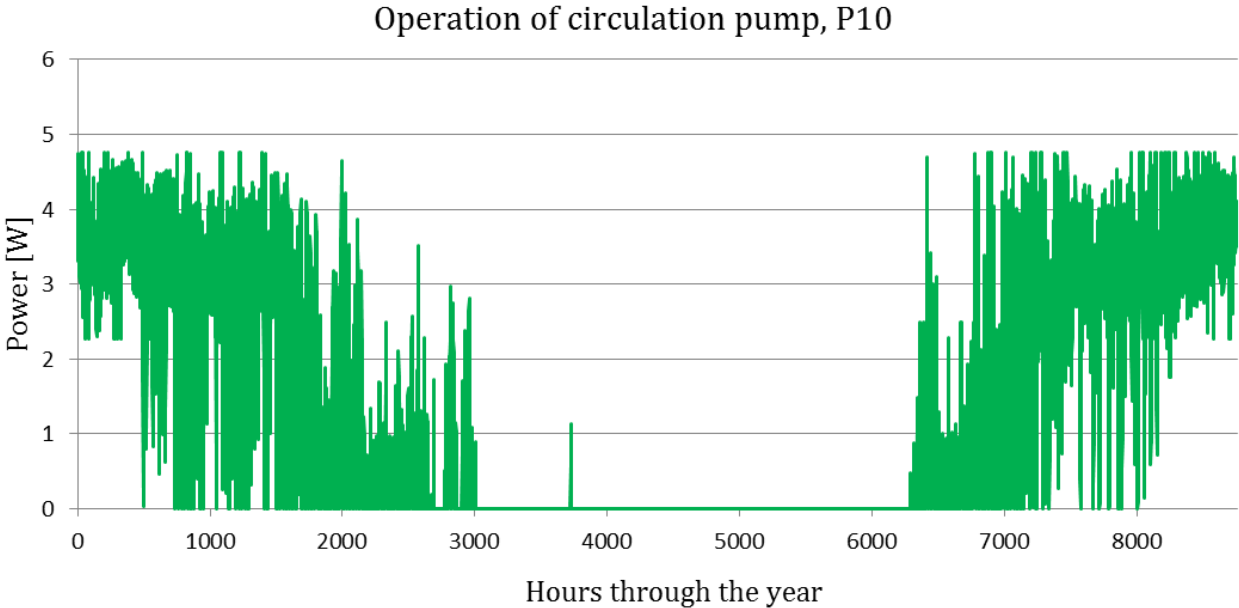


Figure E. 1 - Operation of circulation pump P10 and P11

# APPENDIX F – DESIGN PARAMETER STUDY

Table F. 1 - Effect of solar HE volume

	0.01 m <sup>3</sup>	0.02 m <sup>3</sup>	0.03 m <sup>3</sup>	0.04 m <sup>3</sup>
Annual net utilized solar energy [kWh/a]	4183.5	4183.5	4183.5	4183.5
Annual specific delivered energy [kWh/m <sup>2</sup> ·a]	35.5	35.5	35.5	35.5

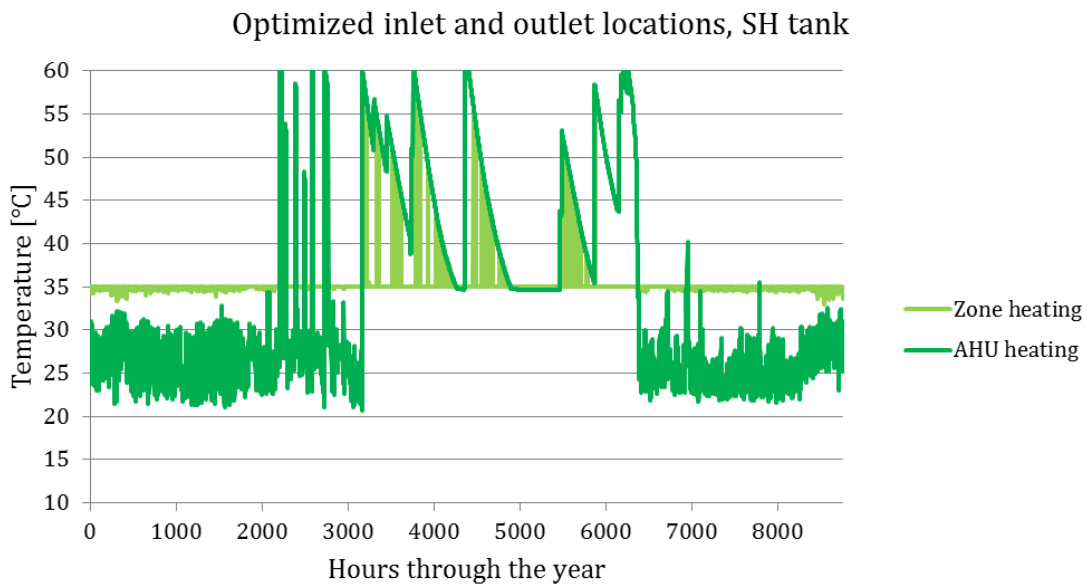


Figure F. 1 - Temperatures for zone and AHU heating - optimized inlet and outlet locations

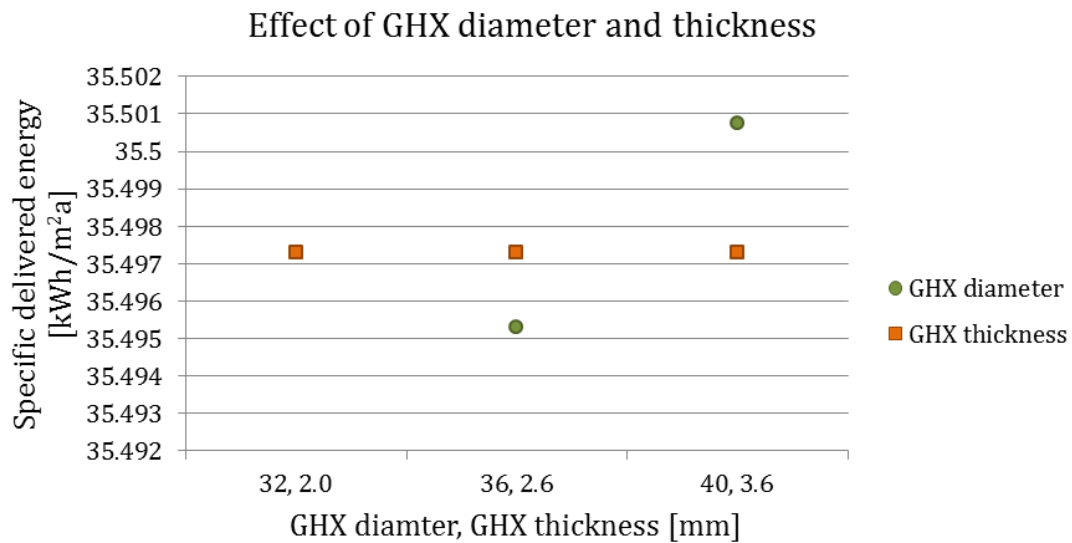


Figure F. 2 - Effect of GHE diameter and thickness - Vertical loop



## APPENDIX G – OPERATION PARAMETER STUDY

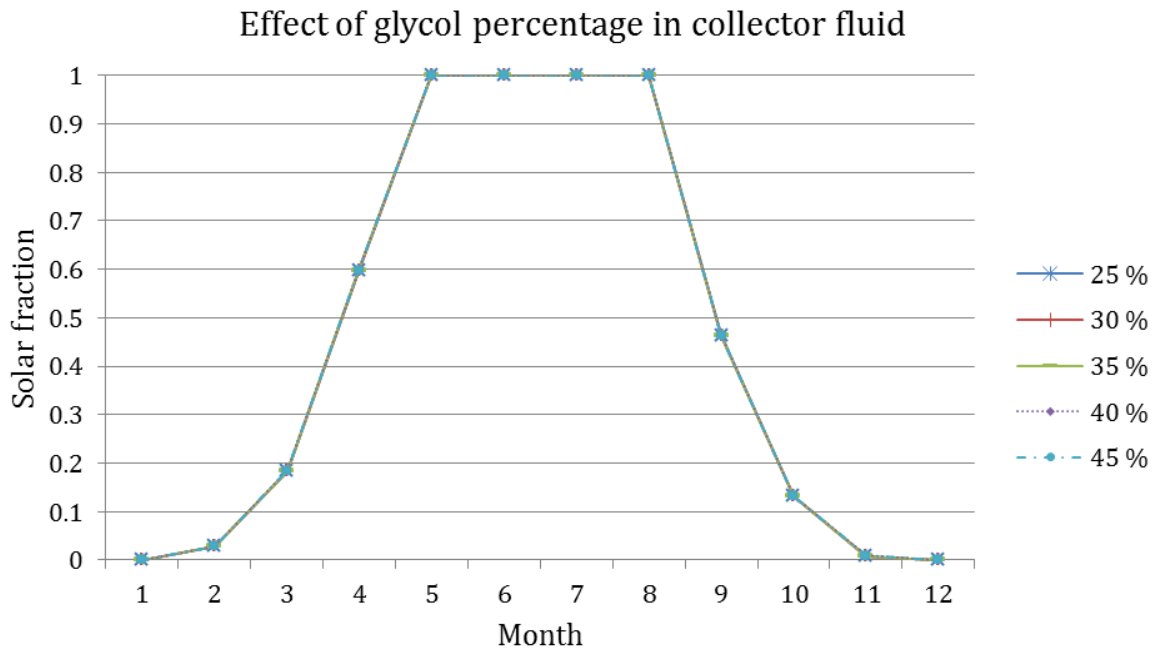


Figure G. 1 - Effect of glycol percentage in collector fluid - Monthly solar fraction

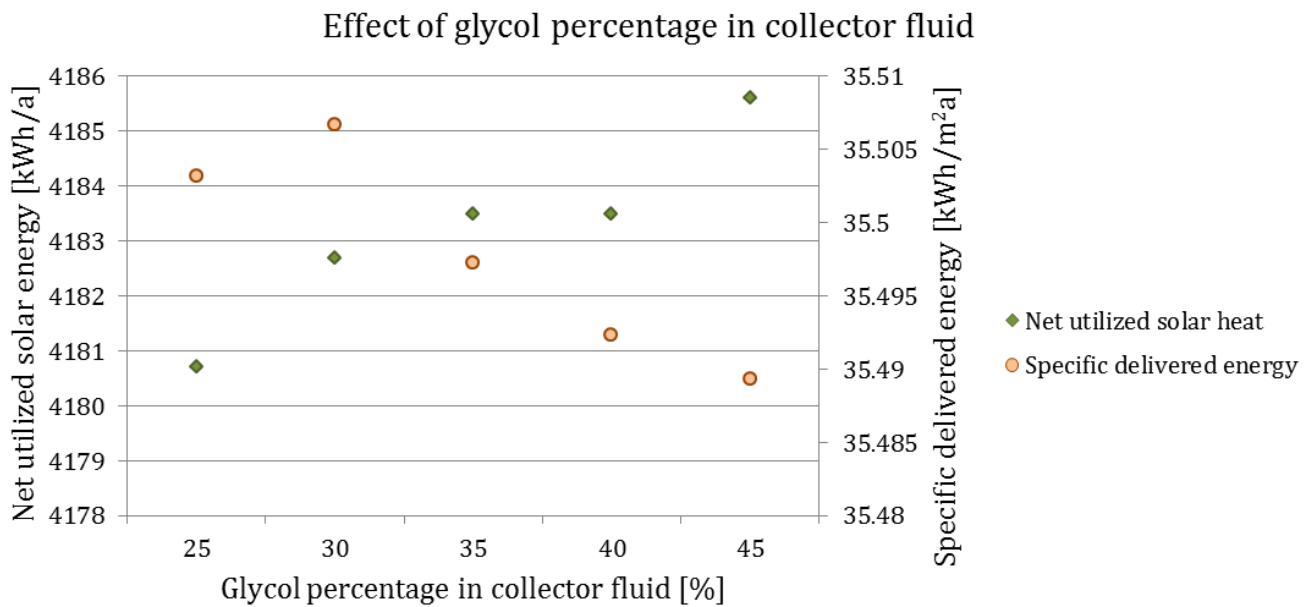


Figure G. 2 - Effect of glycol percentage in collector fluid - Net utilized solar energy and delivered energy

### Effect of GSHE brine

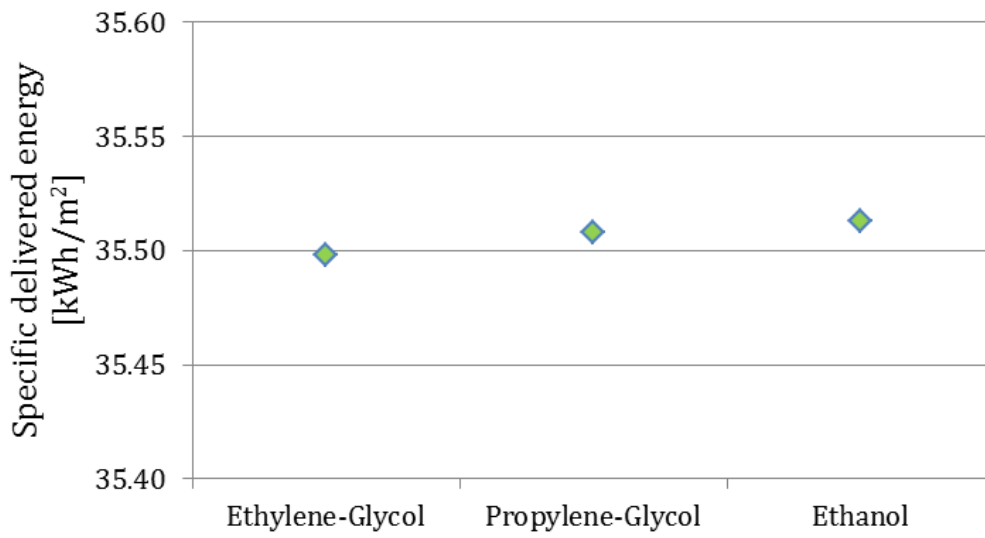


Figure G. 3 - Effect of ground-source heat exchanger brine - Delivered energy

### Effect of GSHE brine mass flow rate

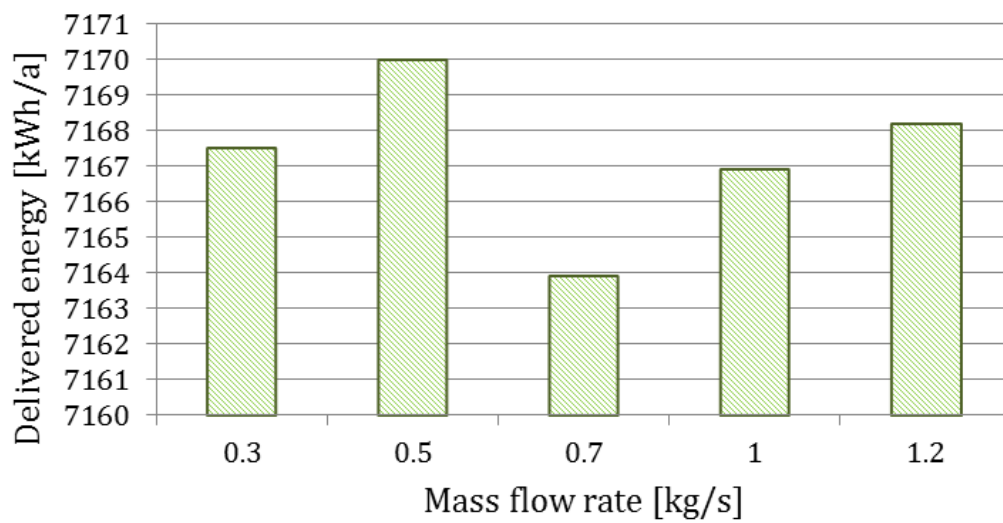
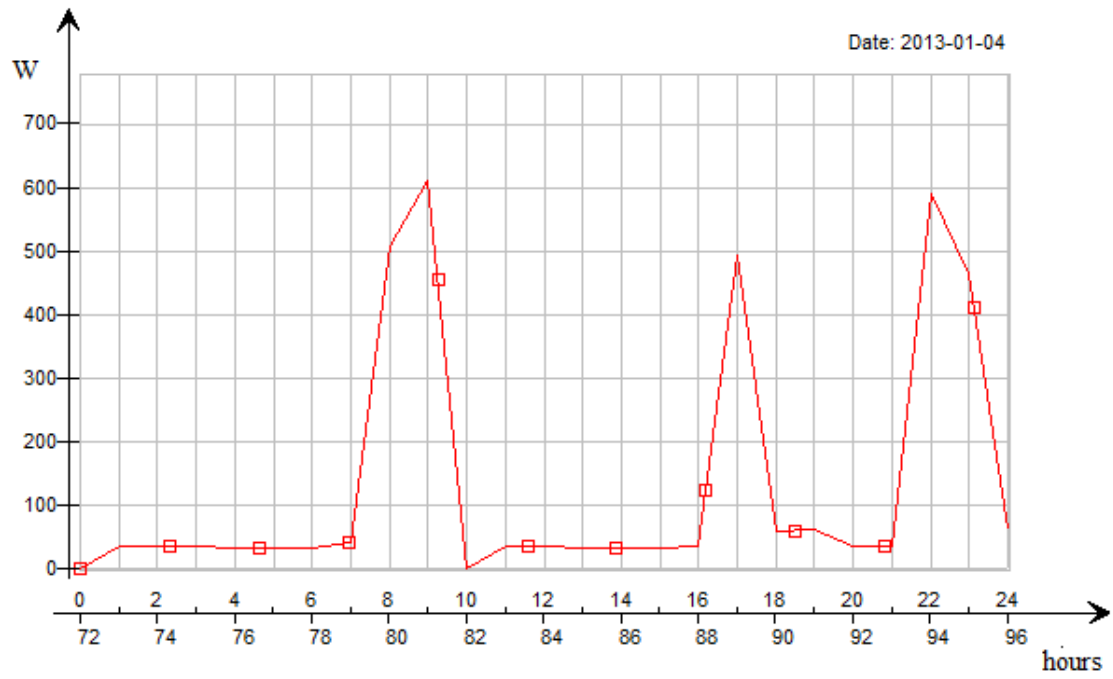


Figure G. 4 - Effect of GSHE mass flow rate - Delivered energy



**Figure G. 5 - Operation of EAHP with new temperature sensor location 2013-01-04**

# APPENDIX H – INDOOR AIR TEMPERATURES

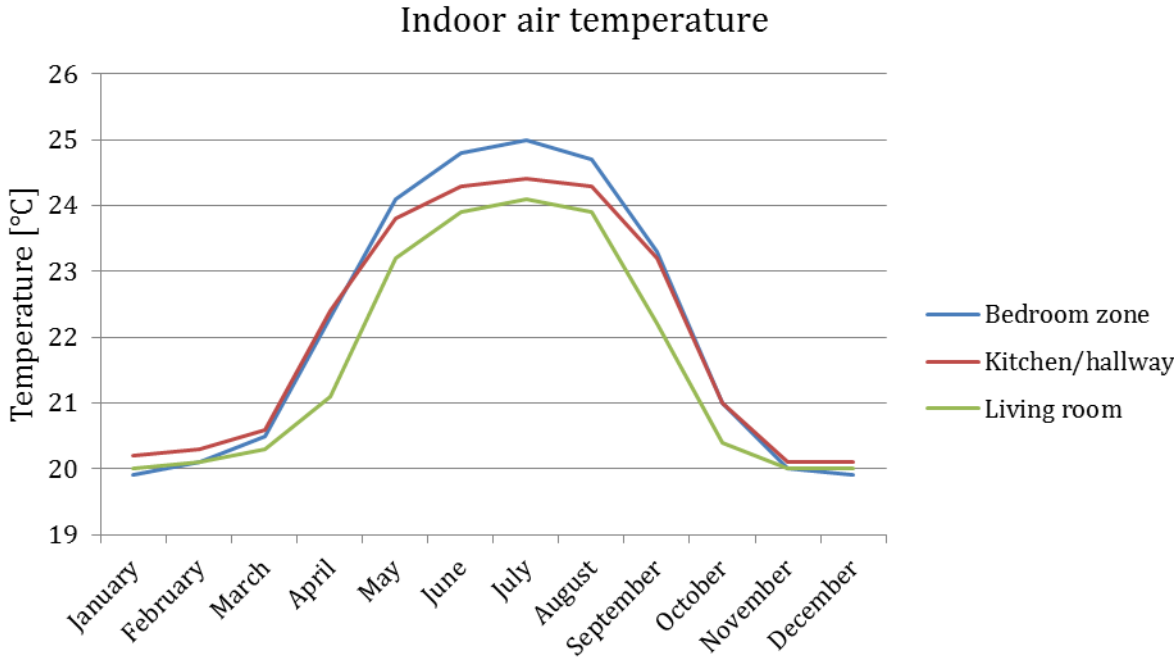


Figure H. 1 - Indoor air temperature - Optimized scenario